The hydraulics of the impacts of dam development on the river morphology

Report to the
Water Research Commission

by

JS Beck and GR Basson

Department of Civil Engineering
University of Stellenbosch
Private Bag X1, Matieland 7602
South Africa

WRC Report No. 1102/1/03
ISBN No. 1-77005-044-2 JUNE 2003

Disclaimer

This report emanates from a project financed by the Water Research Commission (WRC) and is approved for publication. Approval does not signify that the contents necessarily reflect the views and policies of the WRC or the members of the project steering committee, nor does mention of trade names or commercial products constitute endorsement or recommendation for use.

Executive Summary

The construction of a dam can drastically alter the flow regime and sediment load of the river downstream by altering flood peaks and durations, as well as by trapping large amounts of sediment. The imposed changes in the flow can lead to riverbed degradation directly downstream, as a result of very low sediment loads, as well as narrowing of river channels due to decreased transporting capacities further downstream. The increasing number and size of dams built during recent decades has drawn more attention to the impacts that dams can have, so much so that the World Commission on Dams (WCD, 2000a) has completed a worldwide study on dams. In South Africa there have also been some studies focusing on the impacts of river developments on a river system such as interbasin transfer schemes (Rowntree *et al.*, 2000). It has, however, become clear that there are still some issues to be addressed in order to gain a better understanding of the changes in the downstream river morphology that may occur as a result of dam developments

The overall aim of the project is to investigate the impacts of dam developments on the downstream river morphology, specifically:

- The assessment of the changes in the downstream river morphology as a result of different dam development scenarios.
- The development of methods for predicting the downstream river channel geometry for South African conditions.
- An investigation into the effects of clay and silt on the sediment transport behaviour of sediments.
- The development of a methodology to determine required flood magnitudes, duration and frequency downstream of a dam, to maintain (or restore) the river morphology as close as possible to the natural (or desired) conditions, based on fundamental hydraulic principles of sediment transport. This would provide tools with which environmental flow requirements, controlling the river morphology, can be analysed.

The following results have been obtained:

- The impacts of dams on the downstream river morphology depend to a large degree on the operation of the reservoir as well as the reservoir capacity in relation to the MAR,

since these two factors determine the magnitude, duration and frequency of all but the largest floods. Some examples of impacts are presented in **Table 1**:

Table 1 Impacts and causes

Impact	**Cause**
Riverbed degradation	Clear water spillage due to sediment trapped in reservoir
Coarsening of bed material	Clear water releases
Reduced sediment transport capacity	Attenuated flood peaks, coarser bed materials, flatter slopes
Riverbed aggradation	Reduced sediment transport capacity, tributary sediment supply
Increased riparian vegetation	Long periods of low or no flows
Narrowing of river channel	Increased riparian vegetation and smaller floods

- Regime equations describing the average width and depth of a river were developed, based on South African river data. The equations were verified with the aid of international river data, and compared to results obtained from semi-theoretical regime equations developed in the United States. The new regime equations compared favourably to these regime equations.

- The regime equations developed in **Chapter 3**, as well as other international regime equations are not suitable for predicting the channel geometry of rivers downstream of dams with highly unnatural release patterns, mainly as a result of the problems with the determination of the dominant discharge. Alternative regime width equations were developed.

- It has been found, through laboratory experiments, that as little as 7% clay and silt can affect the sediment transport behaviour of sand. When sediments contain more than 23% sand the erosion could be affected by armouring. At higher clay and silt contents (> 7%) almost no bedforms develop.

- A methodology was developed by which the critical conditions for mass erosion of cohesive sediments and cohesive – non-cohesive mixtures can be described in terms of the applied stream power at the bed. The applied stream power at the bed can be related to the percentage clay and silt in the bed material.

- Sediment transport equations in terms of the unit input stream power for cohesive and non-cohesive sediments, as well as mixtures of the two, were developed with data gained from laboratory experiments. The equations were successfully verified against independent flume data, as well as United States river data.

- One-dimensional modelling of the impact of existing and proposed new dams on two South African rivers and an estuary was carried out. By comparing sediment transport characteristics of pre-and post-dam scenarios, problem areas could be identified and mitigating procedures evaluated.

- Procedures were developed by which the impacts of dams on the downstream river morphology can be determined and mitigating measures developed.

- Environmental flood releases at medium and large dams, and sediment sluicing/flushing at small reservoirs (relative to the MAR), are required to limit the upstream and downstream impacts of a dam on the river and estuary morphology. By using observed and simulated discharge-sediment load relationships along a river for various development/operational scenarios, it is possible to design the peak discharge, frequency and duration of these environmental floods.

- Environmental flood releases will cause riverbed degradation close to the dam, but are required for channel maintenance of the greater part of the river further downstream to limit the overall impact of a dam.

The following recommendations can be made:

- Dams have dramatic impacts on the river morphology, far upstream and even further downstream. These impacts should not be underestimated in terms of ecological damage

and costs, and should be investigated in great detail during planning, design and operation of the dam using suitable hydraulic techniques.

- It is recommended that the proposed procedures on the methodology to investigate the morphological impacts of dams be implemented in environmental flood requirement studies. The design of flood releases (or not) considering flood peak, duration, and frequency should be carried out using this methodology.

- Post-dam river width changes can be simulated by using regime equations developed in this study, but for more detailed investigations semi-two-dimensional or two-dimensional modelling should be carried out.

- River morphological simulations should be carried out over at least 15 years. Daily data are often not good enough due to the flood peak averaging.

- Flood flushing and managed flood releases from reservoirs should be implemented to take place simultaneously with a natural flood event for maximum efficiency.

- Generally the quality of the water released from reservoirs is very different than under natural conditions. In order to achieve the desired water quality, the design of multi-level outlet structures should be optimised to allow managed flood releases.

- Hydropower generation, causing large water level fluctuations, can seriously damage a river. Planned flood releases are difficult to implement in order not to interfere with the hydropower generation, so the hydropower releases have to be optimised to reduce geomorphological impacts, by limiting maximum release discharges and rate of change of discharges.

- A problem with determining IFR/EFR requirements is the difficulty in establishing the correct link between the abiotic drivers, e.g. hydrology and sediment transport, and the biotic components, such as the role of fine sediment transport. Detailed hydrodynamic and morphological simulations can yield more information, which can be significant for the biotic components.

- The proposed analysis procedures rely on long-term suspended sediment data taken in rivers to determine a sediment load – discharge relationship. Such data are available on most rivers in Africa and internationally, but are limited in South Africa. It is important that suspended sediment sampling is continued as soon as possible at most of the South African flow gauging stations.

- The natural river geomorphology is generally used as a reference condition against which to evaluate any future changes. At future planned dam sites monitoring of the river morphology should be carried out, such as repeat surveys, in order to establish the reference condition and any subsequent changes.

- The sediment transport theory of sand, gravel and even fine sediment is well established. However, the sediment transport of cobbles and boulders should be investigated to establish characteristics such as the flows necessary to move larger-sized sediment and their sediment transport.

- The impacts of a dam are not limited to rivers, but if the reservoir is large enough or close to the sea, the estuarine and marine environment can also be affected. It is recommended that the flood and sediment transport requirements of the estuarine and marine environment be investigated.

- It has been established that a range of flows is important in forming and maintaining the river geomorphology, but the relative importance between freshets and major flood releases in terms of the sediment transport need to be investigated.

- More data are necessary on the sediment transport of fine sediments and non-cohesive – cohesive mixtures in order to be able to test the theory developed during this project on the critical conditions for mass erosion.

- In order to calibrate the proposed cohesive sediment transport equation for a wider range of sediment sizes, data on other types of cohesive sediments are necessary.

- The effect of consolidation and drying of fine sediments on the sediment transport behaviour should be investigated in greater detail.

Capacity Building

The following students worked on the project, their involvement contributing towards the following qualifications:

- I. Pollard (BEng)
- A. Liebenberg (BEng)
- K.J. Shelly (BEng)
- O.M.F. Mngambi (RND)
- T. Zitumano (Pentech student)
- J. S. Beck (MScEng)

The project team worked closely with the KwaZulu-Natal DWAF regional office to carry out fieldwork during flood releases at Pongolapoort Dam.

The methodology developed during this study has already been implemented at several DWAF studies:

- Sizing of flood release gate for the proposed Skuifraam Dam , Berg River (2001)
- Hydrodynamic flood routing on the Pongola River to design July 2002 flood release to limit flood damage in Mozambique.
- Thukela EFR study (June 2002)

Acknowledgements

The study team wishes to thank the South African Water Research Commission and the Department of Water Affairs and Forestry (DWAF) for sponsoring this research project.

DWAF played an instrumental role in the successful completion of this study and especially the fieldwork would not have been possible without the KwaZulu-Natal regional office's contribution.

Thanks are also due to Mr Chris Viljoen (HDTC) for kindly supplying all the information available about the Ash River upgrading to date.

Finally the Steering Committee members (listed below in no particular order) need to be commended for their role in steering this project from its start in 1999 to its successful completion in 2002:

Mr H. Maaren	Water Research Commission (Chairman)
Mr D.S. van der Merwe	Water Research Commission
Prof S.J. van Vuuren	University of Pretoria
Prof A. Rooseboom	University of Stellenbosch
Prof C.S James	University of the Witwatersrand
Prof K. Rowntree	Rhodes University
Dr C.A. Brown	Southern Waters
Dr N. Armitage	University of Cape Town
Mr P. Huizinga	CSIR
Mr L.E van Rheede van Oudtshoorn	BloemWater
Ms L. Fick	Department of Water Affairs and Forestry
Mr C. Ruiters	Department of Water Affairs and Forestry

Table of Contents

List of Figures

List of Tables

List of Symbols

Symbol	Description
$\frac{d\mathrm{v}}{dy}$	Velocity gradient (s^{-1})
$\left(\tau\frac{d\mathrm{v}}{dy}\right)_0$	Applied unit stream power at the bed (W/m)
ρgQS	Total input stream power (W/m)
α	Exponent of regime equation
β	Exponent of regime equation
γ	Exponent of regime equation
ρ	Specific density of water (kg/m^3)
κ	Von Kármán coefficient
ν	Kinematic viscosity (m^2/s)
γ	Specific weight of clear water (N/m^3)
τ	Bed shear stress (Pa)
τ_c	Critical shear stress in Lacey's bed load formula (kg/m^2)
ρ_d	Dry density of sediment (kg/m^3)
ρ_m	Specific density of sediment laden flow (kg/m^3)
γ_m	Specific weight of sediment-laden flow (N/m^3)
ν_m	Kinematic viscosity of sediment-laden flow (m^2/s)
ρ_s	Specific density of sediment (kg/m^3)
γ_s	Specific weight of sediment (N/m^3)
τ_v	Vane shear strength (kPa)
$\frac{\mathrm{v}S}{w}, \frac{\mathrm{v}_{cr}S}{w}$	Dimensionless unit stream power and critical unit stream power
A	Cross-sectional area (m^2)
A	Reading for VERIFLUX converter (A)
A	Cross-sectional area of return pipe (m^2)
a	Coefficient of regime equations
B	Top width (m)
B	Reading for VERIFLUX converter (m/s)

B_1	Average bankfull width before dam construction (m)
B_2	Average bankfull width after dam construction (m)
b	Coefficient of regime equations
b	River bed width (m)
C	Sediment concentration (mg/ℓ or %)
c	Coefficient of regime equations
C_b	Regression coefficient
C_d	Regression coefficient
C_t	Total sediment concentration (mg/ℓ or %)
C_d	Characteristic sediment coefficient in Lacey's bed load formula (m^3/kg/s)
C_v	Suspended sediment concentration (mg/ℓ or %)
d	Sediment particle size (mm or m)
D	Flow depth (m)
d_{50}	Median particle diameter (mm or m)
d_{84}, d_{90}	Sediment size for which 84% and 90%, respectively, of the material is finer (mm or m)
d_s	Sediment size (m)
Fr	Froude number
F_s	Side factor in *Blench* regime equation
g	Gravitational acceleration (m/s^2)
h_1, h_2	Flow depths at successive reference points 1 and 2 (m)
k_1, k_3	Coefficient of regime equations
k_s	Absolute roughness (m)
L	Distance between successive reference points (m)
L	Total length of reach (m)
L_i	Distance between successive cross-sections (m)
m	Parameter in exponents of *Julien and Wargadalam* regime equations
P	Wetted perimeter (m)
P	Percentage clay or clay and silt
p_i	Proportion of sediments in particle size range i
q_b	Bed load per unit width (m^2/s)
Q	Flow rate (m^3/s)
Q_2, Q_5, Q_{10},	Flood peak with recurrence interval of 2, 5, 10, 20 and 50 years, respectively

Q_{20}, Q_{50}	(m^3/s)
Q_{a1},Q_{a2}	Pre- and post-dam mean annual maximum flood peaks (m^3/s)
Q_{ad1}, Q_{ad2}	Pre- and post-dam Mean annual average daily flow (m^3/s)
Q_m	Average of annual 1-day highest average flows before dam construction (m^3/s)
Q_p	Arithmetic average of annual mean daily flows since dam construction (m^3/s)
Q_{p1}, Q_{p2}	Highest flood peaks for the pre- and post-dam periods (m^3/s)
Q_s	Sediment discharge (m^3/s)
R	Hydraulic radius (m)
S	Slope
s	Specific gravity of sediment
S_i	Bed slope between 2 successive cross-sections
S_o	Bed slope
S_w	Water surface slope
S_f	Energy slope
t	Time (h)
T	Temperature (°C)
U_*	Shear velocity (m/s)
v	Flow velocity (m/s)
v_1, v_2	Mean flow velocities at successive reference points 1 and 2 (m/s)
v_p	Flow velocity in return pipe (m/s)
vS, vS_{cr}	Unit stream power and critical unit stream power (m/s)
w	Particle settling velocity (m/s)
w_i	Sediment particle settling velocity of fraction i (m/s)
w_m	Particle settling velocity in sediment-laden flow (m/s)
w_s	Settling velocity of suspended sediments (m/s)
X	Longitudinal distance (m)
Y	Potential energy per unit weight above a certain datum (m)
z	Side slope of trapezoidal channel shape
z_1, z_2	Elevation above arbitrary datum at successive reference points 1 and 2 (m)

1. Introduction

The construction of a dam can drastically alter the flow regime and sediment load of the river downstream by altering flood peaks and durations, as well as by trapping large amounts of sediment. The imposed changes in the flow can lead to riverbed degradation directly downstream, as a result of very low sediment loads, as well as narrowing of river channels due to decreased transporting capacities further downstream. The increasing number and size of dams built during recent decades has drawn more attention to the impacts that dams can have, so much so that the World Commission on Dams (WCD, 2000a) has completed a worldwide study on dams. In South Africa there have also been some studies focusing on the impacts of river developments on a river system such as interbasin transfer schemes (Rowntree *et al.*, 2000). It has, however, become clear that there are still some issues to be addressed in order to gain a better understanding of the changes in the downstream river morphology that may occur as a result of dam developments.

When attempting to analyse the impacts of dams on the downstream river morphology, there are two fundamental questions that have to be answered:

- What sort of changes are to be expected, e.g. will the river become deeper or shallower and by how much?
- How do these changes come about, e.g. does the river become deeper because of a lack of released sediments, or narrower due to reduced flood peaks?

In order to answer these two questions the first step has to be to determine the factors that influence the channel morphology and the aspects of the river morphology that are likely to change. A study of existing literature offers some answers in that respect since numerous studies have dealt with these aspects.

This does, however, not resolve the question of the magnitude or direction of the changes that are to be expected. What is necessary is to be able to describe the channel geometry in terms of the factors that are likely to have a significant effect. For natural rivers so-called regime equations, which were either empirically or theoretically derived, were used in the past to describe the river channel geometry. A somewhat different approach is necessary for impacted rivers.

An important aspect of all the regime equations has always been the determination of the so-called dominant or effective discharge, responsible for maintaining or forming the river channel. The determination of the dominant or effective discharge is not only important for the regime equations but also plays a vital role in determining a controlled flow regime that will maintain a river in its natural or desired state. For South African conditions this aspect still needs consideration even though other researchers are also working on providing answers in that regard, e.g. Dollar *et al.* (2000).

Once these matters have been dealt with, the second part of the problem has to be addressed. The sediment transport characteristics of the downstream river channel play a vital role in this regard. Generally speaking degradation of the riverbed takes place close to the dam whereas further downstream aggradation is more common, since sediments are supplied by the tributaries, which cannot all be transported because of the lower sediment transport capacities due to the reduced flood peaks. The material that thus becomes deposited may consist of both coarse and fine fractions, including cohesive sediments. Fine materials, consisting of clay and silt fractions, display distinctly different erosion and deposition to non-cohesive sediments, due to the fact that the erosion resistance of fine particles is governed to a large degree by physical and chemical forces. While the entrainment and transport of non-cohesive sediments can already be described adequately, the entrainment and transport of clay and silt, as well as mixtures of cohesive and non-cohesive sediments has not been investigated adequately. Knowledge of the behaviour of fine sediments may also be useful for sediment flushing from reservoirs, since the reservoir deposits usually contain high percentages of clay and silt.

The materials found in the downstream river channel are not the only factors that determine why a river will change as it does. Other key factors are the flows released from the reservoir as well as the amount of sediment supplied by the downstream catchment. The regime equations mentioned above may give an indication of the magnitude and direction that changes in the river morphology may take, but they cannot describe whether a river will change in response to lower flood peaks or longer flow durations. One way in which to accurately determine the effect of a sequence of events is through numerical modelling. A model should take into consideration the effect of fine materials, changes in cross-sectional shape or slope along a river section and also the variability of flows. In this way the long-term impacts of dams can be studied and from the results assessments can be made about the required flood magnitude, duration and frequency.

1.1 Aims

The overall aim of the project is to investigate the impacts of dam developments on the downstream river morphology, specifically:

- The assessment of the changes in the downstream river morphology as a result of different dam development scenarios.
- The development of methods for predicting the downstream river channel geometry for South African conditions.
- An investigation into the effects of clay and silt on the sediment transport behaviour of sediments.
- The development of a methodology to determine required flood magnitudes, duration and frequency downstream of a dam, to maintain (or restore) the river morphology as close as possible to the natural (or desired) conditions, based on fundamental hydraulic principles of sediment transport. This would provide tools with which environmental flow requirements, controlling the river morphology, can be analysed.

1.2 Methodology

This report is structured as follows:

1. An overview of literature on the impacts of dams on downstream river morphology in South Africa and the rest of the world is given in **Chapter 2**.
2. Existing regime equations, as well as other tools that can be employed to determine the resulting equilibrium river channel geometry, are reviewed and regime equations for South African conditions are developed (**Chapter 3**). The concept of a dominant discharge is also explored.
3. The differences in behaviour between cohesive and non-cohesive sediments are investigated with the aid of flume studies and sediment transport equations are calibrated for fine and non-cohesive sediments (**Chapter 4**).
4. A one-dimensional hydrodynamic and morphological numerical model (MIKE 11) is utilized to investigate the impacts of dams by analysing several scenarios (**Chapter 5**) such as:
    - natural conditions,
    - various reservoir capacities and water yields,

- considering the incremental sediment yield downstream of the dam, and
- artificial flood releases.

5. The development of procedures/methodology for the assessment of required environmental floods downstream of dams (**Chapter 6**), taking into account the:
   - sediment yield and sediment load-discharge rating characteristics,
   - reservoir trap efficiency and various operational conditions,
   - sediment transport characteristics of fine and coarse sediments,
   - critical conditions for re-entrainment of sediments,
   - possibility of sediment sluicing through reservoirs, and
   - flood magnitude, duration, frequency and timing.

The regime equations that are explored in **Chapter 3** have been found useful in the past to give and indication of the impacts that a dam can have on the river morphology, by providing a final width, depth or even slope of the river. However, these do not give an indication of the temporal and spatial changes, which in turn affect the sediment balance in the river. For this reason numerical modelling (as described in **Chapter 5**) has been carried out, which incorporates some aspects of the regime theory, such as the reduction in river width as a result of dam development.

Before the numerical modelling could be carried out, however, it was important to look at some sediment transport processes first, in particular cohesive sediment transport characteristics (as described in **Chapter 4**). The reduction in streamflow, which generally occurs after a dam has been constructed, can lead to aggradation in the river, if considerable quantities of sediments are still supplied from the downstream catchments. Sometimes significant portions of this sediment consist of cohesive material, or at least mixtures of cohesive and non-cohesive sediments. Since the erosion and deposition behaviour of cohesive sediment differs significantly form non-cohesive sediments, it was important to investigate cohesive sediment transport in greater detail.

One- and semi-two-dimensional numerical modelling was carried out, incorporating the above-mentioned theories, in order to investigate the impacts of dams on the river morphology (in particular the sediment balance in the river), as well as to develop guidelines to limit these impacts.

2. Downstream Impacts of Dam Developments and Mitigating Measures

Kariba Reservoir on the Zambezi River, Zimbabwe/Zambia, has a surface area of about 5500 km^2 at full supply level and a full supply capacity of over 180 km^3. Gariep Reservoir on the Orange River, South Africa, has an original full supply capacity of 5950 million m^3. Considering the large sizes of these and most of the other dams built during the past 100 years, it is not surprising that they have major impacts on the rivers downstream. However, it is not only large reservoirs that bring about changes in the rivers, but even small structures can disturb an otherwise stable river. A river compensates for the imposed changes due to a dam by adjusting to a new quasi-stable form.

The closure of a dam has an immediate impact on the downstream river channel by changing the natural water discharge and sediment load. The magnitude of this impact depends on various factors:

- Storage capacity of the impoundment in relation to mean annual runoff (MAR):
  Reservoirs with large storage capacities relative to the MAR, typically absorb most of the smaller floods, attenuate larger floods and trap most of the sediments that enter the reservoir (Chien, 1985). Tarbela Reservoir on the River Indus, Pakistan, has a relatively small storage in comparison to flood volume, and thus has little impact on floods with return periods greater than 10 years. Lake Nasser behind the High Aswan Dam on the other hand has such a large storage capacity in relation to the flood volume that even the largest floods are partially absorbed (Acreman, 2000).
- Operational procedure of the dam:
  Typically dams are built for one of the following reasons: storage, hydropower, irrigation or flood detention. Many dams are also built for multiple purposes. The impacts of each type of operation are different. While a storage reservoir may release almost no water unless its storage capacity has been exceeded, a hydropower dam may release a relatively constant high flow for certain times of the day.
- Bed materials:
  Coarser bed materials like cobbles and boulders and even gravel reduce the degradation below a dam to some degree, whereas sand bed rivers are more susceptible to degradation or erosion.

- Outlet structures:

  If a dam has the necessary outlet structures, sediment can be released from a reservoir, through sluicing incoming sediments or flushing deposited sediments. The effect of the released sediment on the river channel of course depends on the operation of the outlet works.

- Sediment load:

  A dam will have a much greater impact on a river with a high natural sediment load than on a river with a low natural sediment load, because the former will experience a much greater reduction in sediment load than the latter. Also the sediments supplied by tributaries downstream of a dam can have a major effect on a river in that the flow can become oversaturated if the sediment transport capacity of the river is reduced.

There was a dramatic increase in the number and size of the dams being built after the Second World War, peaking during the 1970's worldwide (**Figure 2.1**). In South Africa the trend was similar (**Figure 2.2**, based on a list of surveyed dams obtained from the Department of Water Affairs and Forestry). This increase in both size and capacity of reservoirs has made the impacts of dams even more obvious. Numerous studies (e.g. Williams and Wolman (1984), Chien (1985), and Hadley and Emmett (1998)) have been carried out that describe both the impacts and their causes. The primary impacts are the attenuation of flood peaks and the trapping of sediments in reservoirs, leading to changes in channel cross-section, bed particle size, channel pattern and roughness.

2.1 Changes in Discharge

The magnitude and duration of the flows released vary from one dam to another, because of the different purposes for which dams are built. Due to the relatively large storage capacities of most reservoirs, floods are either absorbed or at least attenuated and only very large floods move through a reservoir relatively unchanged. The result is a decrease in the natural variability of streamflow, as is the case below Gariep Dam on the Orange River, South Africa (WCD, 2000b). **Figures 2.1.1** and **2.1.2** give an indication of what the possible impact of the proposed Jana Dam (DWAF Website) on the Thukela River, South Africa, could be on the streamflow at the dam, once the reservoir is fully utilised, without any environmental flood releases.

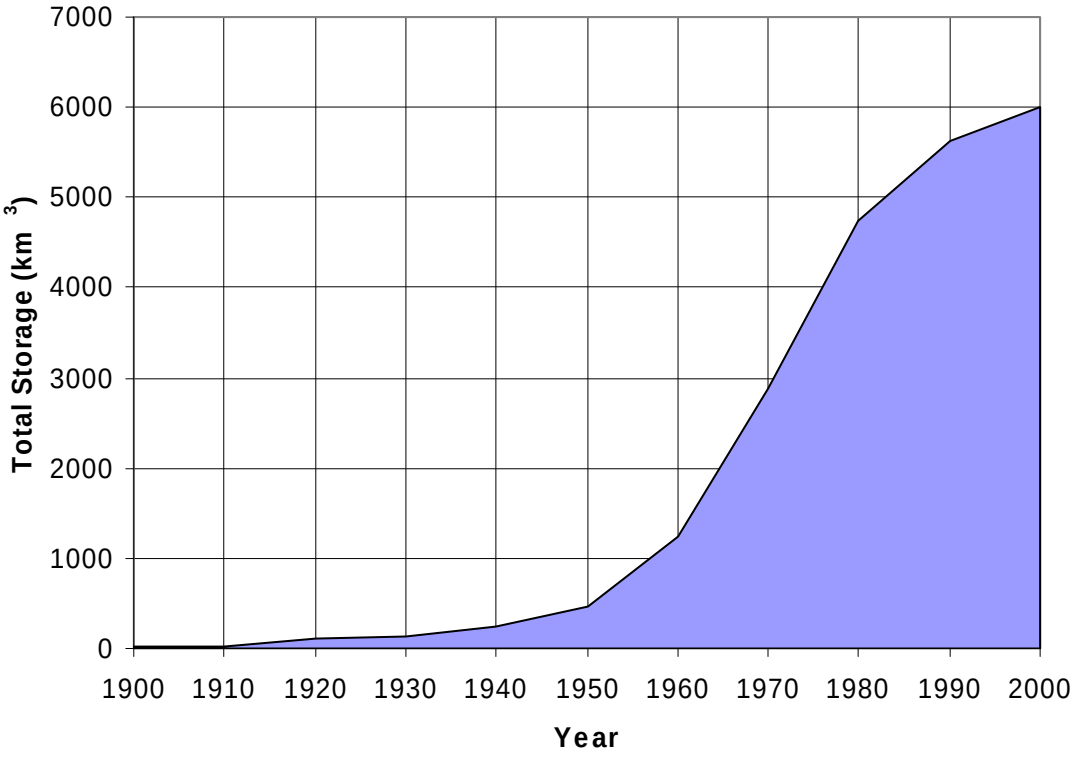

Figure 2.1 Cumulative storage capacity of dams worldwide (dams > 15 m) (White, 2000)

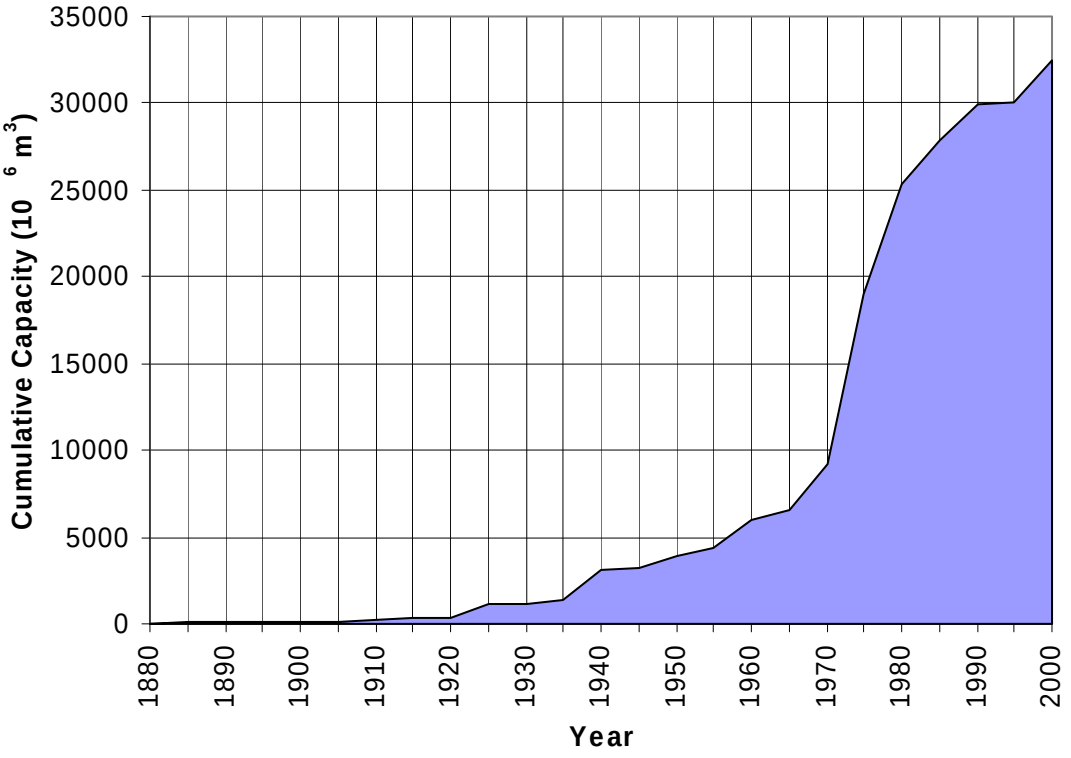

Figure 2.2 Cumulative storage capacity of dams in South Africa

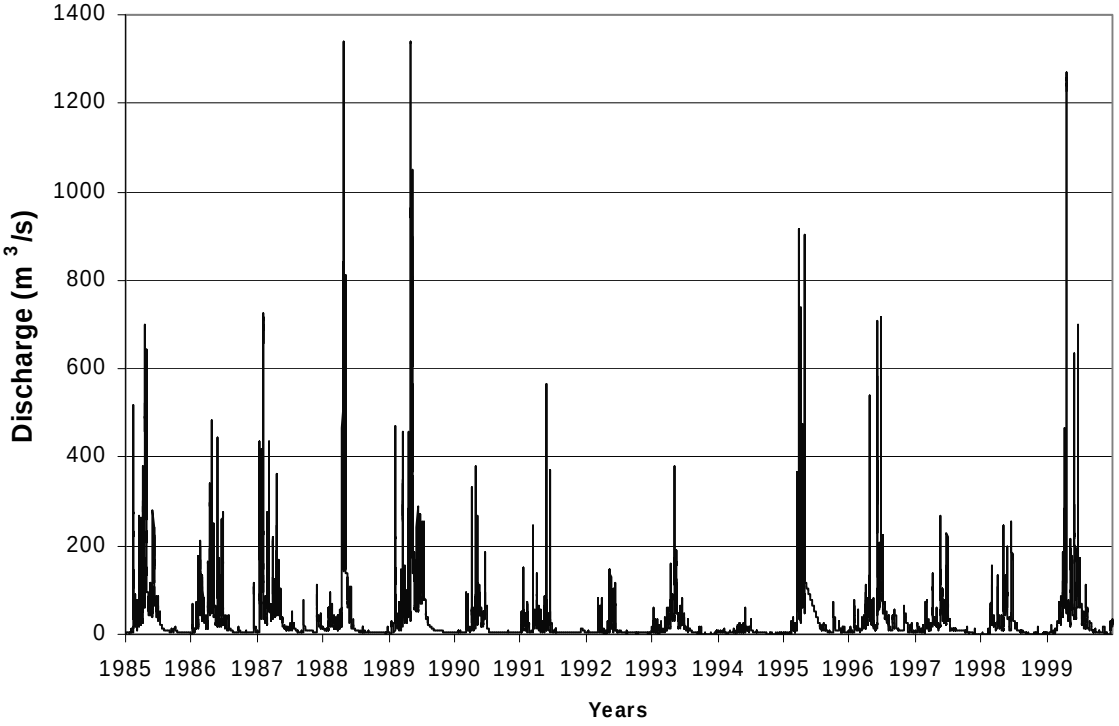

Figure 2.1.1 Pre-dam streamflow (hourly data) at proposed Jana Dam site, Thukela River, South Africa

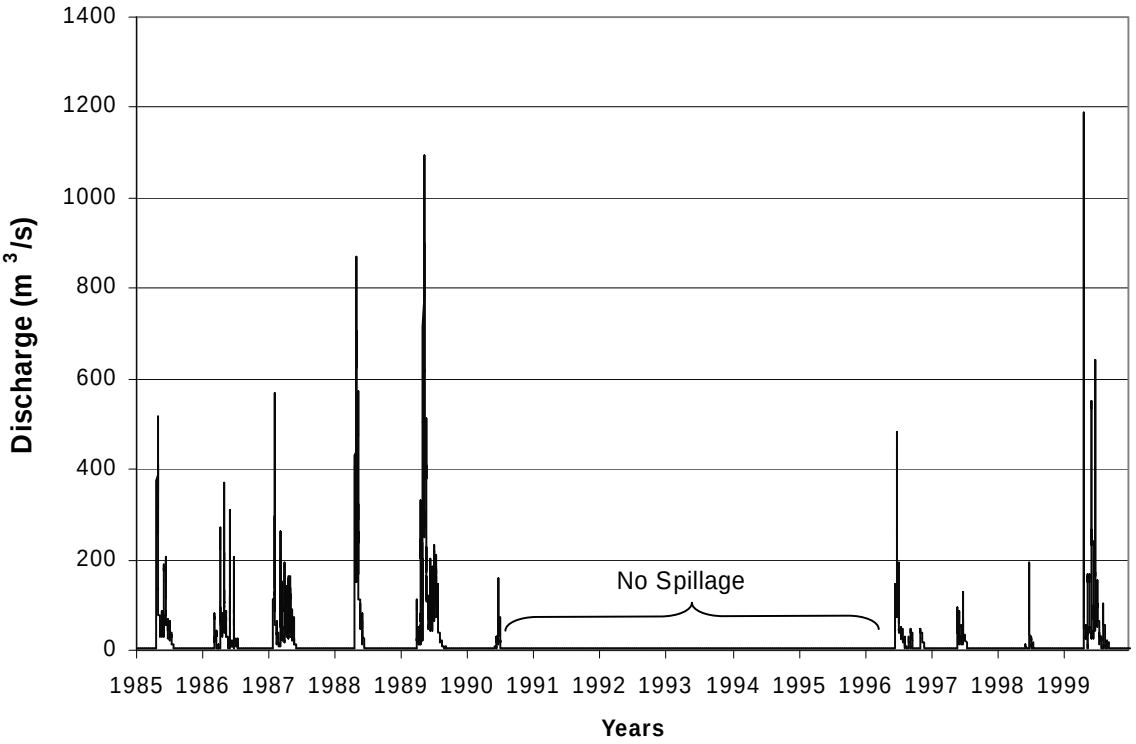

Figure 2.1.2 Post-dam streamflow (hourly data) at proposed Jana Dam site, Thukela River, South Africa

Generally the low flow duration increases and the magnitude of the flood peaks decreases. Gunnison Gorge on the Gunnison River, USA, is downstream of four reservoirs and an interbasin transfer. The 1:10-year flood peak has decreased by 53% from 422 m^3/s to 198 m^3/s while the low flow duration increased threefold according to Hadley and Emmett (1998). Andrews (1986) reported that no flows larger than 5000 ft^3/s (about 142 m^3/s) have been released from Flaming Gorge Reservoir on the Green River, USA, while the mean annual flow has not changed.

In flood detention reservoirs the low and medium flows are usually allowed to pass through the reservoir with no or limited damming, but the larger floods are greatly attenuated. According to Chien (1985), Guanting Reservoir on the Yellow River, China, has reduced the peaks by 78% from 3700 m^3/s to 800 m^3/s. Sanmenxia Reservoir, also on the Yellow River, has been operated for flood detention, with sediment sluicing, and storage since 1974, after being used solely for storage from the time it was built in 1960 to 1964. The flood peaks have been reduced from 12400 m^3/s to 4870 m^3/s, while the duration of the mean daily flows (1000 – 3000 m^3/s) has increased from 130 days a year to 204 days a year.

Reservoirs operated for irrigation decrease flows during the wet season to store water, and increase flows during the dry season, thereby maintaining relatively constant low flows, usually higher than pre-dam conditions. Hydropower dams on the other hand possess highly variable release patterns, with relatively large flows being released during certain times of the day and no or low flows during the rest, although Kariba Reservoir on the Zambezi River, Zimbabwe/Zambia, manages to release a minimum flow of 283 m^3/s (SI and CESDC, 2000), which is rather the exception. The effect of hydropower generation at Glen Canyon Dam, USA, on the Colorado River streamflow can be seen in **Figure 2.1.3**. Construction work officially began on Glen Canyon Dam in 1956 and turbines and generators were installed between 1963 and 1966 (Glen Canyon Dam Website, 2002).

2.2 Changes in Sediment Load

Together with the reduction in flood peaks a drastic decrease in the sediment volumes released from a reservoir is experienced, unless the dam is equipped to sluice or flush

sediments through the reservoir. Williams and Wolman (1984) reported that the trap efficiency of large reservoirs is commonly greater than 99% in the USA.

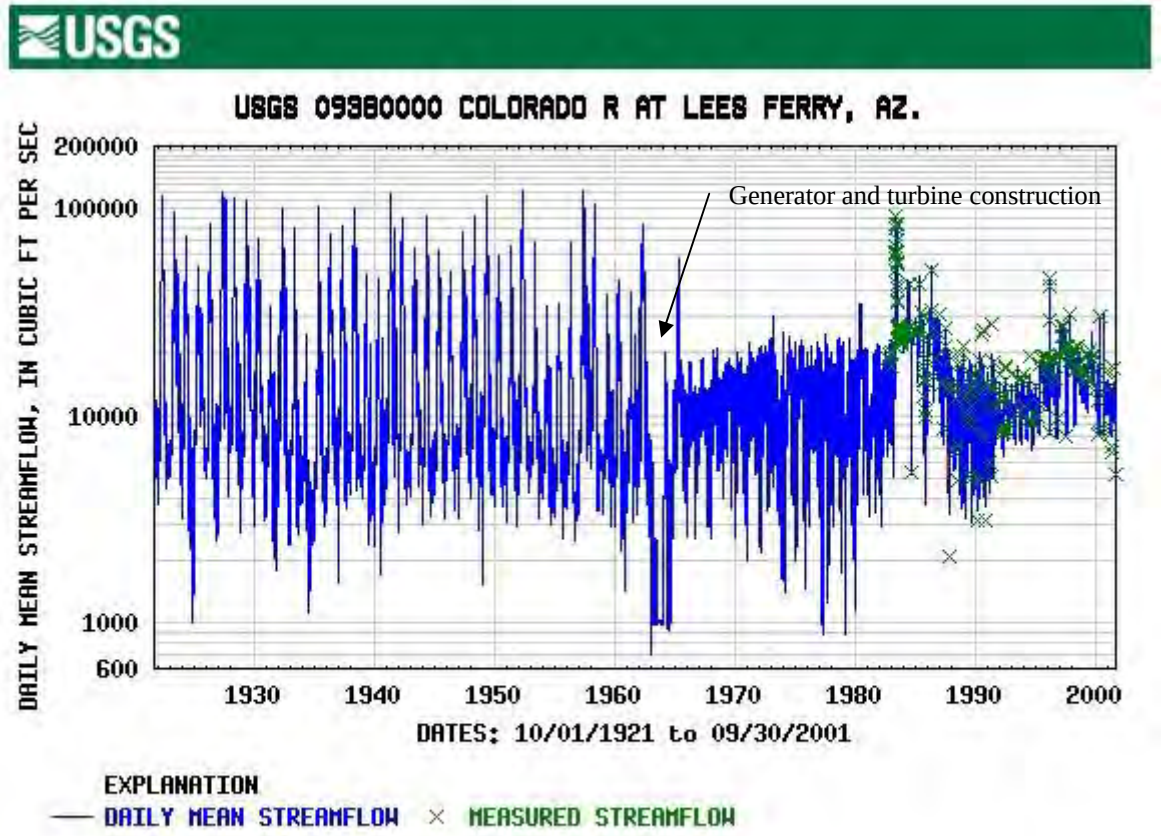

Figure 2.1.3 Colorado River streamflow downstream of Glen Canyon Dam, USA, before and after dam construction (USGS, 2002a)

Glen Canyon Reservoir (**Figure 2.2.1**) on the Colorado River has reduced the average annual suspended sediment load by 87% from 126 million tons/a to 17 million tons/a (Williams and Wolman, 1984). The downstream station at which the measurements were taken is 150 km away from the dam, which shows that the dam's influence extends far downstream. The impact of a dam on the sediment load however decreases with distance from the dam, as can be seen downstream of Canton Dam on the North Canadian River, USA (**Figure 2.2.2**). The control station included in the figure indicates that the upstream sediment load has remained unchanged, whereas the downstream reach has experienced a considerable reduction in sediment load. Also below Flaming Gorge Dam on the Green River, USA, tributaries have replenished the sediment supply within 68 miles downstream according to Andrews (1986).

Figure 2.2.1 Glen Canyon Dam with Lake Powell in the background

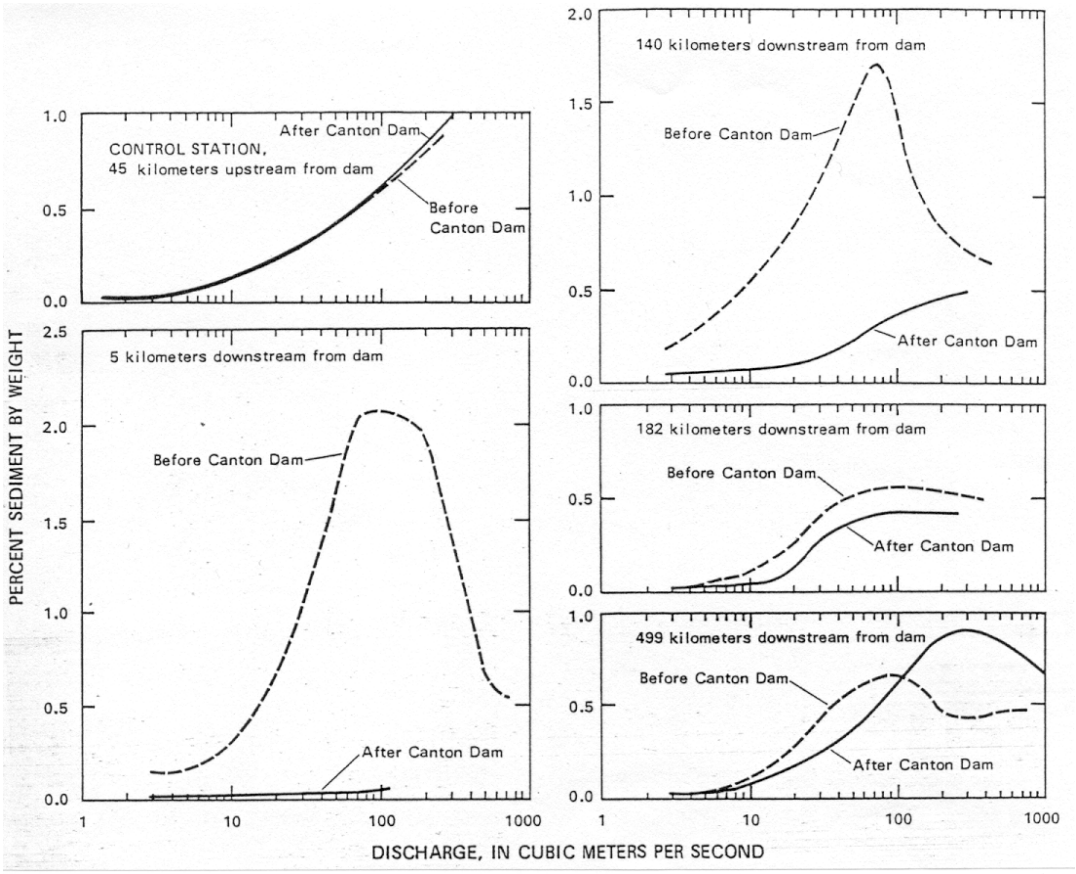

Figure 2.2.2 Suspended sediment loads at successive downstream stations before and after the closure of Canton Dam on the North Canadian River, USA (Williams and Wolman, 1984)

Not only are sediments trapped in a reservoir, but the transport capacity in the downstream channel also decreases due to the attenuated flood peaks and is diminished by coarsening of the bed and flatter bed slopes associated with bed degradation. Downstream of Danjankou Dam on the Han River, China, the sediment concentration at flows of 3000 m^3/s was reduced by 60.4% (Chien, 1985) and downstream of the High Aswan Dam on the Nile, the suspended sediment concentration typically measured during August decreased from 3500 mg/ℓ to 100 mg/ℓ (Schumm and Galay, 1994).

2.3 Changes in Channel Depth

The changes in flow regime and sediment load have a dramatic effect on the channel morphology, since these are two of the controlling factors. Due to the large amounts of clear water released from most reservoirs the most common response of the river channel downstream is degradation. After the completion of Sanmenxia Dam, the average bed degradation was between 0.6 m and 1.3 m during the first four years of storage operation (Chien, 1985). Williams and Wolman (1984) reported much greater impacts below Hoover Dam on the Colorado River, USA, where the maximum degradation 13 years after the completion of the dam was 7.5 m. In most cases the maximum degradation will occur directly below or near the dam, which is the case at the High Aswan Dam with a maximum degradation of 0.7 m (Schumm and Galay, 1994), whereas at Glen Canyon Dam a 7.25 m bed level lowering was measured 16 km downstream of the dam (Williams and Wolman, 1984). **Figure 2.3.1** shows the variation in bed degradation, nine years after the completion of the dam, with distance downstream of the dam.

The amount of degradation will depend on local controls such as bedrock or the development of an armour layer. Armouring occurs when fine materials in the bed are eroded, leaving the coarser fractions behind. These create a protective layer that limits erosion of the underlying particles. Likewise flattening of the channel slope will decrease the flow competence, which will control degradation.

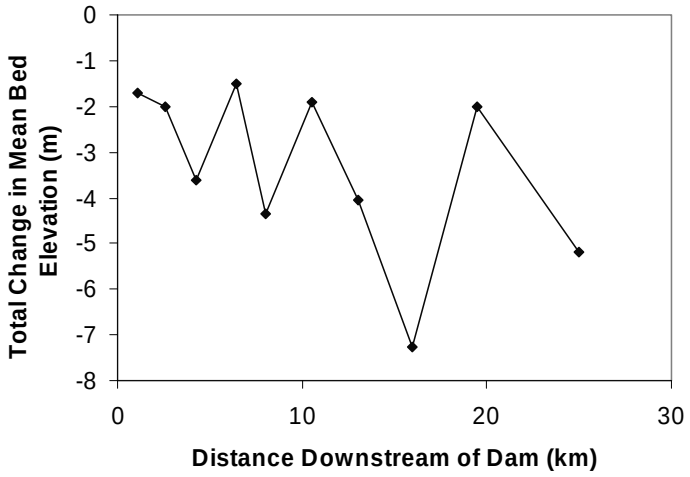

Figure 2.3.1 Variation of bed degradation (nine years after closure of the dam) downstream of Glen Canyon Dam, USA (Williams and Wolman, 1984)

The Lesotho Highlands Water Project (LHWP) tunnel transfers water from Lesotho to South Africa. En route electricity is generated in Lesotho before the water is discharged, via the Delivery Tunnel, into the Ash River, South Africa. The hydropower station was constructed only after the water transfer system had been operational for some time and once the hydropower station was operated at peak discharge (with discharges up to a maximum of 50 m^3/s (equivalent to a 1:10-year flood at the outfall) for a few hours each day), problems became apparent within a year. The variable discharge, leading to alternate wetting and drying of the riverbanks, caused substantial degradation of the riverbed (3 to 5 m) and slumping of the riverbanks, changing the river from a small stream to a deep, wide river (see **Figures 2.3.2** to **2.3.5**). **Figure 2.3.2** shows the observed bed degradation that took place within two years, with as much as 6 m scour in places. Also indicated in the figure are the simulated and estimated bed profiles with a proposed weir that is supposed to limit the erosion. The proposed weir will cause local deposition just upstream, but further upstream the erosion will still take place, unless limited by local natural controls.

Fortunately measures were taken fairly quickly and in 2001 a flood attenuation dam was built just downstream of the tunnel outlet (**Figure 2.3.6**), reducing the water level fluctuations to about 300 mm and dissipating much of the excess energy. As a result the riverbanks have flattened to some degree and vegetation has had a chance to establish itself on the riverbanks (**Figure 2.3.7**), thereby stabilising the banks. The bed slope of the river has gradually become flatter again by utilising natural and man-made controls on the river.

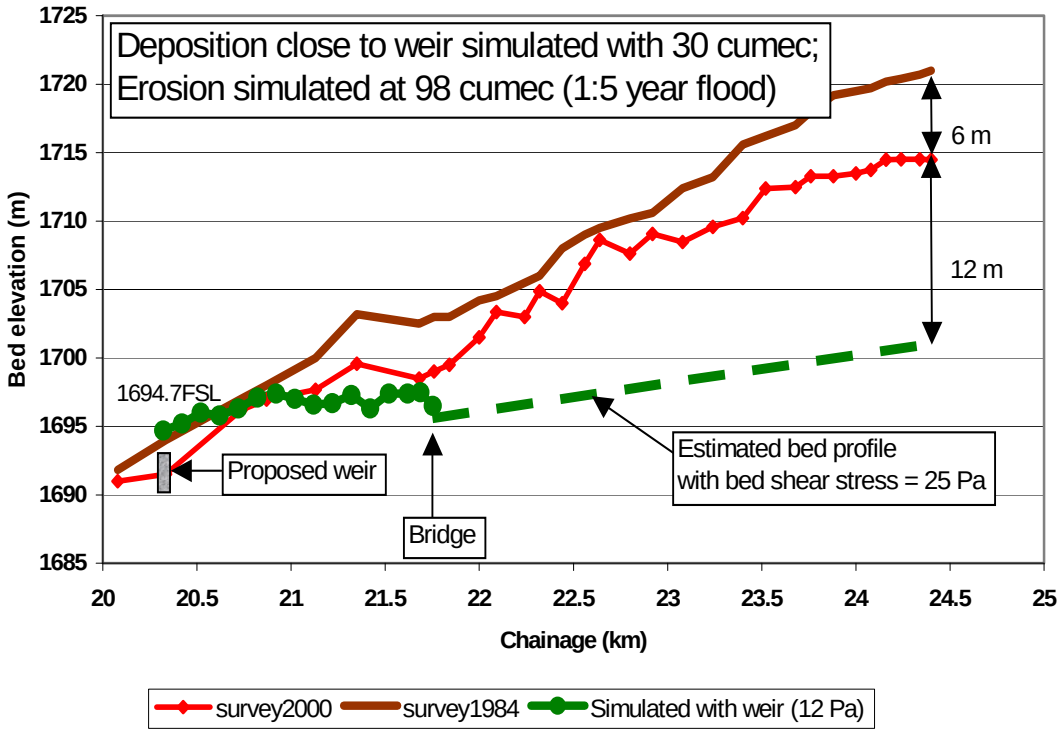

Figure 2.3.2 Ash River longitudinal profile

(at site 26, with site 1 at the tunnel outfall and site 87 at Saulspoort Dam)

Figure 2.3.3 Ash River (site 20) in 1991 (HTDC, 1999)

Figure 2.3.4 Ash River (site 20) in 1997 (HDTC, 1999)

Figure 2.3.5 Ash River bed degradation (HDTC, 2000)

Figure 2.3.6 Flow attenuation dam (site 7) (HDTC, 2002)

Figure 2.3.7 Vegetation established on riverbanks (site 79) (HDTC, 2000)

Rutherford (2000) reported some scour below Keepit Dam on Dumaresq Creek, Australia, but generally scour below dams has been limited in Australia either by the exposure of bedrock or by armouring, which occurred below Glenbawn Dam, Hunter River, and Eildon Dam on the Goulburn River. Another reason for the limited amount of erosion below Australian dams is the naturally low sediment yield of the rivers, so that channels may already be adjusted to low sediment transport rates (Rutherford, 2000).

On the other hand when a certain amount of sediment is released from a reservoir the river experiences aggradation. Naodehai Dam on the Liu River, China, was built for flood detention where most of the sediment is released with the lower flows after a flood has passed. The sediment carrying capacity of the flows is exceeded by the added sediments and thus deposits in the river channel. This resulted in the bed being raised by 1.5 m over a period of 10 years (Chien, 1985). Chien also reported that the maximum aggradation occurred during the flood detention phase of Sanmenxia Reservoir.

Aggradation can also occur due to very low flows, which take place when very little water is released from a reservoir or the releases are depleted by extractions for irrigation for example. Williams and Wolman (1984) cite the Elephant Butte Dam on the Rio Grande, USA, where the decreased flows and sediment contributed by tributaries have allowed the riverbed to rise almost to the same height as the surrounding lands.

2.4 Changes in Channel Width

Unlike the changes in channel depth, which are generally dependent on the discharge, sediment load and sediment characteristics as well as local bed controls, the changes in width are also a function of the bank materials and vegetation. Cohesive banks retard erosion to some degree and an increase in vegetation adds to the stability of the banks as well as trapping of sediments. Reduced sediment loads and longer flow durations on the other hand result in widening of the channel, especially when accompanied by an increase in depth, which leads to bank undercutting and subsequent bank collapse (Williams and Wolman, 1984).

Generally a river channel widens when the channel experiences regular dry and wet periods, characteristic of hydropower dams. This could be a result of bank instability due to alternate

wetting and drying of the riverbanks. Garrison Dam on the Missouri River, USA, was built for flood control and hydropower in 1953. After 23 years the maximum width increase was 625 m (from 525 m to 1150 m) 47 km downstream of the dam. In contrast a river can become narrower when it carries only low flows for long periods. During this time vegetation can encroach onto the river channel. The low flows rarely manage to reach the flood plains and even then are not competent enough to remove the established vegetation. This effectively reduces the channel width. Channel widening has been reported by Rutherford (2000) for several rivers in Australia including the Upper Murray and Swampy Plains Rivers. The channel widening is a result of consistent regulated releases that increase the duration of the near-bankfull flows.

Channel contraction usually occurs on rivers where the flows are low or are cut off completely for most of the time. Jemez Canyon on the Jemez River, USA, was built for flood and sediment control and as a result 1.6 km downstream of the dam the channel width was reduced by 250 m from 270 m to only 20 m (Williams and Wolman, 1984). Parangana Dam on the Mersey River, Australia, diverts the water and as a result the sediment delivered from the tributaries accumulates in the channel and native vegetation encroaches on the river channel. Rutherford (2000) also reported channel narrowing below several other dams in Australia, including Windamere Dam, on the Cudgegong River, and Jindabyne Dam on the Snowy River. Channel contraction can also be seen below Manapouri Lake on the Waiau River, New Zealand (Brierly and Fitchett, 2000). The Manapouri Power Scheme reduced the mean flow by 75%, resulting in a decrease in channel width from 250 m to 175 m.

The two examples from Garrison Dam and Jemez Canyon also show that the maximum change does not occur directly below a dam. In fact there seems to be no trend in the magnitude of the change in width downstream of dams.

Table 2.4.1 lists some South Africa's rivers that have been affected by dams. Generally channel contraction has occurred.

Chelmsford Dam on the Ngagane River, South Africa, was built in 1961 and raised during the 1980's, so that it is now a 2 MAR reservoir. Because of this large storage capacity the annual, 1:2-year and 1:5-year floods are all significantly reduced, with the 1:2-year flood decreasing from 30 m^3/s to 15 m^3/s since 1961 (based on statistical analysis). Aerial photographs from

1944 have been compared with orthophotos of the 1990's, which show in many places that the river has narrowed over the first 10 km downstream of the dam (**Figure 2.4.1**).

Table 2.4.1 River width changes in South Africa

Dam	River	Pre-dam width (m)	Post-dam width (m)	% Change
Erfenis	Groot Vet	24	26	+8.3
Roodeplaat	Pienaars	26	15	-42
Bloemhof	Vaal	92	82	-11
Allemanskraal	Sand	49	21	-57
Krugersdrift	Modder	32	24	-25
Spioenkop	Tugela	53	36	-32
Albertfalls	Mgeni	32	28	-13
Theewaterskloof	Riviersonderend	37	33	-11
Glen Alpine	Mogalakwena	36	24	-33
Gamkapoort	Gamka	67	55	-18
Gariep	Orange	269	255	-5

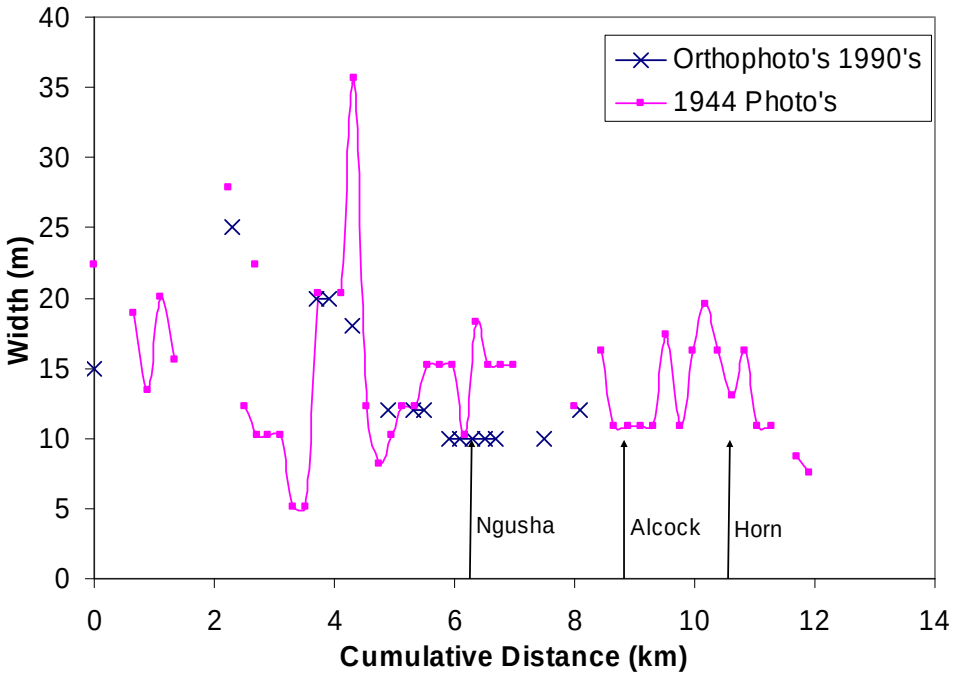

Figure 2.4.1 Ngagane River width changes downstream of Chelmsford Dam, South Africa

Pongolapoort Dam on the Pongola River was used as a case study in this project, and the changes in width were determined from contour maps compiled before the dam was built in 1973, and 1:15 000 aerial photographs from 1996. Of the 158 cross-sections analysed, 90% have narrowed and only 10% have widened. **Figure 2.4.2** shows the difference in the widths. On average the Pongola River has narrowed by 35% over the 80 km analysed. From the figure it can also be seen that the greatest changes have taken place close to the dam, with a 50% reduction in width over the first 20 km. The width has remained almost unchanged at a section close to the Lubambo tributary.

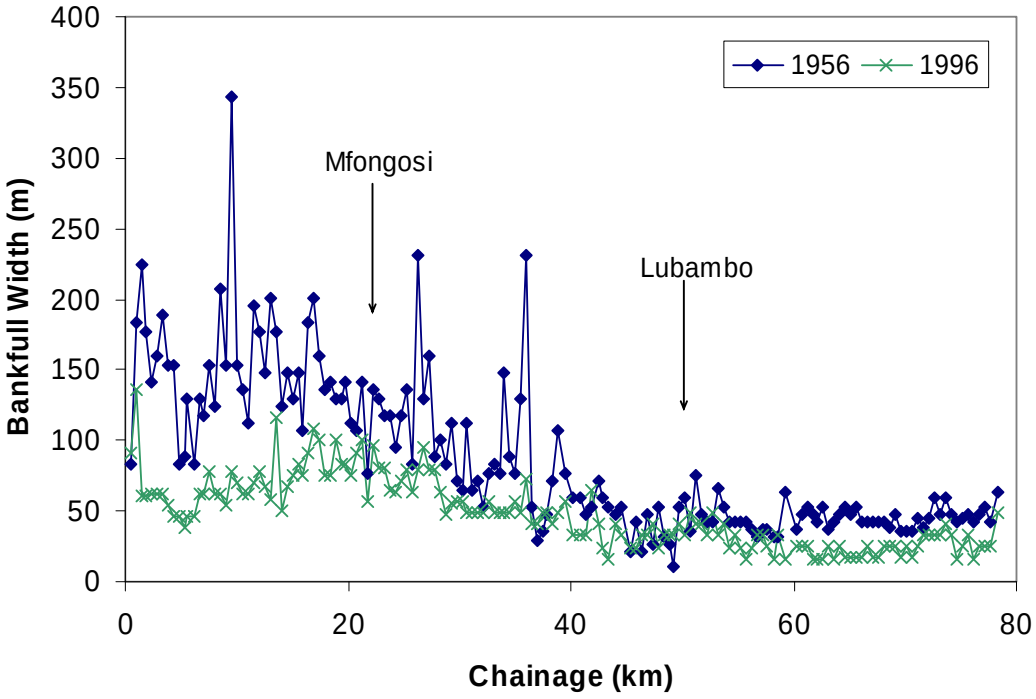

Figure 2.4.2 Changes in channel width of the Pongola River between 1956 and 1996 downstream of Pongolapoort Dam, South Africa (position of tributaries indicated)

2.5 Changes in Bed Material

Due to the decrease in magnitude and frequency of the high flows caused by a reservoir, the released flows are unable to transport the same amount and size of particles as before the dam was built. On the other hand the water released from a reservoir is usually clear and the flows are therefore able to entrain fine materials from the riverbed, while the coarser fractions in the bed are left behind. The relatively clear water releases can also be responsible for removing

complete surface layers from the riverbed if they are composed of finer materials and thereby expose coarser layers.

Downstream of Hoover Dam on the Colorado River, USA, the median bed-particle diameter (d_{50}) increased from 0.2 mm to about 80 mm within seven years after closure of the dam (Williams and Wolman, 1984). Guanting Reservoir has had a similar but less dramatic effect on the bed material of the river. The median particle diameter d_{50} increased from 0.4 mm to about 7 mm (Chien, 1985). In the case of Hoover Dam the substantial increase in d_{50} was a result of the exposure of a layer of gravel, while the released flows downstream of Guanting Dam were not large enough to transport sizes greater than 5 mm. In the case of Glen Canyon Dam, not only was the annual fine sediment supply considerably reduced but also the seasonal pattern of storage and erosion (Topping *et al,* 2000)**.** The result is that newly input sand will only be in storage for about two months, unlike the nine months that it was stored on average before the dam was built.

Changes in mean particle size start taking place immediately after completion of a dam, but will reduce with time, because the availability of the fine materials decreases. **Figure 2.5.1** shows the variation in mean particle diameter with time after dam closure below Parker Dam on the Colorado River, USA. The stabilization could have been the result of fine sediment input from tributaries or the uncovering of fine materials through erosion (Williams and Wolman, 1984).

The coarsening of the bed decreases with distance from a dam. This could be because further downstream tributaries again supply a certain amount of finer sediments, which could be deposited in the river channel. Another reason could be the decrease in bed degradation, which means that the likelihood of uncovering coarser materials is lower. **Figure 2.5.2** shows this trend for Pongolapoort Dam, where d_{50} decreases from 1.7 mm to 0.17 mm over a distance of 60 km. Particle sizes were even bigger nearer the dam, with exposed bedrock at the dam. The mean particle diameter of 0.18 mm before the dam was built was estimated from particle size distributions of samples taken upstream of the dam (Kovacs *et al.*, 1985), such as that shown in **Figure 2.5.2**.

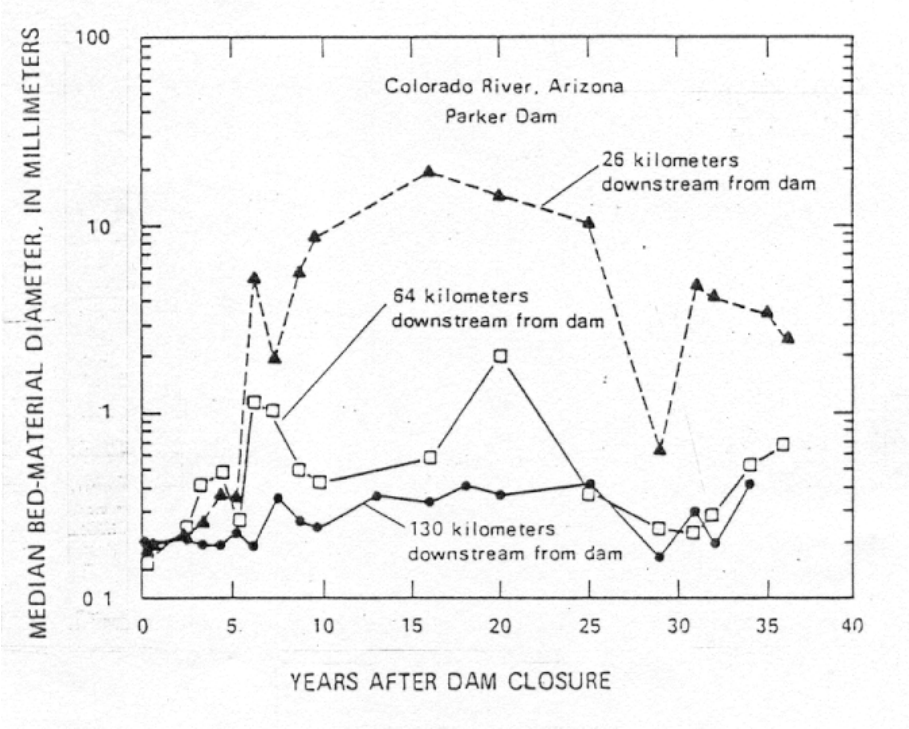

Figure 2.5.1 Variation of d_{50} downstream of Parker Dam, USA (Williams and Wolman, 1984)

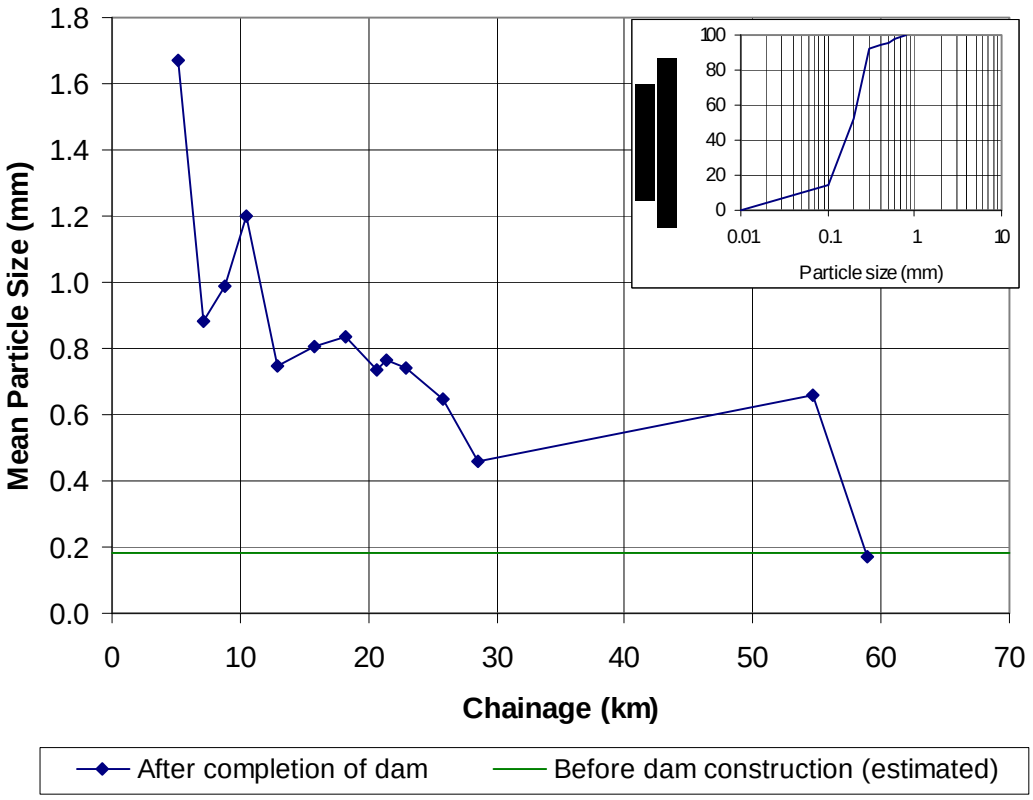

Figure 2.5.2 Variation of d_{50} downstream of Pongolapoort Dam, South Africa

As mentioned above, Sanmenxia Reservoir has had different modes of operation and the effect on the mean particle diameter is shown in **Figure 2.5.3**. During the flood detention phases muddy water was released after the floods had passed through the reservoir, whereas clear water was released during the storage periods. The reversal in trend was immediate, and the mean particle diameter remained relatively constant between 1964 and 1972.

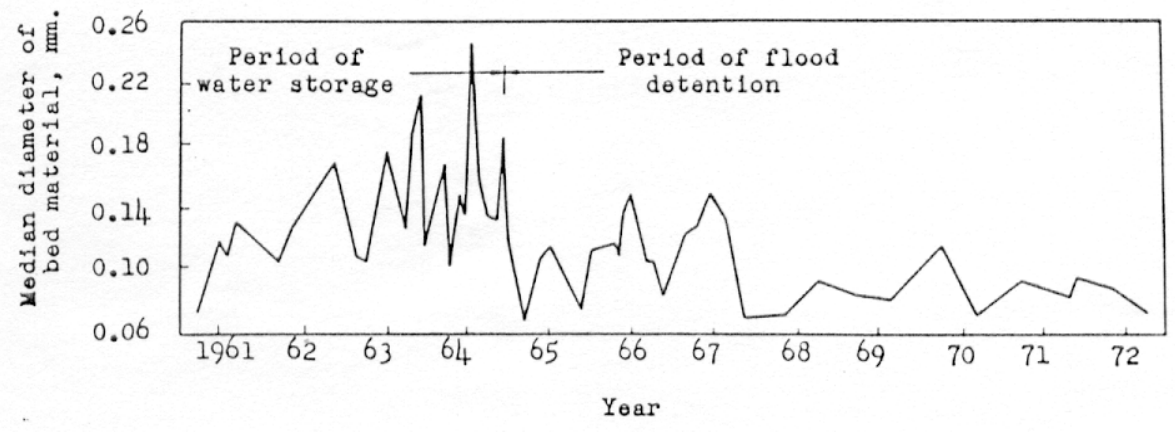

Figure 2.5.3 Variation of d_{50} downstream of Sanmenxia Dam, China, with different modes of operation (Chien, 1985)

Coarsening of the bed leads to an increase in roughness and a subsequent decrease in the transport capacity of the river. Chien (1985) reported that an increase in the mean particle diameter from 0.1 mm to 0.13 mm could reduce the transport capacity by 65%. Development of an armour layer is also important, because it controls degradation. On the Red River downstream of Dennison Dam, USA, 30 to 50% gravel cover limits degradation (Williams and Wolman, 1984). Schumm and Galay (1994) also reported that the Nile River has not degraded as much as expected downstream of the High Aswan Dam because of the coarse material being introduced by wadis along its length.

2.6 Changes in Slope and Channel Pattern

A reduced sediment load in a river channel downstream of a dam is associated with a decrease in transport capacity. This can be achieved by either increasing the bed roughness or by decreasing the channel slope. Flattening of the slope is usually only minor because it is easier to decrease the transport capacity by coarsening of the riverbed than by changing the slope (Chien, 1985). Large adjustments of the slope are difficult to achieve because the

affected reach is usually very long and degradation would have to be considerable. In many cases the degree of degradation is also limited by the presence of bedrock, which is generally present below dam walls. In many cases there might therefore be no noticeable change in slope over a long reach, but on most rivers there could be small changes over shorter distances. On the other hand bed slope changes can also occur as a result of an increase in sinuosity (Williams and Wolman, 1984).

The Yong-ding River downstream of Guanting Dam shows virtually no change in slope over a 60 km distance. Six years after closure the bed was lowered by the same distance over the full distance (Chien, 1985). The same trend was observed downstream of the High Aswan Dam (Schumm and Galay, 1994), unlike the Colorado River below Glen Canyon Dam where the slope has decreased slightly within three years after the dam was built, and after that increased considerably as shown in **Figure 2.6.1**.

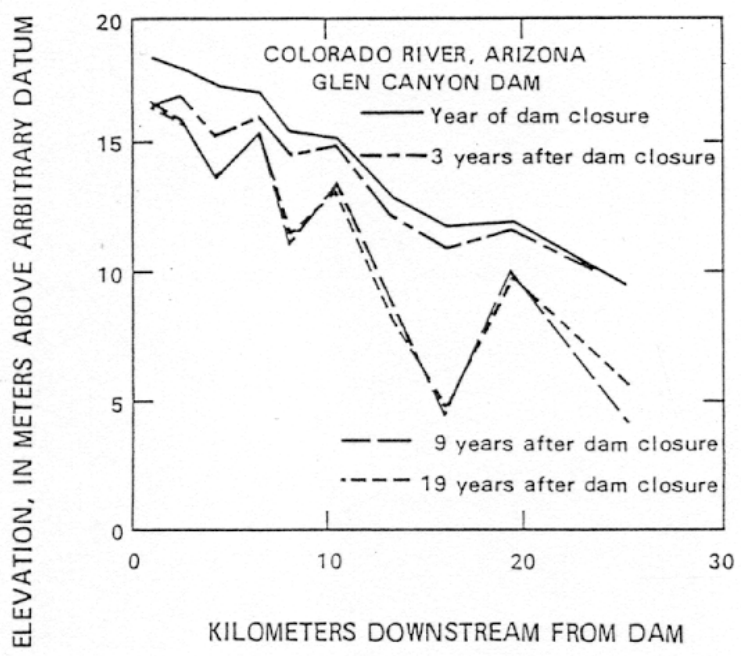

Figure 2.6.1 Changes in slope of the Colorado River below Glen Canyon Dam, USA (Williams and Wolman, 1984)

Since the bed profile downstream of a dam is dependent on factors like variations in bed material, water discharge, local controls and tributary contributions, the changes in slope along a certain reach are generally highly variable. This variability is evident downstream of

Fort Randall Dam, Missouri River, where aggradation, degradation and no change occurred from one cross-section to another (Williams and Wolman, 1984).

A change in slope can be accompanied by a change in channel pattern. Leopold and Wolman (1957) have pointed out that the kind of channel pattern, which a river follows, depends amongst others on the channel slope. Braided rivers generally occur on steeper slopes than meandering rivers. As the river may adjust its slope in response to the construction of a dam, there may occur a corresponding change from braided to meandering or vice versa.

Chien (1985) reported that the river channel downstream of Naodehai Dam has become even more braided after the dam came into operation, while the effect of Sanmenxia Reservoir was a reduction in braiding during the impoundment phase due to severe degradation of the river bed (Zhou and Pan, 1994). The effect of the Lake Nasser on the relatively straight Nile River has not occurred as rapidly as for the two abovementioned examples, but Schumm and Galay (1994) reported that the thalweg has begun to show meandering tendencies over short reaches.

2.7 Changes in Vegetation

The reduced flows downstream of a dam will generally also reduce the frequency of overbank flooding, but at the same time the main channel can experience longer periods of low lows. The fact that the main channel carries water for longer periods encourages vegetation to grow closer to the channel. The reduced overbank flooding means that there is less overbank scouring and the vegetation will therefore develop a stronger hold.

The increased vegetation can block part of the river channel and thereby reduce the flow area and also trap sediments, which leads to aggradation of the bed. The vegetation can also increase bank stability due to the binding and protective effects of the vegetation (Williams and Wolman, 1984).

According to Schumm and Galay (1994) the bank erosion of the Nile River has in part been controlled by the growth of natural vegetation. The same was reported by Hadley and Emmett (1998) for Bear Creek, USA, downstream of Bear Creek Lake. The width increased only by 0.5 m over a period of 15 years, which they accredited to the growth of woody vegetation.

The increase in vegetation on the banks and floodplains leads to an increase in hydraulic roughness. This can result in higher flood levels.

2.8 Affected Distance

The river reach affected by a dam increases with time, until the river has adjusted to the new flow and sediment regime. The length of the reach affected by a dam depends on several factors. The location and number of major tributaries has a significant effect, as they are essential in replenishing both the sediment and water discharge, and the type of material they transport is also important. Andrews (1986) has reported for the Green River below Flaming Gorge Dam that tributaries have replenished the sediment supply within 68 miles (about 109 km).

Downstream base-level controls such as another reservoir or a weir can stop the progression of erosion, as can a reduction in transport capacity (either by a reduction in the slope or through coarsening of the bed material). All of these factors make it difficult to predict the exact extent of the affected reach. In the case of the Ash River (**Section 2.3**) only 15 km were affected by hydropower generation, partly as a result of the presence of a reservoir (Saulspoort Dam) 15 km downstream of the tunnel outlet. However, there were indications that just upstream of the dam the river was close to achieving an equilibrium state, which indicates that even without the dam the affected reach would probably not have been much longer.

Chien (1985) attempted to describe the process of degradation below a dam. The clear water released from the dam picks up sediment from the channel until the incoming load becomes equal to the sediment transporting capacity of the flow and the flow becomes saturated. This is called the point of concentration recovery and at the beginning of reservoir operation this also represents the point to which degradation progresses. After some time has elapsed, the bed material becomes coarser upstream of the point of concentration recovery, which means the transported sediment becomes coarser and the load becomes less than the transport capacity. On the other hand the coarsening of the bed material also results in a considerable reduction in the transport capacity of the flow. The result is that the point of concentration recovery actually moves towards the dam with time. However below the point of concentration recovery enough fine material still exists and the transporting capacity of the

flow is larger than the incoming load. This results in further erosion and coarsening downstream. If the flow conditions remain unchanged the whole process will continue, causing degradation to extend far downstream of the dam. Chien however did not account for the effect of tributaries or downstream controls.

The length of the degraded reach below Hoover Dam was 120 km long, 13 years after closure, and there was no indication that the reach had stopped lengthening (Williams and Wolman, 1984). Below Sanmenxia Dam the affected distance was even longer at 480 km, as reported by Chien (1985). This is partly due to the fact that there are no major tributaries on the Yellow River below Sanmenxia Dam and it is feared that the whole river course of over 800 km could degrade over time.

2.9 Mitigating Measures

The release of artificial floods and flood flushing can be a viable option to restore and maintain the downstream river morphology that has been altered as a result of a dam, because the reduction of flood peaks and the trapping of sediment within the reservoir are two of the key factors affecting the extent of the dam's impact. Artificial flood releases and flood flushing design and operation have to be carefully planned and carried out, because poor management can have negative effects on the downstream river. Also many dams, due to their design, are not able to release artificial floods or to pass sediment, but if this is possible they could aid in restoring the natural sediment balance in the downstream river reach or at least maintain a desired state.

2.9.1 Environmental Flood Releases

Glen Canyon Dam, USA:

Glen Canyon Dam on the Colorado River, USA, (**Figure 2.9.1**) was completed in 1963 and flows have been regulated substantially since 1965. The primary purpose of the dam is to allocate runoff between several US states, with hydropower generation an incidental, though significant, purpose of the dam. The hydropower generation has caused large daily flow fluctuations, sometimes ranging between 109 m^3/s and 770 m^3/s, causing up to 4 m changes in the water surface elevation at some stations downstream of the dam (Andrews and Pizzi, 2000). The flow fluctuations have resulted in severe sand bar erosion as well as the

establishment of dense exotic vegetation at the approximate elevation of the maximum power plant release. Sand slumps and liquefaction along the margins of the sand bars have been observed (Andrews and Pizzi, 2000). In 1992 operating restrictions were imposed, reducing the maximum release to 566 m^3/s (approximately 25% below power plant capacity) and restricting the maximum hourly changes in discharges for increasing and decreasing flows.

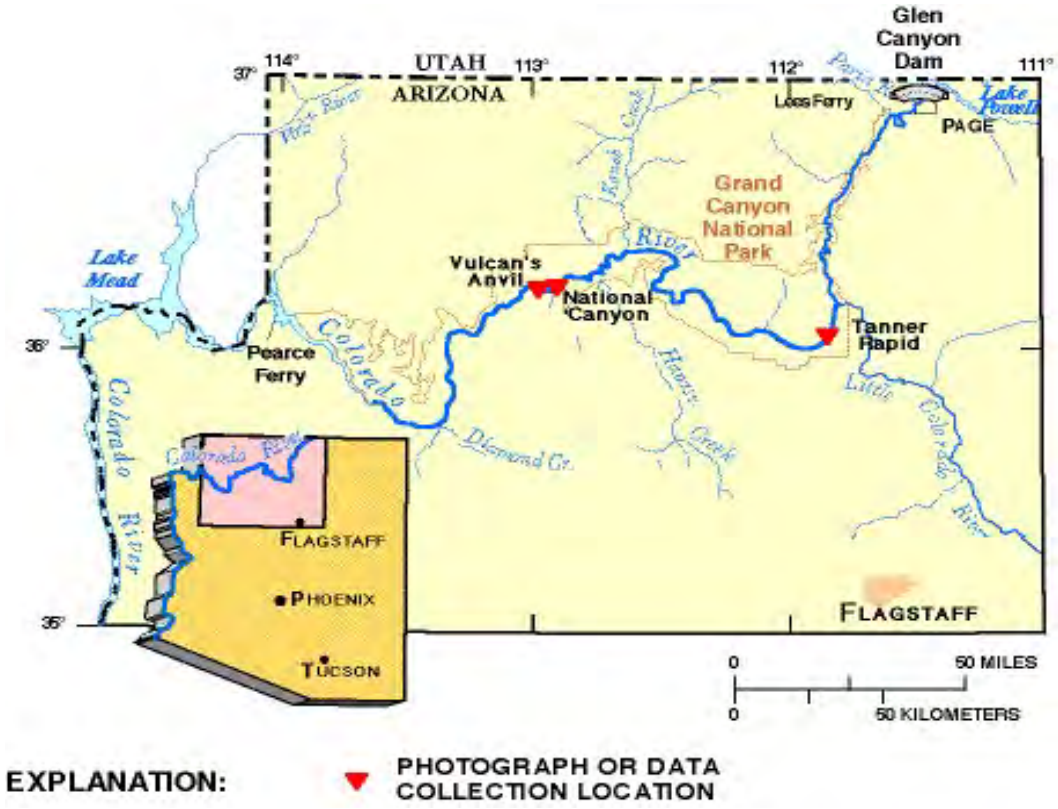

Figure 2.9.1 Glen Canyon Dam location (USGS, 2002b)

Glen Canyon releases essentially clear water. The pre-dam annual suspended sediment loads were 66 million ton at Lees Ferry gauging station (35 km downstream of Glen Canyon) and 86 million ton at Grand Canyon gauging station (a further 50 km downstream). The post-dam annual suspended sediment load at the Grand Canyon gauging station is approximately 25% of the pre-dam load. However, this decrease is not due to a lack of sediment, because the tributaries supply enough sediment, but because much of the sand is being deposited on the riverbed. The loss of the sandbars is not caused by an impoverishment of sand (Andrews and Pizzi, 2000).

During March and April of 1996 the first environmentally designed flood was released from Glen Canyon Dam. It was intended that the releases would restore and maintain the Colorado

River's sediment sources through Grand Canyon, downstream of the dam, rebuild sandbars and simulate some of the dynamics of the river's pre-dam natural flow (Wegner, 1996). The flood was started at 225 m^3/s held constant for three days, after which it was built up to a maximum of 1275 m^3/s within 10 hours (**Figure 2.9.2**), which lasted for seven days after which the discharge was once again reduced to 225 m^3/s and held constant for three days (**Figure 2.9.3**). Surveys did show that sediment was mobilized from the bottom of the river channel and re-deposited along the river corridor in the Grand Canyon (see **Figures 2.9.4** and **2.9.5**). Another smaller flood (reaching 875 m^3/s, lasting for 48 hours) was released in November 1997. The reason for the flood was again to redistribute sediment along the riverside beaches in the Marble Canyon that had been deposited by summer high flows (USBR, 2002).

Future flood releases are planned to either protect the river sediment storage downstream or to reshape the river topography, redeposit sediment and enhance aquatic habitat. Future bar building releases will probably take place once every six years, when an uncontrolled spill is unlikely (Andrews and Pizzi, 2000).

Figure 2.9.2 Glen Canyon Dam 1275 m^3/s flood release (USGS, 2002b)

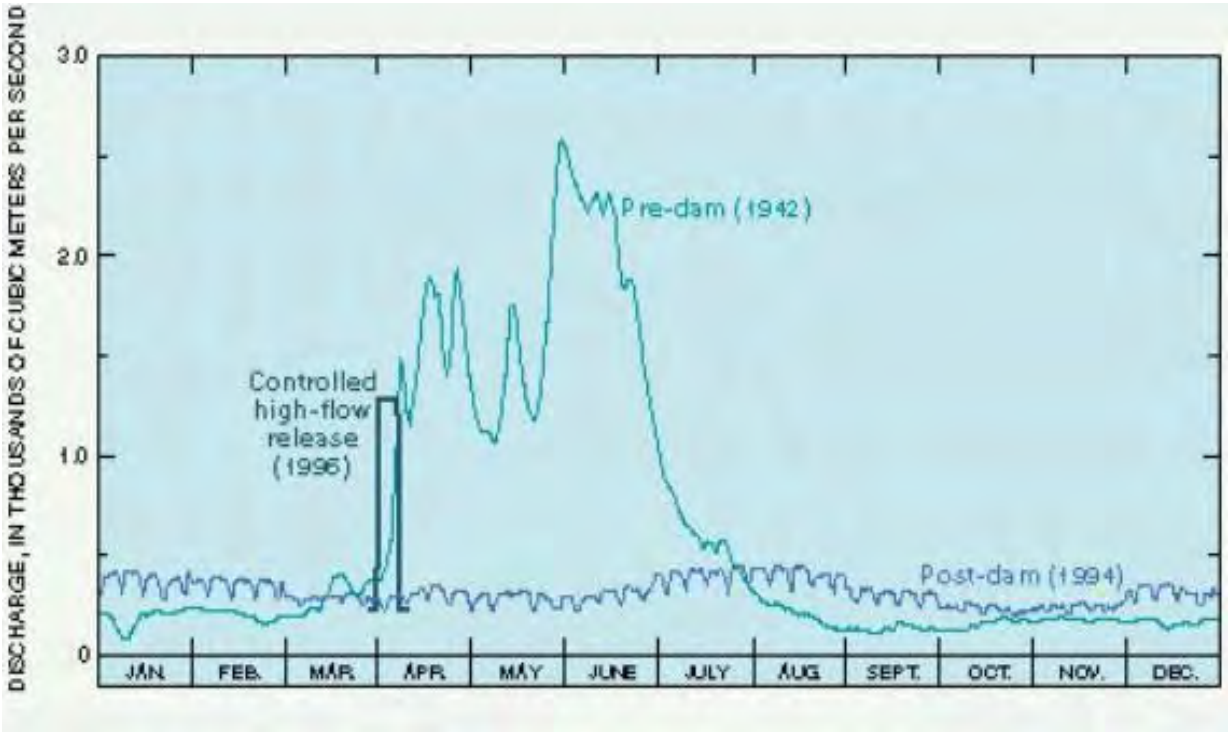

Figure 2.9.3 Relation of the controlled high flow release of 1996 to a typical snowmelt runoff hydrograph (1942) before dam construction and to typical power plant releases (1994) (USGS, 2002b)

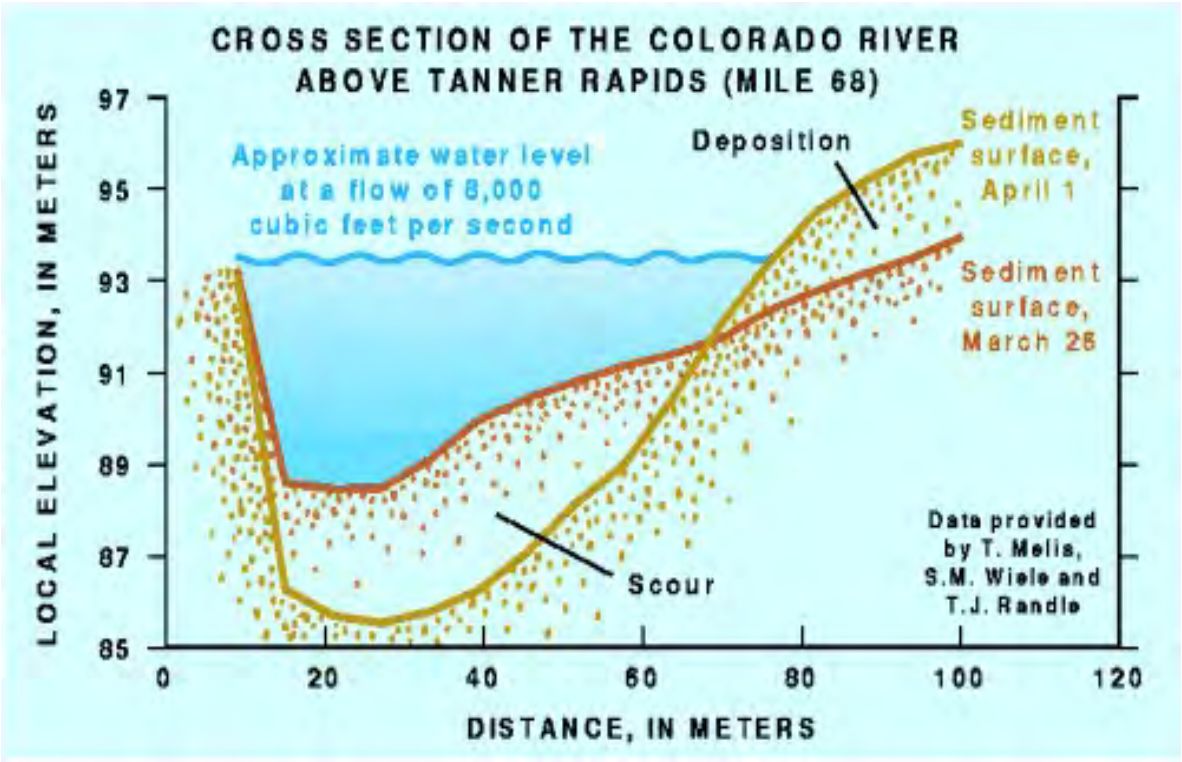

Figure 2.9.4 River cross-section changes above Tanner Rapids (USGS, 2002b)

Figure 2.9.5 Beach changes at National Canyon (Mile 166) at 255 m^3/s and 340 m^3/s, respectively (USGS, 2002b)

Pongolapoort Dam, South Africa:

Managed flood releases have been made from Pongolapoort Dam on the Pongola River, South Africa, since the mid 1980's, once or twice a year. The volume and peak discharge that can be released depend to a large degree on whether these floods will cause damages to low-lying agricultural lands and dwellings in Mozambique (the border between South Africa and Mozambique is just over 100 km downstream of Pongolapoort Dam). The volume released has varied between about 70 and 600 million m^3, with peak discharges of between 300 and 800 m^3/s. The main reasons for these flood releases were to draw down the water level in the reservoir in anticipation of the coming rainy season, as well as to recharge many of the pans downstream of the dam and provide water for the fish habitats, on which the local population depends. In recent years field investigations have been carried out during these flood releases to determine what geomorphological effect these floods have had on the Pongola River and to determine whether they could be improved upon in terms of the magnitude, frequency and timing of these flood releases. More details about these investigations can be found in **Chapter 5**.

2.9.2 Flood Flushing of Sediments

Sanmenxia Dam, China:

The Yellow River in China has one of the highest sediment loads in the world, which makes it essential to operate the reservoirs correctly. As mentioned in **Section 2.1** Sanmenxia Dam on the Yellow River, China, was built initially for year-round impoundment, but after severe sedimentation occurred in the reservoir, the operation was changed to flood detention. In 1964 and 1969 the outlet works were reconstructed (**Figure 2.9.6**) so that the reservoir can now be operated for sediment sluicing, flood control and hydropower. Clear water is stored in the non-flood season and muddy water released in the flood season (**Figure 2.9.7** and **2.9.8**), thereby the reservoir capacity is maintained and the sediment transport capacity of the downstream river channel increased (Qian *et al*., 1993). Before the reservoir operation was changed, severe aggradation occurred in the downstream river due to the reduced flood peaks. Now only major floods are detained and the smaller floods together with the sediment load and previous deposits are released. The outflow varies between 2000 and 6000 m^3/s, with a maximum mean daily discharge of 8000 m^3/s. The channel aggradation was alleviated.

Figure 2.9.6 Reconstruction of the bottom outlets at Sanmenxia Dam

Figure 2.9.7　Sediment flushing at Sanmenxia Dam

Figure 2.9.8　Sediment flushing at Sanmenxia Dam (side outlet)

Tributaries still pose a large threat in that they carry large quantities of sediment, which could block the main channel. In 1966 a small flood (peak discharge 3660 m^3/s) from one of the tributaries in the upper reaches of the Yellow River carrying around 16.5 million ton of sediment (runoff was around 23 million m^3), blocking the main channel of the Yellow River for a short while. Should the discharge of the main river have been regulated, the blockage would have been more serious and the discharge necessary to break the blockage would have been much greater.

3. River Channel Morphology

A natural river is never completely stable because of the natural variability of the factors that control the morphology especially the water discharge and sediment load. Even though the variability can be great, as is the case in the semi-arid climate of South Africa, a river will strive to attain a state of dynamic or quasi-equilibrium, by changing its cross-section, slope and even channel pattern to obtain optimal transport of water and sediments. Such a river is said to be in regime, meaning that it has obtained a long-term stable configuration, with only minor adjustments. Major changes tend to only occur as a result of significant events like a 1:100-year flood or the construction of a dam.

In order to analyse the effects that a dam can have on the downstream river channel, it is important to be able to describe the stable river morphology. There are two approaches to describing the hydraulic geometry of alluvial rivers: the empirical approach and the theoretical or analytical approach. The empirical approach attempts to derive relationships from available data and is thus dependent on the quality of the data. The theoretical or analytical approach relies on fundamental hydraulic processes like flow resistance and sediment transport, where the identification of the dominant processes is very important. A first attempt is generally the development of empirical regime equations that provide at least an indication of the direction of the changes. Regime equations based on hydraulic processes occur in very much the same format as the empirical equations, with the same input variables. The one difference is that the theoretical/analytical regime equations are generally applicable to a wider range of conditions. Another way of describing the channel geometry is through some form of extremal hypothesis, e.g. the minimization of stream power approach by Chang (1979, 1988).

A river has at least three degrees of freedom in its width, depth and slope, while Chang (1979) added the channel pattern to the list. The velocity is not regarded as a degree of freedom because it is determinable from the discharge and channel geometry. The factors that control or influence these variables are the water discharge, sediment load, and bed and bank materials. The water and sediment discharge are by far the most dominant factors also as a result of their great variability. The bed and bank materials remain relatively unchanged under stable conditions, and generally only change as a result of a change in water and sediment

discharge. This is also why dams have such far-reaching impacts on a river, because they disturb the flows and sediment load to such a high degree.

3.1 Dominant Discharge

The water discharge is by far the most important parameter responsible for the geometrical shape of a channel and it is obvious that identifying the correct discharge is of utmost importance. Although a whole range of flows normally shapes a river, there is a general consensus that one steady flow rate, the dominant discharge, should produce the same channel dimensions as a sequence of events. This channel-forming discharge can be defined as either the flow rate that determines particular channel parameters or that cumulatively transports the most sediment.

Many researchers have equated the dominant discharge with the bankfull discharge. Bankfull discharge is the flow rate that just fills the channel to the tops of the banks, corresponding to the condition of incipient flooding. Ackers (1988) argued that sediment transport would decrease once the flow goes overbank, because of an increase in overall resistance and reduction in erosive tendencies of the flow, while Ackers and Charlton (1970) found that the bankfull discharge works best for describing sinuosity and meander wavelength. Carling (1988) reasoned that at bankfull level the resistance to flow is a minimum and the sediment transport rate a maximum. The dominant discharge has also been linked to a recurrence interval of approximately 1-2 years by several researchers (Harvey, 1969), but most of these studies actually established a much wider range for bankfull flow recurrence intervals between 1 and 10 years.

There are several problems regarding the use of bankfull discharge as the dominant discharge. The biggest is that there exist numerous definitions of the bankfull level, as Williams (1978) pointed out. These include either the elevation of certain benches or the active floodplain, the lower boundary of perennial vegetation or the elevation at which the width/depth ratio becomes a minimum. The determination of the discharge corresponding to the bankfull elevation presents an additional problem. The most common ways of determining this discharge are by means of a rating curve, hydraulic geometry or flow equations. Considering all the different approaches it is not surprising that by comparing the various methods, Williams (1978) obtained a wide range of results, in most cases varying by more than 100%.

He also observed that obtaining a bankfull discharge at one cross-section is questionable since it can be radically different a few meters upstream or downstream.

In regions with highly variable runoff the bankfull discharge may not represent the dominant discharge because the water rarely flows at bankfull for long periods of time. The assumptions of a return period of 1 – 2 years also does not hold true in drier climates, because these floods are not nearly large enough to shape a channel extensively. On the other hand large floods have the capacity to reshape the channel geometry, but they occur too infrequently to have a lasting effect and the river changes back to a more stable channel. Wolman and Miller (1960) observed that the greater the variability in runoff, the larger the percentage of sediment carried by infrequent floods, which means the dominant discharge is bound to have a longer recurrence interval than 1 - 2 years. Osterkamp and Hedman (1979) studied ephemeral rivers and found that their widths are more indicative of more unusual discharges than the mean discharge. They related the channel width of ephemeral streams to the 1:10-year flood. Clark and Davies (1988) also found that the dominant discharge had an average return period of 10 years.

For the bankfull discharge to actually occur at bankfull level, means that the river channel must have already adjusted to accommodate that flow, because as soon as the flow regime changes the frequency of the former bankfull discharge will either increase or decrease depending on the changes in regime. This means that the former bankfull discharge will not have the same effects as before and that a different “bankfull” discharge with a different magnitude will emerge. If this is smaller than the original bankfull discharge, the channel will be too big and the “bankfull” discharge will actually not fill the channel to the top of the banks. On the other hand if the flows should increase in magnitude the “bankfull” discharge will actually flow over the banks. The river channel will adjust to the changed flow regime and it will thus take a while before the “bankfull” discharge will actually flow at bankfull level, and only then will it have reached its full effectiveness. Considering that the bankfull discharge has been related to the dominant discharge, because of the extraordinary conditions at bankfull level, i.e. maximum sediment transport rate, the bankfull discharge is a misleading concept in the formation of a river channel’s geometry, while it might be more likely to maintain a river channel once it has adjusted to a new flow regime.

When establishing mathematical or analytical tools describing the changes in channel geometry after the construction of a dam, it might be more correct to use a discharge that can actually be predicted with accuracy. Although it is difficult to link the dominant discharge to a specific recurrence interval, it seems that for a region like South Africa the river channels are formed by discharges that occur rather infrequently, with a recurrence interval between 5 and 20 years.

3.2 Existing Regime Equations

Regime equations have been used to describe river channel geometry for over a century, starting with the first attempts by Kennedy for irrigation canals in 1895. Further attempts were made by Lacey and Blench on straight canals, both having incorporated factors relating to sediment transport. Leopold and Maddock were among the first to develop regime equations for straight alluvial rivers. Later attempts were made to extend the equations to gravel-bed rivers, as well as to meandering rivers.

These regime equations were all empirically derived. The problem with the empirical regime equations is that they are only applicable to the range of conditions for which they were derived. Analytically or theoretically derived regime equations on the other hand are applicable to a wide range of conditions. Nonetheless it is important to correctly identify the dominant processes involved in the formation of a stable channel geometry. Since these processes are rather complex, it is mostly necessary to simplify the equations by deriving coefficients empirically, leading to semi-theoretical or semi-analytical regime equations.

3.2.1 Width Equations

The width generally shows the greatest adjustment after a change in flow regime, and some of the regime equations that have been derived are summarised in **Table 3.2.2**, which shows that most equations are expressed only in terms of discharge. This is because the water discharge is by far the most important factor influencing the channel geometry. From the summarised equations the following qualitative observation can be made regarding the effects of changing input variables on the channel width (**Table 3.2.1)**. A plus or minus exponent denotes an increase or decrease in the variable considered (Schumm, 1969).

Table 3.2.1 Effect of changing input variables on channel width

Input variable	Input variable change	Associated change in B
Q	+	+
	-	-
d	+	+
	-	-
S	+	-
	-	+

with Q = discharge

B = channel top width

d = particle size

S = channel slope

An increase in discharge will thus lead to an increase in width due to its increased erosive tendency, while an increase in the particle size leads to a decrease in channel width because coarser particles are more difficult to erode. Usually the change in particle size is related to the change in discharge, so both will change together. The coarsening of the bed material may thus be a way for the river to counteract the effect of the increasing discharge. Considering that the exponent of discharge in the width equations is generally close to 0.5 and thereby almost twice as large as the particle size exponent, which is usually less than –0.2, the effect of a change in discharge will outweigh a change in particle size.

Most of the variables under consideration will not change in isolation, but rather in response to, or together with another variable. An increase in discharge, which causes channel widening, is generally accompanied by a decrease in slope. Thus a decrease in slope can be associated with an increase in width. The same principle applies to an increase in sediment concentration, which is a consequence of an increase in discharge. A widening of the river channel can therefore be expected when the sediment concentration increases in this way.

Table 3.2.2 Summary of width equations (adapted from Wargadalam, 1993)

Author	Equation	Units	Remarks
Lacey (1930)	$P = 2.667\ Q^{0.5}$	ft	Bankfull discharge, sand-silt canals
Blench (1957)	$B = b\ Q^{0.5}\ d^{0.25}$	ft	Bankfull discharge, sand-silt canals, $d = d_{50}$ (mm), $b = \sqrt{(1.9(1 + 0.012C)/F_s)}$
Leopold & Maddock (1953)	$B = a\ Q^{0.5}$	ft	Bankfull discharge, alluvial rivers, *a* varies for individual streams
Henderson (1963)	$B = 0.93\ Q^{0.46}\ d^{-0.15}$	ft	Design discharge, narrow channels, $d = d_{50}$
Kellerhals (1967)	$B = 1.8\ Q^{0.5}$	ft	Dominant discharge, gravel-bed rivers
Chitale (1966)	$P = 2.187\ Q^{0.523}$	ft	Sand-silt canals
Bray (1982)	$B = 2.38\ Q^{0.527}$	ft	1:2-year discharge, gravel-bed rivers
Bray (1982)	$B = 2.08\ Q^{0.528}\ d^{-0.07}$	ft	1:2-year discharge, $d = d_{50}$, gravel-bed rivers
Hey & Thorne (1986)	$B = k_1\ Q^{0.5}$	m	Bankfull discharge, gravel-bed rivers, k_1 = f(bank vegetation)
Nouh (1988)	$B = 28.30\ (Q_{50}/Q)^{0.83} + 0.018\ (1 + d)^{0.93}\ C^{1.25}$	m	Mean annual discharge, $d = d_{50}$, ephemeral channels (arid zone)
Julien & Wargadalam (1995)	$B = 0.512\ Q^{\alpha}\ d_s^{\beta}\ S^{\gamma}$	m	Dominant discharge, $\alpha = (2 + 4m)/(5 + 6m)$, $\beta = -4m/(5 + 6m)$, $\gamma = (-2m - 1)/(5 + 6m)$, $m = 1/\ln(12.2D/d_s)$

3.2.2 Depth Equations

The depth is generally the first to change when the natural flows of a river are altered. The magnitude of this change is not as considerable as that of the width, because the depth can be controlled to a much larger degree by armouring or the exposure of bedrock.

A summary of some depth equations is provided in **Table 3.2.4.** The same variables that determine the width also describe the depth. Although the discharge is still the most important factor, more equations describe the depth in terms of discharge and particle size, meaning that the particle diameter has a greater effect on the depth than the width. From the summarised equations the following observation can be made regarding the effects of changing input variables on the channel depth (**Table 3.2.3**).

Table 3.2.3 Effect of changing input variables on channel depth

Input variable	Input variable change	Associated change in D
Q	+	+
	-	-
d	+	-
	-	+
S	+	-
	-	+

with D = channel depth

Much the same patterns can be observed here as those that were encountered for the width equations. A deeper channel can occur as a result of an increased discharge, coarser bed material or a decrease in channel slope. The one difference is that a river channel becomes deeper with a decrease in sediment concentration. A decreasing sediment concentration signifies that the transport capacity of the flow is not fully utilised and more sediment will be picked up from the bed, leading to a deeper river channel.

Table 3.2.4 Summary of depth equations (adapted from Wargadalam, 1993)

Author	Equation	Units	Remarks
Lacey (1930)	$R = 0.405\ Q^{0.333}\ d^{-0.167}$	ft	Bankfull discharge, sand-silt canals
Blench (1957)	$D = c\ Q^{0.333}\ d^{-0.333}$	ft	Bankfull discharge, sand-silt canals, $d = d_{50}$ (mm), $c = [F_s/(1.9(1 + 0.012C))]^{0.333}$
Leopold & Maddock (1953)	$D = b\ Q^{0.3}$	ft	Bankfull discharge, ephemeral streams, *b* varies for individual streams
Henderson (1963)	$R = 0.12\ Q^{0.46}\ d^{-0.15}$	ft	Design discharge, narrow channels, $d = d_{50}$
Kellerhals (1967)	$D = 0.166\ Q^{0.4}\ k_s^{-0.12}$	ft	Dominant discharge, gravel-bed rivers, $k_s = d_{90}$
Chitale (1966)	$R = 0.486\ Q^{0.341}$	ft	Sand-silt canals
Bray (1982)	$D = 0.266\ Q^{0.333}$	ft	1:2-year discharge, gravel-bed rivers
Bray (1982)	$D = 0.256\ Q^{0.331}\ d^{-0.025}$	ft	1:2-year discharge, $d = d_{50}$, gravel-bed rivers
Hey & Thorne (1986)	$D = 0.22\ Q^{0.37}\ d^{-0.11}$ $R = k_3\ Q^{0.41}\ Q_s^{0.02}\ d^{-0.14}$	m	Bankfull discharge, $d = d_{50}$, gravel-bed rivers, k_3 = f(bank vegetation)
Nouh (1988)	$R = 1.29\ (Q_{50}/Q)^{0.65} - 0.01\ (1 + d)^{0.98}\ C^{0.46}$	m	Mean annual discharge, $d = d_{50}$, ephemeral channels (arid zone)
Julien & Wargadalam (1995)	$D = 0.2\ Q^{\alpha}\ d_s^{\beta}\ S^{\gamma}$	m	Dominant discharge, $\alpha = 2/(5 + 6m)$, $\beta = 6m/(5 + 6m)$, $\gamma = -1/(5 + 6m)$, $m = 1/\ln(12.2D/d_s)$

3.2.3 Slope Equations

Apart from changes in width and depth an alluvial river can also change its slope in response to an altered flow regime. A change in channel slope can have far reaching consequences as it can be accompanied by a change in channel pattern, but it usually takes much longer for an appreciable change in slope than a change in width or depth to become evident, which means that changes in channel pattern may take even longer to occur.

Table 3.2.6 gives an overview of some slope equations. As with the width and depth, discharge and particle size are the two dominant variables that determine the slope. Generally however the slope equations have very poor coefficients of determination.

Table 3.2.5 Effect of changing input variables on channel slope

Input variable	Input variable change	Associated change in S
Q	+	-
	-	+
d	+	+
	-	-

As mentioned before, the relationship between discharge and channel slope is such that as the discharge decreases the slope becomes steeper, which also follows from the slope equations in **Table 3.2.6**. This occurs because the transport capacity of the river channel decreases as the discharge is reduced and the increase in channel slope is a measure to increase the transport capacity again. The particle size *d* on the other hand is directly proportional to the slope. This probably is due to the fact that on steeper slopes the transport capacity increases and most of the finer material is washed away. Judging by the magnitude of the particle size exponent, *d* also plays a much greater role in determining the slope than the depth or width. Although in this case it is more likely that the slope determines the particle size, whereas the depth and width are definitely influenced by the particle size.

Table 3.2.6 Summary of slope equations (adapted from Wargadalam, 1993)

Author	Equation	Units	Remarks
Lacey (1930)	$S = 0.00118\ Q^{-0.167} d^{0.833}$	ft	Bankfull discharge, sand-silt canals
Leopold & Maddock (1953)	$S = a\ Q^{-0.95}$	ft	Bankfull discharge, ephemeral streams, *a* varies for individual streams
Henderson (1963)	$S = 0.44\ Q^{-0.46} d^{1.15}$	ft	Design discharge, narrow channels, $d = d_{50}$
Kellerhals (1967)	$S = 0.12\ Q^{-0.4}\ k_s^{-0.92}$	ft	Dominant discharge, $k_s = d_{90}$
Chitale (1966)	$S = 0.0005\ Q^{-0.165}$	ft	Sand-silt canals
Bray (1982)	$S = 0.0354\ Q^{-0.342}$	ft	1:2-year discharge, gravel-bed rivers
Bray (1982)	$S = 0.0965\ Q^{-0.334}\ d^{0.586}$	ft	1:2-year discharge, $d = d_{50}$, gravel-bed rivers
Hey & Thorne (1986)	$S = 0.087\ Q^{-0.43}\ Q_s^{0.1}\ d_{50}^{-0.09}\ d_{84}^{0.84}$	m	Bankfull discharge, gravel-bed rivers,
Nouh (1988)	$S = 18.25\ (Q_{50}/Q)^{-0.35} - 0.88\ (1+d)^{1.13}\ C^{0.36}$	m	Mean annual discharge, $d = d_{50}$, ephemeral channels (arid zone)
Julien & Wargadalam (1995)	$S = 12.4\ Q^{\alpha}\ d_s^{\beta}\ S^{\gamma}$	m	Dominant discharge, $\alpha = -1/(3 + 2m)$, $\beta = 5/(4 + 6m)$, $\gamma = (5 + 6m)/(4 + 6m)$, $m = 1/\ln(12.2D/d_s)$

The reason for the poor coefficients of determination of most slope equations may be that the slope takes so much time to adjust to the altered flows and that it may only change over short distances. The measured field slopes might therefore not be equilibrium slopes, making it incorrect to use them in calibration or verification processes.

3.3 Proposed Regime Equations for South African Conditions

In this chapter an attempt is made to develop a set of regime equations for South African rivers much like those listed in **Chapter 3.2**.

3.3.1 Theory

The concept of stream power has been used in one way or another to describe various aspects of a river's morphology. Bagnold (1966) introduced the concept of stream power to the study of sediment transport. The unit stream power approach was used by Yang (1973) to explain the behaviour of meandering rivers as well as sediment transport. He argued that the suspended sediment concentration C is related to the unit stream power $\rho g \mathrm{v} S$ and particle settling velocity w:

$$C \propto \frac{\mathrm{v}S}{w} \quad \text{..... 3.3.1}$$

vS/w is the dimensionless unit input stream power.

Integrating the unit stream power over the cross-sectional area of the channel gives the total input stream power per unit channel length ρgQS, which is proportional to the total sediment load Q_s.

$$Q_s \propto \frac{\rho gQS}{w} \quad \text{..... 3.3.2}$$

Apart from the water discharge the sediment load is one of the major factors determining the channel geometry, and it therefore follows that the channel geometry, i.e. width B and depth D, should be determined by the total stream power. This means:

$$B = f(Q, S, w) \quad \text{.....} \quad .3.3.3$$

$$D = f(Q, S, w) \quad \text{.....} \quad .3.3.4$$

Since the settling velocity w is a function of the median particle diameter d_{50}, it follows that

$$B = f(Q, S, d_{50}) \quad \text{.....} \quad 3.3.5$$

$$D = f(Q, S, d_{50}) \quad \text{.....} \quad 3.3.6$$

From **Tables 3.2.2** and **3.2.4** it can be seen that the general form of the regime equations is basically the same regardless of the approach followed to establish these. For example Bray's (1982) equations are purely empirical and in the form:

$$B = C_b Q^{\alpha} d_{50}{}^{\beta} \quad \text{.....} \quad .3.3.7$$

$$D = C_d Q^{\alpha} d_{50}{}^{\beta} \quad \text{.....} \quad .3.3.8$$

where α, β, C_b, C_d are regression coefficients.

Julien and Wargadalam (1995) on the other hand used the following four fundamental relationships to derive hydraulic geometry equations:

1. Flow rate
2. Resistance to flow
3. Particle mobility
4. Secondary flow

To simplify the established equations for practical applications, some coefficients had to be empirically determined, leading to the semi-theoretical equations in **Tables 3.2.2** and **3.2.4**.

The basic forms of the regime equations, describing the downstream channel morphology, developed during this project are therefore:

$$B = C_b Q^{\alpha} S^{\beta} d_{50}{}^{\gamma} \quad \text{..... 3.3.9}$$

$$D = C_d Q^{\alpha} S^{\beta} d_{50}{}^{\gamma} \quad \text{..... 3.3.10}$$

The calibration of these two equations is discussed in the following section.

3.3.2 Calibration of New Regime Equations

3.3.2.1 Data Set

For the calibration of the channel geometry equations, data from a large number of South African rivers were utilised. The data were in the form of cross-sectional surveys taken by the Department of Water Affairs and Forestry (DWAF) at 59 sites upstream of where dams were to be built. Some of these sites were on the same river, but since a river is never the same over its entire length, the sites were used as if they represented a different river. For each site five consecutive cross-sections were chosen, typically between 250 m and 2 km apart depending on the size of the proposed dam, and a representative slope *S* was determined from topographical maps of various scales for that reach, by weighting the slopes between cross-sections according to the respective distance between cross-sections.

$$S = \frac{\sum_i (S_i * L_i)}{L} \quad \text{..... 3.3.11}$$

where S_i = slope between two successive cross-sections

L_i = distance between successive cross-sections

L = total length of the reach

In addition to the cross-sectional surveys, peak discharges of return periods between 2 and 200 years (DWAF, 1998), as well as other catchment data (i.e. sediment yield, particle size) were available for the sites (see **Appendix A1**). The particle sizes could not be determined from field data because dams have had an impact on the river reaches under consideration, and any field data taken at this stage would not reflect natural conditions. The particle sizes were therefore determined from the erodibility index of the sediment yield map of Southern Africa (Rooseboom, 1992). For each catchment the proportions of area having low, medium

and high erodibility were determined and particle sizes representing coarse (0.5 mm), medium (0.05 mm) and fine (0.005 mm) sediments, associated with each erodibility index, estimated. A representative particle size was thus determined.

With the use of computer software the width *B*, hydraulic radius *R*, wetted perimeter *P* and cross-sectional area *A* were determined for various water levels for every cross-section. Using the Chezy resistance equation, the channel slope *S* and assuming an absolute roughness k_s of 1 m, which was estimated to be representative of field conditions for alluvial rivers during floods (Le Grange, 1994), the discharge corresponding to each water level was calculated:

$$Q = 18\log\left(\frac{12R}{k_s}\right)\sqrt{RS}\ A \quad \text{..... 3.3.12}$$

For the 1:2-, 1:5-, 1:10- and 1:20-year peak discharge the following hydraulic parameters were determined: top width, average depth, hydraulic radius and velocity. The peak discharges with return periods greater than 20 years were not used because these probably do not occur frequently enough to determine the equilibrium channel morphology. They might be able to radically change the channel morphology, but the channel will not remain in that form for long. The smaller floods that occur more frequently will modify the changes brought about by the larger floods.

Of the 295 cross-sections that were originally selected, some 50 cross-sections, depending on the return period, were discarded for the following reasons:

- Above a certain level the cross-sections exhibit one or two secondary channels besides the main channel (**Figure 3.3.1**). Below level A there is no problem and the cross-section can be used for the analysis. Above level A however the problem is that it is not known whether the water first fills the main channel and then overflows into the side channels (level C), or if at some point upstream the river temporarily splits into two channels and the water therefore runs in both of these channels at that particular cross-section (level B). The two scenarios are hydraulically very different. Therefore all the data for a cross-section was discarded once the water level rose above level A. However once the water level rose above level D the data was again included because at that stage the water flows in a single channel again.

- Data were also discarded for cross-sections where the water just reached the stage where it overflows onto the floodplain. The floodplain is a different system from the river channel, and our interest lies in the river channel geometry.

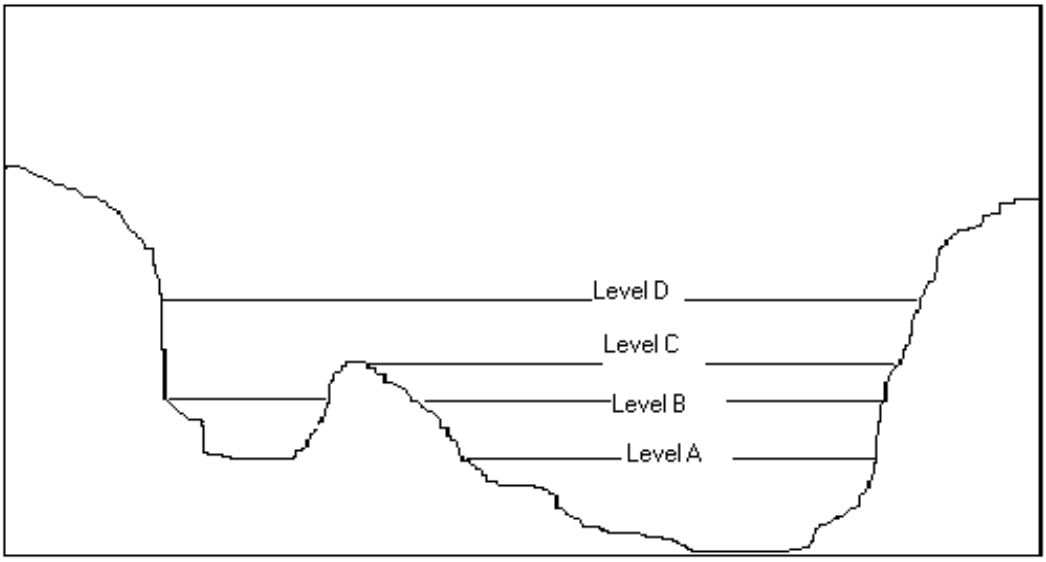

Figure 3.3.1 Cross-sectional levels (indicating which sections could not be used)

The results from the remaining cross-sections for each reach were used to determine an average width, depth, hydraulic radius and velocity for that reach, leaving 59 data sets to work with for each of the four peak discharges.

3.3.2.2 Calibration

In order to calibrate **Equations 3.3.9** and **3.3.10** all the pertinent values were first log-transformed and the coefficients and exponents derived by linear regression analysis. All the regression values were then de-transformed to obtain the final calibrated equations. In addition to **Equations 3.3.9** and **3.3.10** the following relationships were also tested to determine the relative importance of each of the three independent parameters (water discharge Q, channel slope S and particle size represented by d_{50}):

$$B = C_b Q^{\alpha} \quad \text{.....} \quad 3.3.13$$

$$B = C_b Q^{\alpha} S^{\beta} \quad \text{.....} \quad 3.3.14$$

$$B = C_b Q^{\alpha} S^{\beta} d_{50}{}^{\gamma} \quad \text{.....} \quad 3.3.9$$

$$D = C_d Q^{\alpha} \quad \text{.....} \quad 3.3.15$$

$$D = C_d Q^{\alpha} S^{\beta} \quad \text{..... 3.3.16}$$

$$D = C_d Q^{\alpha} S^{\beta} d_{50}{}^{\gamma} \quad \text{..... 3.3.10}$$

where B (m), D (m), Q (m^3/s), S (m/m), d_{50} (m)

All the width equations were first calibrated for four peak discharges with recurrence intervals of 2, 5, 10 and 20 years using the corresponding top widths. The 1:10-year discharge gave the best coefficients of determination for all cases. This would mean that the 1:10-year discharge is the discharge that has the dominant impact on the channel morphology. All further calibrations are therefore carried out with Q_{10} as the dominant discharge. The results of the regression analysis for the other peak discharges are shown in **Appendix A4**.

The range of values of each parameter used in the calibration is shown in **Table 3.3.1**, while the results of the regression analysis are shown in **Table 3.3.2**. The best correlation was achieved with all three independent parameters and the new regime equations are thus:

$$B = 4.034 Q_{10}{}^{0.365} S^{-0.228} d_{50}{}^{0.053} \quad \text{..... 3.3.17}$$

$$D = 0.071 Q_{10}{}^{0.374} S^{-0.154} d_{50}{}^{-0.02} \quad \text{..... 3.3.18}$$

However, the parameter d_{50} has very little impact on the accuracy of the equations and the regime equations in terms of the discharge and slope only can also be used (i.e. **Equation 3.3.14** and **3.3.16**).

Table 3.3.1 Variability of channel parameters

Parameter	Range
Discharge Q_{10} (m^3/s)	68 – 5200
Width B (m)	22 – 351
Average Depth D (m)	0.51 – 5.90
Hydraulic Radius R (m)	0.49 – 6.40
Slope S	0.00015 – 0.07198
d_{50} (mm)	0.005 – 0.5

Table 3.3.2 Results of regression analysis

Dependent Variable	Equation	C_b / C_d	α	β	γ	r^2
B	3.3.13	4.417	0.485	-	-	0.51
B	3.3.14	2.488	0.357	-0.230	-	0.66
B	3.3.9	4.034	0.365	-0.228	0.053	0.67
D	3.3.15	0.125	0.462	-	-	0.72
D	3.3.16	0.085	0.377	-0.153	-	0.82
D	3.3.10	0.071	0.374	-0.154	-0.020	0.82

It should be remembered that **Equations 3.3.17** and **3.3.18** only predict the average width and depth, whereas these two variables can vary considerably from one section to another on a river. For the rivers under consideration, it was found that on average the widths could be 30% larger or smaller than the average width over a certain river reach. This means that a river with an average width of 100 m is likely to be between 70 and 130 m wide. For the depths a slightly smaller variation of 20% was established.

From **Table 3.3.2** it can be seen that all the depth equations have better coefficients of determination than the width equations. This is probably due to the fact that not all the factors influencing the width are included in the analysis. Although the water discharge is the major controlling factor for widths, bank material and type and amount of vegetation on the banks also determine the width. The depth on the other hand seems to be more adequately related to the three chosen parameters. The correlations of **Equations 3.3.9** and **3.3.10** are shown in **Figures 3.3.2** and **3.3.3**. The lowest coefficients of determination for both the depth and width relationships occur when the discharge is the only independent variable. Looking at the results of the regression analysis for **Equation 3.3.13** however, it can be seen that the exponent is very close to 0.5, which is in agreement with traditional regime relationships. The inclusion of the channel slope improves the relationship, while the inclusion of the particle size has very little impact on the correlation as well as on the exponents. The magnitude of the exponents gives an indication of the relative importance of the three independent variables. As already mentioned the discharge is the most influential parameter and the channel slope is also relatively important, but the particle size seems to have very little effect on both the width and depth.

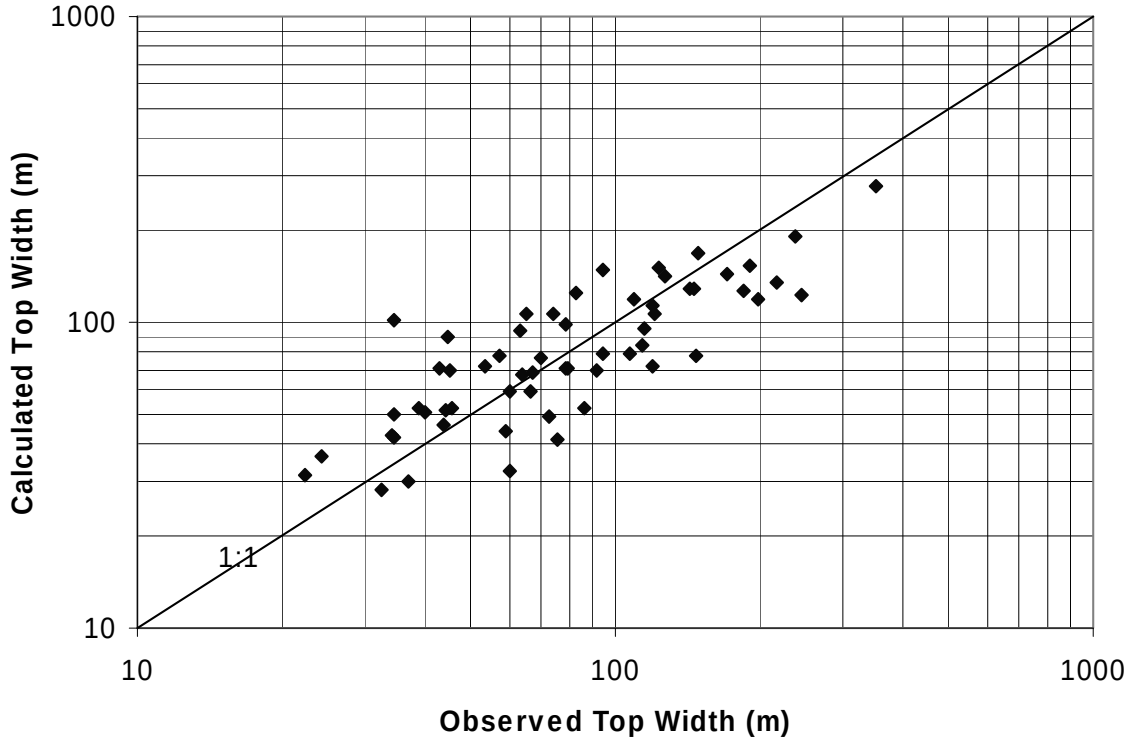

Figure 3.3.2 Calibration of South African regime width equation

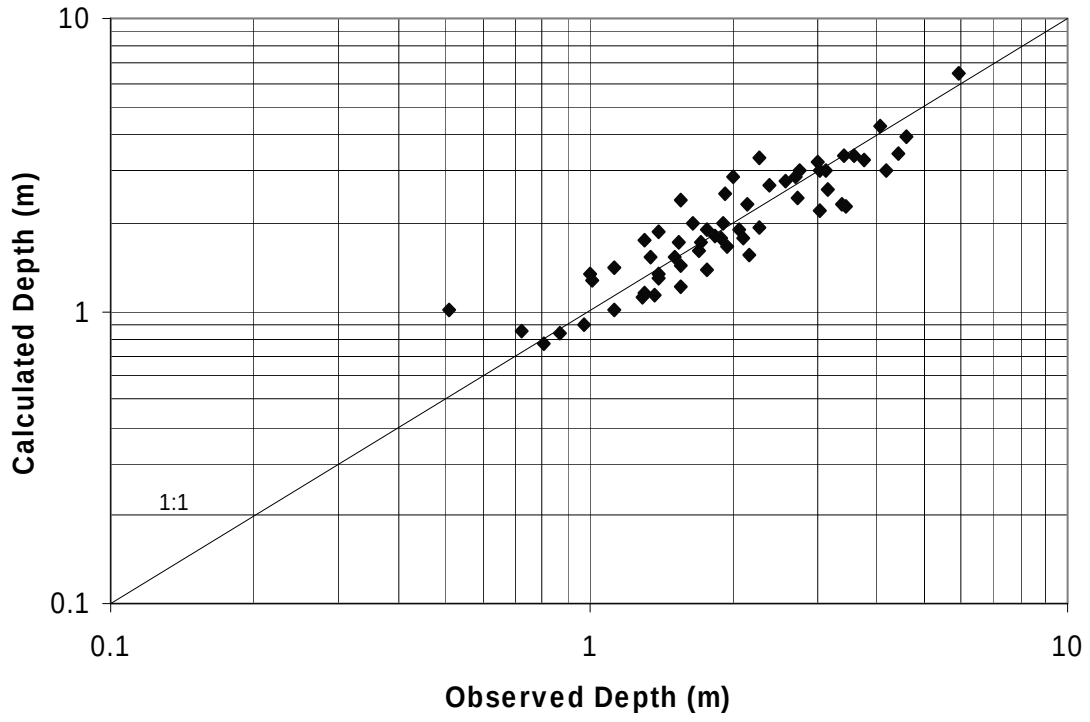

Figure 3.3.3 Calibration of South African regime depth equation

In addition to the coefficient of determination it is sometimes useful to express the accuracy of the relationships in terms of their ability to predict the width and depth within certain accuracy ranges, as indicated in **Tables 3.3.3** and **3.3.4**.

Table 3.3.3 Accuracy of new width relationships

Equation	$0.67 < \frac{B_{calculated}}{B_{observed}} < 1.5$	$0.5 < \frac{B_{calculated}}{B_{observed}} < 2$	$0.33 < \frac{B_{calculated}}{B_{observed}} < 3$
3.3.13	57 %	92 %	98 %
3.3.14	75 %	97 %	100 %
3.3.9	75 %	97 %	100 %

Table 3.3.4 Accuracy of new depth relationships

Equation	$0.67 < \frac{D_{calculated}}{D_{observed}} < 1.5$	$0.5 < \frac{D_{calculated}}{D_{observed}} < 2$	$0.33 < \frac{D_{calculated}}{D_{observed}} < 3$
3.3.15	85 %	97 %	100 %
3.3.16	90 %	98 %	100 %
3.3.10	90 %	98 %	100 %

From **Tables 3.3.3** and **3.3.4** the same trends can be observed as from the coefficients of determination of **Table 3.3.2**. The accuracy in predicting the width and depth improve dramatically once the channel slope is included in the analysis, especially for calculating widths. Considering that for all except one equation, more than 95% of the observations fall within 50% and 200% of the calculations, the new regime equations fit data fairly well.

3.3.2.3 Comparison and Verification

In order to establish the applicability of the new regime equations they are verified using an independent set of data, as well as comparing them to the semi-theoretical channel geometry equations developed by Julien and Wargadalam (1995). These are applicable to a very wide range of conditions, since they are theoretically based and also calibrated on an extensive set of data. The semi-theoretical relations are as follows:

$$B = 1.33 Q^{(2+4m)/(5+6m)} d_{50}^{\ -4m/(5+6m)} S^{-(1+2m)/(5+6m)} \quad \text{..... 3.3.19}$$

$$D = 0.2Q^{2/(5+6m)} d_{50}{}^{6m/(5+6m)} S^{-1/(5+6m)} \quad \text{..... 3.3.20}$$

where $$m = \frac{1}{\ln\left(\frac{12.2D}{d_{50}}\right)} \quad \text{..... 3.3.21}$$

The data set used for the comparison is taken from Wargadalam (1993), shown in **Appendix A2**. It consists of 28 sets of data from various sand bed rivers. The data were used by Wargadalam to verify **Equations 3.3.19** and **3.3.20**. The data were initially used to determine the exponents of **Equations 3.3.19** and **3.3.20**, then both widths and depths are determined from these equations and the results are compared to the original data as well as values computed from **Equations 3.3.17** and **3.3.18**.

The first point that became obvious was that the exponents of **Equations 3.3.19** and **3.3.20** vary very little for this particular data set, except for β. The ranges of coefficients are shown in **Table 3.3.5**, with α, β and γ indicating the exponent of discharge, particle size and slope, respectively, for the width and depth equations.

Table 3.3.5 Range of exponents

		α	β	γ
Width	Minimum	0.422	-0.092	-0.218
	Maximum	0.437	-0.054	-0.211
	Average	0.426	-0.066	-0.213
Depth	Minimum	0.345	0.081	-0.218
	Maximum	0.368	0.138	-0.181
	Average	0.361	0.099	-0.212

Using the average values does not compromise the accuracy of the equations, but it makes it easier to compare the equations with the newly developed South African regime equations. Substituting the average coefficients into **Equations 3.3.19** and **3.3.20** yields the following:

$$B = 1.33Q^{0.426} d_{50}{}^{-0.066} S^{-0.213} \quad \text{..... 3.3.22}$$

$$D = 0.2Q^{0.361} d_{50}^{\ 0.099} S^{-0.212} \quad \text{..... .3.3.23}$$

These two equations are very similar to the regime equations (**Equations 3.3.17/18**) developed during this project and the computed widths are almost identical as shown in **Figure 3.3.4.** It does seem though that **Equation 3.3.23** overestimates the depth considerably as shown in **Figure 3.3.5**. The fact that the semi-theoretical channel geometry equations by Julien and Wargadalam (1995) and the new regime equations of this project generally produce similar results and also have similar accuracy ranges, give **Equations 3.3.17** and **3.3.18** a sound basis.

The same data is used to verify **Equations 3.3.17** and **3.3.18.** As with the calibration process the accuracy of the new regime equations are expressed in terms of their ability to predict data within certain accuracy ranges, shown in **Table 3.3.6** and **3.3.7**.

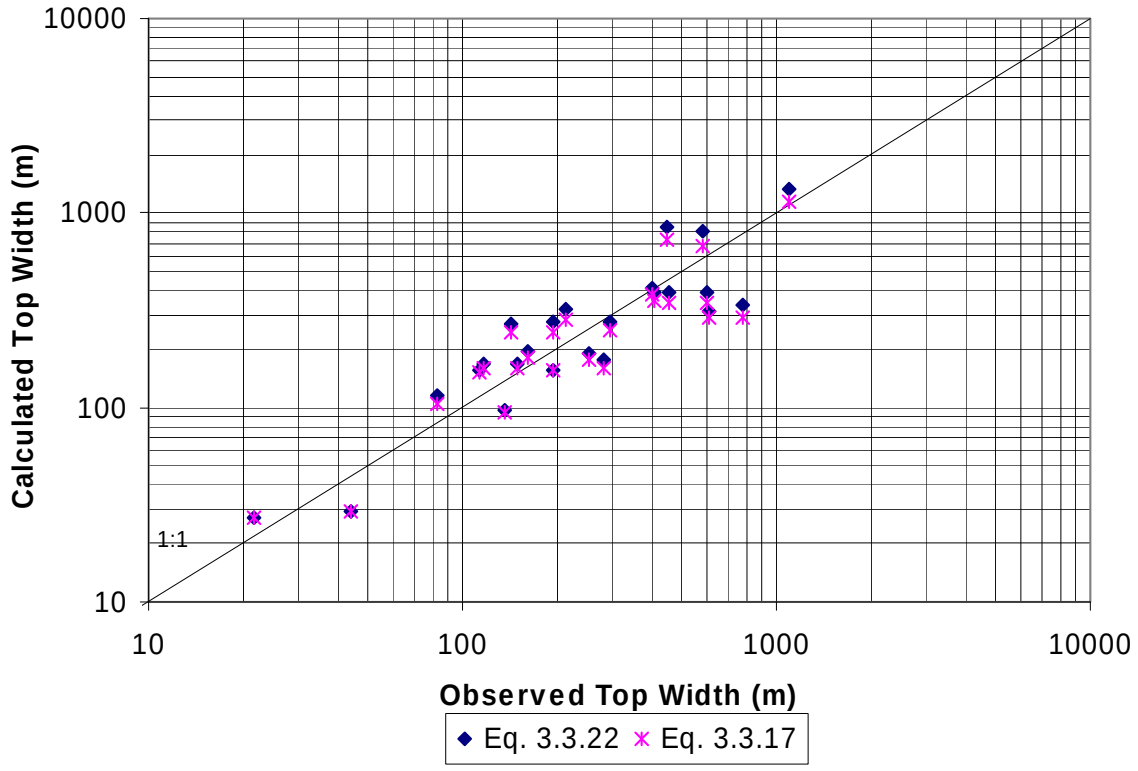

Figure 3.3.4 Comparison of existing and new width equations

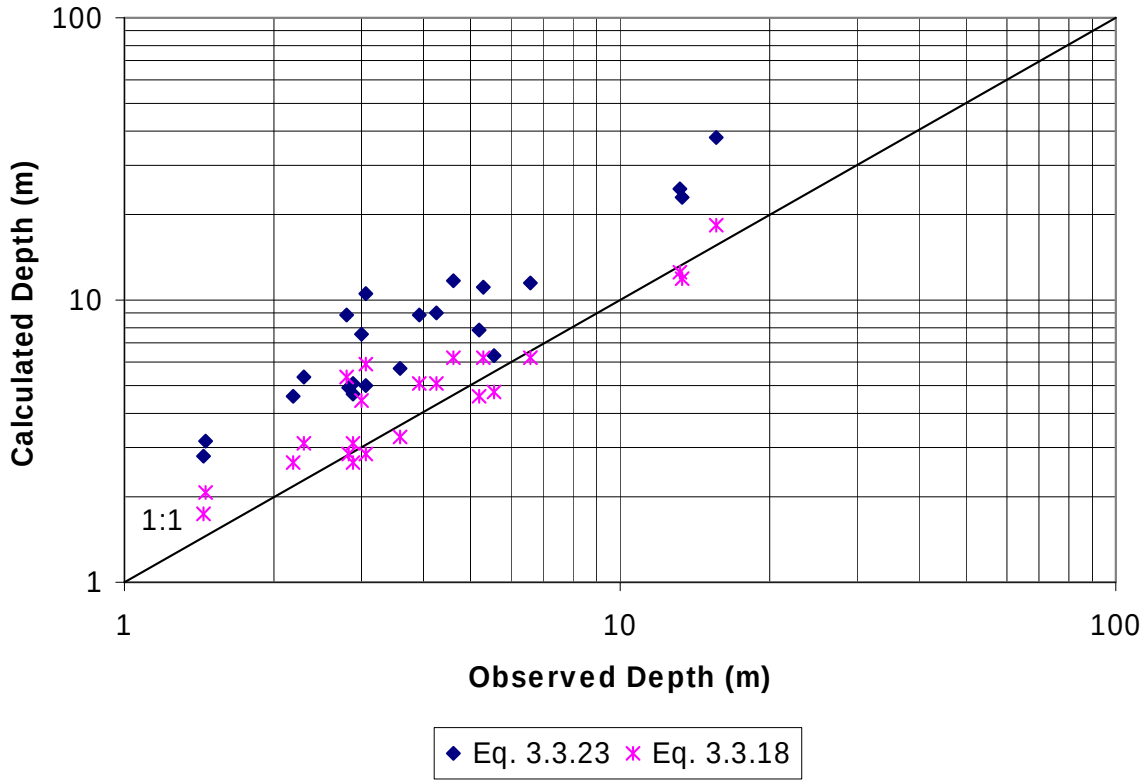

Figure 3.3.5 Comparison of existing and new depth equations

Table 3.3.6 Accuracy ranges of width relationships (independent river data)

Equation	$0.67 < \frac{B_{calculated}}{B_{observed}} < 1.5$	$0.5 < \frac{B_{calculated}}{B_{observed}} < 2$	$0.33 < \frac{B_{calculated}}{B_{observed}} < 3$
New	64 %	79 %	96 %
Julien, et al.	61 %	89 %	100 %

Table 3.3.7 Accuracy ranges of depth relationships (independent river data)

Equation	$0.67 < \frac{D_{calculated}}{D_{observed}} < 1.5$	$0.5 < \frac{D_{calculated}}{D_{observed}} < 2$	$0.33 < \frac{D_{calculated}}{D_{observed}} < 3$
New	82 %	100 %	100 %
Julien, et al.	54 %	93 %	100 %

Table 3.3.6 and **3.3.7** show very much the same trends as **Table 3.3.3** and **3.3.4**, except that the accuracies are sometimes lower, which is to be expected because of the use of independent data in the verification process. However the accuracies are still good and compare well to the accuracies of Julien and Wargadalam's relations.

3.4 Minimization of Stream Power

Apart from the regime equations the hydraulic geometry of a river channel in quasi-equilibrium can also be determined through some form of extremal hypothesis, involving the maximization or minimization of one parameter. This hypothesis usually forms part of a set of equations, with the other equations being for the sediment transport capacity and flow resistance.

3.4.1 Theory and Application

Given a flow resistance equation and a sediment discharge equation, Chang (1979) proposed the hypothesis of minimum stream power as the third required relation. He stated that an alluvial channel with a given water discharge Q and sediment load Q_s will establish its width, depth and slope such that the stream power is a minimum. The input stream power per unit channel length is given by ρgQS. Since Q is a given parameter, minimum ρgQS means minimum channel slope S. This concept of minimum stream power is similar to the concept of minimum unit stream power proposed by Yang (1973), which also implies maximum sediment transport.

Chang (1988) used the flow resistance formula of Lacey and the DuBoys' bed load formula in conjunction with the minimization of stream power to develop a design procedure for stable alluvial canals, approximating the channel shape as a trapezoid with bank slope z. He also stated that the procedure is not limited to Lacey's and DuBoys' formulas, but that both can be replaced by any other valid formulas. In this project the same procedure was followed, but Chezy's flow resistance formula (**3.4.1**) was substituted for Lacey's formula.

$$\mathrm{v} = 18\log\left(\frac{12R}{k_s}\right)\sqrt{RS} \quad \text{..... 3.4.1}$$

$$q_b = C_d\tau\left(\tau - \tau_c\right) \quad \text{..... 3.4.2}$$

where q_b = bed load per unit width

C_d = characteristic sediment coefficient = $\dfrac{0.17}{d^{3/4}}$ 3.4.3

d = sediment diameter

τ = shear stress exerted on the bed

τ_c = critical shear stress = $0.061 + 0.093d$ 3.4.4

The basic procedure is outlined below as well as in **Figure 3.4.1** (Chang, 1979):

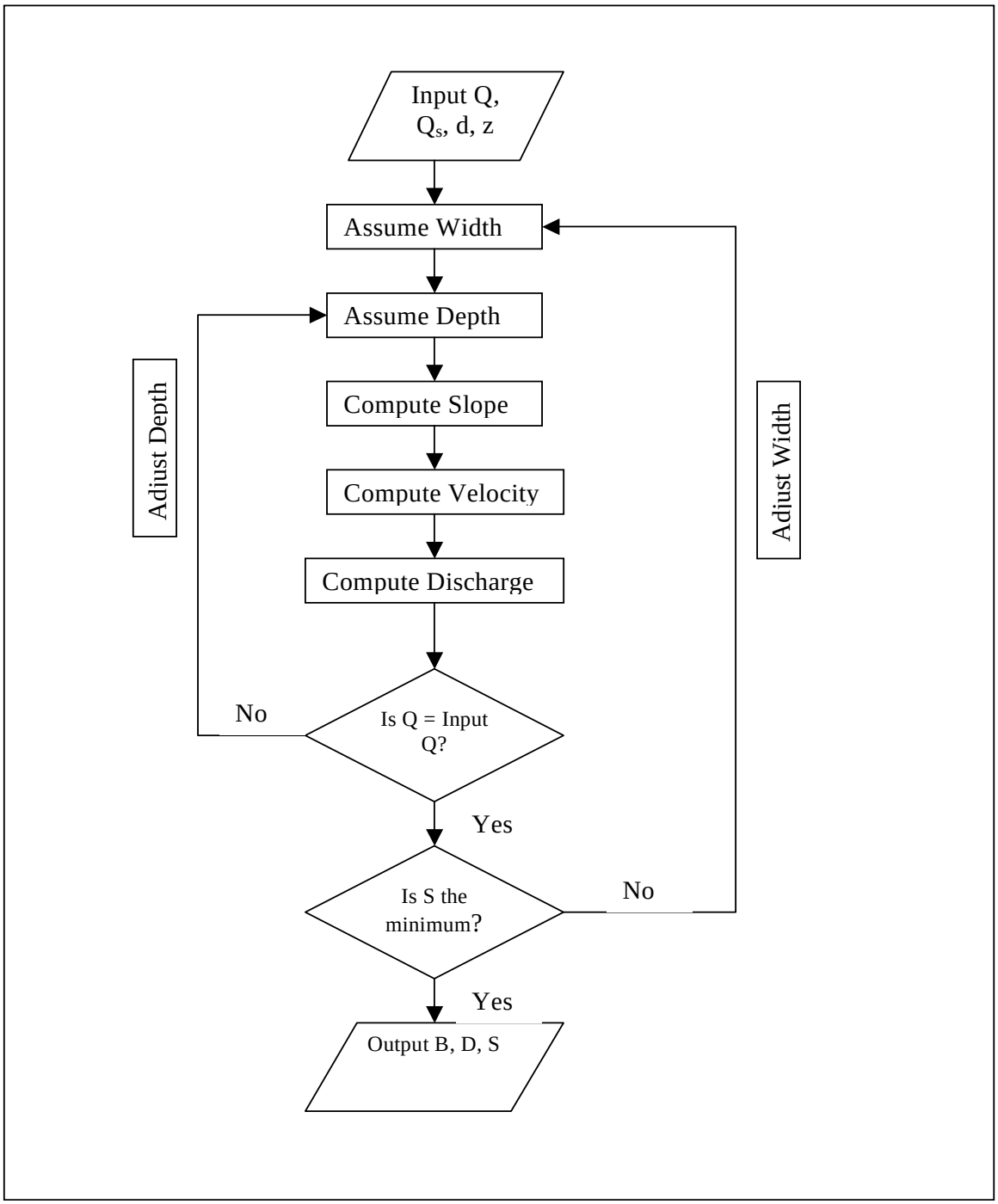

Figure 3.4.1 Flow chart showing major steps of calculation (Chang, 1979)

- Select a set of independent variables Q, Q_s, d, z as input variables, with z the channel side slopes.
- Assume a set of incremental widths B and for each width assume a depth D. Compute the slope from the sediment transport formula and the velocity from the flow resistance formula. In order to calculate the slope it is more convenient to rewrite DuBoys' transport formula to express the slope in terms of the specified variables.

$$Q_b = q_b b = \frac{0.17}{d^{3/4}} \rho g R S (\rho g R S - (0.061 + 0.093 d)) b \quad \text{..... 3.4.5}$$

and

$$S = \frac{\rho g R(0.061 + 0.093 d) + \sqrt{(\rho g R(0.061 + 0.093 d))^2 + 4(\rho g R)^2 \frac{Q_b d^{3/4}}{0.17 b}}}{2(\rho g R)^2} \quad \text{..... 3.4.6}$$

Calculate the discharge and compare it to the input discharge. Change the depth and repeat the procedure until the input discharge and the calculated discharge are equal, then go to the next width.

- The stable width and depth correspond to the minimum slope computed.

3.4.2 Discussion

Chang (1988), using the procedure set out above, explained the variation of stream power expenditure with channel width as follows. The stream power $\rho g Q S$ or slope S attains a minimum under certain counteractive forces. Starting with a large width, where the bank effect is small the channel slope decreases with decreasing width because the flow is more concentrated in a smaller channel and therefore the transport efficiency increases. This means that Q and Q_s are transported at lower power expenditure. The surface areas of the channel banks contribute relatively little to bed load transport so that when the channel width decreases so does the effective (bottom) width for bed load transport, meaning that the bank effect increases. Consequently the channel slope has to become steeper at some point to transport the given discharge and sediment load, and the power expenditure increases. When

the two opposing forces are balanced the channel attains a stable width when the channel slope is a minimum.

Chang (1988) and Brandt (1999) have successfully applied the procedure outlined in **Section 3.4.1**, both using Lacey's resistance formula and DuBoys' bed load formula. In this project DuBoys' bed load formula was tested together with Chezy's resistance formula, but this resulted in a very small minimum slope and unrealistic depths. Substituting Manning's resistance formula produced much the same results. It was also found that a total load formula like Engelund and Hansen's did not produce a minimum slope at all. It is therefore very important to verify which formulae are applicable before applying the minimisation of stream power theory. The concept, however, is still valid and is incorporated in a numerical model (GSTARS), which is explained in further detail in **Chapter 5**.

3.5 Channel Patterns

Apart from the width, depth and channel slope, a river can also adjust its channel pattern in response to imposed changes in the flow regime and sediment load. The three major patterns are straight, meandering and braided, which are very much linked to the channel slope. There exist several thresholds or discontinuities between these channel patterns and if the channel slope should be close to the critical or threshold slope, the river pattern can change. A small change in channel slope can therefore lead to a definite change in river pattern.

3.5.1 Theory and Background

An index used to describe the channel planform is the sinuosity, defined as the ratio of channel length to valley length. Leopold and Wolman (1957) have stated that a reach could be considered meandering when the sinuosity is greater than or equal to 1.5. The value is arbitrary, but they argued that a sinuosity of 1.5 indicates a truly meandering river. Chang (1988) as well as other researchers have adopted that value.

The channel patterns and their relationships with the channel slope can therefore be identified as follows:

- Truly straight rivers (sinuosity < 1.1), rarely occurring in nature and are usually artificially maintained.

- Straight rivers (sinuosity < 1.5) generally occur on flat slopes with small width/depth ratios and low velocities. Although a river may have a relatively straight alignment the thalweg usually has a distinct meandering pattern.
- On steeper slopes the river becomes meandering (sinuosity > 1.5) and the width/depth ratio increases, as does the velocity.
- On even steeper slopes the sinuosity generally decreases and the river becomes braided, in conjunction with an even higher width/depth ratio.

Several researchers have identified thresholds between different channel patterns, but they differ somewhat from one study to another, which is a result of the different data sets being used as well as the difference in the definitions of the various channel patterns.

The discharge-slope relation developed by Leopold and Wolman (1957) separates meandering and steeper braided streams:

$$S = 0.0125Q^{-0.44} \quad \text{3.5.1}$$

where Q is the bankfull discharge in m^3/s.

The following meandering-braided threshold has been developed by Begin (cited in Carson, 1984):

$$S = 0.0016Q^{-0.33} \quad \text{3.5.2}$$

Carson (1984) pointed out the importance of including the sediment particle size in the relationship, since streams with gravel beds must plot higher on a Q-S diagram than sand bed rivers, simply because it requires more power to transport gravel than sand. Henderson (cited in Chang, 1988) obtained the following equation for gravel-bed rivers:

$$S = 0.0002d_{50}^{1.15}Q^{-0.46} \quad \text{3.5.3}$$

Chang (1979) developed channel pattern thresholds, based on the minimisation of stream power theory. Unlike other researchers, however, he argued that there can be a transition from

straight to braided, before a river becomes meandering. With an increase in valley slope, however, the river tends to become less sinuous and more braided again, as indicated in **Figure 3.5.1**

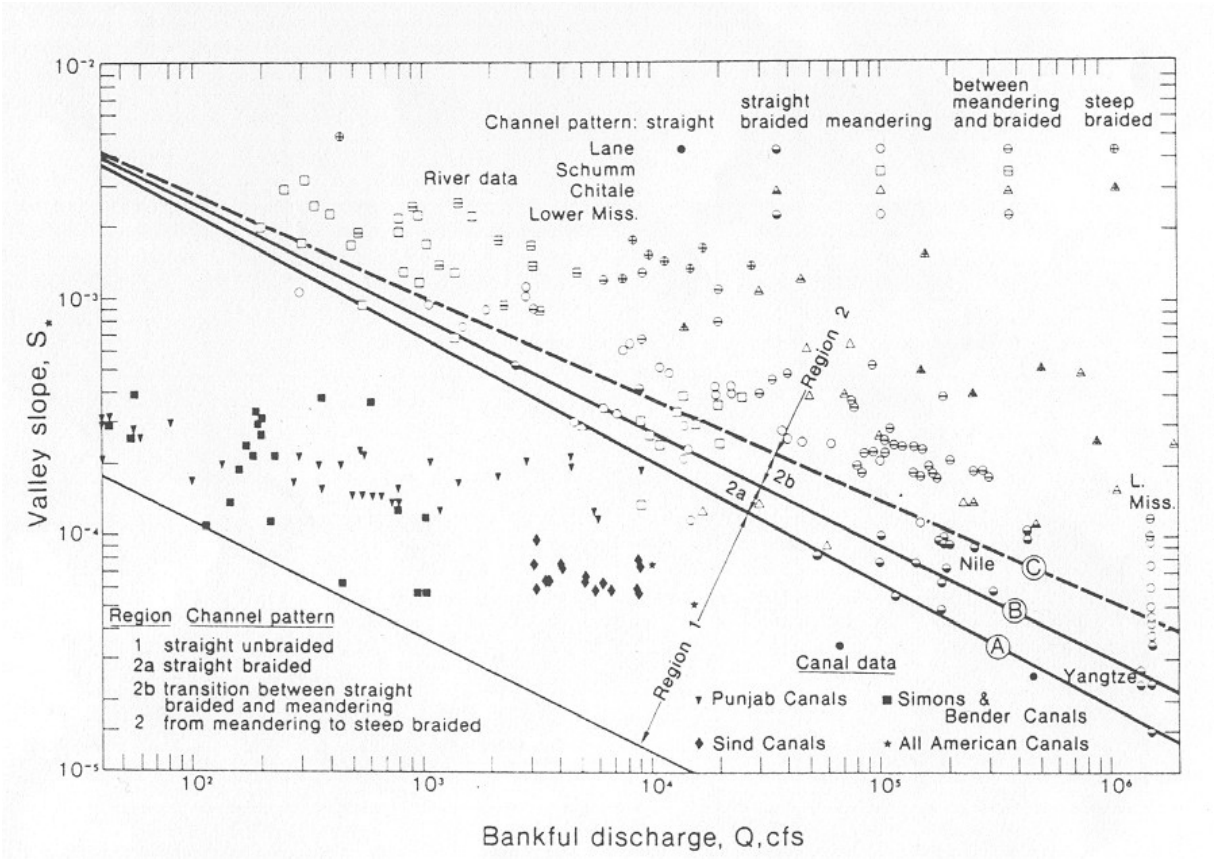

Figure 3.5.1 Channel patterns of sand streams (Chang, 1979)

3.5.2 Development of a Discharge - Slope Relationship for South African Rivers

As mentioned in **Section 3.5.1** a small change in channel slope can result in a major change in channel pattern, and it is therefore useful to establish a discharge-slope relationship applicable to South African rivers.

The same set of rivers used for the calibration of the South African regime equations in **Section 3.3** were used to determine the Q-S relationship. Sinuosities for each river were determined from 1:50 000 topographical maps (see **Appendix A3**). Each section was chosen to be representative of the river reach under consideration, by disregarding for instances reaches that were obviously prevented from developing normally either by natural controls

such as rock formations or manmade controls. The sinuosities were then plotted (as labels) together with the corresponding 1:10-year discharges and slopes as shown in **Figure 3.5.2**.

The fact that a meandering river is defined as having a sinuosity of greater than 1.5 is mentioned in **Section 3.5.1** and braided rivers generally occur on slopes steeper than those of meandering rivers. The position of the threshold separating meandering and braided rivers would therefore be expected to be found in the upper region of **Figure 3.5.2** where the sinuosities start decreasing. A threshold was observed, based on a trend of increasing sinuosities in the lower part of the graph, followed by a decrease in sinuosities in the upper part. The data in **Figure 3.5.2** indicate that braided rivers are separated from meandering channels by a line described by the following equation:

$$S = 0.159Q_{10}^{-0.557} \quad \text{..... 3.5.4}$$

The Eerste River, Hex River and Vaal River data are all shown in **Figure 3.5.2**. All three rivers have braided reaches and plot just above the threshold line.

Several observations can be made from the data set:

1. There is only a weak trend of increasing sinuosity with increasing slope for meandering rivers, which makes it impossible to determine a threshold between straight and meandering rivers.
2. No trend could be found for increasing width/depth ratios with increasing slopes or that coarser grained particles plot at higher Q-S combinations than finer particles.
3. There is no indication of different thresholds for different particle sizes as suggested by Carson (1984), but this could be because the particles sizes of the data analysed, all fall into the range of fine to medium sand. The effect of the particles size might only become obvious when a wider range of particle sizes is investigated.

The absence of any real trend of increasing sinuosity or width/depth ratio with increasing slopes, has already been pointed out by Carson (1984) amongst others, and **Equation 3.5.4**, seeing that it is only a best-fit relationship, should really only be used as a rough guide to determine whether a river might change its channel pattern as a result of a change in discharge and sediment load due to the construction of a dam.

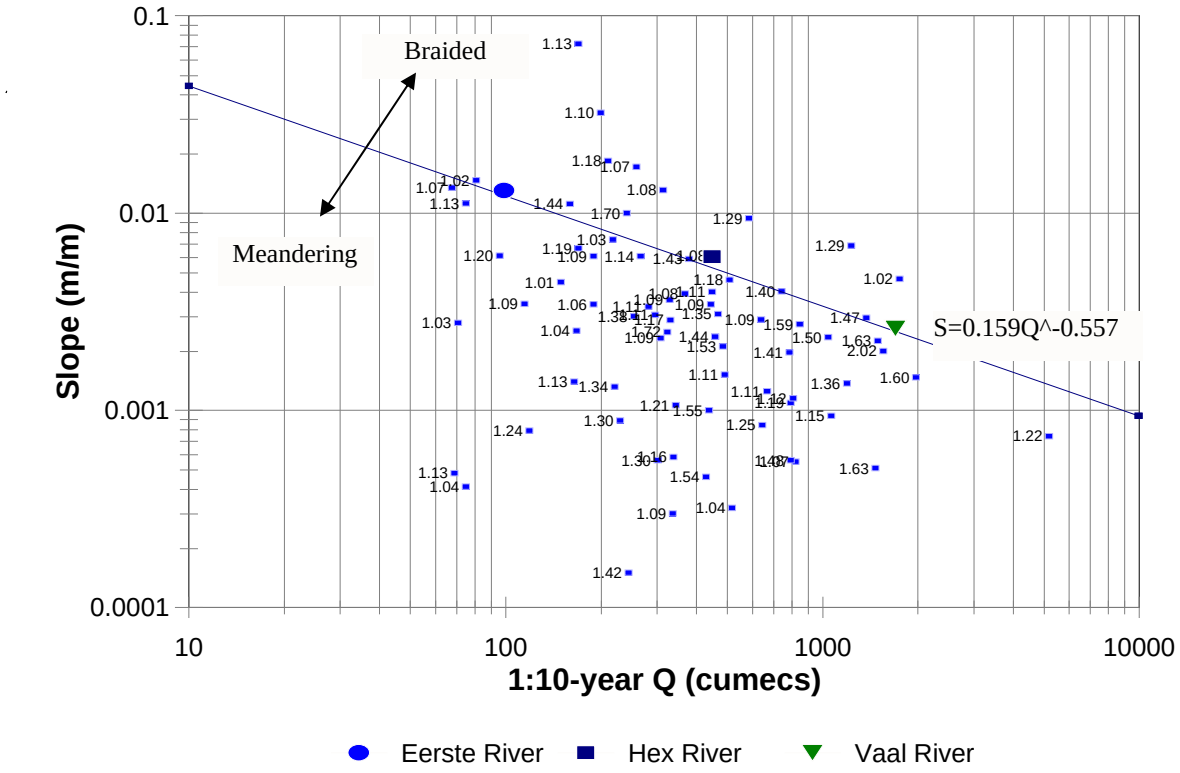

Figure 3.5.2 Threshold line separating meandering and braided rivers (sinuosity indicated)

3.6 Applications

In this section the applicability of the methods developed in the previous sections is tested using the Pongola River, downstream of Pongolapoort Dam, as an example (see **Chapter 5** for further details on Pongolapoort). The following data are of interest (where average values are mentioned they were determined over the first 20 km downstream of the dam in order to get a representative value):

- 1:10-year flood peak:

  Both flood peaks (before and after the dam was built) were determined through statistical methods with data obtained from DWAF. The flood peak determined for the period after the dams was built, was however based on a rather short record of only 16 years.

- Median particle size:

The median particle size for the period before the dam was built was estimated from particle size distribution curves of samples taken upstream of the dam (Kovacs *et al*., 1985). For the period after the dam was built the average median particle size was determined from samples taken during flood releases at Pongolapoort during 2000.

- Channel slope:

  The channel slope before the dam was built was determined from topographical maps and the slope does not seem to have changed appreciably.

- Top width and mean depth:

  The width and depth of the river before the dam was built were obtained from surveys by DWAF. For the period after the dam was built the average width was determined from aerial photographs taken in 1996. Only one depth could however be obtained for the period after the dam was built, which was determined from a surveyed cross-section 2 km below the dam (DWAF). The widths before and after the dam's construction are listed in **Appendix C1**.

The 1:10-year flood changed from 1877 m^3/s to 759 m^3/s after dam construction and the median particle size changed from 0.19 mm to 1 mm. The channel geometry of the natural river, the impacted river and the predicted values for both are summarised in **Table 3.6.1**. The ranges for the observed data given in the table indicate the natural variability of both the width and depth, as pointed out in **Section 3.3.2.2**.

Table 3.6.1 River channel geometry of the Pongola River

	Natural		
	Observed	**Calculated (eq. 3.3.17/18)**	**Calculated (eq. 3.3.22/23)**
Average width	148 m	176 m	207 m
Range (width)	83 - 343 m	-	-
Average depth	4.6 m	3.8 m	6.0 m
Range (depth)	3.7 - 5.5 m	-	-
Slope	0.0015	-	-

Table 3.6.1 continued

	After Dam		
	Observed	**Calculated (eq. 3.3.17/18)**	**Calculated (eq. 3.3.22/23)**
Average width	60 m	139 m	129 m
Range (width)	39 - 135 m	-	-
Average depth	4.7 m	2.7 m	4.9 m
Range (depth)	-	-	-
Slope	0.0015	-	-

From **Table 3.6.1** it can be seen that the average predicted values for the natural river differ only by about 17% for the regime equations developed during this project, whereas the predicted widths for the altered river differ considerably. The rather small widths observed from aerial photos 23 years after the dam was built could be a result of an almost constant release of 5 m^3/s from the dam in recent years. The constant releases could have created favourable conditions for vegetation, which could have encroached onto the river channel thereby reducing the channel width. The Domoina flood of 1984 with a peak inflow of 13 000 m^3/s, was almost completely absorbed by the dam, which was almost empty when the flood reached the dam. This means that the river reach below the dam has not experienced any large floods since the dam was built, which could also have contributed to the fact that the river channel has narrowed to such a degree.

The statistical methods (Alexander, 1990) used to determine the 1:10-year discharge for the post-dam period might not be applicable here, since the 1:10-year discharge is not very different from the 1:20-year discharge, which is 800 m^3/s. What has not been considered is the duration of the discharges. Whereas a 1:10-year flood would have maybe lasted one or two days naturally, the flood releases from the dam occurred over one week or longer, with a very different effect from a duration of only one day. The 1:10-year discharge seems to have lost it’s meaning in this case.

Evidently the methods available for predicting stable channel geometries are not very precise because they do not take into consideration all the factors that determine the channel geometry. Considering however that it is almost impossible to account for all these factors

and often very little information is available, the methods outlined in this chapter are still very valuable for natural rivers. In the case of a river affected by a dam these regime equations may be useful if the releases/spills from the dam do not differ drastically from the natural flow pattern. The regime equations are however not applicable to rivers where the flow pattern has changed drastically. In order to determine the morphological changes a river undergoes when affected by a dam, more detailed analyses are necessary.

3.7 Alternative Width Equations

Since it seems that the use of a 1:10-year flood peak, or any other flood peak calculated by means of conventional statistical methods, for predicting the resulting channel geometry is unreliable, a different approach will have to be used. More reliable results could be obtained by using basic discharges such as the mean daily flow. Williams and Wolman (1984) have done a study of the impacts of dams on a large number of North American rivers. They have found that the average width downstream of a dam can best be described as follows:

$$B_2 = 13 + 0.5Q_m + 0.1Q_p \quad \text{..... 3.7.1}$$

where B_2 = average bankfull width after dam construction (m)

Q_m = arithmetic average of annual mean daily flows since dam construction (m^3/s)

Q_p = average of annual 1-day highest average flows before dam construction (m^3/s)

A similar type of equation was sought with South African river data. The following data (**Appendix A1**) were collected for 12 rivers on which dams had been built:

- Pre- and post-dam widths (B_1/B_2) in m
- Pre- and post-dam mean annual runoff (MAR_1/MAR_2) in m^3/s
- Pre- and post-dam mean annual maximum flood peaks (Q_{a1}/Q_{a2}) in m^3/s
- Highest flood peaks for the pre- and post-dam periods (Q_{p1}/Q_{p2}) in m^3/s
- Mean annual average daily flow (Q_{ad1}/Q_{ad2}) in m^3/s

It was of course found that the width before dam construction had the biggest effect on the width after dam construction, as well as the mean annual runoff. To a somewhat lesser degree the mean annual maximum flood and the highest flood peak also play a role. The mean annual

maximum flood is significant due to its frequency, while the highest flood peak is important because of its magnitude, although it is not clear which of these two discharges is more important. Therefore the following two equations are presented, which yield very similar results, with practically the same accuracies:

$$B_2 = -3.40 + 0.856 \cdot B_1 + 0.142 \cdot MAR_2 - 0.0013 \cdot Q_{p_1} \quad \text{..... 3.7.2}$$

$$B_2 = -1.02 + 0.805 \cdot B_1 + 0.183 \cdot MAR_2 - 0.00036 \cdot Q_{a1} \quad \text{..... 3.7.3}$$

The r^2 values are in both cases 0.99, with the accuracy ranges shown in **Table 3.7.1** and the observed (aerial photographs) and predicted widths shown in **Table 3.7.2**.

Table 3.7.1 Accuracy ranges for alternative width equations

Equation	$0.67 < \frac{B_{calculated}}{B_{observed}} < 1.5$	$0.5 < \frac{B_{calculated}}{B_{observed}} < 2$	$0.33 < \frac{B_{calculated}}{B_{observed}} < 3$
3.7.2	100 %	100 %	100 %
3.7.3	100 %	100 %	100 %

Table 3.7.2 Post-dam observed and predicted widths

Dam	**River**	**Observed width (m)**	**Predicted width (m) Eq. 3.7.2**	**Predicted width (m) Eq. 3.7.3**
Albertfalls	Mgeni	27.6	24.8	26.0
Gamkapoort	Gamka	55	53.8	52.9
Gariep	Orange	255	255.9	255.3
Krugersdrift	Modder	24	22.9	24.3
Roodeplaat	Pienaars	60	59.0	54.5
Spioenkop	Thukela	36.3	43.2	43.8
Theewaterskloof	Sonderend	33	29.0	29.7
Pongolapoort	Pongola	60	59.0	62.0
(Vioolsdrif)	Orange	208	206.2	206.9

3.8 Summary

This chapter was mainly concerned with the development of regime equations for South African rivers. The concept of a dominant discharge was discussed and while many researchers equate the bankfull discharge with the dominant discharge, it seems that for South African conditions the dominant discharge will be more in line with the 1:10-year flood peak. Existing international regime equations were studied and new regime equations were calibrated with South African river data and verified against international river data. The new equations (**3.3.17** and **3.3.18**) compare favourably with international regime equations. However, these new regime equations were found to be unsuitable for rivers that are highly impacted by dams, and alternative width equations (**3.7.2** and **3.7.3**) were developed for these rivers.

With these regime equations it is possible to predict the equilibrium (stable) river width and depth. However, they do not take into considerations any temporal or spatial changes. In order to determine the sediment balance in the river, the variations in discharge and channel geometry, which influence the sediment transport, have to be known, as well as the sediment transport processes that drive these changes. These will be further discussed in the following chapters.

4. Sediment Transport

It was shown in **Section 3.6** that regime equations alone cannot adequately predict the changes in channel morphology after a dam has been built, especially if the dam has drastically altered the flow in the river. The fact is that other aspects than just the 1:10-year discharge, channel slope and particle size, play a role in determining the channel geometry, although they certainly are some of the most important aspects. The sediment transport capacity of a river, the type of sediment in a river, i.e. cohesive or non-cohesive, sediment grading and riparian vegetation all may have a large effect on the river morphology. The regime equations do not take these factors into consideration, except for the sediment size, which makes it necessary to deal with the first two aspects mentioned above in more detail. While the theory of non-cohesive sediment transport has been researched extensively, it is necessary to gain more knowledge of the initiation of motion and the sediment transport of cohesive sediments. The erosion and deposition of cohesive sediments differ significantly from those of non-cohesive sediments, and the presence of even small percentages of clay or silt in the riverbed can drastically alter the transport behaviour of the sediment (Panagiotopoulos *et al.*, 1997). Many sand-bed rivers contain some fraction of cohesive material, and a dam can cause that fraction to increase through lowering of the flood peaks, which are not able to transport the incoming sediments from downstream tributaries, causing deposition of even fine sediments.

The theory of critical conditions for the entrainment of cohesive sediments is investigated in detail in this chapter. A cohesive sediment transport theory is also developed, calibrated and verified with laboratory and field data.

4.1 Cohesive Sediment Transport Processes

Cohesive sediments are essentially mixtures containing silt and clay that possess various degrees of cohesion. The particles are small enough so that the surface physico-chemical forces become much more important than their weight, which is the determining factor in the erosion of non-cohesive sediments (Partheniades, 1971). Depending on the physical and chemical properties of the water and the composition of the fine sediments the net effect of the interparticle forces can be repulsion or attraction, where the fine particles tend to cling to

each other and to form flocs. These flocs or aggregates have much greater sizes and settling velocities than the individual particles. The growth of these aggregates is determined by the concentration, physical-chemical properties of the water-sediment mixture, as well as the flow conditions. At some stage, generally at concentrations greater than 10 000 mg/ℓ (Mehta *et al.*, 1989), the aggregates will become too big and will start to hinder each other and the settling velocity decreases rapidly. However, flocculation will probably not occur during turbulent flow and sediment transport conditions experienced in South Africa (Basson and Rooseboom, 1997) and therefore settling velocities for individual particles were used in this project. The behaviour of cohesive sediments can also be modified by the properties of the fluid (temperature, salinity) or the clay properties themselves (clay type, organic content).

4.1.1 Sand and Clay Mixtures

The presence of clay in the sediment in the bed can dramatically alter the behaviour of the sediment, depending mainly on the amount of clay present. Approximately 5 – 10% of clay minerals, by dry weight, are considered sufficient to control the soil properties (Panagiotopoulos *et al.*, 1997). With increasing clay content the sediment deposits become more plastic and swelling, shrinkage and compressibility increase. The result is that the resistance to erosion generally increases as the clay content increases, although some researchers have found that the resistance to erosion can increase with increasing sand content (Panagiotopoulos *et al.*, 1997).

Panagiotopoulos *et al.* (1997) have carried out experiments to determine the influence of clay on the erosion threshold of sand beds. They found that with clay contents less than approximately 11%, the increase in the critical threshold conditions with increasing clay content is smaller than for clay contents larger than 11%, and that the sediment mixtures with high clay contents are more difficult to erode. These observations prove again that clay contents of about 10% are enough to limit sediment erosion. Panagiotopoulos *et al.* (1997) have argued that at clay contents less than 10% the sand particles are still close enough to be in contact with each other and so pivoting is the main mechanism for the initiation of sediment motion (**Figure 4.1.1**). At higher clay contents, however, the clay particles fill the voids between the sand particles, which are no longer in contact with each other. The pivoting

mechanism is not the dominant mechanism any longer, but the erosion is instead controlled by the resistance of the clay fraction.

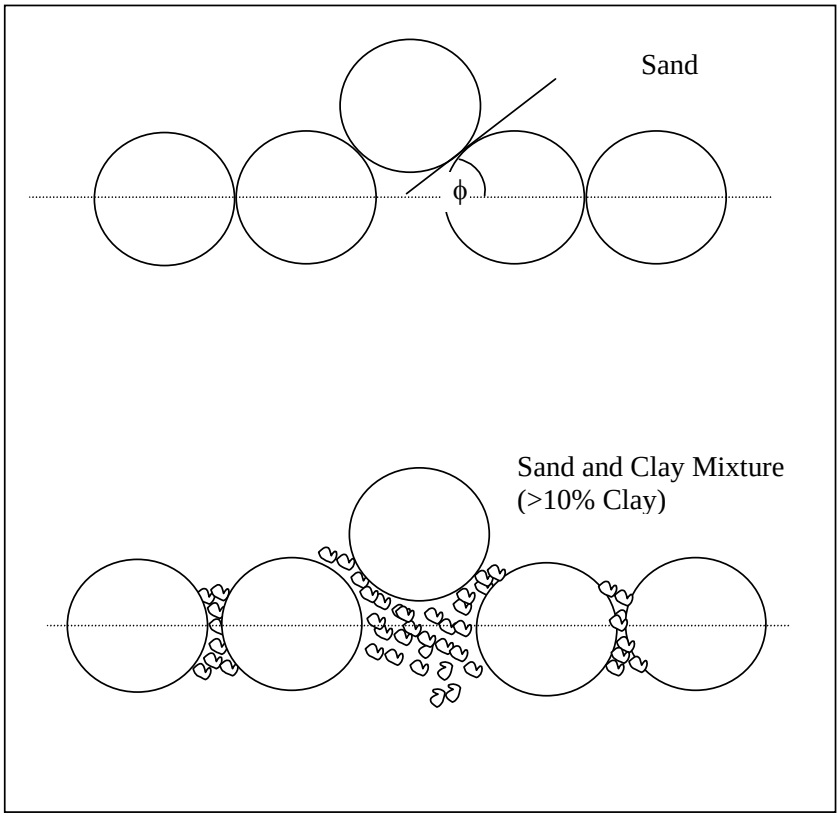

Figure 4.1.1 Mechanism for initiation of motion
(adapted from Panagiotopoulos *et al.*, 1997)

Experiments carried out by Torfs *et al.* (1994) have shown results very similar to those of Panagiotopoulos *et al.* (1997), although they also observed a transition zone between cohesive and non-cohesive behaviour. Sediment mixtures with less than 7% fines (clay and silt) behaved as non-cohesive sediments, forming ripples and dunes. The fine particles were washed out from the top layer leaving the sand behind. Sediments with higher contents of fines behaved as cohesive sediments. No bedforms were observed and very high shear stresses were needed to start erosion. For fines contents ranging between 7 and 13%, a transitional behaviour pattern was observed, exhibiting irregular bedforms.

4.1.2 Erosion

The amount and type of clay minerals, the clay properties and the physical and chemical properties of the water affect the shear stress required to erode cohesive sediments. The

erosion of cohesive sediments is also dependent on the shear strength of the bed, which is why placed beds and deposited beds have different erosion characteristics. There exist two main types of erosion:

- Surface erosion: aggregates in the surface layer are broken up and entrained.
- Mass erosion: the bulk strength of the sediment is exceeded and the plane of failure lies deep in the bed. Above that plane resuspension is almost instantaneous.

4.1.2.1 Surface Erosion

Mehta *et al.* (1989) investigated the erosion of both placed and deposited beds in order to determine the resuspension potential of cohesive sediments. The shear strength of deposited beds, which are characterised by high water contents and increasing shear strength with depth, is usually much lower than for placed beds. Placed beds, where sediments have been placed or poured into the apparatus and sometimes compacted, have a much more uniform variation of shear strength with depth and also lower water contents. The rate of surface erosion of these beds becomes nearly constant with time unlike the rate of erosion of deposited beds, which tends to become zero after a while. Parchure and Mehta (1985) have argued that in the latter case the eroded bed has reached a layer with critical shear strength equal to the applied bed shear stress. Partheniades and Paaswell (1970) reported that the ratio of strengths of the remoulded to the deposited bed was about 100:1. However, the minimum scouring shear stress was about the same for both beds. They concluded that the shear strength is not the only factor governing erosion.

4.1.2.2 Mass Erosion

Although many researchers have investigated the erosion of cohesive materials, because of the complexity of the problem many arbitrary and subjective criteria were established (Kamphuis and Hall, 1983). The critical shear stresses obtained from these studies vary greatly, with results ranging between 11.5 – 72 Pa for one project. The large variation is a result of experimental error, variation in experimental procedure, simplistic interpretation of sediment properties, and the use of different criteria for defining the onset of erosion. Kamphuis and Hall (1983) found that the critical shear stress is dependent on the amount and type of clay, water content, pH and temperature of the fluid, and the chemical composition of the pore fluid and eroding fluid.

Kamphuis and Hall (1983) conducted experiments to determine the onset of erosion of consolidated clays, investigating the effect of different consolidation pressures and clay contents. They found a linear relationship between critical shear stress and compressive strength as well as vane shear strength. The resistance to erosion increases with increasing clay content and consolidation pressure.

Basson and Rooseboom (1997) have argued that a more appropriate approach would be to use the applied stream power at the bed $\left(\tau \frac{dv}{dy}\right)_0$ instead of the critical shear stress at the bed to describe the critical conditions for erosion. It also takes the effect of increasing or decreasing roughness into account through the inclusion of the variable k_s:

$$\left(\tau \frac{dv}{dy}\right)_0 = \frac{30\rho g DS\sqrt{gDS}}{\kappa k_s} \quad \text{..... .4.1.1}$$

with ρ = density

D = flow depth

S = slope

κ = Von Kármán coefficient

k_s = absolute roughness

$\frac{dv}{dy}$ = velocity gradient

τ = bed shear stress

They assumed κ = 0.4 and $k_s = d_{50}$ (not enough data were given by Kamphuis and Hall to calculate k_s), and derived a relationship between the critical applied stream power and vane shear strength, % clay and consolidation pressure, shown in **Figure 4.1.2**. The correlation coefficient so obtained was 0.91, which is good. The assumption of $k_s = d_{50}$ is however not entirely correct, which became evident during laboratory test performed for this project, as is described later in the chapter.

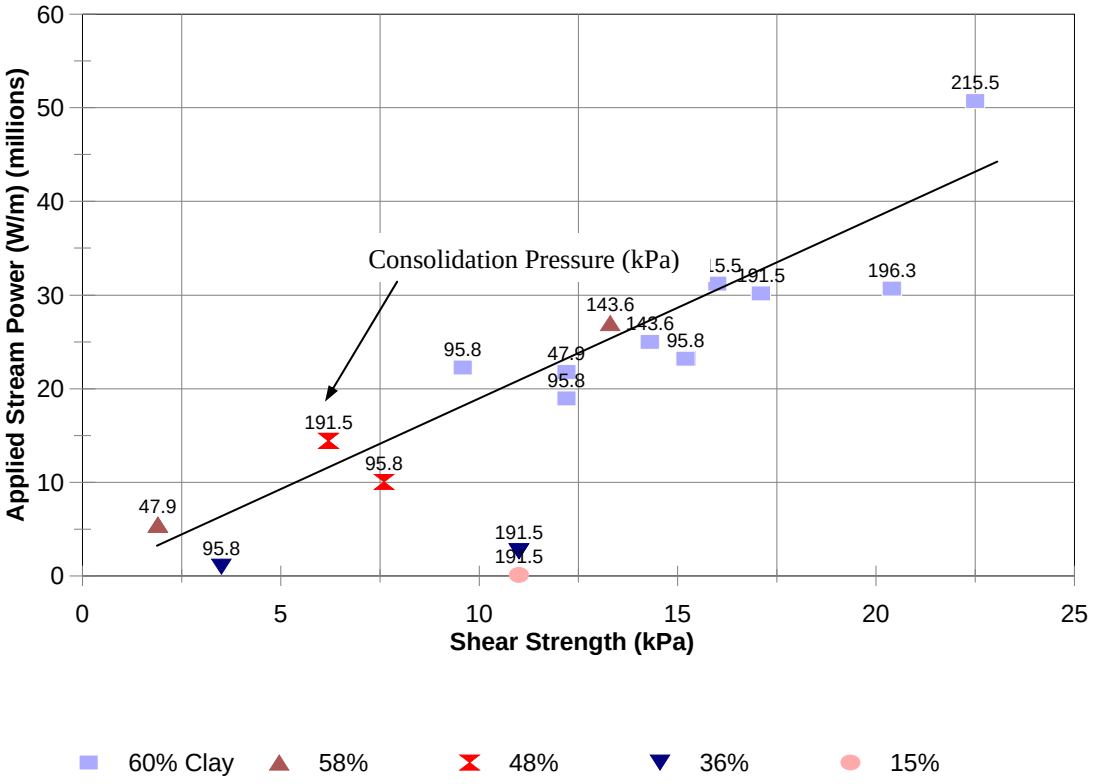

Figure 4.1.2 Correlation between critical applied stream power and vane shear strength, % clay and consolidation pressure (Basson and Rooseboom, 1997)

4.2 Equilibrium Sediment Transport

Sediments can be transported in a river as suspended load and/or bed load. The bed load is that part of the load that is moving on or near the bed, whereas the suspended load consists of particles usually finer than those found in the bed. Of the vast amount of sediment transport equations developed there are those that predict bed load, suspended load or the total load, i.e. the bedload and suspended load combined. Because of the complexity of the sediment transport processes, the sediment transport rate cannot be predicted following a purely theoretical approach. The sediment transport equations have all needed to be calibrated using either laboratory or field data, or both. This means that most equations will only yield accurate results within certain ranges or for certain conditions. The problem with the accuracy of most transport equations is also that many sediment transport processes are not fully understood yet. One problem is that most equations are derived for uniform sediments, but natural sediments are usually non-homogeneous. The approach is generally to use a

representative particle size or to model different particle sizes, each with its own sediment transport capacity. What also has to be taken into consideration is that the presence of different particle sizes can lead to bed armouring and sorting, further affecting the sediment transport. Another problem is the prediction of the transport of fine sediments (clay and silt), which is complicated by aspects such as cohesion and flocculation.

The sediment transport equations developed so far have been based on different approaches, such as shear stress, statistics and stream power. The stream power approach is explored in greater detail.

4.2.1 Stream Power Concept

The concept of stream power has been used in various forms to determine the sediment transport, such as Bagnold (1966) and Yang (1972).

Bagnold used the stream power per unit area to relate the rate of energy dissipation used in transporting sediment particles to the sediment transport capacity, with two separate components for bedload and suspended load.

Yang (1972) defined the unit stream power as the rate of potential energy expenditure per unit weight of water:

$$\frac{dY}{dt} = \frac{dX}{dt}\frac{dY}{dX} = \mathrm{v}S \quad \text{..... 4.2.1}$$

where Y = Potential energy per unit weight above a certain datum

X = longitudinal distance

t = time

vS = unit stream power

Yang argued that since the sediment transport is related to the strength of the turbulent flow conditions, the rate of total sediment transport rate or concentration should be directly related to the unit stream power. The basic form of Yang's unit stream power equation is:

$$\log(C_t) = \alpha + \beta \log(\mathrm{v}S - \mathrm{v}S_{cr}) \quad \text{.....4.2.2}$$

where C_t = total sediment concentration in ppm

α, β = coefficients

$\mathrm{v}S_{cr}$ = critical unit stream power

Yang found that both α and β are dependent on the water depth and that β is also dependent on the particle size. In 1973 Yang sought to improve on **Equation 4.2.2** through dimensional analysis. He found the following:

$$C_t = \Phi\left(\frac{\mathrm{v}S}{w} - \frac{\mathrm{v}_{cr}S}{w}, \frac{U_*}{w}, \frac{wd}{\nu}\right) \quad \text{..... 4.2.3}$$

where w = particle settling velocity

U_* = shear velocity = $\sqrt{gDS}$

ν = kinematic viscosity

d = particle size

Equation 4.2.4, which is the basic form of **Equation 4.2.3,** is very similar to **Equation 4.2.2**:

$$\log(C_t) = \alpha + \beta \log\left(\frac{\mathrm{v}S}{w} - \frac{\mathrm{v}_{cr}S}{w}\right) \quad \text{..... 4.2.4}$$

where α, β = coefficients

$\frac{\mathrm{v}S}{w}, \frac{\mathrm{v}_{cr}S}{w}$ = dimensionless unit stream power and critical unit stream power, respectively

When the concentrations are more than 100 ppm the dimensionless critical unit stream power is relatively small in relation to the value of the unit stream power and the $\left(\frac{\mathrm{v}_{cr}S}{w}\right)$ term can be excluded (Yang and Molinas, 1982).

$$\log(C_t) = \alpha + \beta \log\left(\frac{\mathrm{v}S}{w}\right) \quad \text{..... 4.2.5}$$

Based on laboratory and field measurements the coefficients α and β were determined through regression analysis. Yang's sediment transport equation for sand, including the critical unit stream power term, is as follows:

$$\log(C_t) = 5.435 - 0.286\log\left(\frac{wd}{\nu}\right) - 0.457\log\left(\frac{U_*}{w}\right) + \left(1.799 - 0.409\log\left(\frac{wd}{\nu}\right) - 0.314\log\left(\frac{U_*}{w}\right)\right)\log\left(\frac{\mathrm{v}S}{w} - \frac{\mathrm{v}_{cr}S}{w}\right) \quad \text{..... .4.2.6}$$

For concentrations of more than 100 ppm the incipient motion criterion does not play a significant role and the following equation can be used:

$$\log(C_t) = 5.165 - 0.153\log\left(\frac{wd}{\nu}\right) - 0.297\log\left(\frac{U_*}{w}\right) + \left(1.780 - 0.360\log\left(\frac{wd}{\nu}\right) - 0.480\log\left(\frac{U_*}{w}\right)\right)\log\left(\frac{\mathrm{v}S}{w}\right) \quad \text{..... 4.2.7}$$

The dimensionless critical average flow velocity can be computed as follows (Yang, 1973):

$$\frac{\mathrm{v}_{cr}}{w} = \frac{2.5}{\log\left(\frac{U_*d}{\nu}\right) - 0.06} + 0.66\,; \quad 1.2 < \frac{U_*d}{\nu} < 70 \quad \text{..... 4.2.8}$$

$$\frac{\mathrm{v}_{cr}}{w} = 2.05\,; \quad 70 \le \frac{U_*d}{\nu} \quad \text{..... 4.2.9}$$

Yang *et al.* (1996) modified **Equation 4.2.5** for use in sediment-laden flows with high concentrations of fine materials. The modifications included the particle settling velocity, viscosity and relative specific weight, with the coefficients being unchanged. The modified formula is as follows:

$$\log(C_t) = 5.165 - 0.153\log\left(\frac{w_m d}{\nu_m}\right) - 0.297\log\left(\frac{U_*}{w_m}\right)$$
$$+\left(1.780 - 0.360\log\left(\frac{w_m d}{\nu_m}\right) - 0.480\log\left(\frac{U_*}{w_m}\right)\right)\log\left(\frac{\gamma_m}{\gamma_s - \gamma_m}\frac{\mathrm{v}S}{w_m}\right) \quad \text{..... .4.2.10}$$

with:

$$w_m = w(1 - C_v)^{7.0} \quad \text{..... 4.2.11}$$

$$\nu_m = \frac{\rho}{\rho_m} e^{5.06 C_v} \quad \text{..... 4.2.12}$$

$$\rho_m = \rho + (\rho_s - \rho) C_v \quad \text{..... 4.2.13}$$

where w, w_m = particle settling velocity in clear water and sediment-laden flow, respectively

ν_m = kinematic viscosity of sediment-laden flow

ρ, ρ_m, ρ_s = specific density of clear water, sediment-laden flow and sediment, respectively

γ, γ_m, γ_s = specific weight of clear water, sediment-laden flow and sediment, respectively

C_v = suspended sediment concentration by volume

Equations 4.2.10 to **4.2.12** are however only applicable to the Yellow River, China with hyper-concentrations. For any other river with high concentrations of fine sediments these equations will have to be recalibrated.

Basson and Rooseboom (1997) argued that the applied stream power would be a more appropriate basis for determining the sediment transport, as the applied stream power is determined by basic hydraulic variables. They have developed a sediment transport equation that is based on the applied stream power $\left(\tau \frac{d\mathrm{v}}{dy}\right)$, which has been calibrated extensively with laboratory and river data:

$$C = \left(\left(\frac{\rho}{\rho_s - \rho} \right) (gDS)^{1.5} \right)^{1.969} (0.4k_s)^{-1.146} w^{-3.286} \left(\frac{k_s}{D} \right)^{0.856} \left(\frac{w}{0.4\sqrt{gDS}} \right)^{2.560} \quad \text{..... 4.2.14}$$

where C is the sediment concentration in % (by weight).

Besides **Equation 4.2.14** Basson and Rooseboom have also developed a sediment transport equation for implementation in a numerical model based on the unit input stream power approach:

$$\log(C_t) = 4.31 + 0.343 \log\left(\frac{vS}{w} \right) \quad \text{..... 4.2.15}$$

where C_t = sediment concentration in ppm

Equation 4.2.15 has been calibrated with data from a large number of South African reservoirs for flood flushing and storage operations, which means that it has been calibrated with fine sediment fractions. **Equation 4.2.15** may however not be applicable to rivers because it has been calibrated on reservoir data, which were obtained under non-uniform flow conditions, unlike river or laboratory data.

Equations 4.2.6 and **4.2.7**, as well as **Equation 4.2.14** give excellent results for a wide range of particle sizes; however, they do not extend to finer particles in the clay and silt range. Yang's attempt to modify his original transport equation for sediment- laden flow with high concentrations of fine materials is only partially successful, since his equation is only applicable to the Yellow River and also dependent on the suspended sediment concentration. **Equation 4.2.10** gives the total sediment concentration, i.e. bedload and suspended load combined, but before the equation can be used the suspended sediment concentration must be known. In very few cases is it known how much sediment is carried in a river at a given flow rate. This makes **Equation 4.2.10** difficult to apply, even when calibrated for different rivers. But the unit input stream power concept is still one of the best approaches to describe sediment transport because it can be theoretically derived and it is dimensionally homogeneous. The unit input stream power approach will therefore be used to develop a sediment transport equation, in the form of **Equation 4.2.5**, for fine sediments.

4.3 Laboratory Flume Studies

The objective of the experiments was to obtain hydraulic and sediment data on non-cohesive and cohesive sediments at equilibrium, as well as mixtures of cohesive and non-cohesive sediments, to determine the effect of fine sediment on the hydraulic and sediment transport characteristics. The data obtained were used to describe critical conditions for mass erosion of cohesive sediments, as well as to calibrate a sediment transport equation for fine sediments.

4.3.1 Equipment

The experiments were carried out in the Hydraulics Laboratory at the University of Stellenbosch in a recirculating flume (0.6 m wide, 1.5 m deep and 17 m long) and return pipe (∅ 150 mm) system as shown in **Figure 4.3.1**. The flow rate could be varied from 0 to 100 ℓ/s by adjusting both the variable speed pump and the two valves. The slope of the flume was adjustable and baffles were placed at the entrance of the flume to ensure energy dissipation and a uniform flow rate at the entrance. The sampling point for suspended sediments was located on the return pipe to ensure that sediment and water were completely mixed.

Velocities were determined with the use of an electromagnetic VERIFLUX VAC 0.075 kW flow meter installed on the return pipe. Readings were taken with the aid of the VERIFLUX Series 2-2 Converter (**Figure 4.3.2**). The velocities are determined as follows:

$$v_p = \frac{A \cdot B}{10} \quad \text{..... 4.3.1}$$

where A, B = readings from the converter

v_p = velocity in return pipe (m/s)

The types of sediments that were used, are summarized in **Table 4.3.1**, and the gradings shown in **Figure 4.3.3**. The cohesive - non-cohesive mixtures were obtained by combining certain percentages (by weight) of sand and clay. The following fine contents (< 0.03 mm) were aimed at: 10%, 20%, 60% and 80%, but the actual mixtures are shown in **Table 4.3.1**.

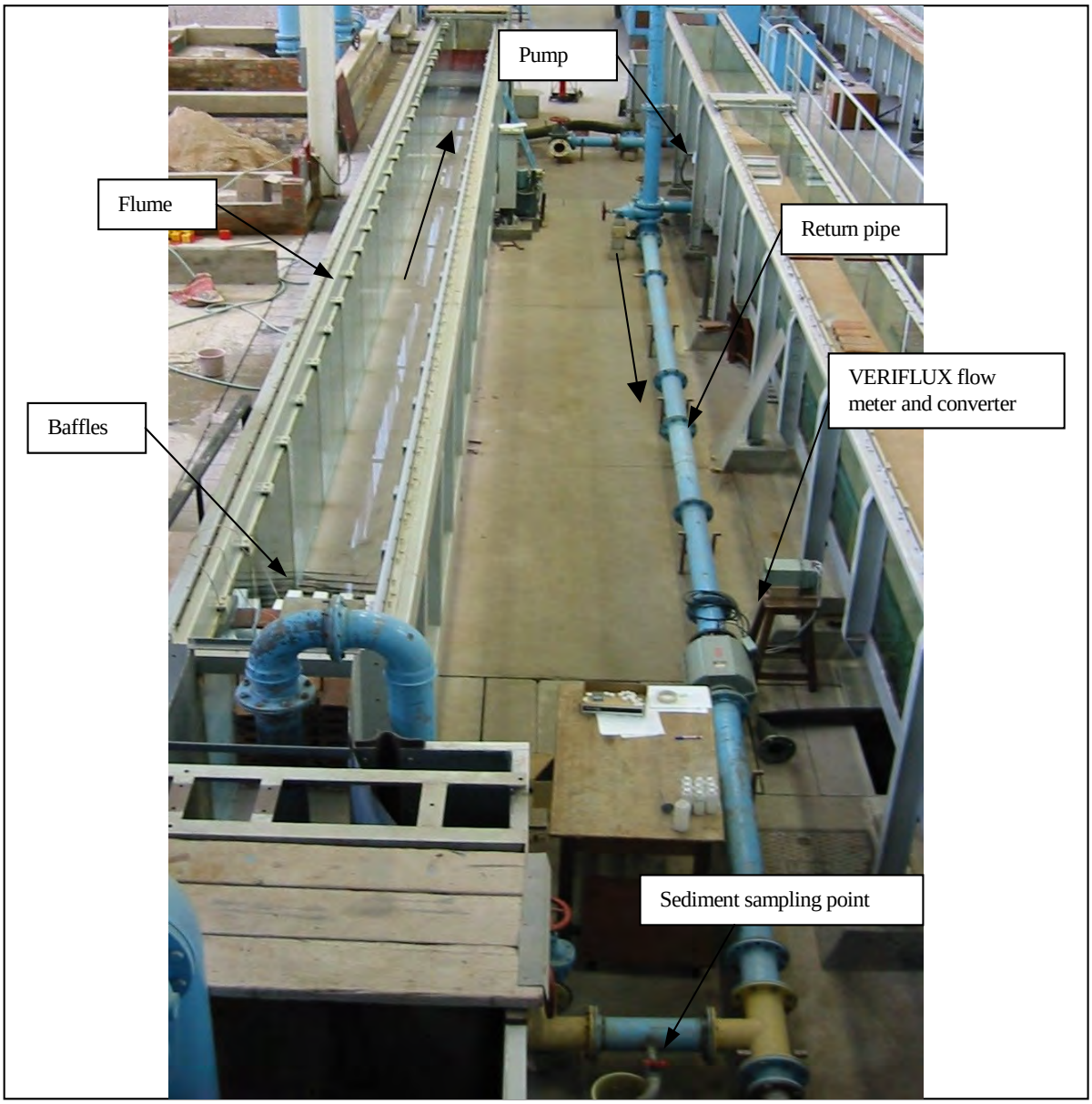

Figure 4.3.1 Layout of laboratory system

Table 4.3.1 Sediment types

Sediment Type	Median Particle Diameter (mm)
Sand	0.12
Clay: 88% Fines	< 0.001
Mixture 1: 77% Fines	< 0.001
Mixture 2: 54% Fines	0.017
Mixture 3: 20% Fines	0.105
Mixture 4: 7% Fines	0.11

Figure 4.3.2 VERIFLUX flow meter and converter

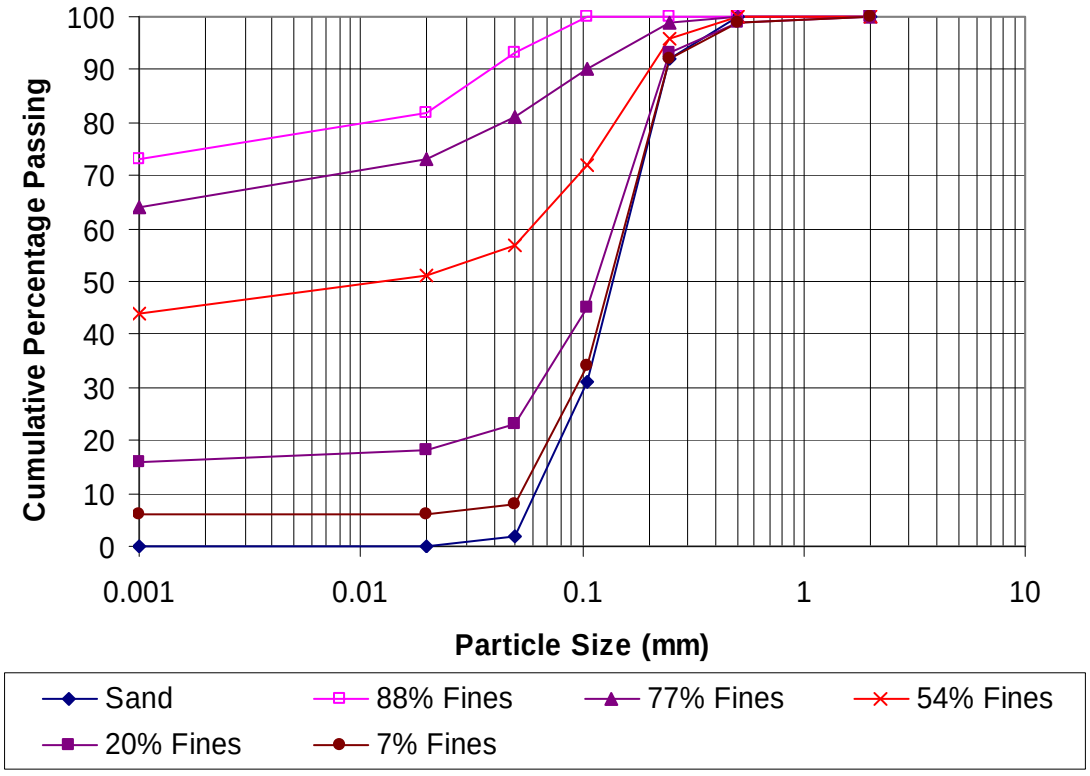

Figure 4.3.3 Particle size distribution curves

The shear strength of the sediment was determined through the use of the vane shear test. The densities were determined with the aid of a TROXLER moisture-density gauge (Model 3411-B), shown in **Figure 4.3.4,** after draining the water from the flume. Density measurements were performed by utilizing a radioactive source and gamma ray detectors.

Figure 4.3.4 TROXLER moisture-density gauge

4.3.2 Laboratory Procedure

For all the experiments the basic procedure was to recirculate a given water-sediment mixture in the flume at a preset slope until equilibrium conditions were reached. The following conditions had to be satisfied for equilibrium to be considered as established:

- Sand: the average water surface slope and the bed slope were found to have remained constant and parallel, and the bed configuration was consistent throughout the test section, both with respect to time.

- Clay and clay/sand mixtures: the average energy slope remained constant with respect to time, and the suspended-sediment concentration was observed to be constant.

The different procedures for the different sediments were as follows:

♦ **Sand:**

The slope of the flume was adjusted to 1:500, and the sand was allowed to reach its equilibrium bed slope. A 150 mm layer of dry sand was then placed in the flume by hand, levelled as best as possible and clear water was slowly added without disturbing the sediment. The runs were started at a low flow rate and measurements were taken at various time intervals until equilibrium was reached. For the first seven runs the flow rate was increased each time, with the bed forms changing from ripples in run 1 up to antidunes in runs 6 and 7. Run 8 was added to obtain more data in the dunes range. The time it took each run to be completed varied from 2.5 to 18 hours, depending on the bed configuration. Runs 6 and 7 took the least time because of the high rates of erosion.

♦ **Clay and clay/sand mixtures:**

The slope of the flume was adjusted to 1:20 000 and a 170 mm layer of dry pottery clay was placed in the flume by hand, levelled as best as possible and clear water was added without disturbing the clay too much. The clay was then left to consolidate for four days, and then the water was pumped at a high flow rate so that most of the clay could erode, after which the clay was allowed to deposit again whilst the water was still flowing. The clay was allowed to consolidate for one, four and seven days, respectively, under saturated conditions and then the runs were again started at a very low flow rate. The same measurements were taken as for the sand, except at shorter time intervals, as each run only took 2 to 3 hours. After equilibrium was reached the flow rate was immediately increased for the next run, allowing for three to four runs each day. The pump was not allowed to run throughout the night and to ensure continuity throughout all runs, the flow rate was raised in steps to the desired flow rate at the start of the second and following days, to make sure that the same conditions were present as at the end of the previous day. The experiments ended when the erosion changed from surface to mass erosion. Mass erosion was defined as that stage at which the bed started to exhibit noticeable scouring throughout the whole test section. An additional test was carried out on clay that was left to dry for 35 days. For this experiment an open flow system was used in order to reach higher velocities than could be obtained with the closed pump system.

For the mixtures, about two-thirds of the clay was removed from the flume and certain amounts of sand were added and mixed by hand. The mixtures were then left to consolidate for four days under water and the same procedures were followed as for the clay alone. In order to compare all the runs, more or less the same flow depths and flow rates were used for each mixture, and the runs with the same flow rate and flow depth given the same numbers. In **Appendix B1/2** the runs with the same numbers for the mixtures and the clay are therefore directly comparable. Because the data obtained for the first few runs of each experiment varied very little, it was decided to leave out some of the lower flow rates and to add higher flow rates for the mixtures containing larger amounts of sand.

The following data were determined for all sediments:

- Average water surface slope S_w
- Average bed slope S_o
- Average depth of flow D
- Water discharge Q
- Suspended-sediment concentrations C
- Water temperature T
- Particle size distribution of sediment
- Particle settling velocity w

The water surface and bed level were measured at 1 m intervals along a 10 m test section, which was chosen to exclude all entrance and exit influences. The flow depth was determined from the difference between water surface and bed levels, and the discharge was obtained from the velocity meter, which had been installed in the pipe:

$$Q = A\mathrm{v}_p \quad \text{..... .4.3.2}$$

where Q = discharge

v_p = velocity in return pipe

A = cross-sectional area of pipe

Suspended-sediment samples were taken at the start and end of each run and the temperatures were recorded to the nearest half degree Centigrade. The particle size distributions were

determined from samples taken from the bed before and after each experiment to determine any changes in bed material.

From the measured data the following variables were computed:

- Average energy slope S_f: The energy slope was determined from the energy equation:

$$z_1 + h_1 + \frac{v_1^2}{2g} - z_2 - h_2 - \frac{v_2^2}{2g} = h_f \quad \text{..... 4.3.3}$$

$$S_f = \frac{h_f}{L} \quad \text{..... 4.3.4}$$

where z_1, z_2 = elevation above arbitrary datum

h_1, h_2 = flow depths

v_1, v_2 = mean flow velocities

h_f = friction losses between sections 1 and 2

L = distance between points 1 and 2

- Mean velocity v: The mean velocity was determined from the observed values of discharge Q, depth D and width B of flume by means of the continuity equation:

$$v = \frac{Q}{DB} \quad \text{..... 4.3.5}$$

- Shear stress at bed τ: The shear stress at the bed was calculated as follows:

$$\tau = \rho g D S_f \quad \text{..... 4.3.6}$$

- Froude number Fr: The Froude number was calculated from the formula:

$$Fr = \frac{v}{\sqrt{gD}} \quad \text{..... 4.3.7}$$

- Absolute roughness k_s: The resistance factor was determined from Chezy's resistance formula:

$$k_s = \frac{12D}{10^{\frac{\nu}{18\sqrt{DS}}}} \quad \text{.....} \quad 4.3.8$$

- Particle settling velocity w: The settling velocity was calculated from the following two equations:

For $d < 0.1$ mm (Stokes range): $$w = \frac{1}{18}\frac{(\rho_s - \rho)gd^2}{\nu\rho} \quad \text{.....} \quad .4.3.9$$

For $0.1 < d < 1$ mm (Zanke, 1977): $$w = 10\frac{\nu}{d}\left(\sqrt{1 + \frac{0.01(s-1)gd^3}{\nu^2}} - 1\right) \quad \text{.....} \quad 4.3.10$$

Since non-uniform sediments were used for some of the experiments the effective settling velocities were calculated as the summation of the settling velocities for certain particles sizes w_i (**Table 4.3.2**) according to their proportion p_i (by mass) in the sediment grading curve:

$$w = \sum p_i w_i \quad \text{.....} \quad 4.3.11$$

Table 4.3.2 Particle size ranges

Particle Size Range (mm)
2 –0.5
0.5 – 0.25
0.25 – 0.106
0.106 – 0.05
0.05 – 0.02
0.02 – 0.002
< 0.002

4.4 Analysis of Results

The laboratory results (**Appendix B1 - B3)** show that as the clay content decreased the sediment did not exhibit any non-cohesive behaviour until the fines content was only 20%. At that point some irregular bedforms appeared towards the end of that series of runs (**Figure 4.4.1**). These took a few hours to develop throughout the flume, whereas the bedforms of the sand alone developed almost immediately throughout the test section. During the tests done on the sediment with 7% fine content, larger dunes and ripples appeared (**Figure 4.4.2**). These sometimes did not develop throughout the whole test section, and generally took more than a day to stabilize. At the end of this set of runs the bed also did not display scouring as experienced during the tests with higher fine contents, with a rough uneven surface, but rather a smooth flat bed developed, as evident during the transitional phase of the experiments on the sand alone.

Figure 4.4.1 Irregular bedforms after the flume was drained (20% clay and silt content)

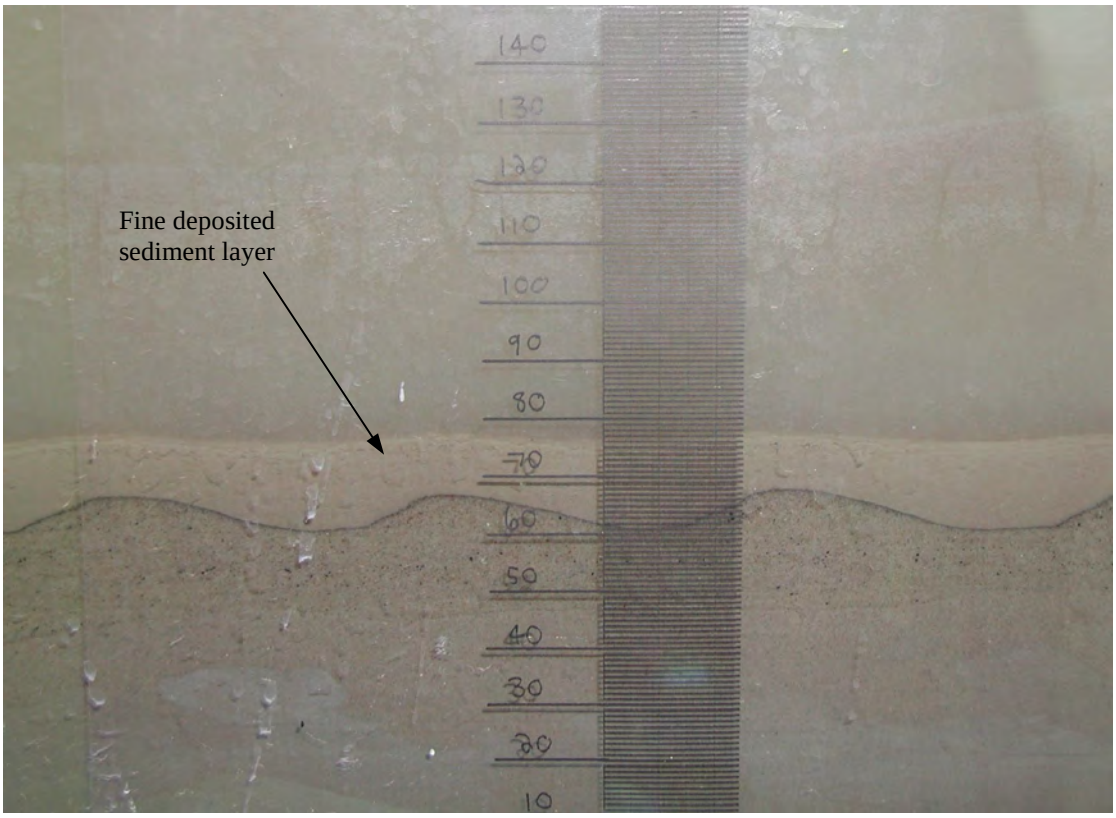

Figure 4.4.2 Bedforms developed during runs made with 7% clay and silt content (fine deposited layer developed after runs were stopped)

The bedforms that developed with 7 and 20% fines content seemed to develop on top of the original mixed layer (**Figure 4.4.3**). There was a noticeable difference in the composition of the bedforms and the lower mixed layer, in that the bedforms seemed to be entirely made up of sand. This together with the fact that the suspended sediments were made up almost entirely of fine materials means that instead of transporting the same fractions of particle sizes as present in the bed, the finer sediments were washed out and only a small fraction of the coarser material was transported. The sediment transport of graded sediment therefore seems to be based on the sediment transport capacity of each fraction.

In order to induce mass erosion for the dried clay (**Figure 4.4.4**), higher velocities were expected than for any of the other experiments. However, during the drying the clay had detached from the floor of the flume and when the tests were run water managed to get between the clay blocks and the floor thereby lifting the clay blocks up and washing them away much quicker than expected.

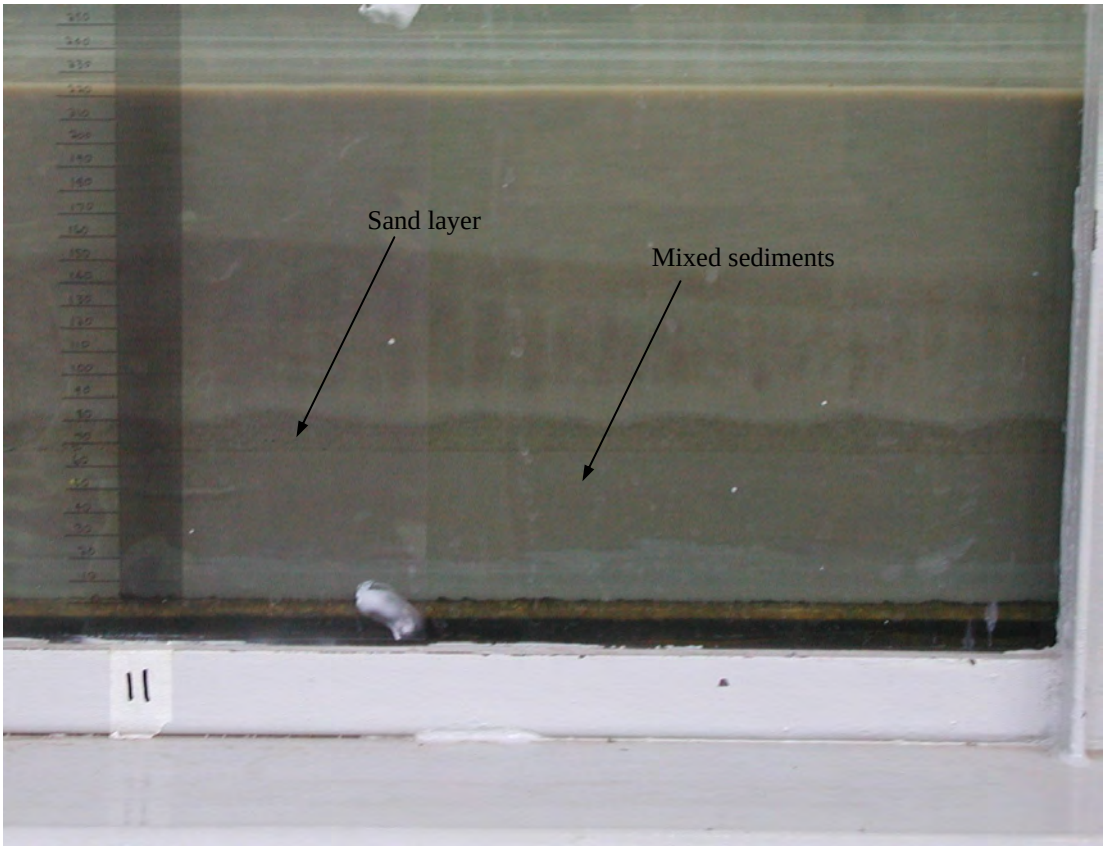

Figure 4.4.3 Layers of sediment developed during runs with 7% clay and silt content

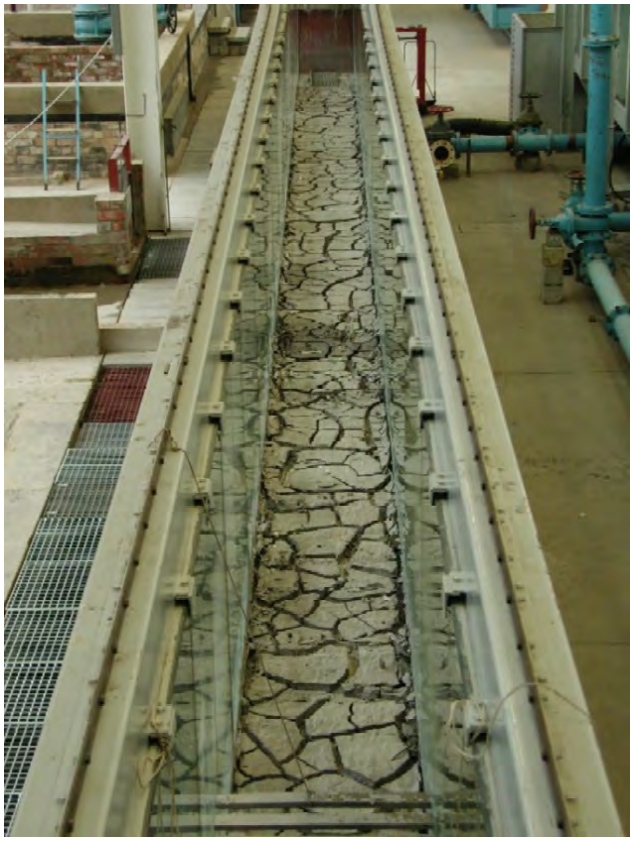

Figure 4.4.4 Dried clay in flume

The fact that fines contents of 7% and greater can dominate the erosion behaviour of sediments can also be seen from **Figure 4.4.5**, which shows the correlation between applied stream power and clay content. The points represent the series of runs made for each of the six sediments (with a consolidation time of four days).

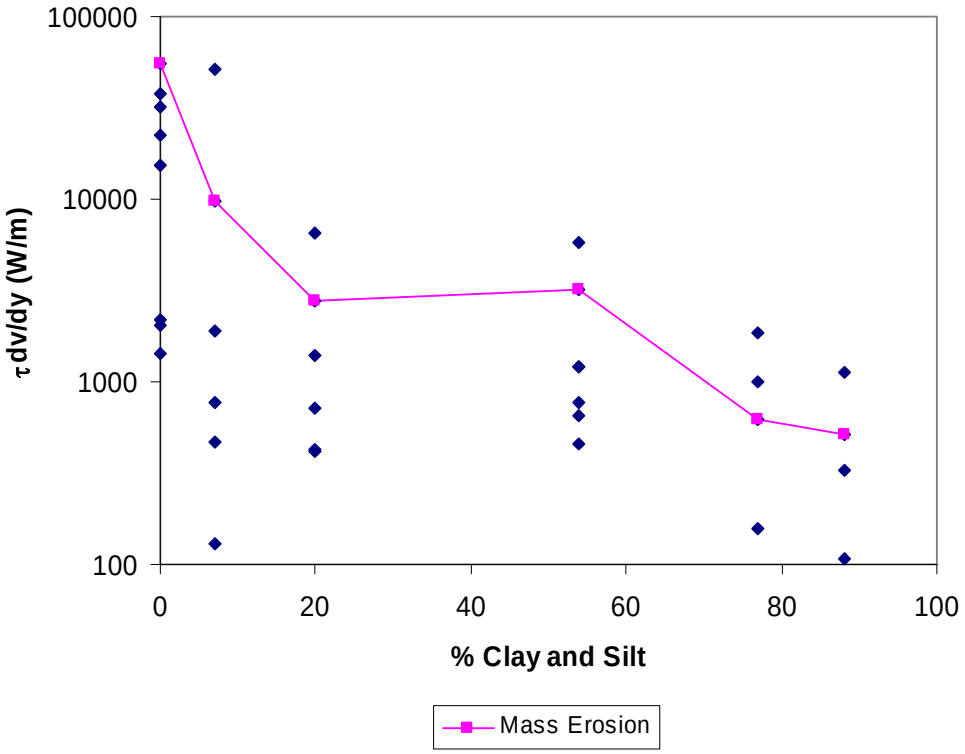

Figure 4.4.5 Correlation between applied stream power and fine particle content (consolidation time – four days)

To be able to compare the mass erosion states of the various sediments, an equivalent state had to be defined for the non-cohesive sediments. Since relatively large amounts of sediments are transported and there is an almost immediate change to a smooth flat bed for the transition phase of non-cohesive sediments, this state was chosen. The solid line in **Figure 4.4.5** connects the points indicating mass erosion. There appear to be two points of change, which divide the graph into three regions. The first occurs with between 7 and 20% fines content, which is where the clay and silt start dominating the erosion pattern of the sediments. The second change occurs between 54 and 77% clay and silt. This could be a point where there is enough sand present to affect the erosion through armouring.

The differences in erosion behaviour between the different consolidation times for the saturated clay were not very noticeable while the experiments were running, but some

differences became apparent during the analysis of the results as discussed in the following section.

4.4.1 Critical Conditions for Mass Erosion

Kamphuis and Hall (1983) and Torfs *et al.* (1994) amongst others have defined the critical conditions for erosion of cohesive sediments in terms of the critical shear stress or critical velocity. **Figure 4.4.6,** however, shows that the critical shear stress ρgDS may not be a clear indicator for mass erosion. Generally the critical shear stress τ_{cr} increases with increasing clay content, which is true for up to 54% clay content, after which the critical shear stress decreases dramatically. This could be due to the fact that the critical shear stress is highly susceptible to even small changes in both depth and slope. During the experiments the slope was difficult to determine accurately because it was so small and also because of water surface fluctuations.

The fact that the critical shear stress is only dependent on the depth and slope is one of the reasons to consider the use of the applied stream power $\left(\tau \frac{d\mathrm{v}}{dy}\right)_0$ at the bed to describe the critical conditions for erosion (**Figure 4.4.7**).

$$\left(\tau \frac{d\mathrm{v}}{dy}\right)_0 = \frac{30\rho gDS\sqrt{gDS}}{\kappa k_s} \quad \text{..... .4.1.1}$$

The applied stream power takes into consideration the effect of roughness, which is an important parameter in sediment transport (Basson and Rooseboom, 1997).

Basson and Rooseboom (1997) have used Kamphuis and Hall's data to develop a relationship between the applied stream power and the shear strength, % clay and consolidation pressure. They assumed $k_s = d_{50}$, since k_s could not be determined from the Kamphuis and Hall data. The roughness values determined from the flume experiments are however much greater than the mean particle size, especially when the fine particle contents were substantial (**Table 4.4.1**).

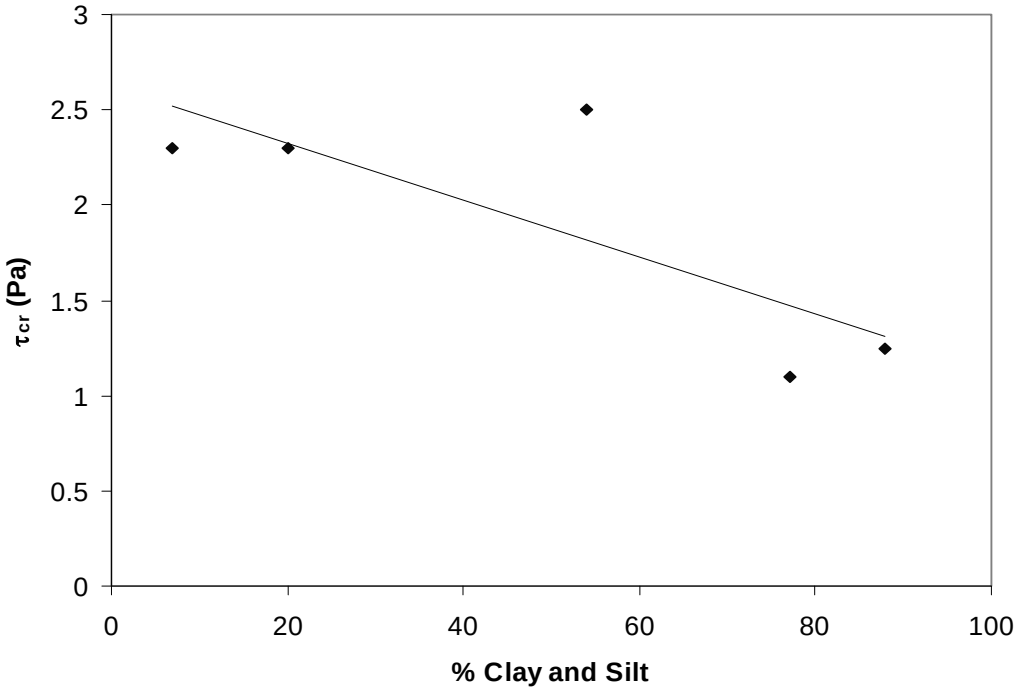

Figure 4.4.6 Correlation between critical shear stress and fine particle content

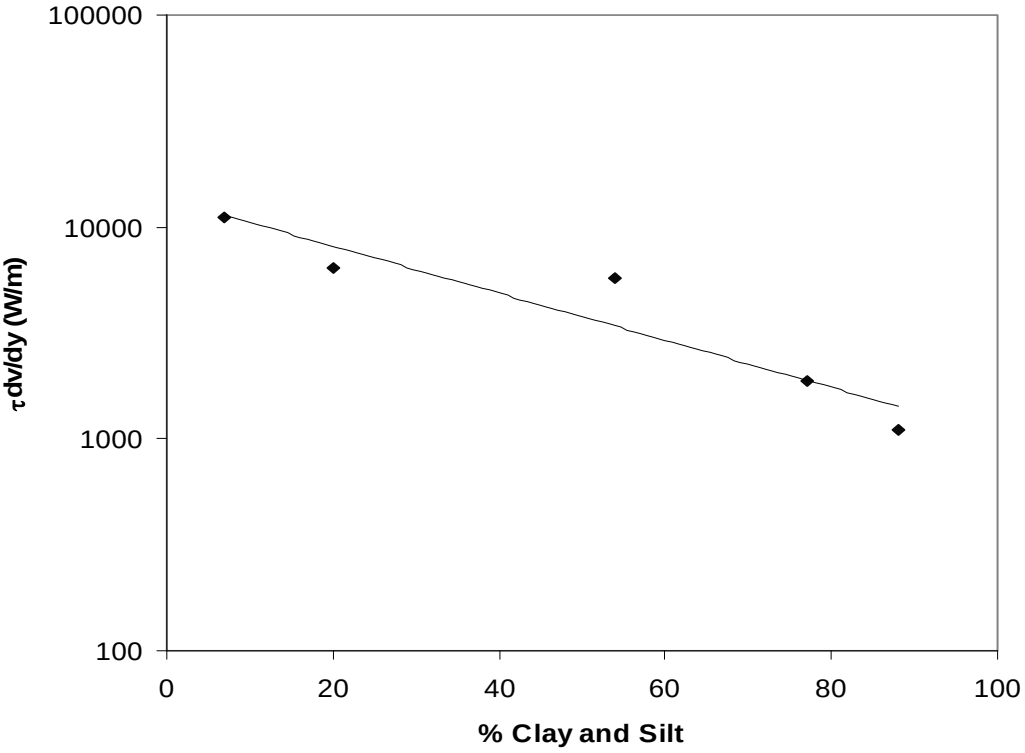

Figure 4.4.7 Correlation between applied stream power and fine particle content (mass erosion only)

Table 4.4.1 Variation of absolute roughness with % clay and silt, and d_{50}

k_s (m)	d_{50} (mm)	% Clay and silt
0.003	< 0.001	88
0.0014	< 0.001	77
0.0016	0.017	54
0.0013	0.105	20
0.0001	0.11	7
0.076	< 0.001	88 (dried)

The consolidation pressure is also not as easily obtainable as the sediment density, which is also an indicator for the amount of consolidation. In this project, therefore, a relationship was sought between the applied stream power and the shear strength, clay and silt content, and sediment density. However, from **Figures 4.4.7** to **4.4.9** it can be seen that there only exists a definite relationship between the applied stream power and the clay and silt content, which illustrates a decrease in the applied stream power necessary to induce mass erosion with an increasing clay and silt content. This is contrary to most theories that argue that higher fine material contents will offer greater resistance to erosion, due to the cohesive properties of the particles. On the other hand greater amounts of sand may very well hinder the erosion process through armouring, which seems to have occurred during the laboratory experiments done for this project. The relationship between the density and the applied stream power is not clearly defined and there does not seem to be any relationship between the applied stream power and the vane shear strength.

The effect that the time of consolidation has on the both the applied stream power and critical shear stress is illustrated in **Figures 4.4.10** and **4.4.11**. As one expects, there is a general trend of increasing critical shear stress and increasing applied stream power necessary to induce mass erosion with increasing consolidation time.

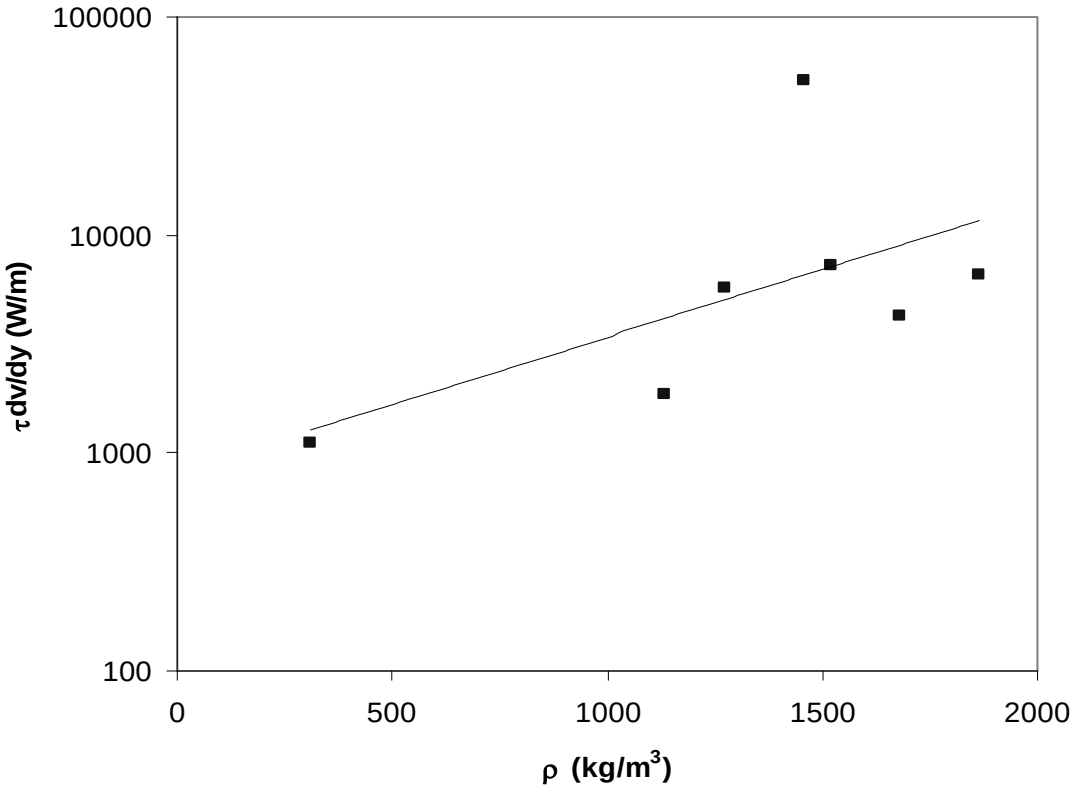

Figure 4.4.8 Correlation between applied stream power and dry density

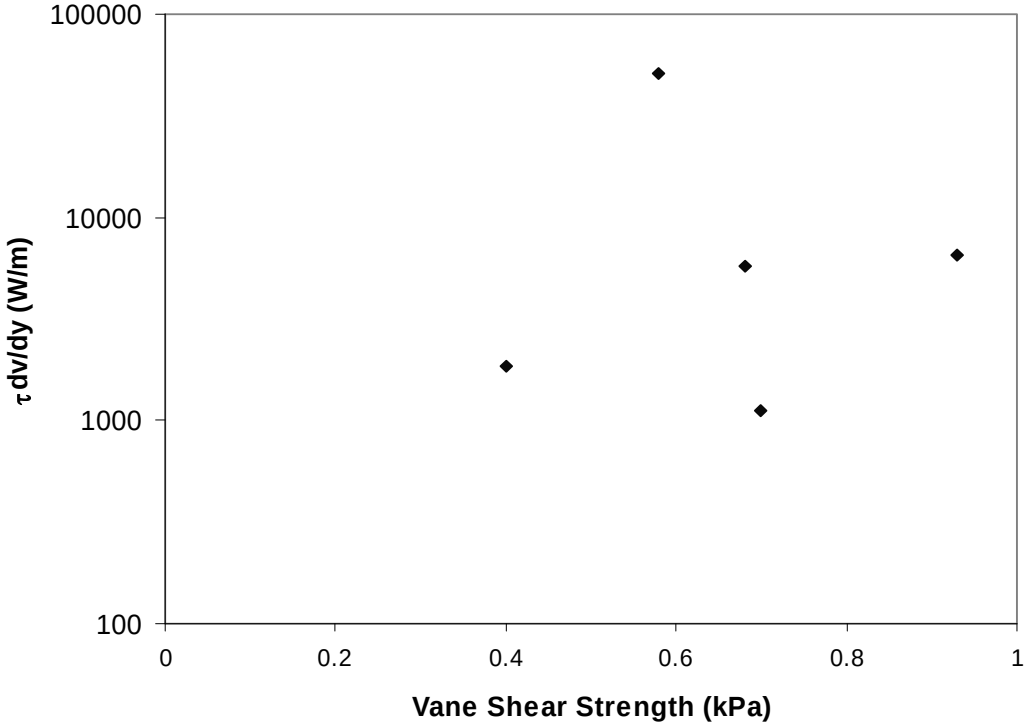

Figure 4.4.9 Correlation between applied stream power and shear strength

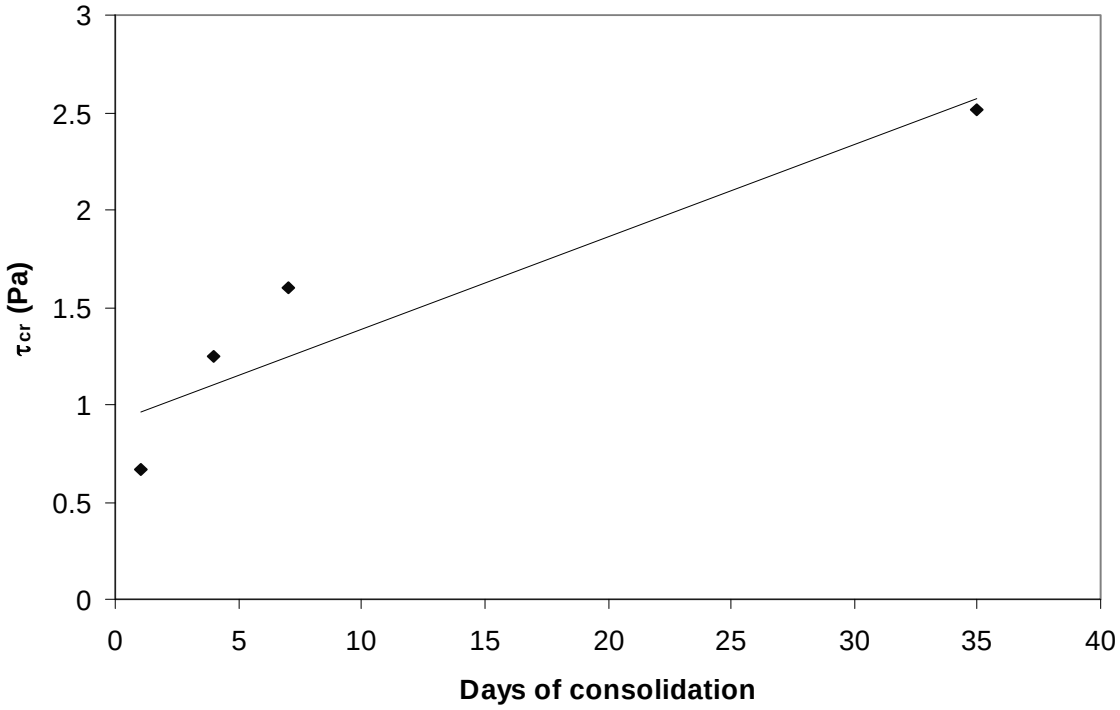

Figure 4.4.10 Correlation between critical shear stress and consolidation time

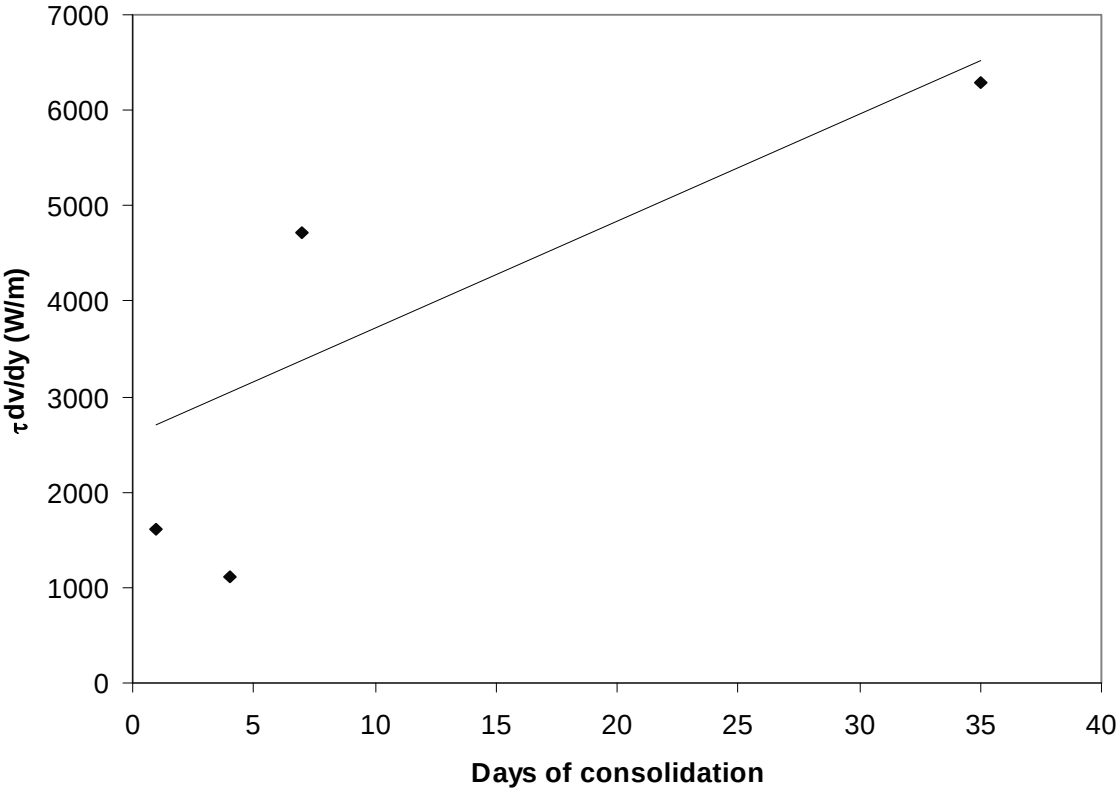

Figure 4.4.11 Correlation between applied stream power and consolidation time

The fact that no clear relationships could be found between the applied stream power and the density or vane shear strength could be a result of the fact that the measurements of these two properties could not be done accurately because the equipment could not operate properly under the conditions under which the experiments were carried out. Both the high humidity levels in the laboratory and the walls of the narrow flume affected the readings.

For this reason only a relationship between the clay and silt content and the applied stream power should be considered. By taking $\kappa = 0.4$ it is possible to derive **Equation 4.4.1** through regression analysis, relating the critical applied stream power to the clay and silt content.

The applied stream power can be calculated as follows:

$$\left(\tau \frac{dv}{dy}\right)_0 = 60674P^{-0.777} \quad \text{..... 4.4.1}$$

where P = percentage of clay and silt

The coefficient of determination r^2 is 0.76, which is rather good (see **Figure 4.4.12**), but more data will be necessary to develop a reliable relationship for general use. Additional data could also help determine whether there do exist relationships between the applied stream power and the density as well as the shear strength. Kamphuis and Hall (1983) have argued that the onset of erosion could be related to various soil properties such as the clay content and consolidation pressure. As mentioned before they found through their experiments that there exists a linear relationship between the critical shear stress and the compressive strength as well as vane shear strength.

Even though the relationship between density and applied stream power did not become apparent during these experiments, there is a definite correlation between the applied stream power and the time of consolidation. The density generally increases with increasing consolidation time, and therefore a relationship should exist between the applied stream power and both the percentage clay and silt, and the density. A relationship between these three variables could therefore be as follows:

$$\left(\tau \frac{d\mathrm{v}}{dy}\right)_0 = 182 \cdot P^{-0.472} \cdot \rho^{0.685} \quad \text{.....} \quad .4.4.2$$

Equations 4.4.1 and **4.4.2** provide a methodology by which the critical conditions for mass erosion of cohesive sediments and cohesive/non-cohesive mixtures can be described in terms of the applied stream power at the bed.

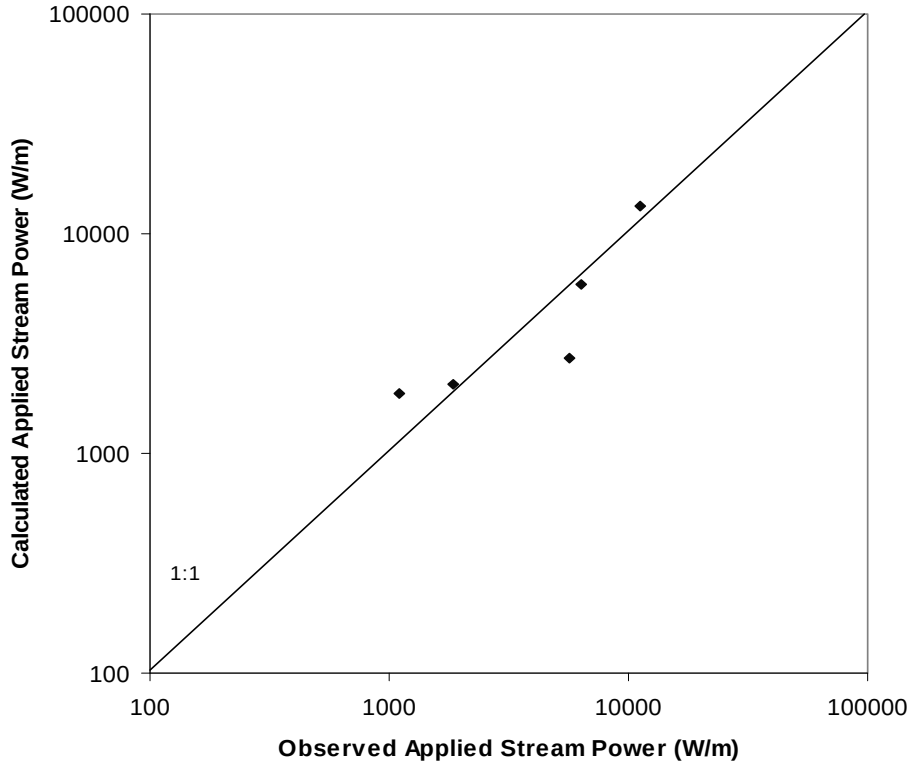

Figure 4.4.12 Observed versus calculated critical applied stream power for mass erosion

4.4.2 Evaluation and Calibration of Sediment Transport Equations for Fine and Non-Cohesive Sediments

In addition to the data obtained from the experiments, data sets from other researchers were also used for the calibration and verification process. One data set, compiled by Guy *et al.* (1966), was used to supplement the limited sand data that was obtained during this project because the experiments were mostly done on cohesive sediments. From the data set of Guy *et al.* only the data for concentrations greater than 100 mg/ℓ were used, because all of the

concentrations obtained during laboratory experiments done for this project were also greater than 100 mg/ℓ, and the critical unit stream power $\left(\frac{\mathrm{v}_{cr}S}{w}\right)$ is negligible (Yang and Molinas, 1982). The data of Guy *et al.* and the laboratory data were used to calibrated the following sediment transport relationship:

$$\log(C_t) = \alpha + \beta \log\left(\frac{\mathrm{v}S}{w_s}\right) \quad \text{..... 4.2.5}$$

In **Equation 4.2.5** the effective settling velocity w_s was determined for the particles found in suspension. For the sediment mixtures this was found to be predominantly clay and silt with median particle diameters of less than 0.001 mm. The gradings are shown in **Appendix B4**.

4.4.2.1 Calibration

Figure 4.4.13 shows the relationship between the dimensionless input stream power $\frac{\mathrm{v}S}{w}$ and the sediment concentrations for both the laboratory data obtained during this project as well as data from Guy *et al.*, which represents a data set of 305 observations. The calibrated sediment transport equation has a coefficient of determination of 0.75 and is shown in **Figure 4.4.14**:

$$\log(C_t) = 4.472 + 0.978 \log\left(\frac{\mathrm{v}S}{w_s}\right) \quad \text{..... .4.4.3}$$

with C_t = suspended sediment concentrations (mg/ℓ)

In **Figure 4.4.14** it can be seen that the data lie in two slightly different regions, with the data associated with clay and silt situated slightly lower on the graph and at a different slope. This would explain the relatively low coefficient of determination. The divergence occurs because of the difference in the particle sizes that are in suspension. For the sediments containing at least 7% clay and silt, most of the suspended sediments were found to be predominantly clay and silt, whereas for sediments with less than 7% fine particles most of the suspended sediment was sand. There are two ways to overcome that problem. One would be to separate the settling velocity as a term from the dimensionless input stream power term. The second

option would be to separate the data associated with clay and silt form the non-cohesive data, and to calibrate two sediment transport equations.

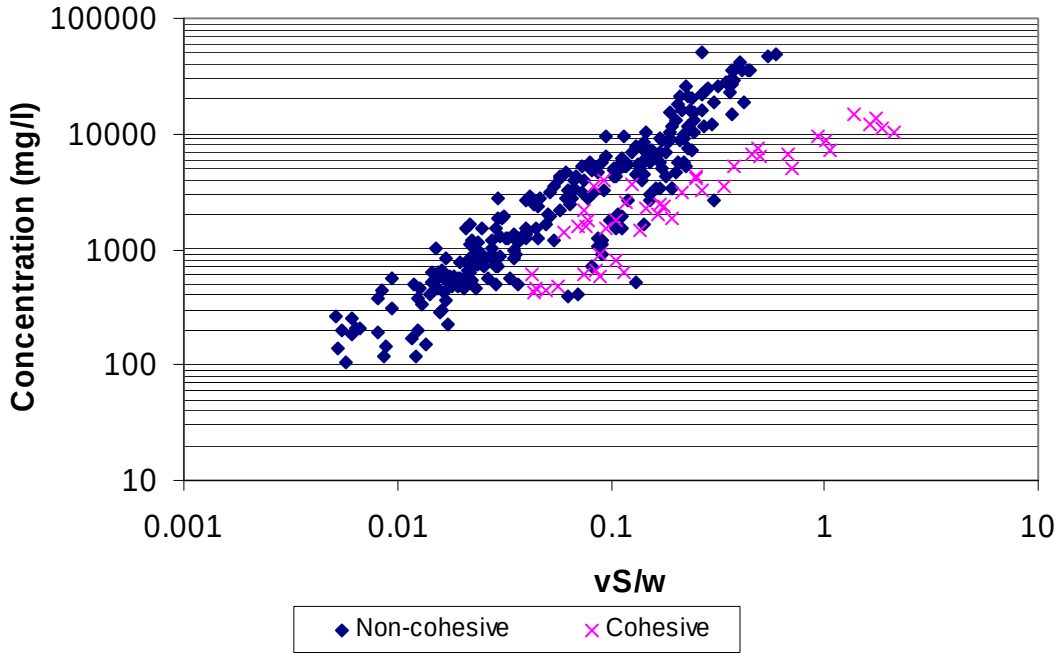

Figure 4.4.13 Correlation between dimensionless unit stream power and concentration for both cohesive and non-cohesive sediments

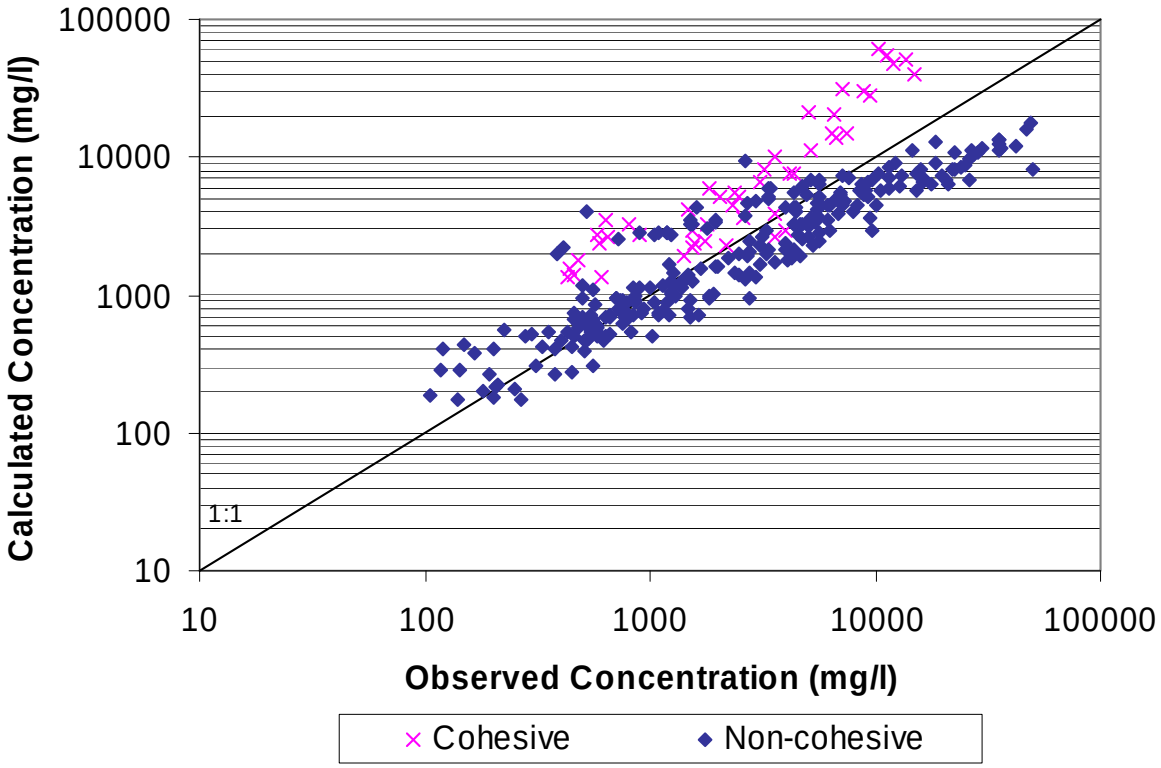

Figure 4.4.14 Calibration of sediment transport equation for both cohesive and non-cohesive sediments

a) Calibration of sediment transport equation with settling velocity as a separate term

The calibrated equation has a relatively good coefficient of determination (0.84) and is as follows (see also **Figure 4.4.15**):

$$\log(C_t) = 5.038 + 1.14\log(\mathrm{v}S) - 0.853\log(w) \quad \text{.....4.4.4}$$

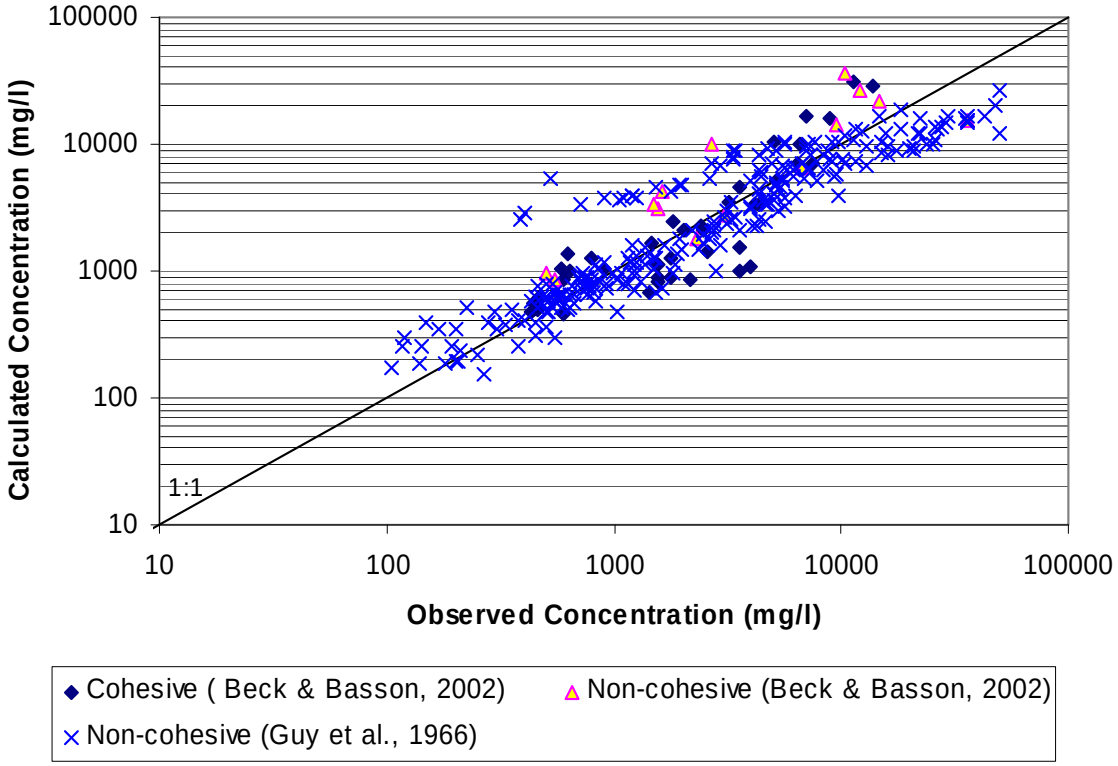

Figure 4.4.15 Calibration of sediment transport equation for both cohesive and non-cohesive sediments (with separate settling velocity term) (Equation (4.4.4))

b) Calibration of two separate equations

For cohesive sediments the effective settling velocity of the materials in suspension was determined from the particle size distribution curve of the suspended sediments. The same particle size ranges were used as shown in **Table 4.3.2**. The effective particle size for the suspended sediments was found to be 0.025mm. **Equation 4.4.5** has only been calibrated for that effective particle size. The correlation is illustrated in **Figure 4.4.16**.

$$\log(C_t) = 3.964 + 0.812\log\left(\frac{\mathrm{v}S}{w_s}\right) \quad \text{..... 4.4.5}$$

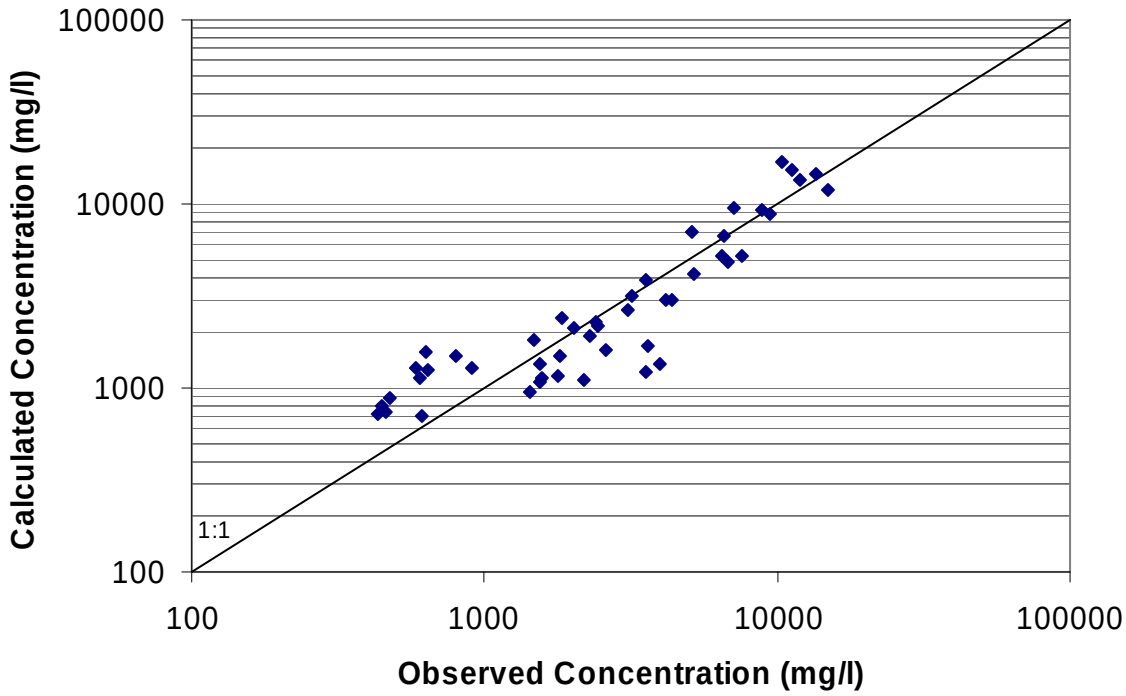

Figure 4.4.16 Calibration of sediment transport equation for cohesive sediments

For non-cohesive sediments the effective particle sizes vary between 0.15mm and 0.93mm. For the data of Guy *et al.* it was assumed that the effective particle size and d_{50} are very similar, since they used uniform sediments. The sediment transport equation for non-cohesive sediments is:

$$\log(C_t) = 4.765 + 1.160 \log\left(\frac{\mathrm{v}S}{w_s}\right) \quad \text{..... 4.4.6}$$

The calibrated function is illustrated in **Figure 4.4.17**. With coefficients of determination of 0.81 and 0.86, respectively, the two equations show a significant improvement over **Equation 4.4.3**.

The accuracies of the newly developed equations (**4.4.4** to **4.4.6**) for cohesive and non-cohesive sediments are relatively good, as indicated in **Table 4.4.2**, with more than 80% of the predicted values varying by no more than a factor of 2.

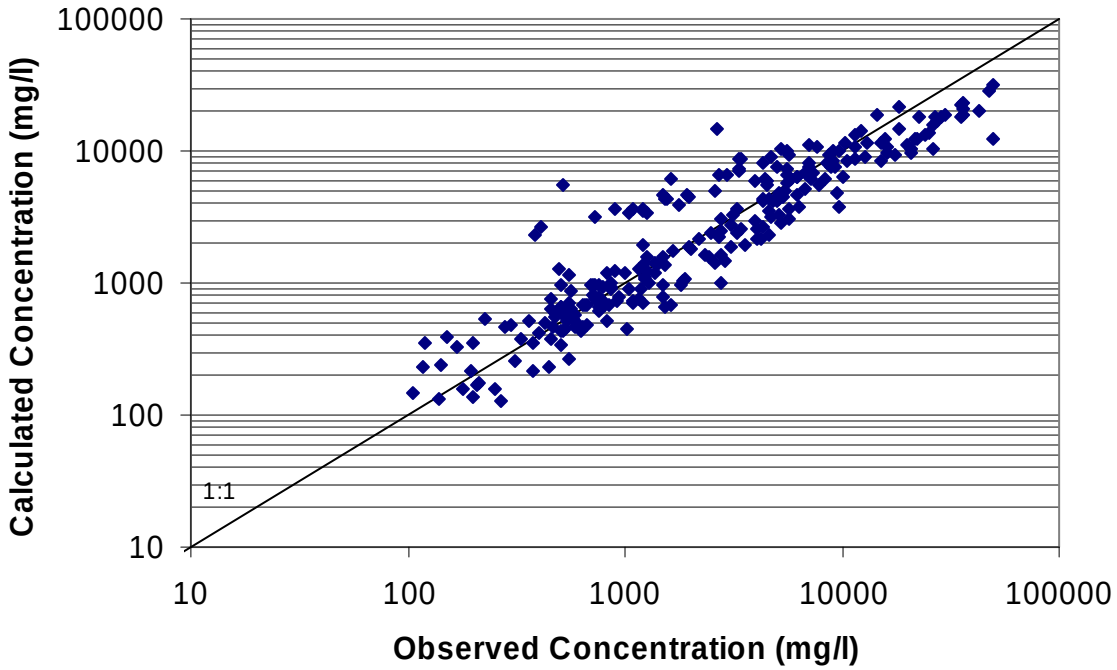

Figure 4.4.17 Calibration of sediment transport equation for non-cohesive sediments

Table 4.4.2 Accuracy ranges of sediment transport equations

Data	$0.67 < \frac{C_{calc}}{C_{obs}} < 1.5$ *	$0.5 < \frac{C_{calc}}{C_{obs}} < 2$ *	$0.33 < \frac{C_{calc}}{C_{obs}} < 3$ *	**No. of Observations**
Cohesive and Non-cohesive Sediments (4.4.4)	61 %	89 %	95 %	305
Cohesive Sediments (4.4.5)	64 %	89 %	100 %	47
Non-cohesive Sediments (4.4.6)	59 %	84 %	95 %	258

*: C_{calc}/C_{obs} – Calculated and observed concentrations, respectively

4.4.2.2 Comparison

To examine the applicability of the three proposed sediment transport equations they are compared to the unit stream power equations developed by Yang (**Equation 4.2.7**), and Basson and Rooseboom (**Equation 4.2.15**).

The comparison between the new sediment transport equation **(4.4.4)** for both cohesive and non-cohesive sediments, and Yang's sediment transport equation is presented in **Figure 4.4.18**, which shows that both equations give much the same results with similar accuracy ranges. Much the same results can be found when Yang's relationship is compared to the new sediment transport equation for non-cohesive sediments alone (**Figure 4.4.19**). In **Figure 4.4.20** the comparison between Basson and Rooseboom's (1997) unit stream power equation and the new cohesive sediment transport equation is shown, but **Equation 4.2.15** for the most part predicts much higher concentrations than were observed, which could be due to the fact that the equation has been calibrated with reservoir data and non-uniform flow conditions.

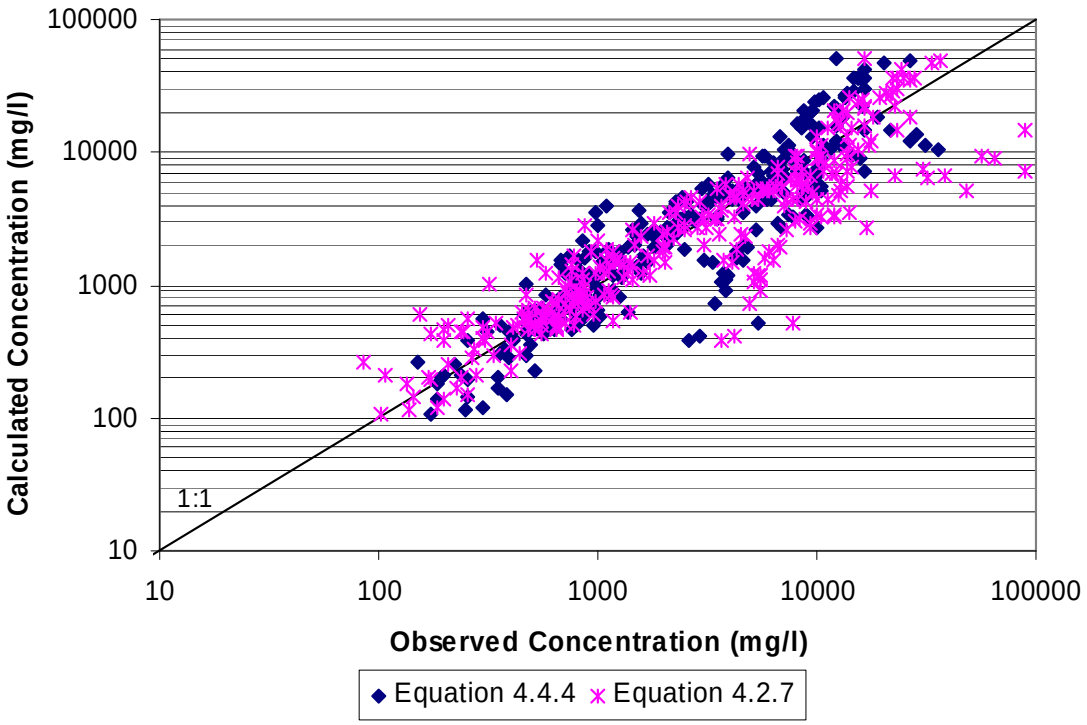

Figure 4.4.18 Comparison between sediment transport equation for cohesive and non-cohesive sediments and Yang's relationship

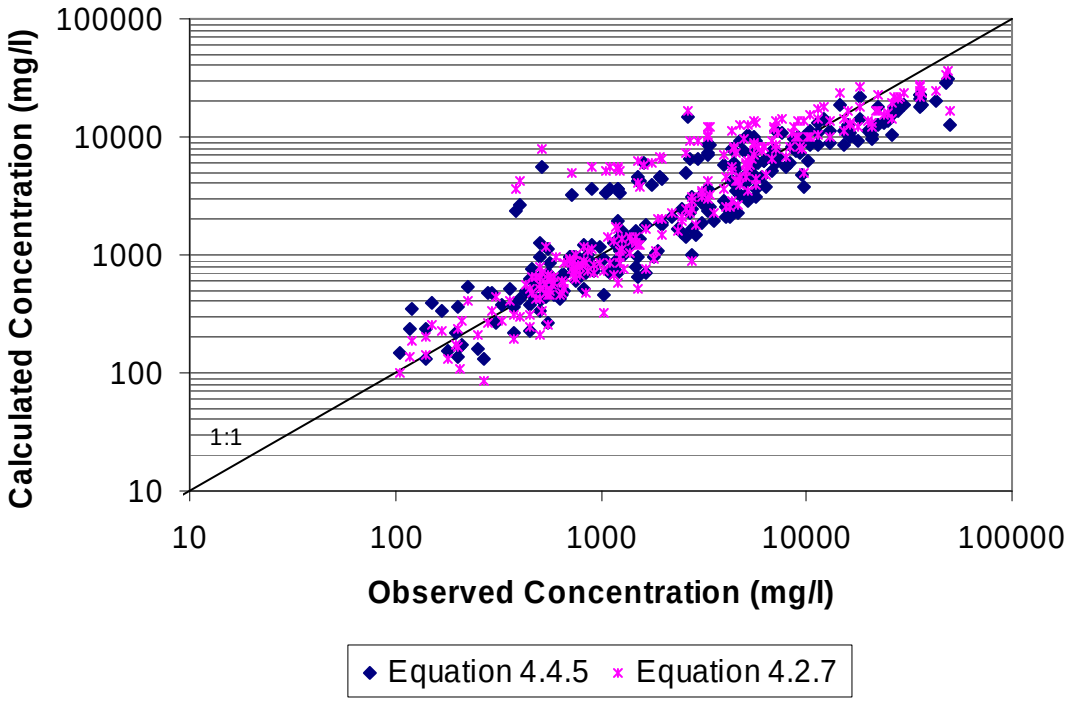

Figure 4.4.19 Comparison between sediment transport equation for non-cohesive sediments and Yang's relationship

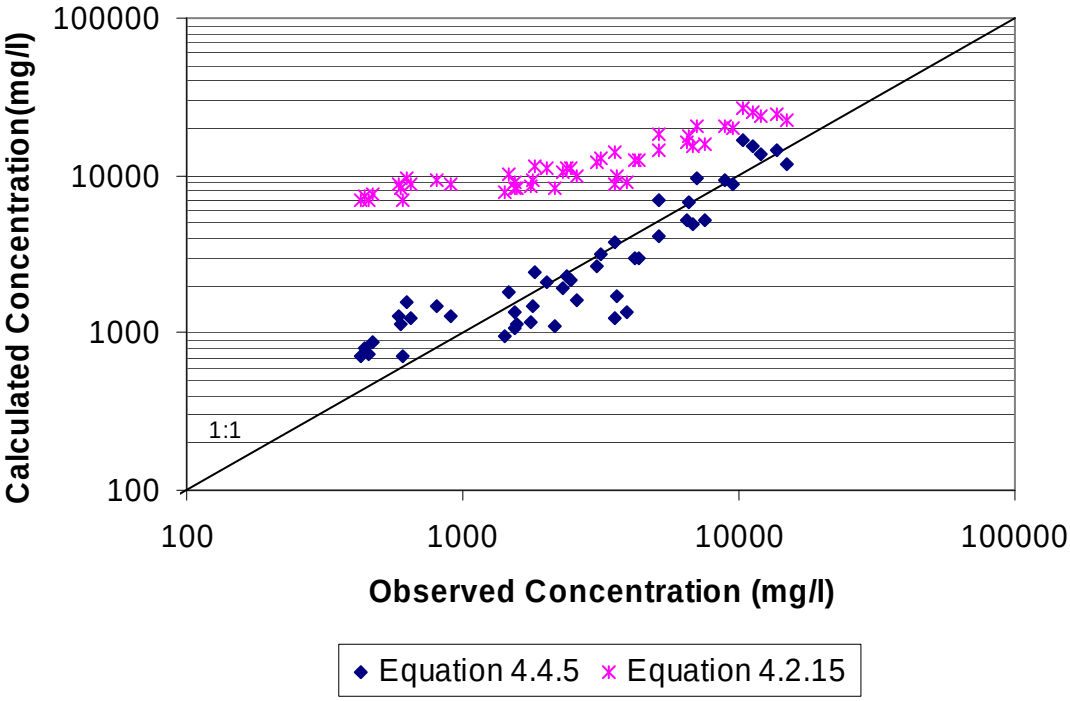

Figure 4.4.20 Comparison between sediment transport equation for cohesive sediments and Basson & Rooseboom's relationship

4.4.2.3 Verification

Two of the new sediment transport equations (**Equation 4.4.4** and **4.4.6**) are verified using both laboratory data compiled by Gilbert (1914) and United States river data published by Bagnold (1966). **Equation 4.4.5** could not be verified at this stage because not enough cohesive sediment data were available.

As with the calibration process the accuracies of the new sediment transport equations are expressed in terms of their ability to predict data within certain accuracy ranges. **Table 4.4.3** is applicable to the sediment transport equation for cohesive and non-cohesive sediments (**Equation 4.4.4**) and **Table 4.4.4** shows the accuracy ranges for the sediment transport equation for non-cohesive sediments only (**Equation 4.4.6**).

Table 4.4.4 shows that the accuracy of **Equation 4.4.6 i**s very good, since the accuracy ranges for the independent flume data are even better than for the data used in the calibration process. This can also be seen in **Figure 4.4.21**, as all the data lie in a very narrow band. **Equation 4.4.6** even predicts river data fairly well with 87% of the predicted values varying by no more than a factor of 2, although the scatter is much greater than for laboratory data (**Figure 4.4.22**). The sediment transport equation for both cohesive and non-cohesive sediments shows slightly lower accuracies, which is to be expected considering that the coefficient of determination is only 0.75.

Table 4.4.3 Accuracy ranges of sediment transport equation for cohesive and non-cohesive sediments (4.4.4) - independent data

Data Source	$0.67 < \frac{C_{calc}}{C_{obs}} < 1.5$	$0.5 < \frac{C_{calc}}{C_{obs}} < 2$	$0.33 < \frac{C_{calc}}{C_{obs}} < 3$	**No. of Observations**
Gilbert Flume Data	63 %	91 %	100 %	615
Bagnold River Data	49 %	63 %	82 %	122

Table 4.4.4 Accuracy ranges of sediment transport equation for non-cohesive sediments (4.4.6) - independent data

Data Source	$0.67 < \frac{C_{calc}}{C_{obs}} < 1.5$	$0.5 < \frac{C_{calc}}{C_{obs}} < 2$	$0.33 < \frac{C_{calc}}{C_{obs}} < 3$	No. of Observations
Gilbert Flume Data	63 %	92 %	100 %	615
Bagnold River Data	56 %	87 %	96 %	122

All three new sediment transport equations give relatively good results, considering that both **Equations 4.4.4** and **4.4.6** compare very well with Yang's sediment transport equation, which has been calibrated with over 1000 sets of laboratory flume data and as well as some field data. All three equations can therefore be used, but **Equation 4.4.4** is more widely applicable because it has been calibrated on both cohesive and non-cohesive sediments.

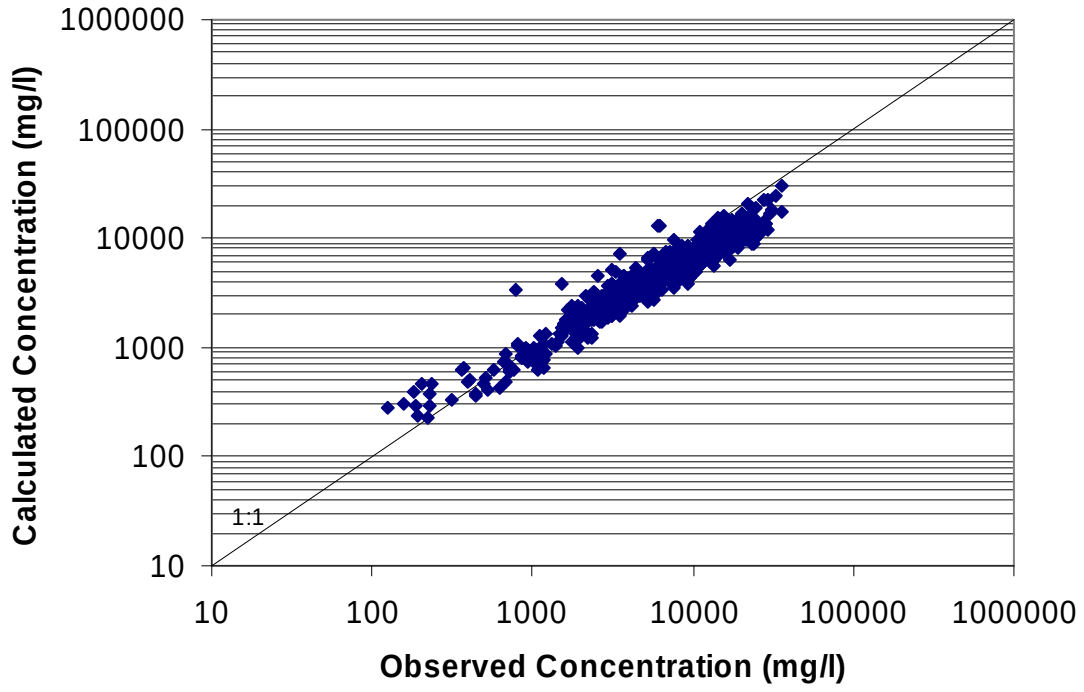

Figure 4.4.21 Verification of sediment transport equation for non-cohesive sediments with independent flume data

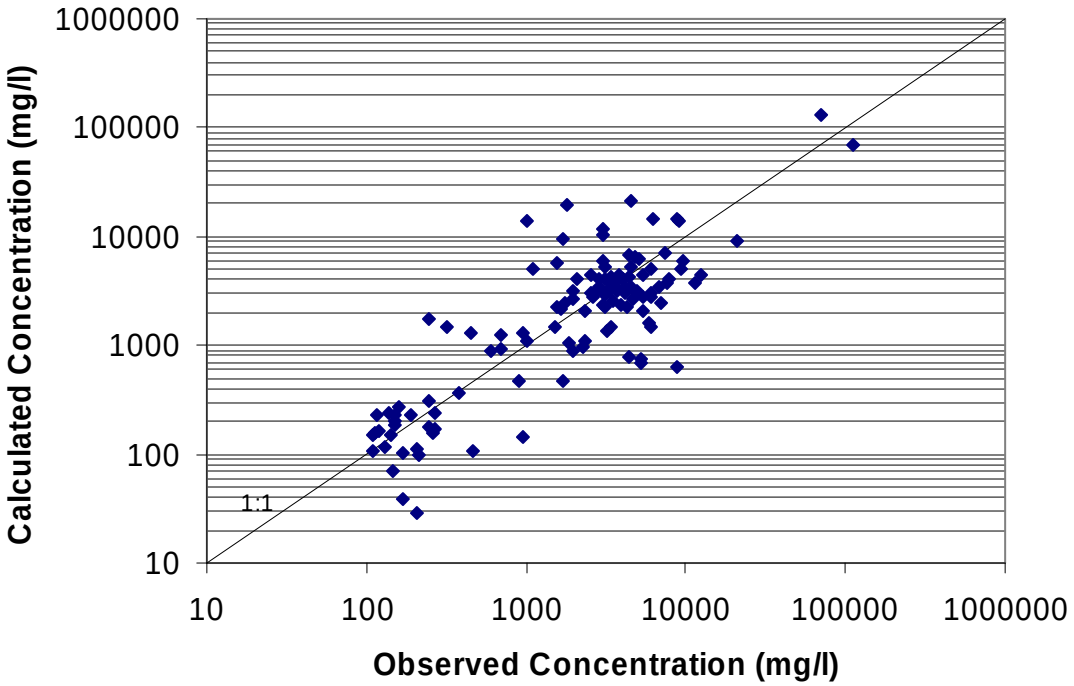

Figure 4.4.22 Verification of sediment transport equation for non-cohesive sediments with independent river data

4.5 Summary

Cohesive sediment transport processes have been investigated with the aid of laboratory experiments. Specifically the sediment transport of mixtures of cohesive and non-cohesive sediments was studied, as well as the critical conditions for the entrainment of cohesive sediments. Existing theories on these topics were taken into account. It was found that with fines content of more than 7% the cohesive properties dominate the erosion behaviour of sediment mixtures. **Equations 4.4.1** and **4.4.2** provide a methodology by which the critical conditions for mass erosion of cohesive sediments and mixtures can be described in terms of the applied stream power at the bed. With the aid of the data obtained from the laboratory experiments, equilibrium sediment transport equations, based on the unit input stream power, for cohesive (**Equation 4.4.5**), non-cohesive (**Equation 4.4.6**) and sediment mixtures (**Equation 4.4.4**) were calibrated and verified with the aid of international laboratory and river data.

5. Numerical Modelling of the River Morphology Downstream of Dams

Chapter 3 has shown that regime equations alone are not adequate in determining the temporal and spatial changes in river morphology that are due to the construction of a dam. As pointed out**,** this is because the regime equations do not take into consideration the effect of increasing or decreasing durations of certain flood peaks, the significance of increased riparian vegetation and the effect of the presence of clay and silt in either the bed material or suspended sediment. Factors such as the duration of certain flows, the effects of smaller flows, the difference in roughness between the river channel and the flood plain and the effect of fine sediments can be dealt with by a numerical model.

The results from the numerical model simulations can be used to establish the sediment balance in the river (or estuary). Factors that will be examined are the annual sediment loads entering and leaving the reach under consideration, as well as the bed material composition and sediment load – discharge relationships. Any changes in these factors from the natural, or reference, condition to the present or any future scenarios will show how much the river will be affected and also make it possible to develop remedial measures, such as environmental flood releases.

A one-dimensional numerical model was utilized to simulate the pre- and post-dam river morphology of the following three case studies (see **Figure 5.1** for locations):

- Pongolapoort Dam – Pongola River
- Proposed Skuifraam Dam – Berg River
- Proposed Jana Dam/ Mielietuin Dam – Thukela Estuary

In addition to the one-dimensional modelling, a semi-two-dimensional numerical model was also used for more detailed, but shorter simulations, with the Pongola River as a case study.

Pongolapoort Dam was chosen as a case study because:

– Relatively long flow records are available both upstream and downstream of the dam.
– Detailed surveys of the river and the flood plains before the dam was built were undertaken.

– Aerial photos from 1996 are available
– Flood releases have been taking place for a number of years.

The other two case studies were included because these are dams that will be built in future, and investigations such as the ones carried out during this project should be carried out at all such dams.

Figure 5.1 Case study locations

5.1 One-Dimensional Mathematical Model

The model used for the simulations is the one-dimensional model MIKE 11, developed by the Danish Hydraulics Institute (DHI) for the simulation of flows, sediment transport and water quality in rivers, estuaries and similar water bodies. The model comprises several models, of which only the first two were used:

- Hydrodynamic
- Non-cohesive sediment transport

- Advection-dispersion
- Water quality
- Rainfall-runoff
- Flood forecast

The overview given here is a short summary of the general descriptions of aspects of the MIKE 11 modelling system, as given in the MIKE 11 Reference Manual (DHI, 1992).

5.1.1 Hydrodynamic Module

The MIKE 11 hydrodynamic (HD) module is an implicit, finite difference model for the computation of unsteady flows in rivers and reservoirs, based on the St Venant equations representing conservation of mass and momentum. The model can describe both subcritical as well as supercritical flow conditions, and modules are incorporated that describe flow past hydraulic structures. The model can be applied to looped networks and quasi two-dimensional flow simulation on flood plains. The HD module provides three different flow descriptions:

- The dynamic wave approach, which uses the full momentum equation.
- The diffuse wave approach, which only models the bed friction, gravity forces and the hydrostatic gradient terms of the momentum equation.
- The kinematic wave approach, where the flow is calculated on the assumption of a balance between the friction and gravity forces. Backwater effects cannot be simulated.

5.1.2 Advection-Dispersion Module

The advection-dispersion (AD) module is based on the one-dimensional equation of the conservation of mass of a dissolved suspended material, i.e. the advection-dispersion equation. The module requires the output from the hydrodynamic module in terms of discharges and water levels. The advection-dispersion equation is solved numerically using the implicit finite difference scheme. Part of the AD module is the cohesive sediment transport (CST) module, which uses the AD module to describe the transport of suspended cohesive sediments, because unlike non-cohesive sediment transport, the cohesive sediment transport cannot be described by local parameters only. The erosion and deposition of cohesive sediments is modelled as a source/sink term in the advection-dispersion equation.

5.1.3 Non-Cohesive Sediment Transport Module

The non-cohesive sediment transport (NST) module can be run in two modes: explicit and morphological. In the explicit mode output is required from the HD module, but no feedback occurs from the NST module to the HD module. In the morphological mode sediment transport is calculated together with the HD module and feedback is given from the NST module to the HD module. The results are in the form of bed level changes, sediment transport rates and bed resistance. The morphological model updates either the whole cross-section or only a part of it (generally the part representing the river channel).

Traditional sediment transport equations are incorporated in the MIKE 11 model for non-cohesive sediment transport. All of these can be run with a single representative particle size or a number of particle sizes.

5.2 Semi-Two-Dimensional Mathematical Model

All three case studies were evaluated with the help of a one-dimensional mathematical model. This means that for a cross-section, only changes in the vertical, but not the horizontal could be evaluated. One way to overcome that problem is to reduce (increase) the with of the cross-section with the aid of the regime equations developed in **Chapter 3** and let the model adjust the depth with the given narrower (wider) cross-section, such as in the case of the Berg River simulations. However, this does then not take into account the period of adjustment to the new width. Two- and three-dimensional models are better suited in that regard. The disadvantage of these models is, however, that long-term simulations are almost impossible due to the large computational power requirements of these models.

A semi-two-dimensional model such as GSTARS (Generalised Stream Tube model for Alluvial River Simulations) does not require a great deal of computational power, and can give an indication of what the effect of reduced streamflow will be on the river morphology, but in order to run long-term simulations relatively long time steps (e.g. daily) have to be used.

GSTARS has the following capabilities (Yang and Simões, 2000):

1. Hydrodynamic:
    - Quasi-steady
    - Use of both the energy and momentum equations for backwater calculations
    - Handles both sub- and supercritical flows, as well as irregular cross-sections with multiple channels
    -
2. Sediment transport:
    - Use of stream tubes in sediment routing computations
    - Hydraulic parameters and sediment routing computed for each stream tube, providing transversal variation in the cross-section
    - Position and width of each stream tube can change, but no sediment or flow can be transported across the boundaries
    - Bed sorting and armouring possible

3. Minimisation of stream power:
    - Channel width adjustments with the aid of simplified version of minimum total stream power

The disadvantage of this program is that it is based on quasi-steady flow calculations, and not unsteady flow calculations. This means the hydrodynamics are not as accurate as could be, which in turn influences the sediment transport.

5.3 Case Study: Pongolapoort Dam – Pongola River

5.3.1 One-Dimensional Modelling

Pongolapoort Dam (**Figure 5.3.1**) was completed in 1973 on the Pongola River (**Figure 5.3.2**) and is located in northern Kwazulu-Natal, South Africa, close to the Swaziland and Mozambique borders (**Figure 5.3.3)**. The Pongola River floodplain below the dam flows through the Makatini Flats, with numerous pans, before reaching the Mozambique border.

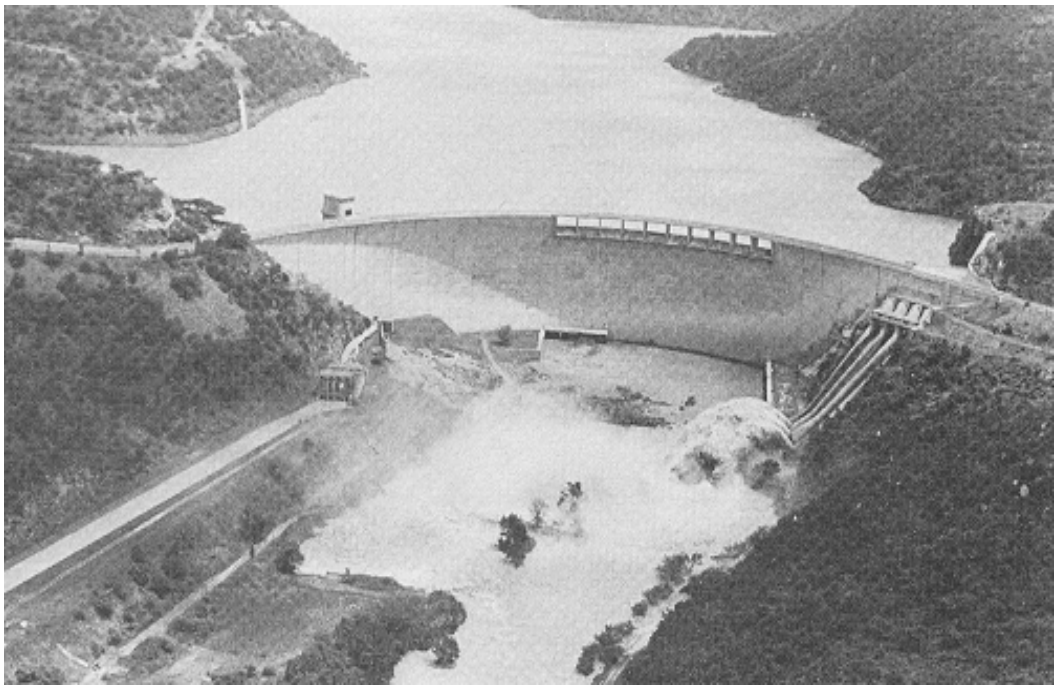

Figure 5.3.1 Aerial view of Pongolapoort Dam (Kovacs *et al,* 1985)

Figure 5.3.2 Pongola River downstream of Pongolapoort Dam with artificial flood releases (October 2000)

Figure 5.3.3 Pongolapoort Dam location

The reservoir is one of the largest in South Africa with a full supply capacity of 2445 million m3 (about 2 MAR). The dam was built mainly for irrigation, storage and domestic use, but the largest quantities of water are actually used for environmental flood releases (sometimes more than 400 million m^3/a). The current water demand placed on the dam is around 190 million m^3/a (~17% of the MAR), excluding the annual environmental flood releases. More typical of South African 2MAR reservoirs would be a yield of up to 60% of the MAR. Most of the pans are situated more than 40 km downstream of the dam. Over 100 km of the river was set up, but due to model constraints only 60 km were investigated during the morphological simulations (**Figure 5.3.4**). However, hydrodynamic flood routing was carried out over the whole 100 km to design the July 2002 flood release to limit flood damage in Mozambique. A report is included in **Appendix D**.

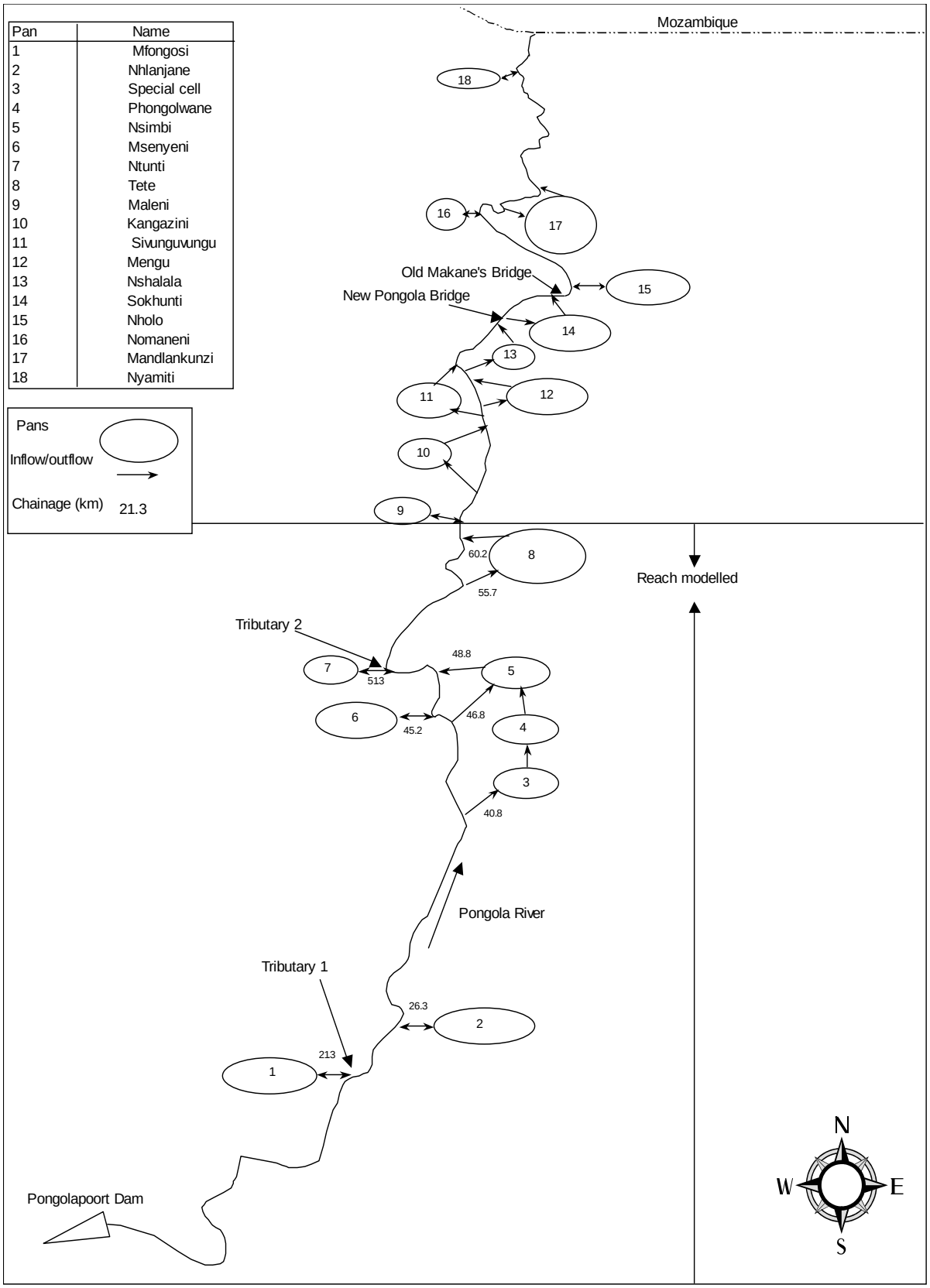

Figure 5.3.4 Pongolapoort model layout

Since the dam was constructed, releases from the reservoir have been strongly controlled with flood peaks of between 300 and 800 m^3/s being released once or twice a year (**Figure 5.3.5**), at the beginning (October) and end (March) of the rainy season. (The natural flood peaks are summarised in **Table 5.3.1**). This was done mainly to draw down the water level in the reservoir in anticipation of the coming wet season, as well as to recharge the pans downstream (**Figure 5.3.6** and **5.3.7**) and to provide water for flood irrigation. The amount of water released has varied, with as much as 590 million m^3 released in March 1985 and only 99 million m^3 released in February 1986 (DWA, 1987). In recent years the annual releases have been between about 200 and 500 million m^3.

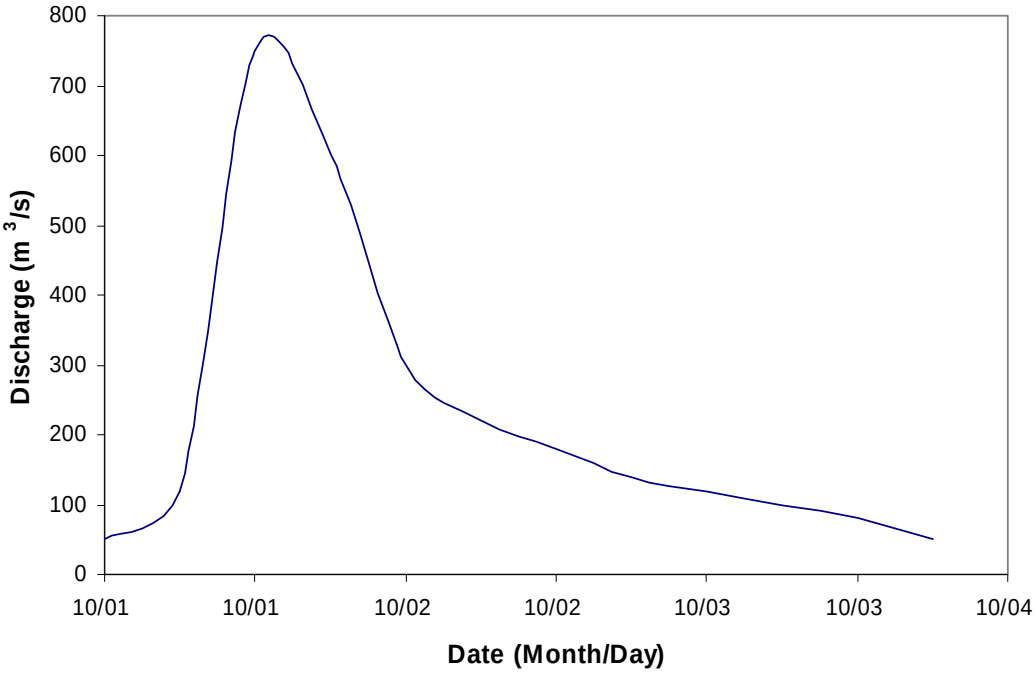

Figure 5.3.5 Typical artificial flood hydrograph

The characteristics of Pongolapoort Dam, such as the storage-area relationship, were used to set up a reservoir balance to determine an outflow sequence that is more representative of normal reservoir operations with and without artificial flood releases. The reservoir basin characteristics such as rainfall and evaporation were obtained from WR90 (Midgley *et al.*, 1990), also shown in **Table 5.3.2**. The inflow sequence (six-hour time steps) and the irrigation demand were obtained from gauging stations from the Department of Water Affairs and Forestry (DWAF). The gauging station from which the inflow sequence was obtained was situated upstream of the dam, but this station had the longest record available (39 years). Using the cumulative discharge curve over that period as a reference, an 18-year

representative period was chosen (1950 – 1968). The demand placed on the reservoir for dam scenarios was obtained from the storage-draft-frequency curves of WR90.

Table 5.3.1 Pongola River flood peaks – natural

Recurrence interval (years)	Flood peak (m^3/s)
2	800
5	1400
10	1900
20	4600
50	10500
100	11200

Table 5.3.2 Pongolapoort Dam - catchment characteristics

MAP (mm)	581
MAE (mm)	1500
MAR (10^6 m^3)	1160
Upstream gauging station (7081 km^2)	W4H002
Irrigation gauging station	W4H014
Catchment area (km^2)	7831
Hydro zone	Q

Figure 5.3.6 Pan before artificial flood releases (October 1999)

Figure 5.3.7 Pan after artificial flood releases (October 1999)

Five scenarios, based on an 18-year streamflow record, were considered for this project (with flow sequences over the 18 year simulated period shown in **Figures 5.3.8** to **5.3.12**):

- **Scenario 1**: Pre-dam conditions
- **Scenario 2**: Pongolapoort Dam (current demand) without artificial flood releases
- **Scenario 3**: Pongolapoort Dam (current demand) with alternating annual artificial flood releases
- **Scenario 4**: scenario 2 with total water demand of 60% MAR
- **Scenario 5**: scenario 3 with total water demand of 60% MAR

The natural conditions were simulated to determine the changes that would have occurred naturally over that period of time, and also to have a basis against which to compare the four other scenarios. The present day reservoir with a larger demand was chosen because Pongolapoort Reservoir, as it is today, without considering the artificial flood releases, only releases a steady 5 m^3/s for environmental purposes and about 20 million m^3/a are available for irrigation, and the reservoir therefore remains relatively full most of the time. There is a significant flood peak attenuation from the natural condition, as can be seen in **Figure 5.3.9**. With a higher demand on the dam, only small flood peaks will be spilling at the dam for four out of the 18 years (which would not be acceptable for the ecology (**Figure 5.3.11**)).

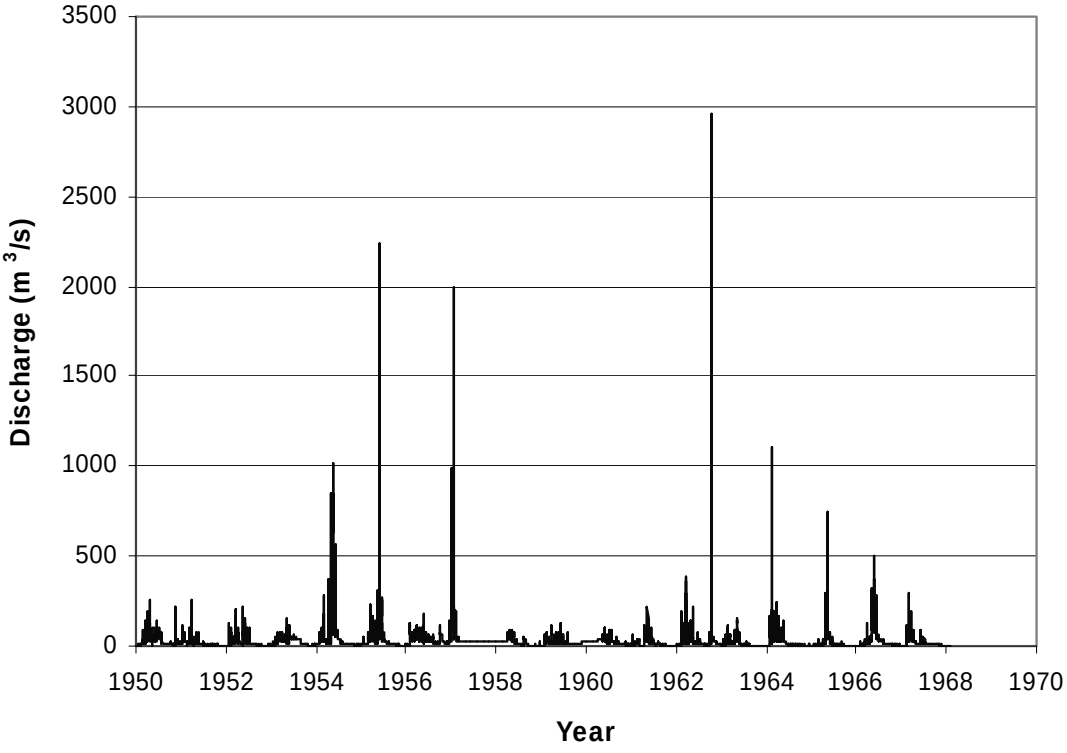

Figure 5.3.8 Scenario 1 - Pre-dam streamflow at dam site (6-hourly data)

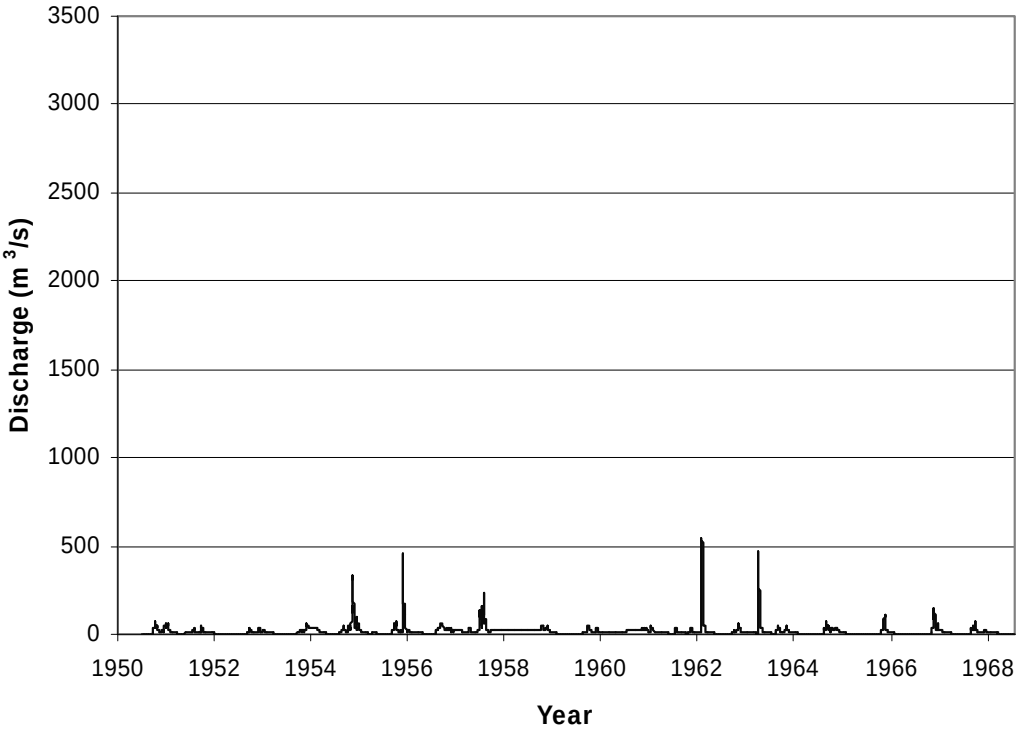

Figure 5.3.9 Scenario 2 - Pongolapoort Dam spillage (6-hourly data)

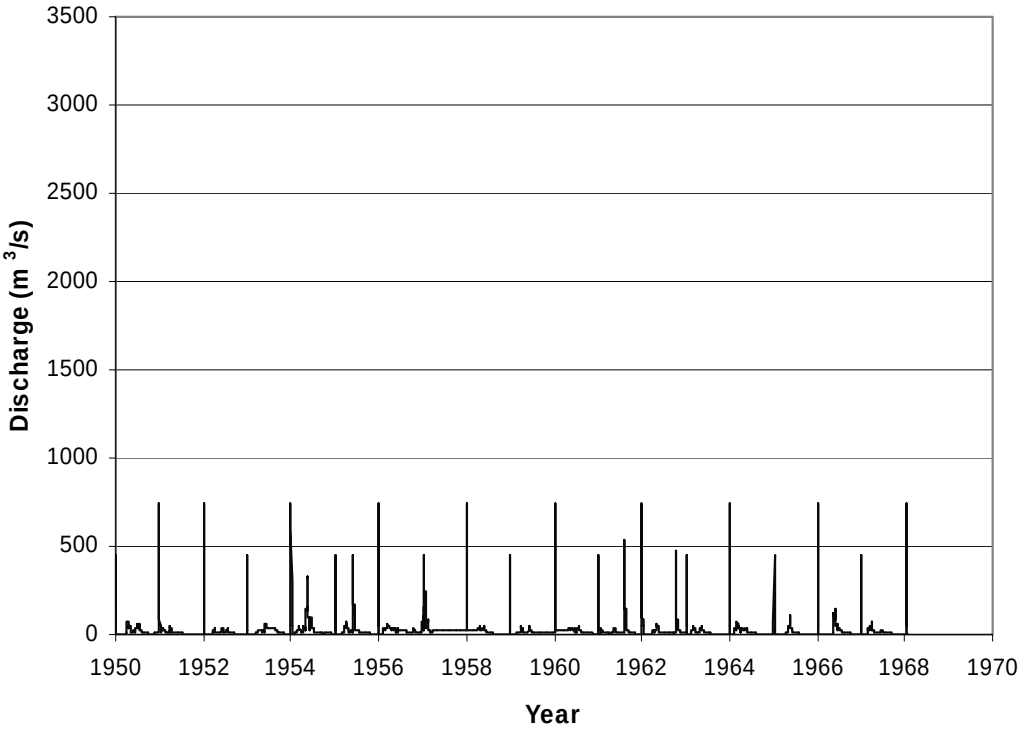

Figure 5.3.10 Scenario 3 - Pongolapoort Dam spillage with artificial flood releases (6-hourly data)

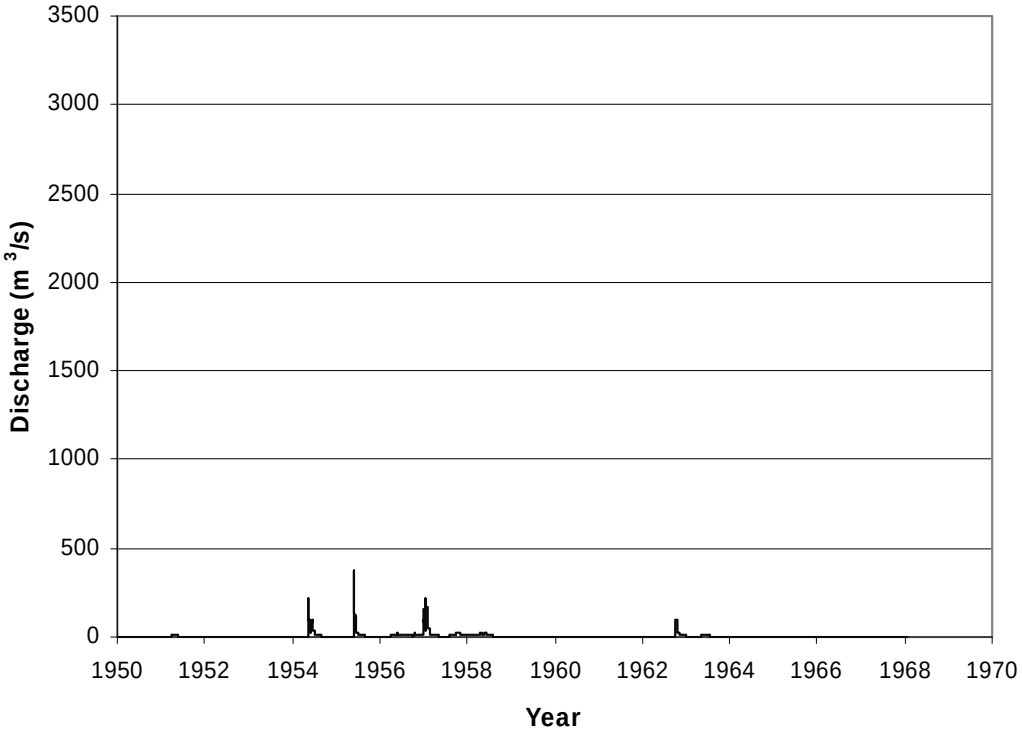

Figure 5.311 Scenario 4 - Pongolapoort Dam spillage (60% MAR demand) without artificial flood releases (6-hourly data)

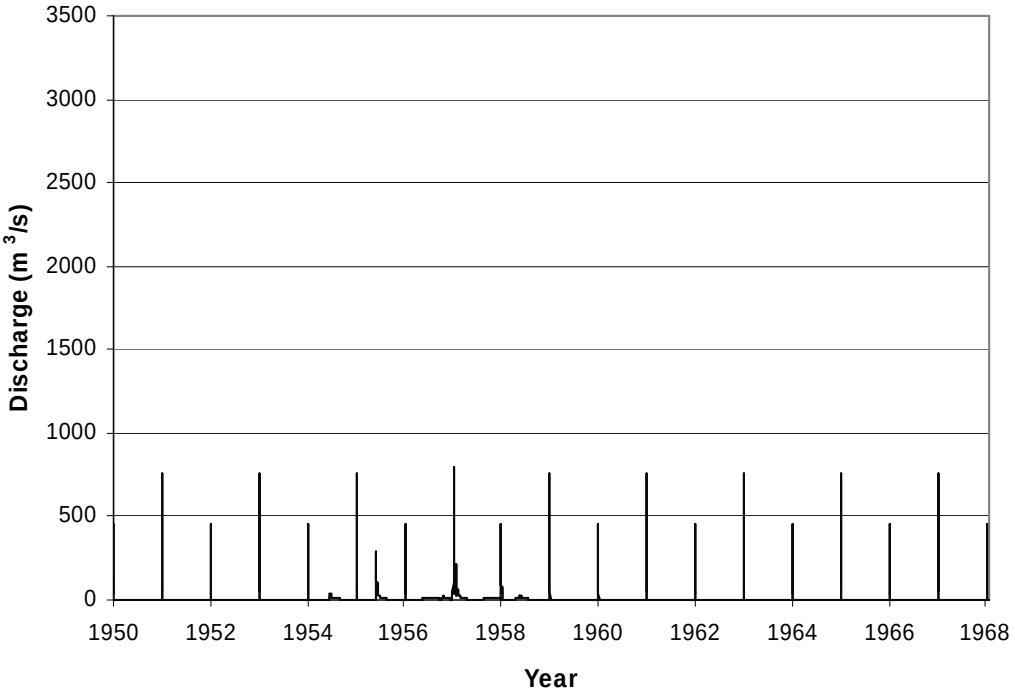

Figure 5.3.12 Scenario 5 - Pongolapoort Dam spillage (60% MAR demand) with artificial flood releases (6-hourly data)

5.3.1.1 Model Input

The following input data were obtained for the simulations:

- Cross-sections: 193 cross-sections of the Pongola River downstream of the dam were obtained from topographical maps (dated 1933 and 1957) for the 100 km reach. Typically the distance between sections is 500 m.

- Tributaries: The effect of two minor tributaries (Mfongosi and Lubambo) was included in the model through water and sediment input at two locations downstream of the dam.

- Pans: Eight pans were identified on 1:50 000 topographical maps as well as from a DWA (1987) report on the 60 km stretch of river modelled. The pans were connected to the river by means of short link channels, where the water level in the river has to rise to a certain level before water spills into the pans, allowing for in- and outflow from the pans. The sill levels were obtained from contour maps as well as the DWA report.

- Bed roughness: Manning n-values were calibrated as 0.05 for the river channel, and 0.075 for the pans and the flood plains. The initial n-value for the river channel was obtained from current meter gaugings carried out by the Department of Water Affairs and Forestry (DWAF), along a section close to the dam and refined during the calibration process. During the simulations the n-values were kept constant at their original values to be able to compare the different scenarios. In reality, however, the n-values will change as the hydraulic radius changes.

- Inflow sequence: 18-year flow sequences were generated for all scenarios. Since no observed data are available for the two tributaries, the upstream inflow sequences were scaled down for the tributaries according to their catchment areas in order to generate flow sequences for these tributaries.

- Sediment fractions in the bed: Only two sediment fractions were used. Fraction 2, with a diameter of 0.24 mm, was estimated from particle size distribution curves of samples taken upstream of the dam (Kovacs *et al.*, 1985) where 0.24 mm was found to be the effective particle size. However, there is usually finer material present in the suspended load that is not found in the bed, since it is generally moved right through the system. By comparing observed sediment concentrations to the calculated sediment transport capacity of the river, it was found that about 60% of the sediment load had to be made up of sediment finer than 0.24 mm, which was represented by fraction 1 during the simulations. The fractions and their respective proportion of the bed material are shown in **Table 5.3.3**.

Table 5.3.3 Sediment fractions of bed sediment

Fraction	Particle size (mm)	Percentage of sediment size in fraction
1	0.035	5
2	0.24	95

- Sediment load: For each scenario, sequences of suspended sediment concentrations were determined by means of a sediment load – discharge relationship, derived from observed data at a gauging station on the Pongola (**Figure 5.3.13**) with a sediment yield of 133 ton/km^2.a, thus accounting for the sediment yield from both the upstream

catchment and the two tributaries. In the case of the dam scenarios no sediment input was specified at the upstream boundary, because it was assumed that almost all the sediment from the upstream catchment would be trapped within the reservoir. In that case only the incremental downstream catchment will supply sediment to the river. The suspended sediment concentrations were adjusted to yield an average sediment yield of 133 ton/km^2.a.

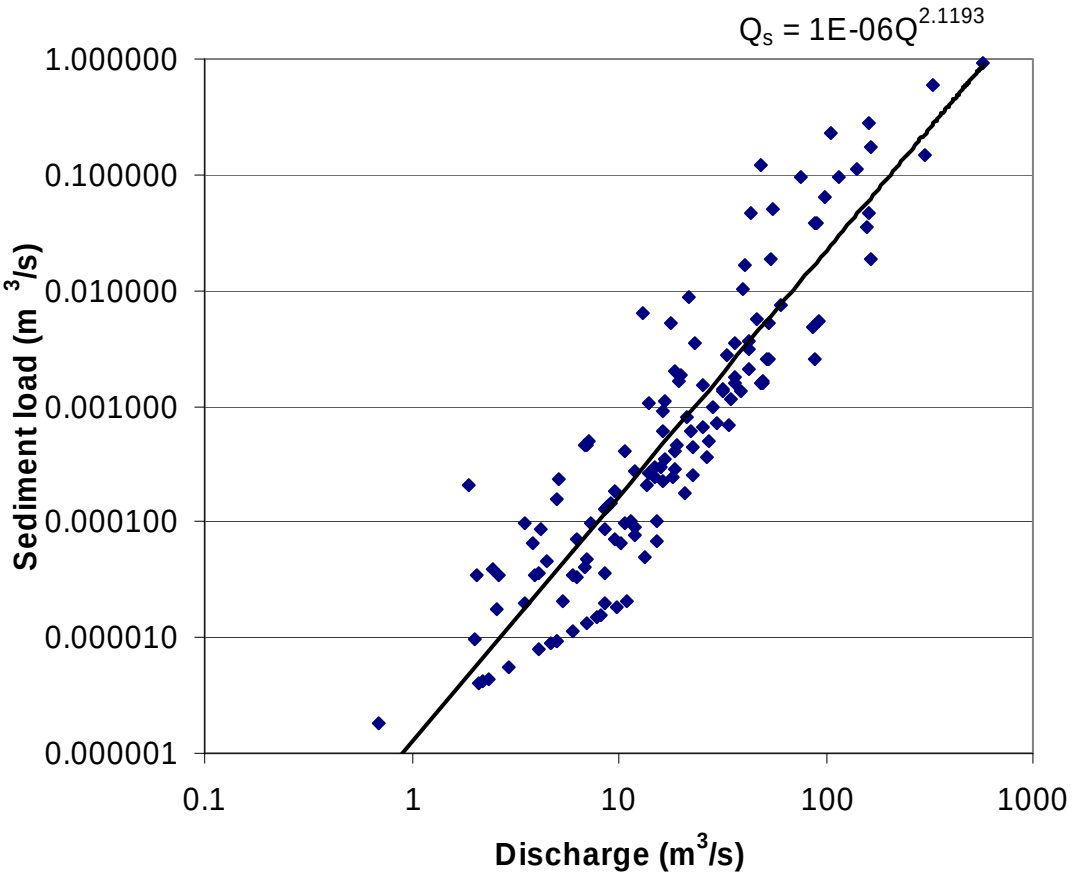

Figure 5.3.13 Sediment load – discharge relationship – Pongola River

- Q-h boundary: at the downstream end of the river reach under consideration a Q-h boundary was set up relating the elevation above mean sea level to the discharge. The characteristics of the cross-section at km 100.63 were taken and the discharge calculated with Chezy's flow resistance formula (**3.3.12**).

- Artificial flood releases: Annual alternating flood releases of 450 m^3/s (annual flood) and 750 m^3/s (1:2-year flood) at the beginning of October were simulated, because these are the kind of floods (in magnitude, duration and frequency) that should be released.

- Bottom level update: Several methods are available in MIKE 11 to update the bottom level. However, due to the long simulations and complex network structure the only method available that did not cause instabilities in the program was the default method. This means that erosion and deposition are uniformly distributed over the whole cross-section below bank level, i.e. not including the floodplains.

- Sediment transport equation: The sediment transport equation used for these simulations is Engelund and Hansen's total load formula.

5.3.1.2 Hydrodynamic Model Calibration

For the hydrodynamic model calibrations, the Pongola River (100 km), as well as all the major tributaries and pans along that reach were included in the simulations. The model was calibrated based on water levels in certain pans taken during the 1984 and 1986 flood releases. The Manning n-value for the main river channel and floodplains was adjusted and extra storage capacity was added to some pans in order to get peak and timing right. The simulated water levels deviated from the observed water levels between –0.65 and +0.65 m, with an average of +0.2 m. The simulated peak generally occurs about half a day too early, which is conservative for flood warnings (see **Figures 5.3.14** and **5.3.15** for some calibration examples). The reason for the poor accuracy on some of the pans is due to the fact that the topographical maps from which the cross-sections were taken are quite old and the river has certainly changed to some degree, especially since the dam has been built.

5.3.1.3 Discussion of Simulation Results

From **Figure 5.3.16** it can be seen that under pre-dam conditions quite a bit of erosion takes place over the first 35 km of the river, with relatively high sediment loads, probably because the river is still relatively steep and the sediment transport capacity is high. The sediment from the subcatchment supplied by one of the tributaries is also responsible for the high sediment load at 35 km. In contrast, at 44 km the annual sediment load is greatly reduced, indicating that deposition occurred between 35 and 44 km. The reason for this could be that the area becomes flat and the first pans appear in this area, which play an important role in attenuating flood peaks.

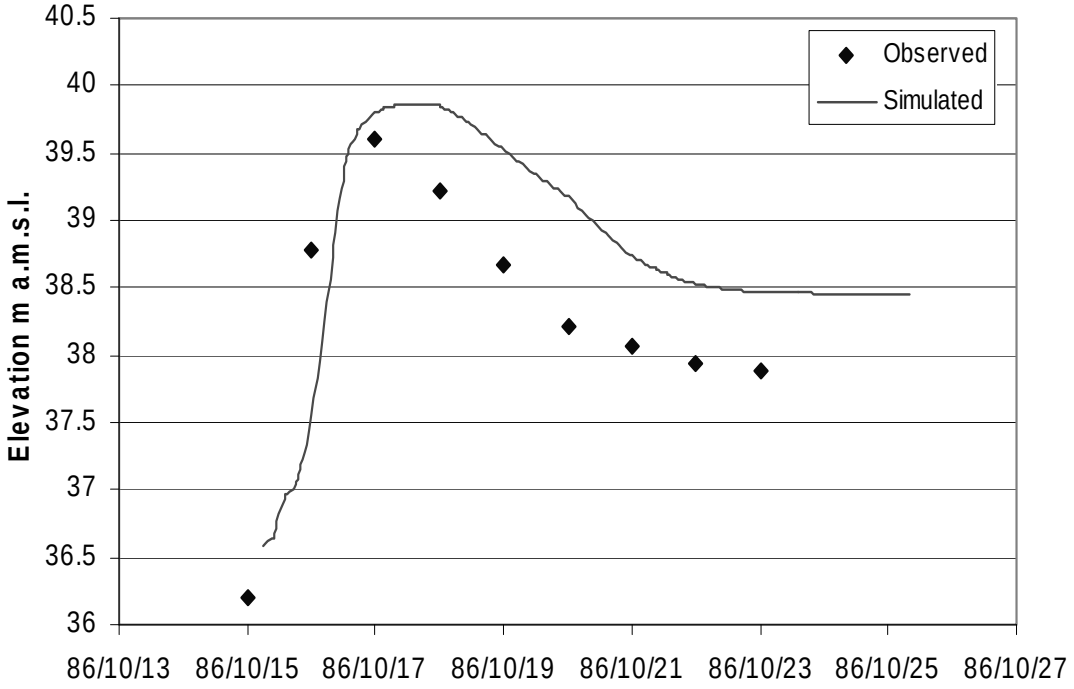

Figure 5.3.14 Observed and simulated water levels at Nsimbi Pan, October 1984

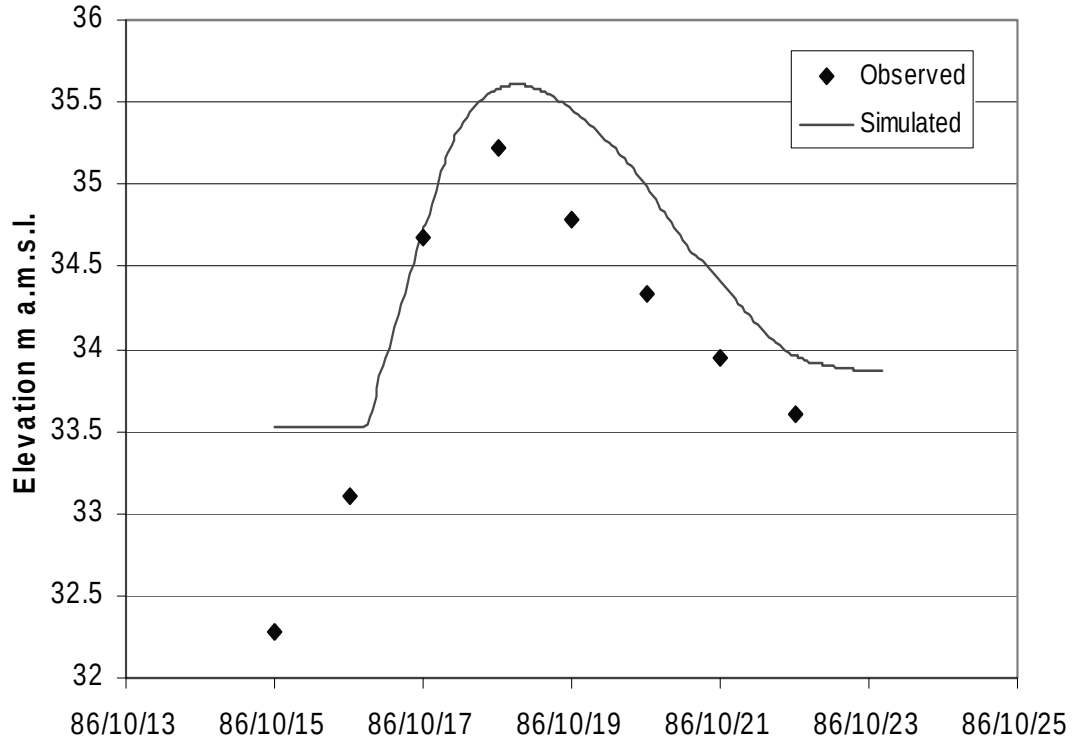

Figure 5.3.15 Observed and simulated water levels at Tete Pan, October 1984

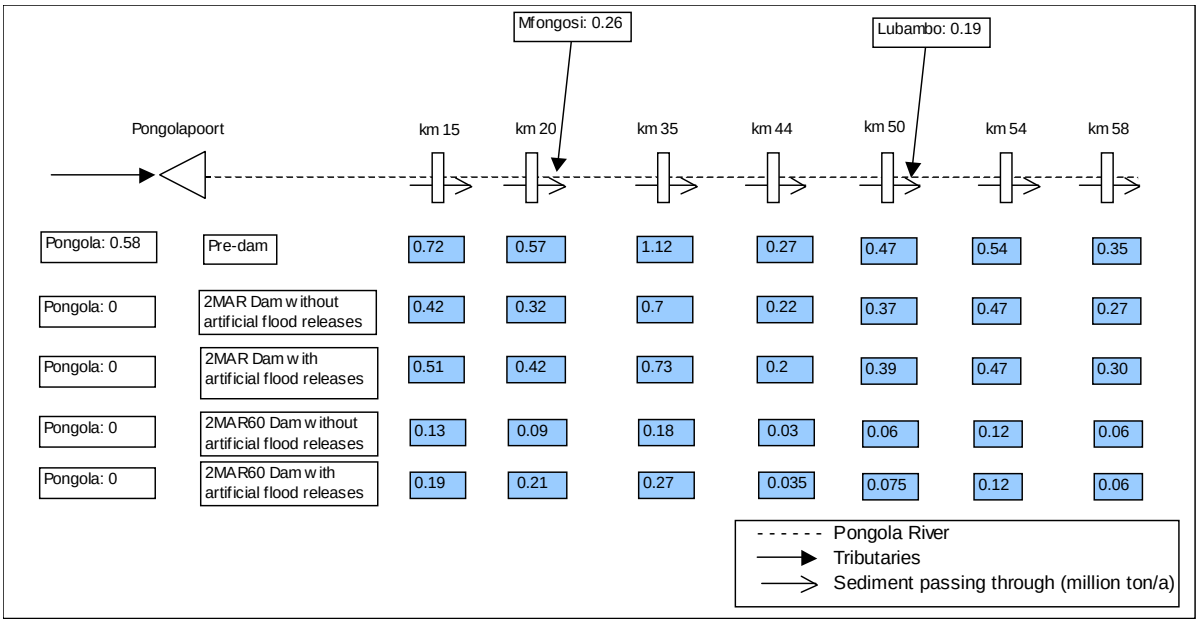

Figure 5.3.16 Long-term simulated sediment balance

With Pongolapoort Dam and its current demand (without the artificial flood releases), the simulated annual sediment loads are definitely reduced along the first 35 km, but not so much over the rest of the river reach under consideration. This seems to indicate that the "naturally" released flows (spillage) are sufficient in maintaining the sediment transport capacity. However, considering that most of the 0.58 million ton/a from the upstream catchment do not pass through the reservoir anymore, quite a large amount of erosion occurred in the river, especially over the first 20 km. The increase in sediment loads between 20 and 35 km can again be attributed to the tributary located at 21 km. Even though the sediment loads have not changed drastically between 35 and 60 km downstream of the dam, riverbed aggradation could still be a problem, because the area is relatively flat.

With the artificial flood releases the simulated sediment loads increase somewhat over the first 20 km, but not to a great extent further downstream, probably because the pans play a major role in attenuating the flood peak, thereby reducing its efficiency. The same trend can be seen from the longitudinal profile in **Figure 5.3.17**. Most of the erosion takes place over the first six kilometres just downstream of the dam, as a result of the clear water spilling from the dam.

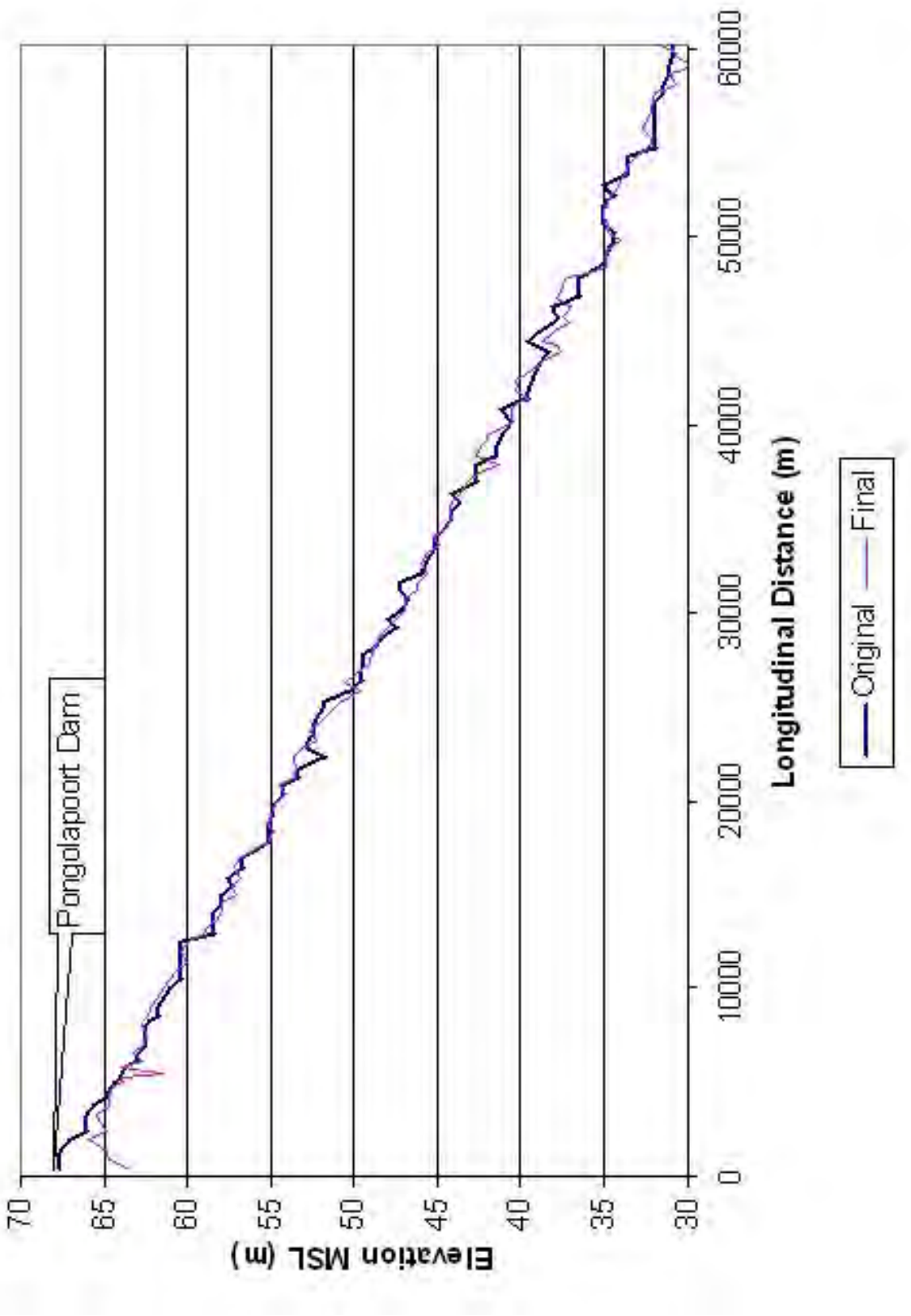

Figure 5.3.17 Longitudinal bed profile – scenario 3

Should a greater demand be placed on Pongolapoort in future, the situation will be very different. The flood peaks as well as spillage from the dam will be reduced dramatically as can be seen in **Figure 5.3.9**. For this reason the simulated mean annual sediment loads along the whole 60 km reach under consideration are very much reduced although the same pattern of erosion and deposition as for the other scenarios is evident. The managed flood releases have some effect in restoring the sediment balance, but only over the first 35 km or so. Further downstream the sediment loads are basically unchanged from those of scenario 4, indicating that more frequent flood releases or higher flood peaks are necessary.

Another way of illustrating the effect of Pongolapoort Dam with and without the artificial flood releases, is by comparing the simulated sediment load-discharge relationships at various locations along the Pongola River. **Figures 5.3.18** to **5.3.20** show these relationships at 15 km, 35 km and 54 km. From **Figure 5.3.18** it can be seen that with the artificial flood releases the relationship plots slightly above that of the pre-dam conditions at the higher discharges. This is a result of the more frequent high flood peaks, where larger quantities of sediment can be transported. Without the artificial flood releases the sediment load-discharge relationship plots below that of the pre-dam conditions, especially at higher discharges. This is to be expected, because of the reduced flood peaks. The relationships of the two greater demand scenarios both plot below that of the natural conditions, with the relationship of scenario 5 plotting slightly closer, indicating that the artificial flood releases have had some effect, though not very much. This is to be expected because apart from the flood releases very little natural spillage occurs at the dam and the flow regime has changed completely from the natural conditions.

At 35 km the situation has changed in that the sediment load-discharge relationships of scenarios 2 and 4 lie just above that of the pre-dam condition, which makes it seem like the sediment transport capacity of the river after the dam is higher than under pre-dam conditions. However, it has to be remembered that the sediment load-discharge relationships of the two scenarios only extend to discharges up to about 500 m^3/s. Flood peaks greater than 500 m^3/s that occurred under pre-dam conditions had the capacity to transport considerable amounts of sediment, which is apparent from the simulated sediment loads of the pre-dam scenario. Therefore the sediment load-discharge relationship of the two scenarios can plot above that of the pre-dam scenario, because due to the absence of the larger floods, more sediment is available to be transported by the smaller flows. The relationships of scenarios 3 and 5 plot

above that of the pre-dam conditions at higher discharges indicating that the artificial flood peaks may have been too large and smaller flows may be more beneficial.

From **Figure 5.3.20** it can be seen that at 54 km the sediment load-discharge relationships of all dam scenarios plot below the relationship of the pre-dam conditions (at flows greater than 100 m^3/s). As mentioned before, the river becomes flatter and therefore sediment deposition is always a problem, even under pre-dam conditions. With the dam scenarios the situation worsens in that the floods that are necessary to remove these deposits periodically, are greatly reduced. The artificial flood releases in the case of scenario 3, however, do not seem to have been sufficient since the relationship is in the same position as the one without the artificial flood releases. In contrast, with a greater future demand the flood releases seem to have restored the sediment balance to at least a state similar to scenarios 2 and 3, which was not evident from the simulated mean annual sediment loads.

The fact that at different locations along the river reach different flows seem to be needed to attempt to restore the sediment balance indicates that there is a whole range of flows that actually maintains a river channel, and that not just the magnitude of the flood peaks but also the variability of flows and flow durations is crucial.

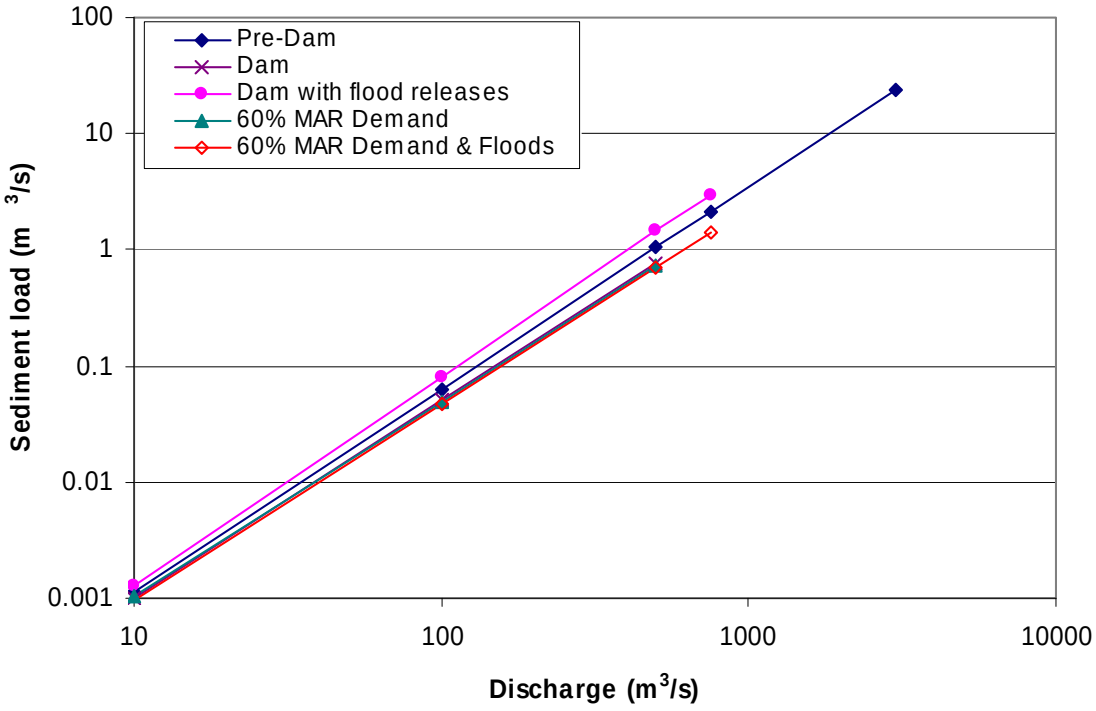

Figure 5.3.18 Sediment load-discharge relationships at 15 km

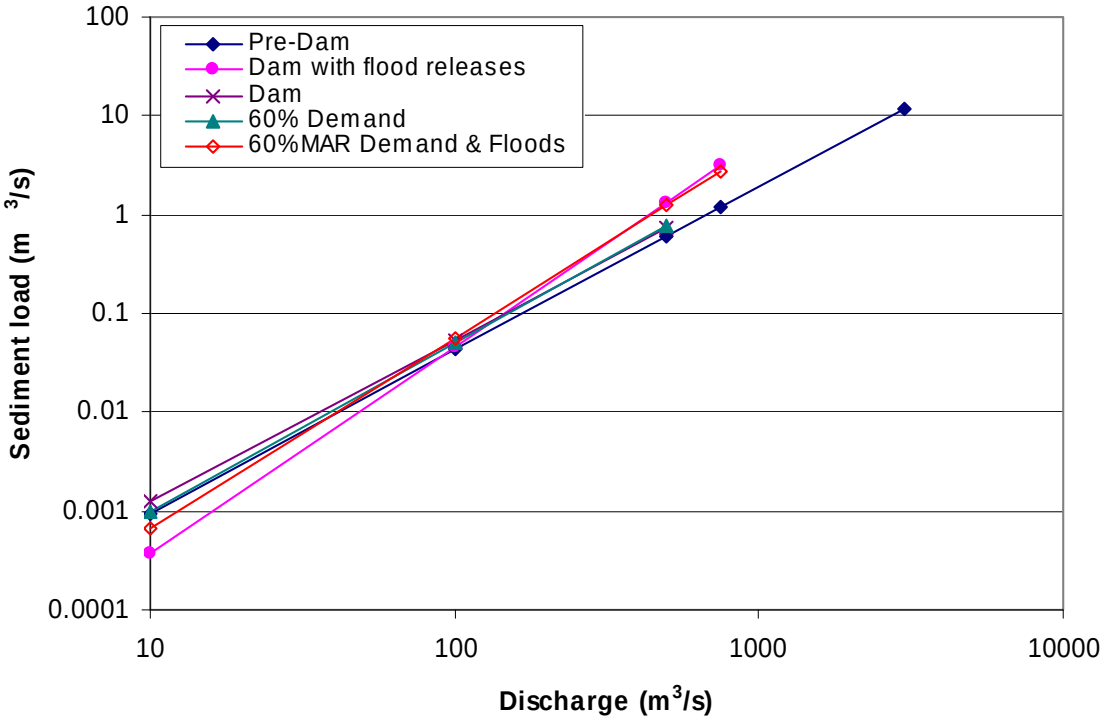

Figure 5.3.19 Sediment load-discharge relationships at 35 km

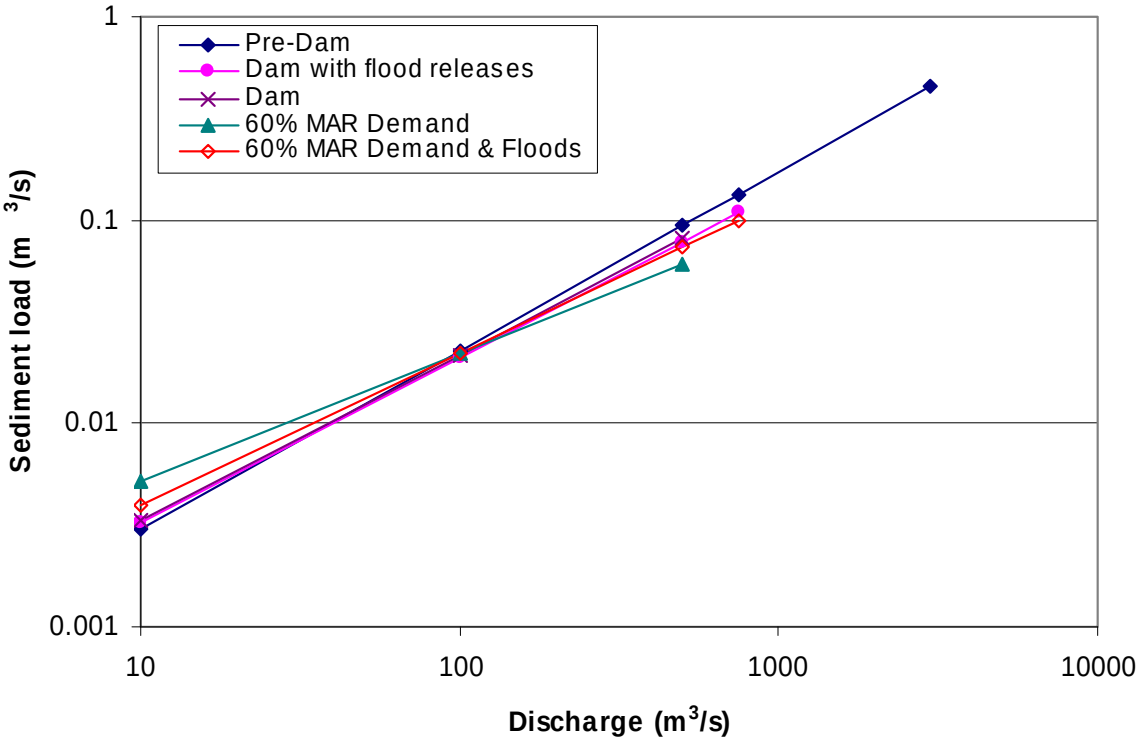

Figure 5.3.20 Sediment load-discharge relationships at 54 km

5.3.1.4 Discussion: Artificial Flood Releases

From the simulations it has become obvious that at present the artificial flood releases may not be more effective in restoring the sediment balance of the Pongola River than the "natural" spillage from the dam, because at 54 km both the sediment load-discharge relationships of the two dam scenarios plot very close to the pre-dam conditions, indicating that even without the artificial flood releases the sediment transport balance seems to have been more or less restored. Should a higher demand be placed on Pongolapoort Dam in future, the situation will be different because considerably less natural spilling occurs and artificial flood releases will definitely be necessary.

A factor that will have to be considered when releasing artificial floods is that they will increase the riverbed scour for some distance just downstream of the dam, which is site-specific, but since the downstream distance affected by a dam can be hundreds of kilometres long, it is important to focus on restoring or maintaining the greater part of the river.

5.3.2 Semi-Two-Dimensional Modelling

The semi-two-dimensional numerical model GSTARS was used to carry out more detailed simulations with regard to river width and depth adjustments of the Pongola River.

5.3.2.1 Model Input and Set-up

Because of model limitations only the first 40 km of the Pongola River downstream of the dam was modelled, with cross-sections every kilometer, without any tributaries or pans. Three sediment fractions were specified (see **Table 5.3.4**) and a sediment rating curve for the incoming sediment load, as shown in **Figure 5.3.13**. Apart from the natural conditions (scenario 1), two dam scenarios were simulated:

- Scenario 2: Pongolapoort Dam with its current demand
- Scenario 3: Pongolapoort Dam with a total water demand of 60% of the MAR

Table 5.3.4 Sediment fractions in bed and suspended material

Particle size range (mm)	Percentage of each fraction in bed material	Percentage of each fraction in suspended sediment
0.07 – 0.17	20	80
0.17 – 0.41	75	19
0.41 – 1.0	5	1

The model was set-up with 6-hour time steps for the hydrodynamic calculations, for a period of four years (1954 – 1958), taken from the 18-year flow record as used for the one-dimensional modelling.

The simulations were run with two stream tubes and the minimisation of total stream power procedure was used to simulate the channel geometry changes in the width and depth.

Yang's 1979 sand transport formula together with the 1984 gravel transport formula was used (Yang, 1979, 1984).

5.3.2.2 Simulation Results

Scenario 1:

Under natural conditions the river is very dynamic and both the longitudinal profile and the cross-sections change continually (**Figures 5.3.21** to **5.3.24**), with every flood. Some cross-sections have become narrower and shallower, but mostly this has occurred close to the upstream boundary where the model first has to deal with the incoming sediment. Further downstream the cross-sections seem more inclined to move from side to side.

It also seems that the model needs a short warm-up period in order to adjust the cross-section width and depth with the aid of the minimisation of total stream power procedure. **Figure 5.3.25** shows the total sediment load exiting the reach together with the streamflow. As can be seen there is a period of higher sediment transport at the beginning, after which the sediment transport levelled off.

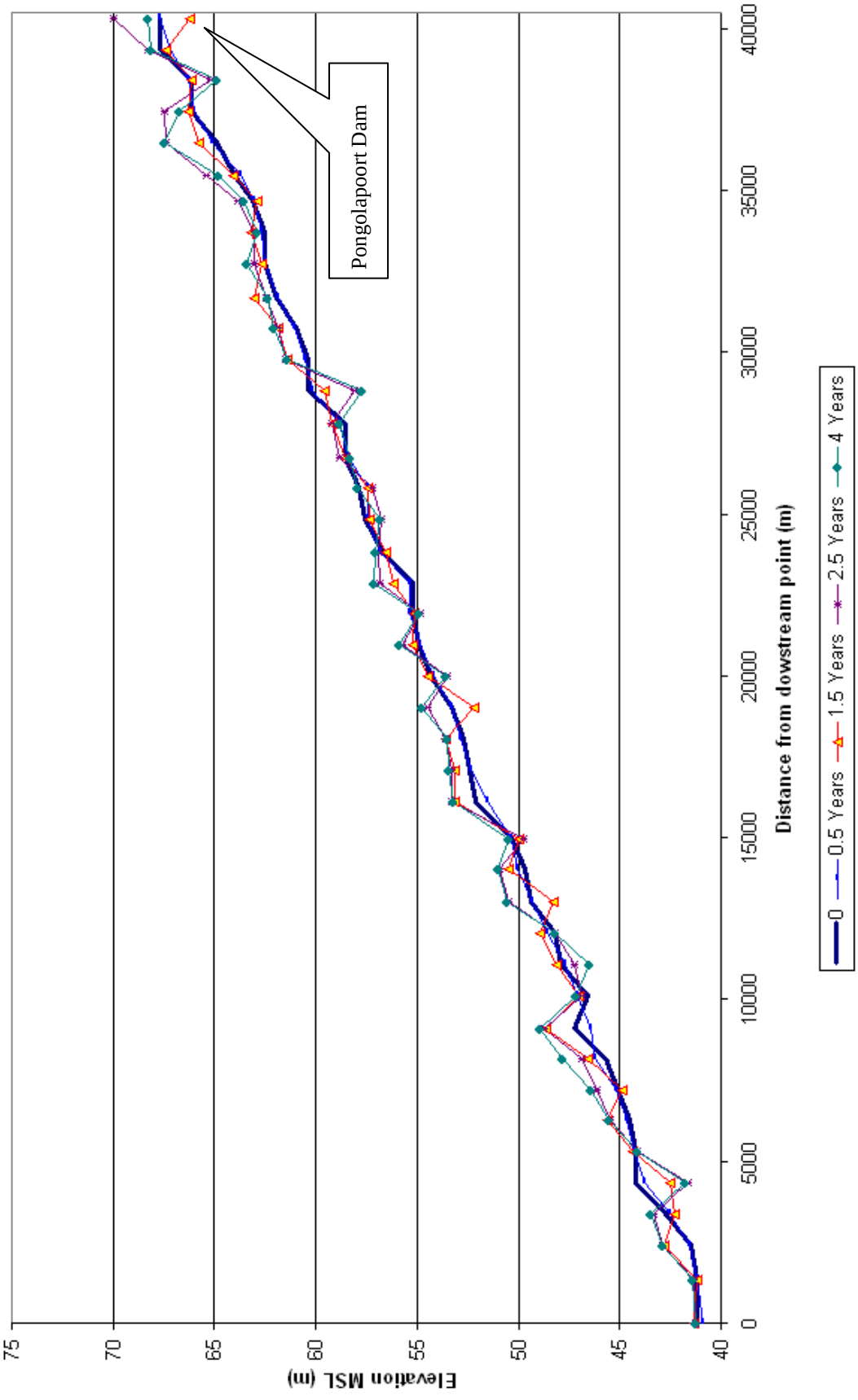

Figure 5.3.21 Longitudinal profile – scenario 1

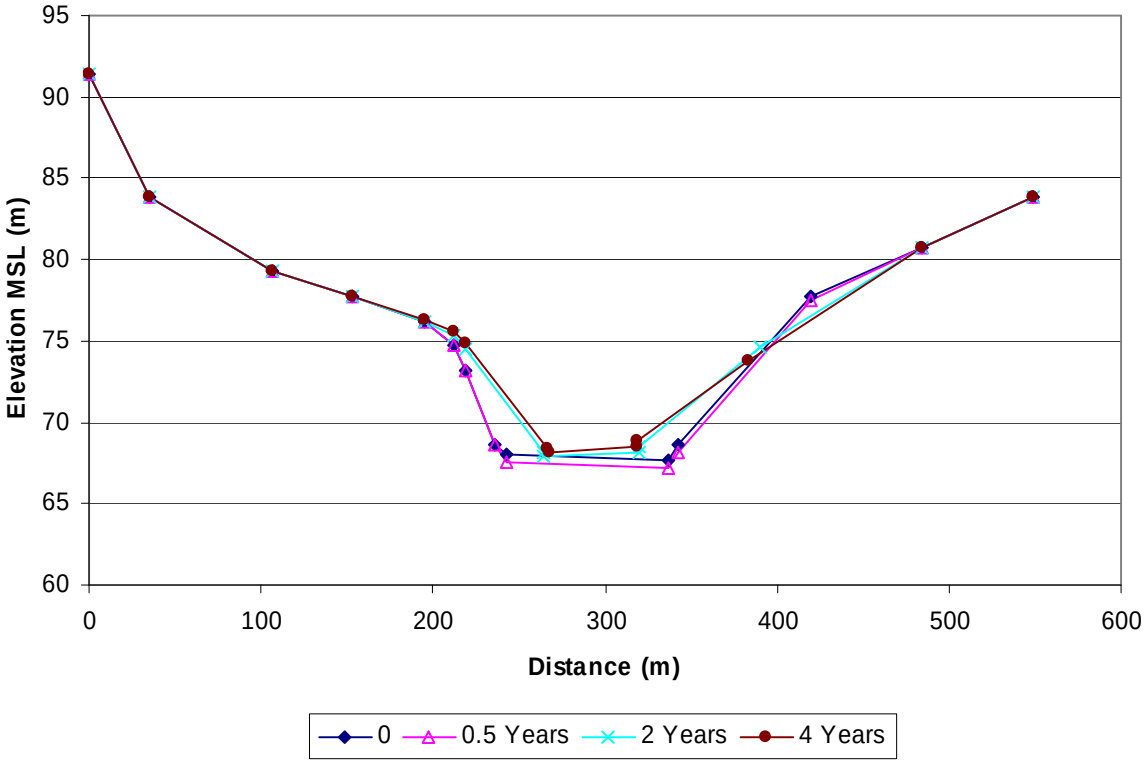

Figure 5.3.22 Cross-section changes with time at 1 km – scenario 1

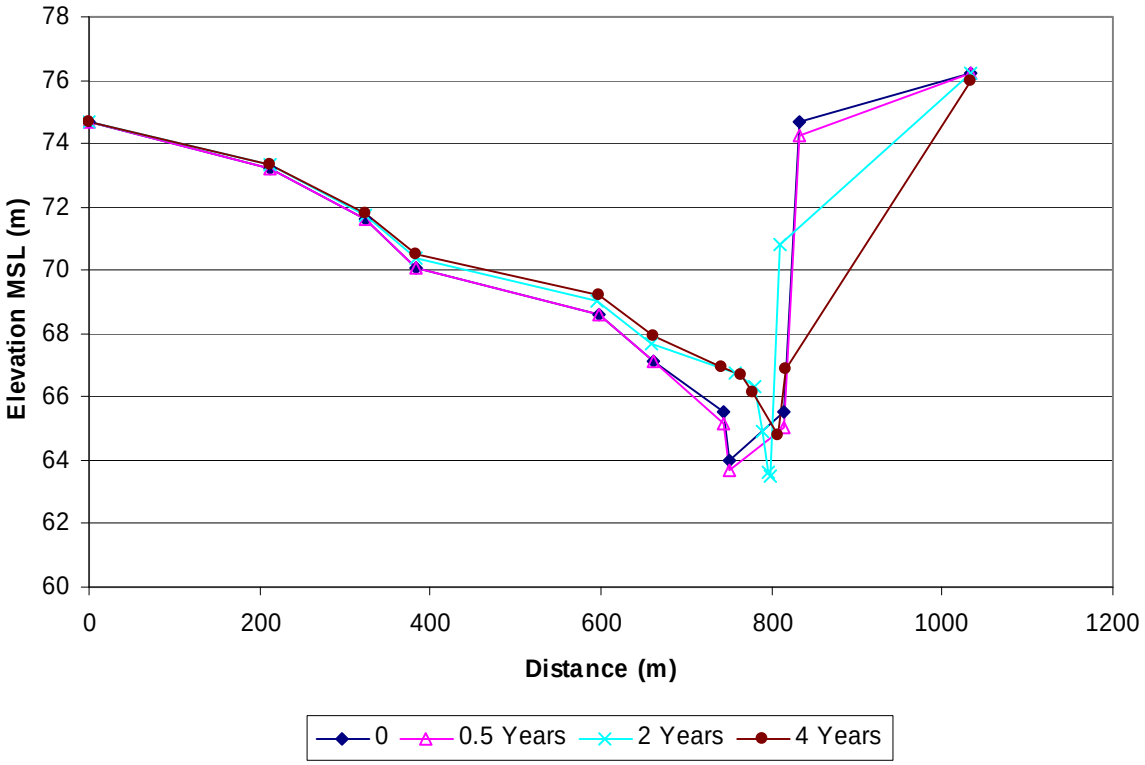

Figure 5.3.23 Cross-section changes with time at 5 km – scenario 1

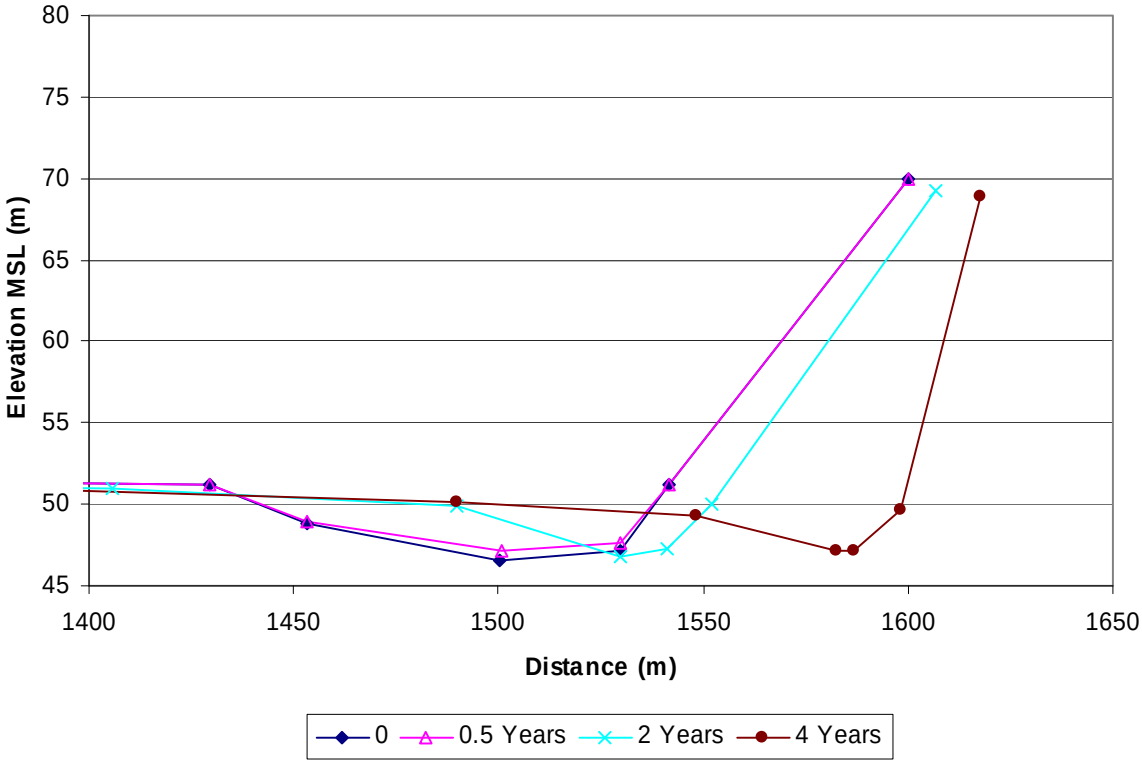

Figure 5.3.24 Cross-section changes with time at 30km – scenario 1

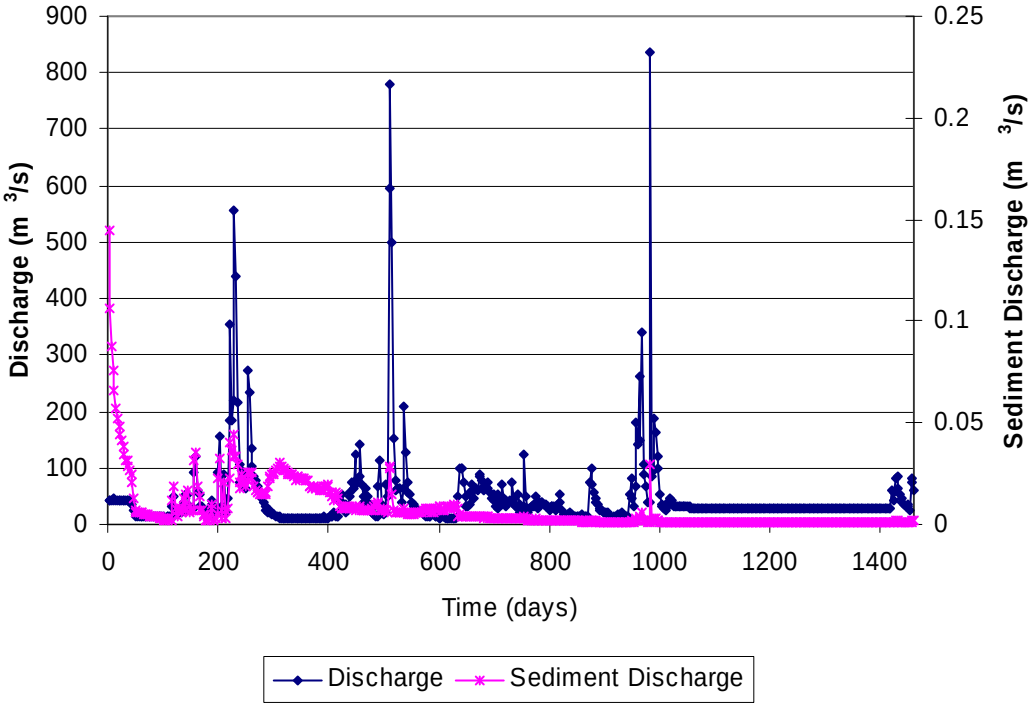

Figure 5.3.25 Streamflow (average over 60 hours) and simulated sediment load exiting the reach – scenario 1

Scenario 2:

Under scenario 2 the trend is much the same, as the dam spills regularly. However, since there is no incoming sediment, scour is taking place close to the dam. Many cross-sections have become deeper (**Figure 5.3.26**) and the slope tended to be somewhat flatter (**Figure 5.3.27**) than the original. Many cross-sections became narrower than under scenario 1, by about 18%, while some were simulated to become wider (**Figure 5.3.28**). Those that were simulated to become narrower were well within the range of what could be observed from aerial photographs. The simulated reduction in width for the cross-section shown in **Figure 5.3.29** was 25 m (from 142 m to 117 m), and the observed reduction in width was 30 m.

Together with the cross-sectional changes the bed material composition also changed somewhat (**Figure 5.3.30**). Fraction 1 (finest) was reduced by about 10 % over the first 8 km, while the percentage of fraction 2 increased by about 10% over that distance. Fraction 3 on the other hand remained almost unchanged. These changes are as observed in the field, with coarser material being exposed close to the dam as most of the fine material is washed away. Had the simulations been done over a longer period, the changes would have been more dramatic, and would probably have shown much the same trend as depicted in **Figure 2.5.2**.

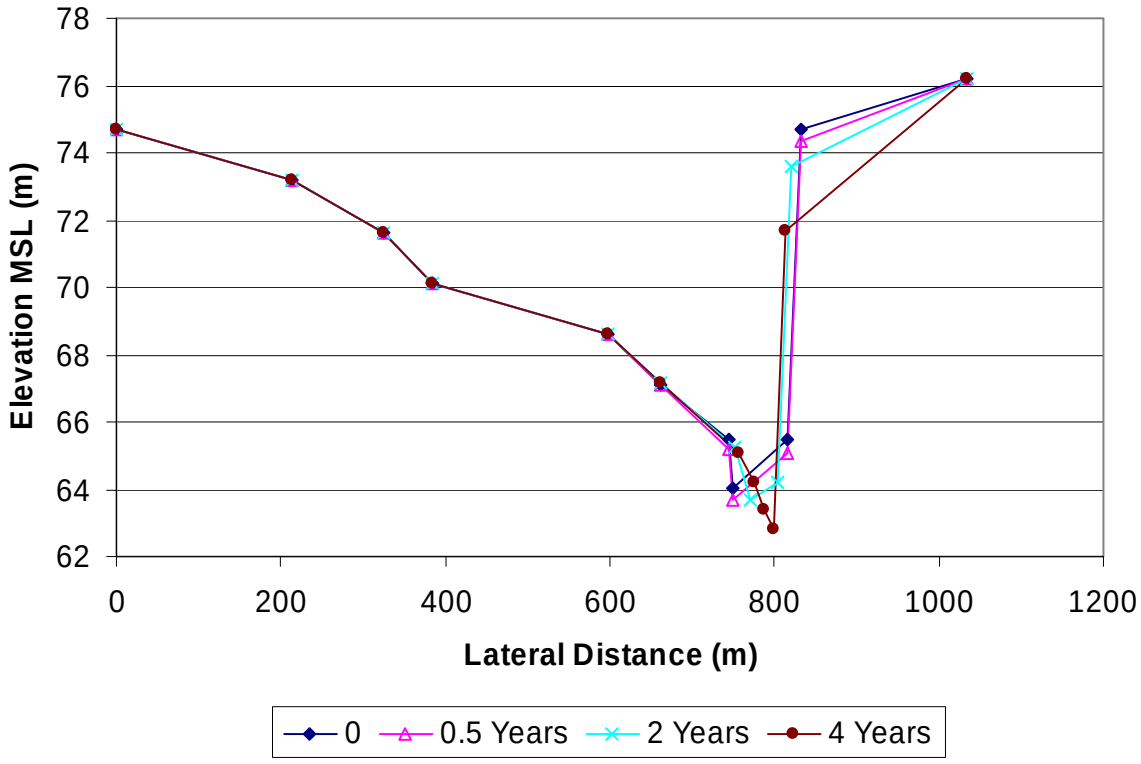

Figure 5.3.26 Cross-section changes with time at 5 km – scenario 2

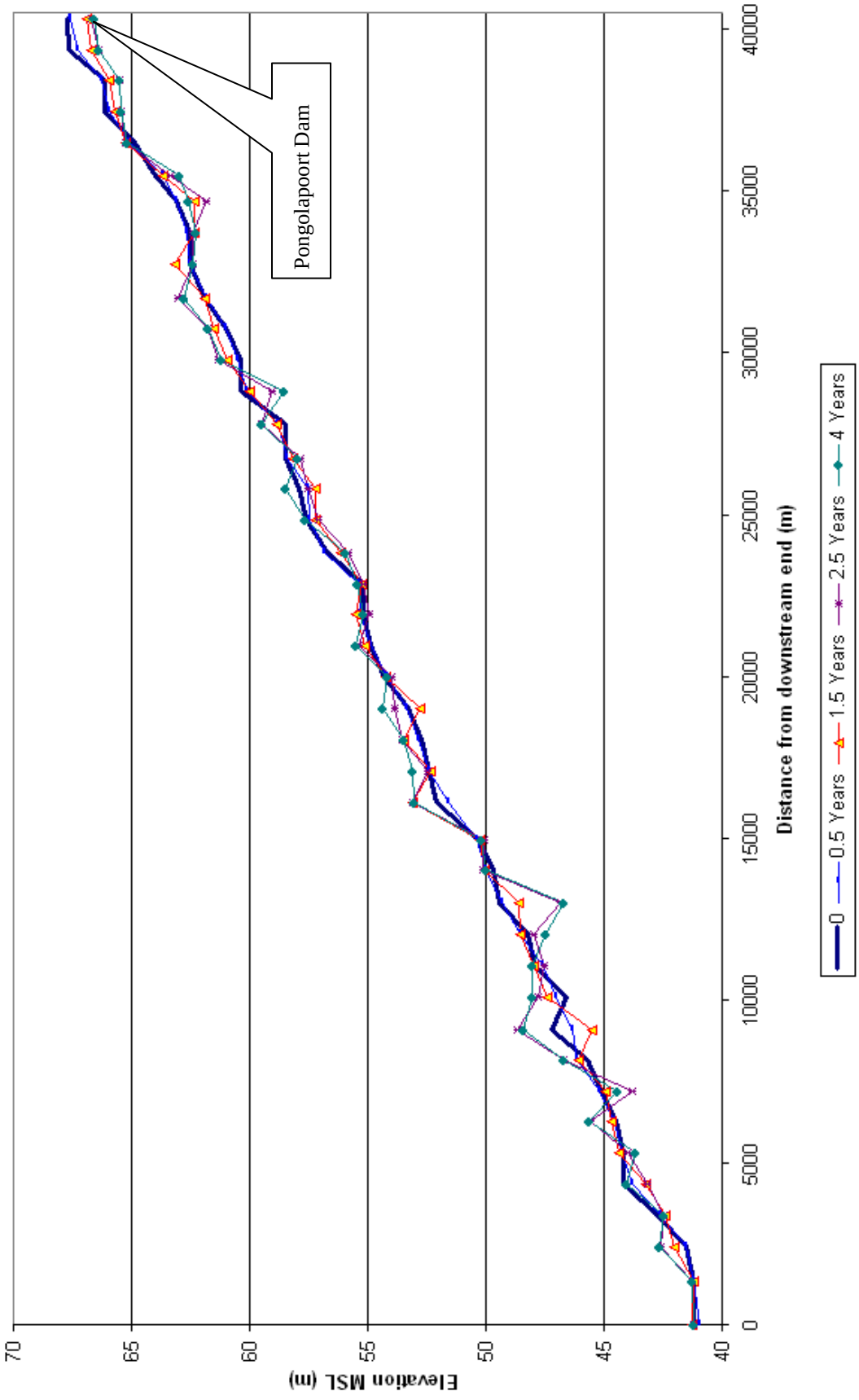

Figure 5.3.27 Longitudinal profile – scenario 2

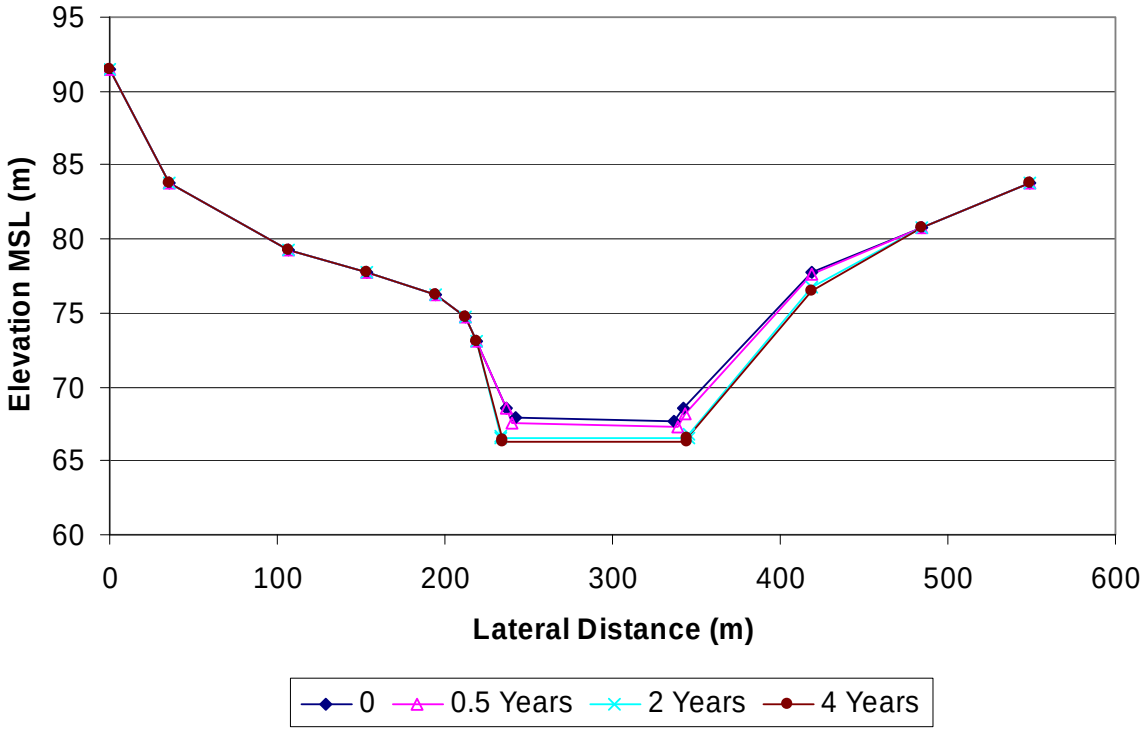

Figure 5.3.28 Cross-sectional changes with time at 1 km –scenario 2

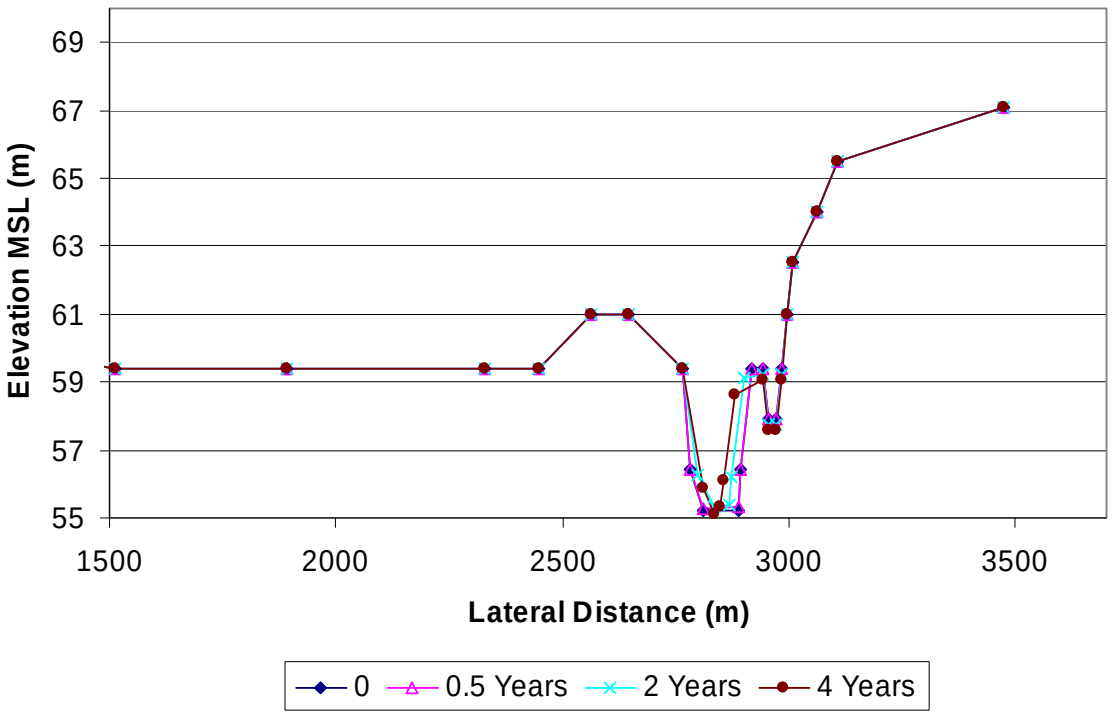

Figure 5.3.29 Cross-sectional changes with time at 18 km – scenario 2

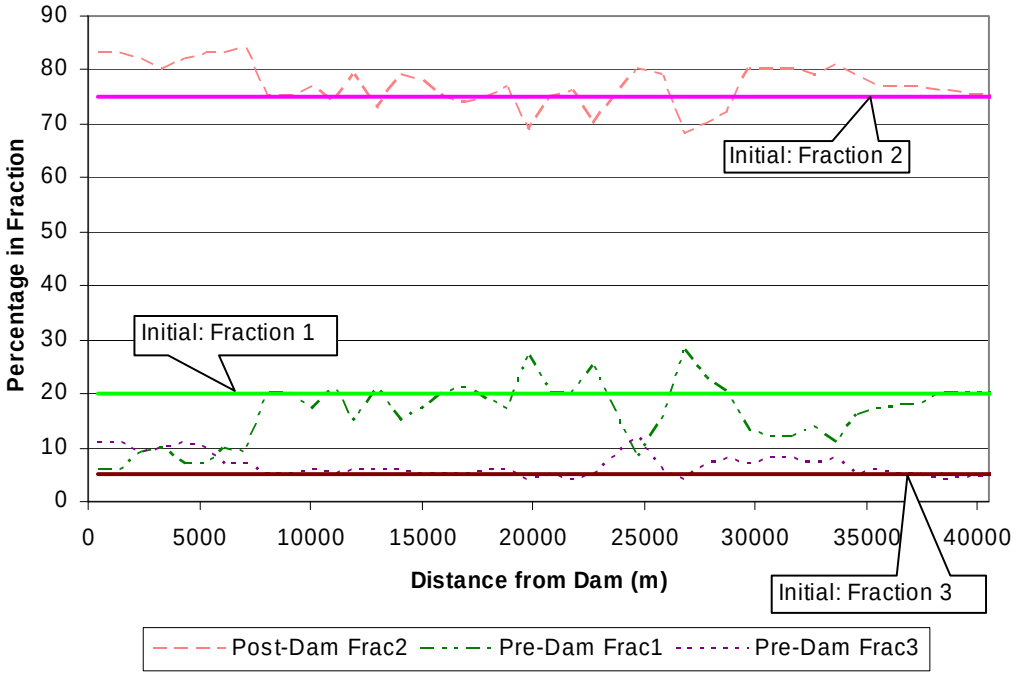

Figure 5.3.30 Bed material changes – scenario 2

Just as for scenario 1, the model seemed to need an initial adjustment period. Through the first few floods higher sediment loads were simulated than during the rest of the simulations (see **Figure 5.3.30**).

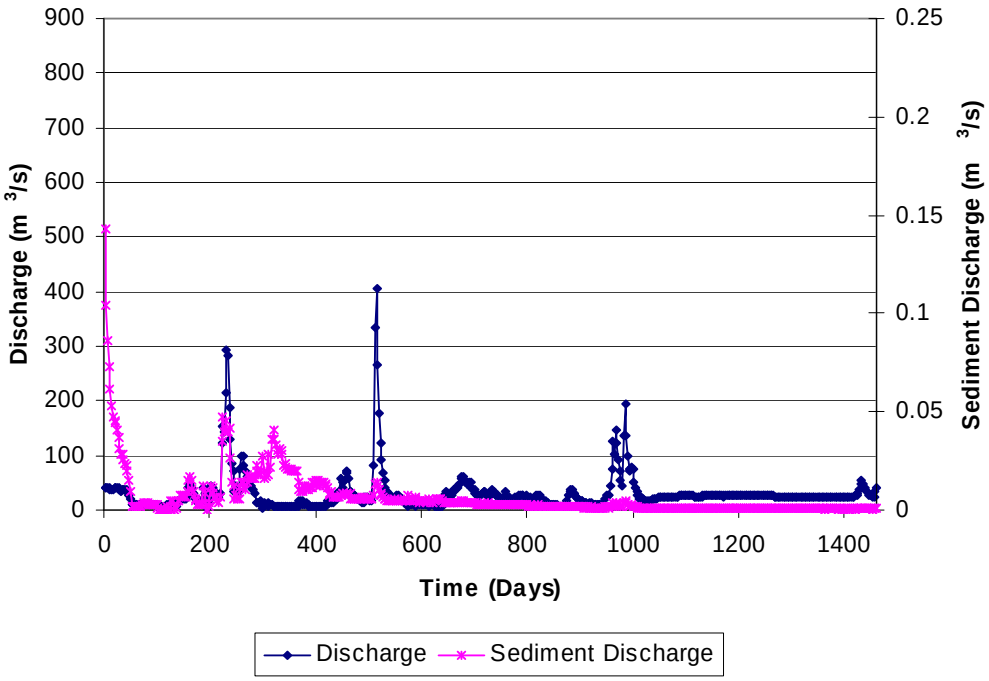

Figure 5.3.31 Streamflow (average over 60 hours) and simulated sediment load exiting the reach – scenario 2

Scenario 3:

Simulations of scenario 3 yielded some very interesting results. In general the river did not change as much as for the other two scenarios. As can be seen from **Figure 5.3.32** the longitudinal profile is very stable, with some areas undergoing degradation, such as close to the dam, while others experience aggradation, but in neither case more than 1 meter.

The width and depth for most cross-sections did not vary considerably with time, but rather remained very close to the original shape (**Figure 5.3.33**), except those very close to the dam, which underwent scouring. The reason for the comparatively little change is that the streamflow variability has been drastically reduced as compared to the first two scenarios. Most of the time the flows are less than 10 m^3/s, which means that practically no sediment transport takes place. Since the minimisation of stream power procedure is dependent on the sediment transport, width and depth adjustments will only take place during larger flows, while the rest of the time the cross-sections will remain more or less unchanged. As a result the cross-sections are actually larger for most of the time than for scenario 2, although one would expect that due to the reduction in streamflow the cross-sections would become smaller. In reality vegetation becomes established on the banks due to the absence of regular floods, and the continuous baseflow could stabilize the river banks to some degree and the river may become deeper and narrower.

Due to the infrequent flooding taking place, a large amount of sediment is available during the floods, because it cannot be transported during the low flows (**Figure 5.3.34**). With the more regular flooding in scenario 2, sediment is transported most of the time, and less sediment is available during floods, mostly less than the sediment transport capacity. In scenario 3, however, the sediment availability is not as much of a factor and therefore in total more sediment can be transported. As can be seen from **Table 5.3.5**, the total cumulative sediment transport over the four year period is about 30% greater than for scenario 2.

Table 5.3.5 Cumulative sediment loads – all scenarios

Scenario	Incoming sediment load (ton/a)	Outgoing sediment load (ton/a)
1	1380 000	385000
2	0	330000
3	0	450000

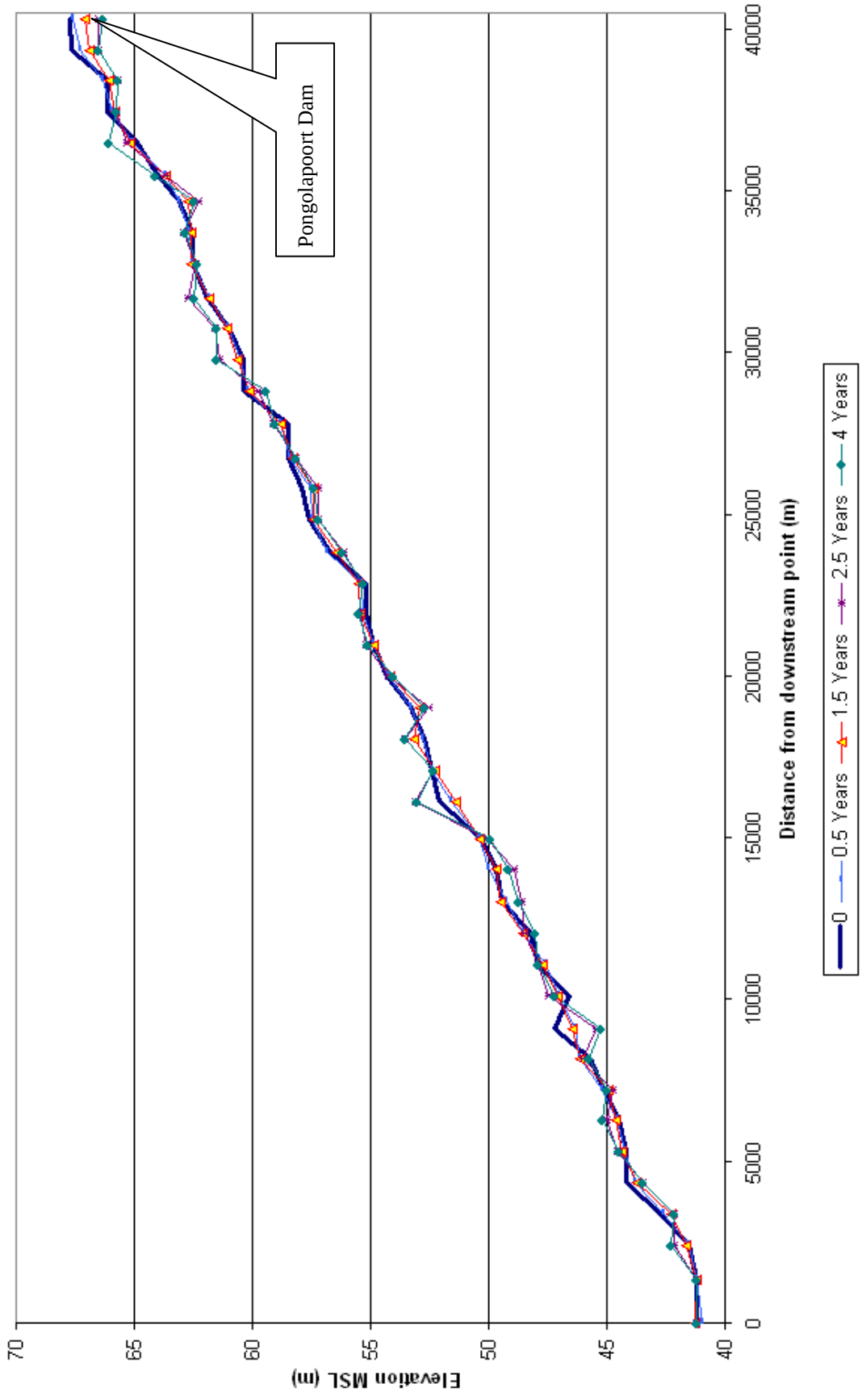

Figure 5.3.32 Longitudinal profile – scenario 3

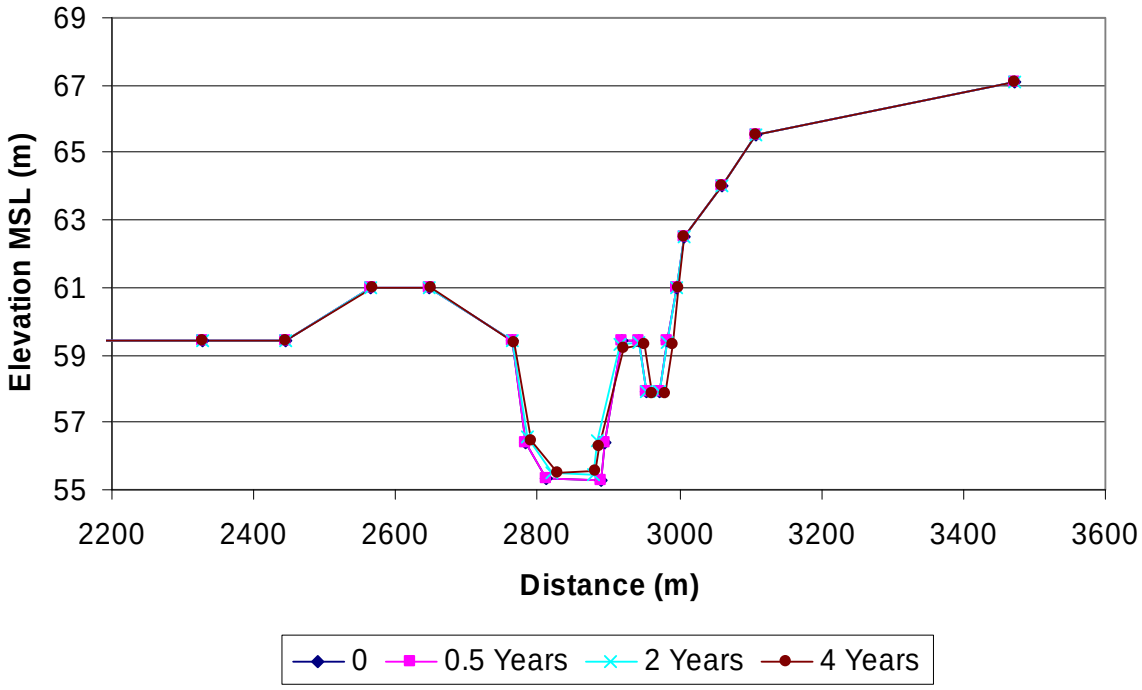

Figure 5.3.33 Cross-sectional changes at 18 km – scenario 3

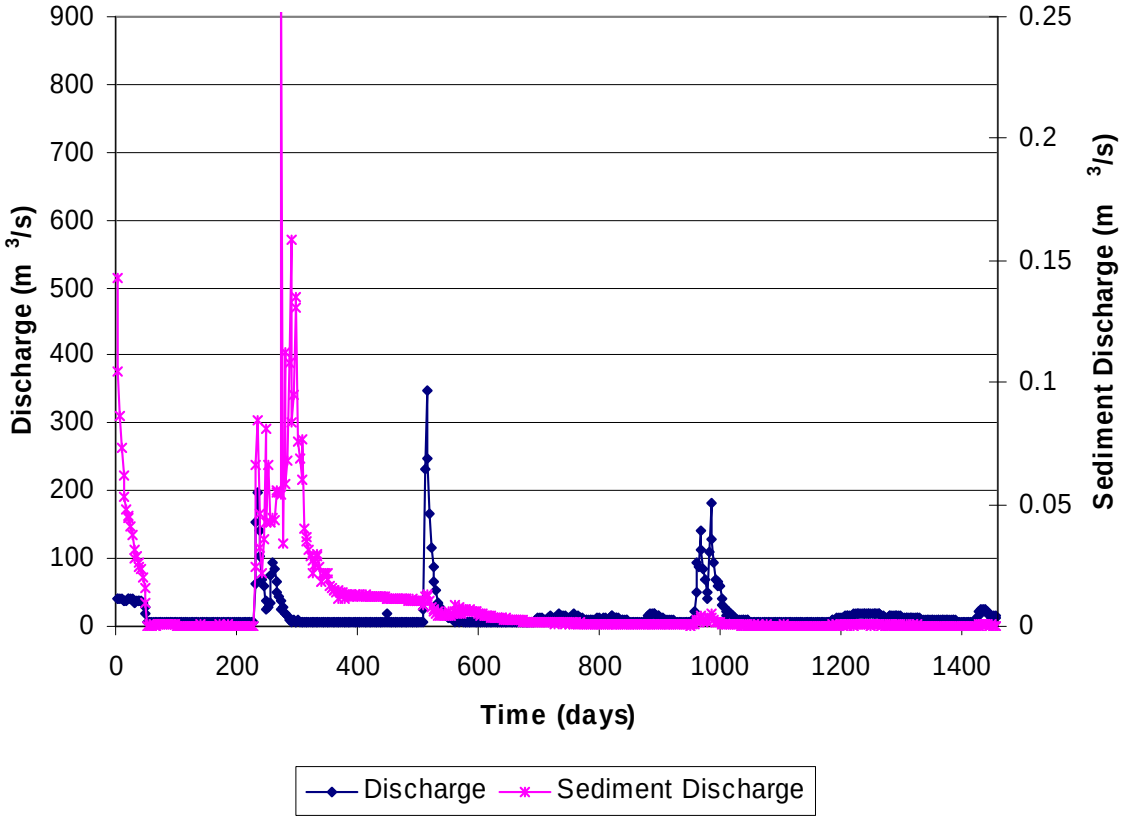

Figure 5.3.34 Streamflow (average over 60 hours) and simulated sediment load exiting the reach – scenario 3

5.4 Case Study: Proposed Skuifraam Dam - Berg River

The upper 73 km of the Berg River downstream of the proposed Skuifraam Dam up to Hermon was used in this case study (see **Figure 5.4.1**). The upper reaches are steep (**Figure 5.4.2)** while downstream of Wellington the slope decreases and the riverbed material consists of sand. While only 73 km of the Berg River was considered, it does not mean that the dam could not have a significant impact on the estuary, especially since the lower Berg River reaches have a low gradient with cohesive bed sediment, which would decrease sediment transport capacity and limit re-entrainment of the sediment.

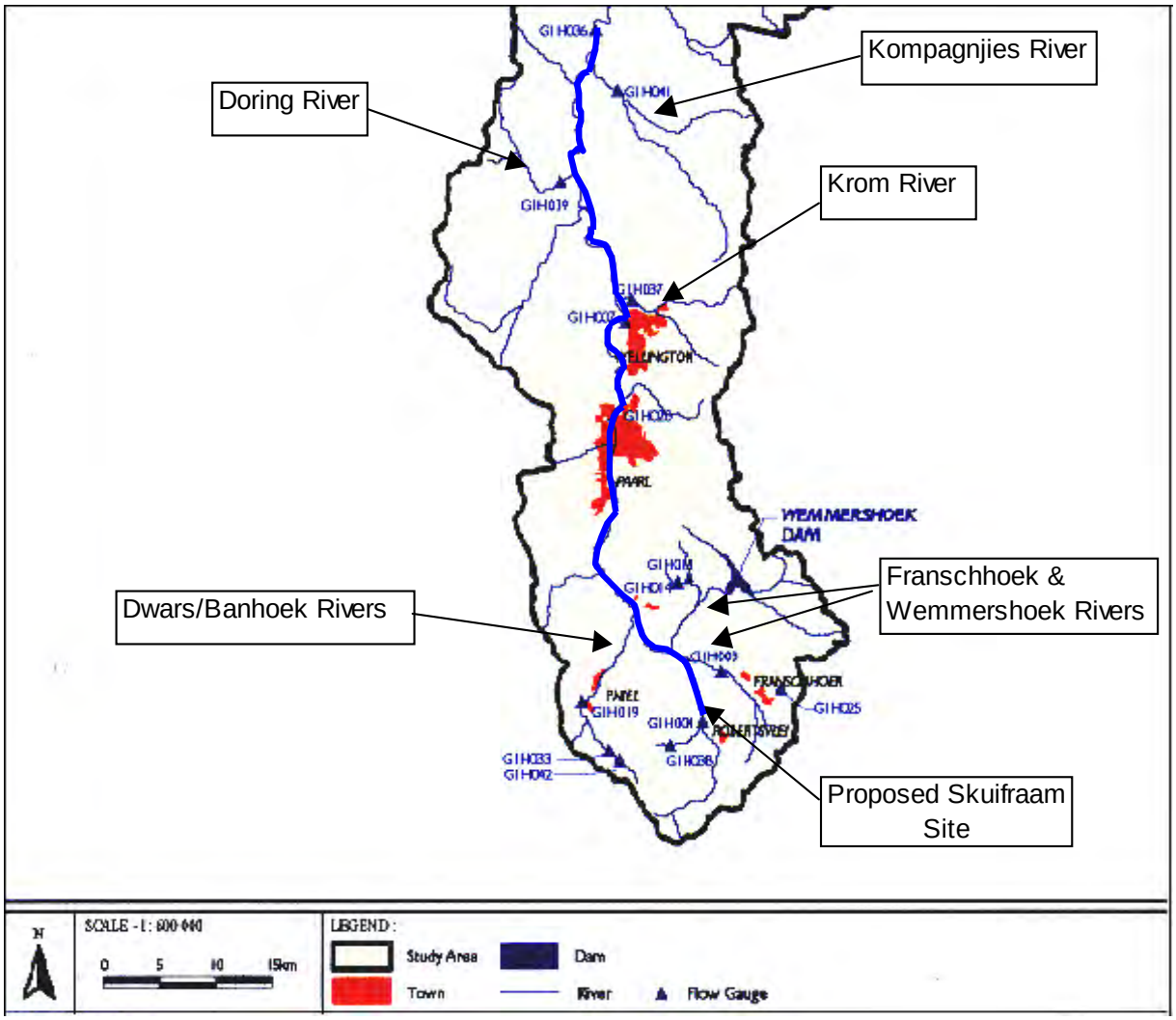

Figure 5.4.1 Berg River system (Nitsche, 2000)

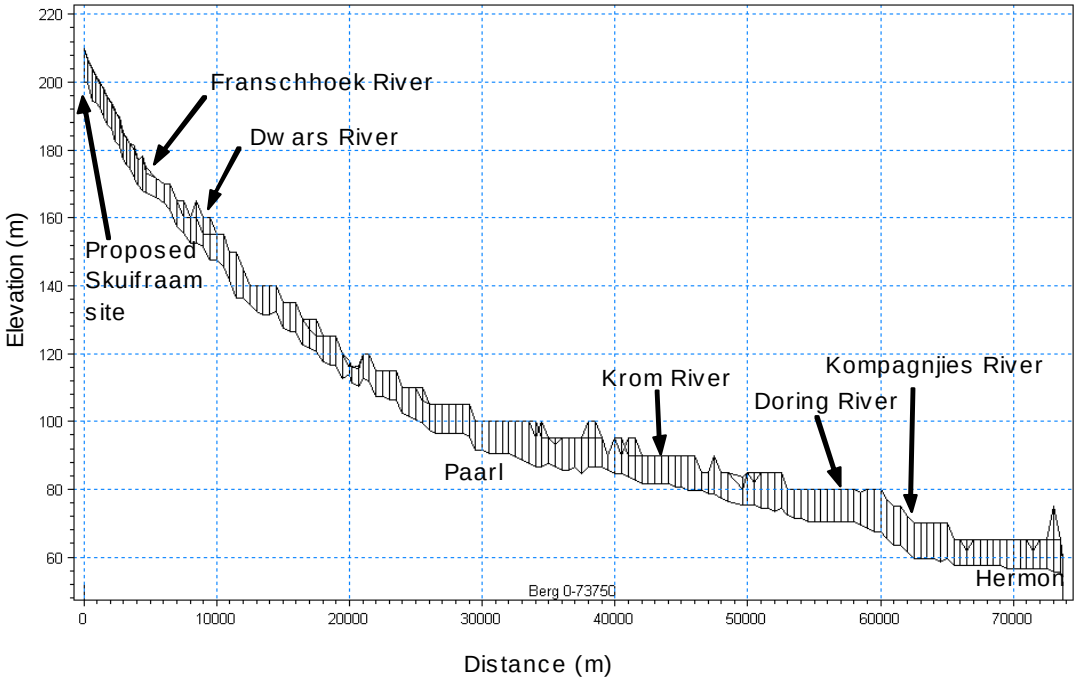

Figure 5.4.2 Longitudinal bed profile of Berg River (vertical lines indicating left and right-hand river bank)

5.4.1 Data Requirements

- River cross-sections

Surveyed river cross-sections of the upper 4 km immediately downstream of the dam were obtained from the Department of Water Affairs and Forestry (DWAF). Other surveyed sections further downstream were obtained from data in a report by Nitsche (2000). Most of the cross-sections were however obtained from orthophotos. The interval between cross-sections typically varies from 300 to 500 m.

- Flow records

Observed flow records are available at three DWAF stations along the Berg River: G1H004, which measures most of the Skuifraam Dam inflow, G1H020 at Paarl, and G1H036 at the Hermon bridge. The discharge table limits for stations G1H004 and G1H036 had to be extended to include medium and large floods and was based on recommended discharge tables of the Western Cape Systems Analysis study (1990).

The tributaries with flow measurement stations that were used in this study are: Franschhoek, Dwars, Krom, Doring and Kompagnjies. The measured tributary flows had to be scaled to

allow for unmeasured catchment areas, and this was done after calibration on the Berg River based on observed flood peak attenuation and the catchment areas at the stations to obtain a relationship as function of catchment area ratio. Wemmershoek River flows had to be simulated by scaling up the Franschhoek River record, since no records on flow releases from the dam were available from DWAF.

Also the flow data for the Krom River does not extend beyond 1992. The flows for that subcatchment were therefore expressed as a fraction of the flows of the Kompagnjies River. The scaling factors used are indicated in **Table 5.4.1**.

Table 5.4.1 Scaling of unmeasured flows

Tributary	**Flow gauging station catchment area (km²)**	**Scaled up catchment area (km²)**	**Flow factor**
Franschhoek (G1H004)	46	308	4.5
Dwars (G1H019)	25	231	9.2
Krom (G1H041/G1H037)	141	69	0.6
Doring (G1H039)	42	307	0.82
Kompagnjies (G1H041)	141	325	0.72

The flow scaling factors of the Krom, Doring and Kompagnjies catchments are relatively low and can only be attributed to the inaccurate extension of the discharge table (DT) limits on the Berg River. The station at Hermon (G1H036) DT is based on current meter gaugings at high flows and should have an accuracy of say 30% at high flows. At this stage it seems as if the discharges at Paarl (G1H020) are overestimated by the DT, but a combination of factors could play a role. The deposition patterns upstream and downstream of Paarl could therefore be worse if the G1H020 floods are in fact smaller.

This exercise was carried out on a 10-year flow record (primary/break point data), 1990 to 2000. The selected flow record contains relatively large floods and is representative of the long-term flow record of the Berg River for current development conditions.

- Artificial annual flood

The originally proposed artificial flood to be released once annually during July, had a peak discharge of 160 m³/s and a relatively long duration with a total volume of 9.8 million m³. A

more “naturally” shaped hydrograph was obtained from Ninham Shand (NS, 2001), with a flood volume of 5 million m³. This flood was used in the sediment transport simulations in this study and is shown in **Figure 5.4.3**. More detailed analysis was also carried out of observed flood hydrographs by NS (2001), but the flood volume is similar to the flood used in this case study.

- Sediment yield

The sediment input into the Berg River system is important in quantifying the sediment balance in the river. The sediment yield can be determined from observed sedimentation volumes in reservoirs or from sediment sampling in the river. Rooseboom (1992) gives a regional sediment yield of 35 t/km².a, based on reservoir basin surveys. Most of these reservoirs are however quite far from the Berg River. No river sediment sampling data are available, not from the DWAF water quality database or from municipal water treatment plants along the river. The approach followed in this case study was to use local observed reservoir sedimentation information instead of a regional approach.

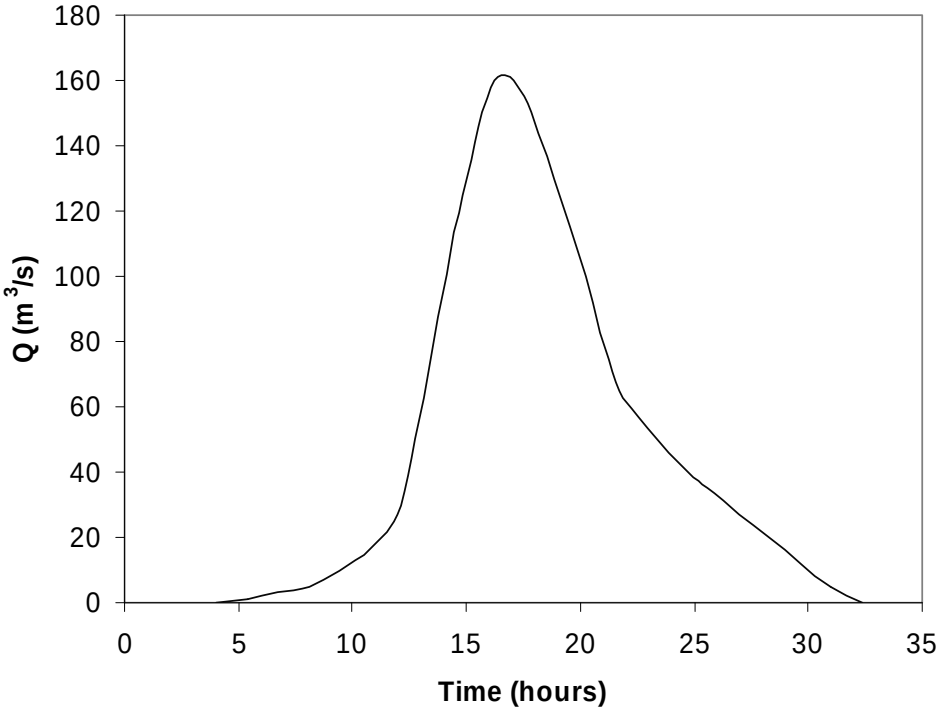

Figure 5.4.3 Artificial flood hydrograph

Wemmershoek and Kleinplaas Dams are the only two dams with relatively large trap

efficiencies that could be used. Kleinplaas Dam is not in the Berg River catchment, but climatically and geologically the conditions are similar. Wemmershoek Dam is located on a tributary of the Berg River and was constructed in 1957. The dam has a catchment area of 86 km² and a survey in 1984 indicated 1.1 million m³ sedimentation. If this volume is converted to a 50-year volume with a density of 1.35 ton/m³, the sediment yield is 270 ton/km².a, which is relatively high. The catchment upstream of the dam consists of Malmesbury shale, which is not that typical of the rest of the Berg River catchment, although the Franshoek River catchment also has Malmesbury shale. Kleinplaas Reservoir lost about 20 % of its capacity due to sedimentation within the first 9 years of operation, which is equivalent to a sediment yield of 120 ton/km².a. This sediment yield is also much higher than the regional yield.

The sediment yield used in this case study is 120 ton/km².a, based on the Kleinplaas Dam data and a site inspection, which indicated easily erodible alluvial sediments downstream of Wemmershoek Dam (**Figure 5.4.4**).

Figure 5.4.4 Wemmershoek catchment erosion

The sediment load input into the Berg River is indicated in **Table 5.4.2**.

Table 5.4.2 Sediment input at simulation boundaries

River	Mean annual sediment load (ton)
Berg (G1H004)	9418
Franschhoek	28209
Dwars	29652
Krom	8298
Doring	32264
Kompagnjies	36535

- Sediment load-discharge relationship

It is important to establish a sediment load-discharge relationship at each inflow into the Berg River. Normally such a relationship should be obtained from observed suspended sediment sampling over at least 5 years, but in this study no such data are available. In this project, it was found that the sediment transport capacity could be used if suspended sediment data are not available. The sediment transport capacity and sediment load are therefore calculated and integrated over the 10-year period, and scaled down due to sediment availability to obtain the sediment yield of 120 t/km².a.

- Sediment particle size fractions

The sediment grading of bed sediment at IFR site 1 (near dam site), is indicated in **Table 5.4.3** (Engelbrecht, 1996).

Table 5.4.3 Sediment grading analysis at IFR site 1

Sediment size range (mm)	Percentage distribution in pool	Percentage distribution in riffle	Percentage distribution in cobble bar
< 2	8	0	0
2 - 8	2	1	0
8 – 16	0	2	1
16 – 64	20	18	18
64 – 128	36	28	31
128 – 256	20	31	25
> 256	14	20	25

The median sediment diameter in the bed (riffle and bar) is 128 mm, while in the pools it is about 94 mm due to the presence of sand. During a field visit in November 2001 of the first 4 km downstream of the dam, sand deposits between boulders were observed in pools, riffles and cobble bars, indicating that even after a relatively "wet" winter in the Western Cape with high floods the sediment transport capacity is limiting the transport of sand. At the Wemmershoek River sand deposits apparently covered all the boulders up to the end of this winter in October, when most of it was finally washed away. **Figure 5.4.5** shows the bed sediment near the dam site.

The field inspection generally indicated more sand in the bed close to the dam site than indicated in **Table 5.4.3**, and this could be a seasonal effect or can be attributed to the bush fire of 1999, which destroyed most of the afforestation in the catchment. Bush fires are however not uncommon in the Western Cape and occur regularly.

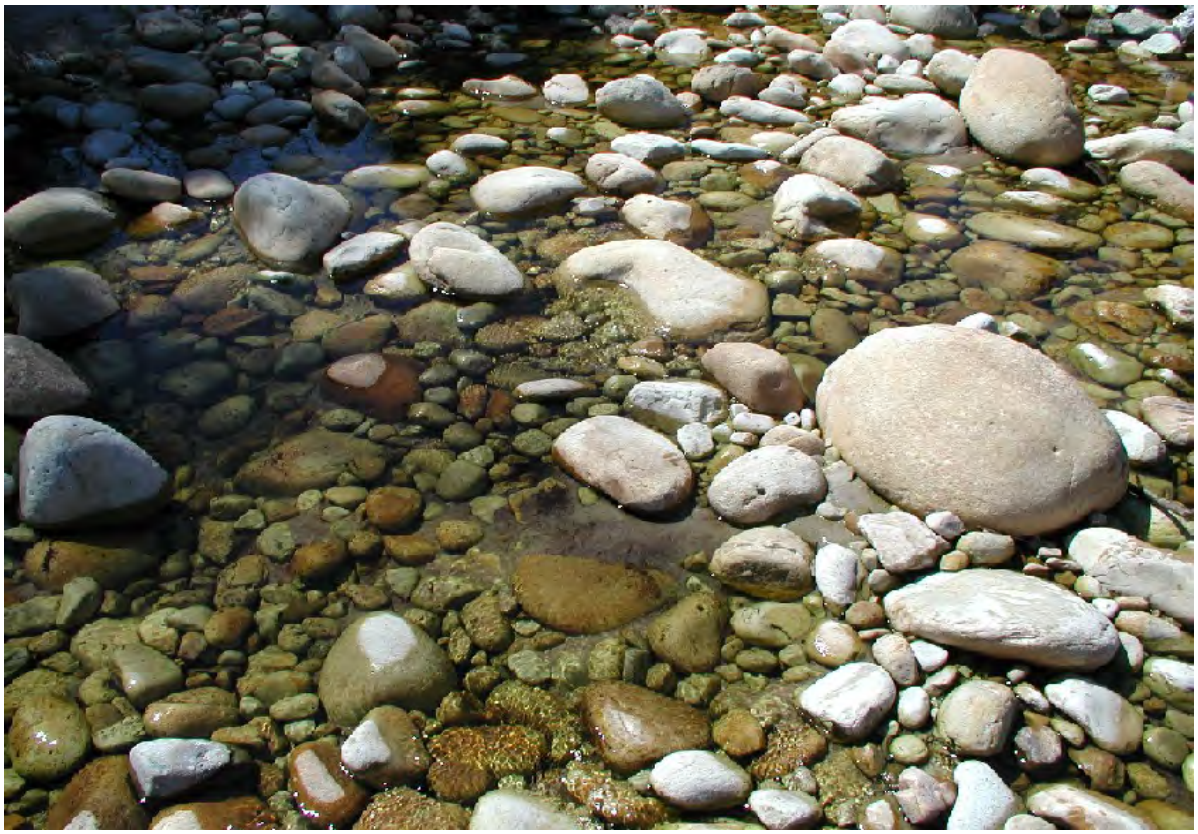

Figure 5.4.5 Upper Berg River bed sediment

Sand bed samples taken 100 m downstream of the dam site and at the Paarl-Franschhoek Road bridge have a median diameter of 0.5 mm. Sediment samples were also obtained further

downstream as indicated in **Table 5.4.4**, and the median diameter decreases to about 0.2 mm, indicating sediment deposition of finer sediment.

Table 5.4.4 Sediment grading analysis downstream of IFR site 1

Sediment size range (mm)	Road bridge (4 km downstream from dam site)	Paarl weir	Paarl-Wellington Road bridge	Hermon bridge
2.36 – 1.18	3.55	7.72	0.45	0.15
1.18 – 0.6	26.84	38.47	12.7	0.31
0.6 – 0.3	61.09	48.47	71.58	26.03
0.3 – 0.15	6.86	3.72	10.98	57.93
0.15 – 0.075	0.3	0	1.65	10.16
< 0.075	0.59	0.57	2.56	4.97

5.4.2 Skuifraam Reservoir Routing

Two of the three scenarios considered in this study include Skuifraam Dam. The proposed reservoir will cause flood attenuation and this effect had to be calculated to create the upstream flow boundary for the computational model. Level pool routing was carried out with the following Skuifraam Dam characteristics as obtained from Ninham Shand (NS, 2001):

- Full supply capacity: 126.4 million m^3
- Full supply level: 250 m
- Net demand on reservoir (including agricultural and environmental releases, as well as inflows from the supplement scheme and Theewaterskloof Dam): 99 million m^3/a
- Spillway length: 150 m

The 10-year flow record 1990 – 2000 was routed through the reservoir, using hourly time steps. The routing was also repeated for the artificial flood release scenario. The artificial floods were incorporated by replacing a naturally occurring flood in July (first flood larger than 50 m^3/s) of each year with an artificial one in order to have them coincide with floods from the subcatchments, which can, however, not be guaranteed. The pre-dam flows at the dam site and the post-dam flows with and without artificial flood releases are indicated in **Figures 5.4.6** to **5.4.8** respectively.

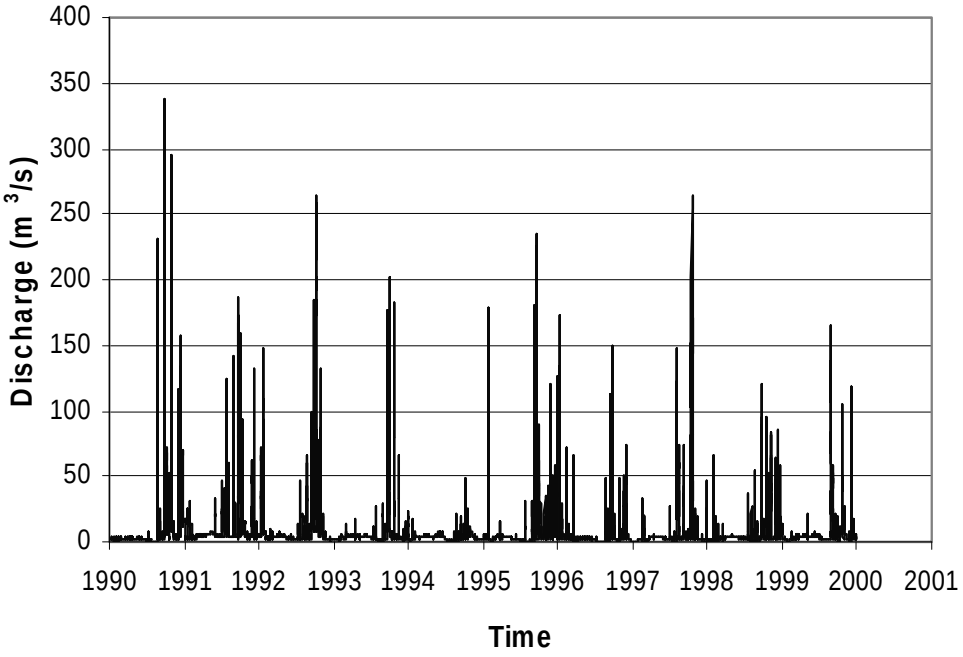

Figure 5.4.6 Current development flows at proposed dam site (hourly data)

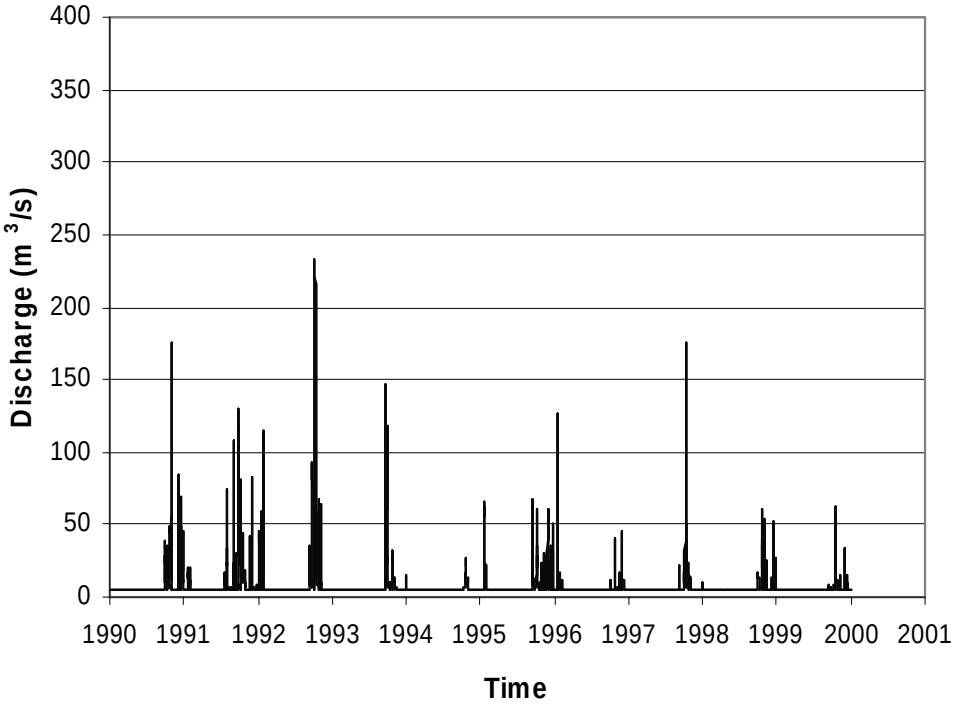

Figure 5.4.7 Post-dam scenario flows at dam without artificial flood releases (hourly data)

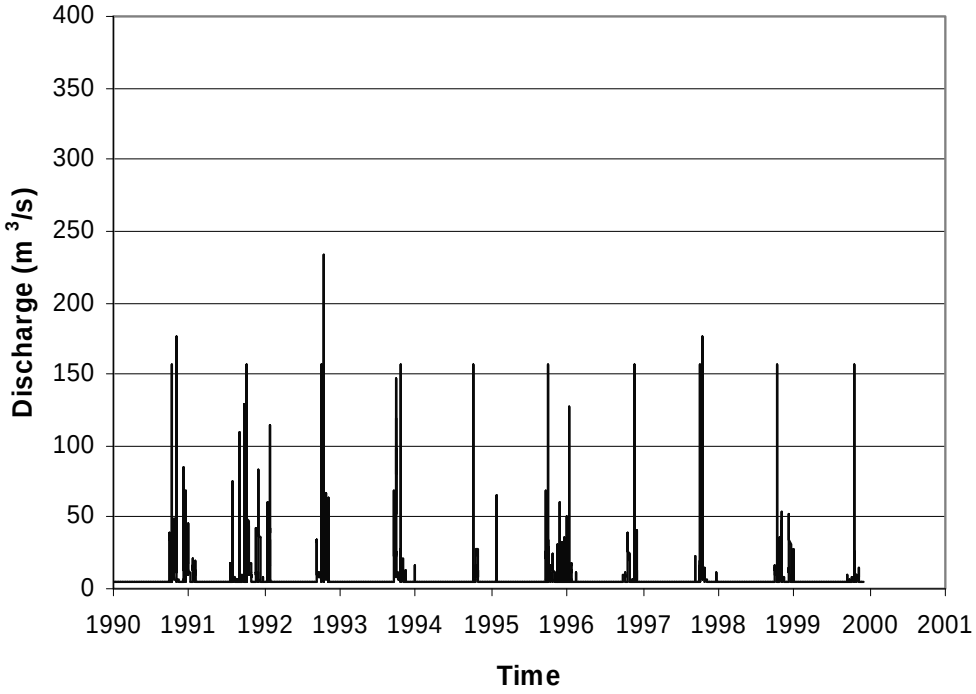

Figure 5.4.8 Post-dam scenario flows at dam with artificial flood releases (hourly data)

5.4.3 Hydrodynamic Model Calibration

The hydrodynamic and morphological model Mike 11 of the Danish Hydraulic Institute has been used in the simulations. The Berg River from the dam site to Hermon Bridge, about 73 km, was included, with tributary inflows at Franschhoek River (scaled up to include Wemmershoek River and ungauged catchment), Dwars River, Krom River, Doring River and Kompagnjies River. Very little time was available for calibration during this study, but a reliable calibration based on observed flows at Paarl and Hermon records could be established. Considering the extension of discharge tables, the observed flood discharges would at best have a 20 % accuracy to typically 30 %. The observed and simulated flow records on the Berg River at Paarl and Hermon are indicated in **Figures 5.4.9** and **5.4.10** respectively.

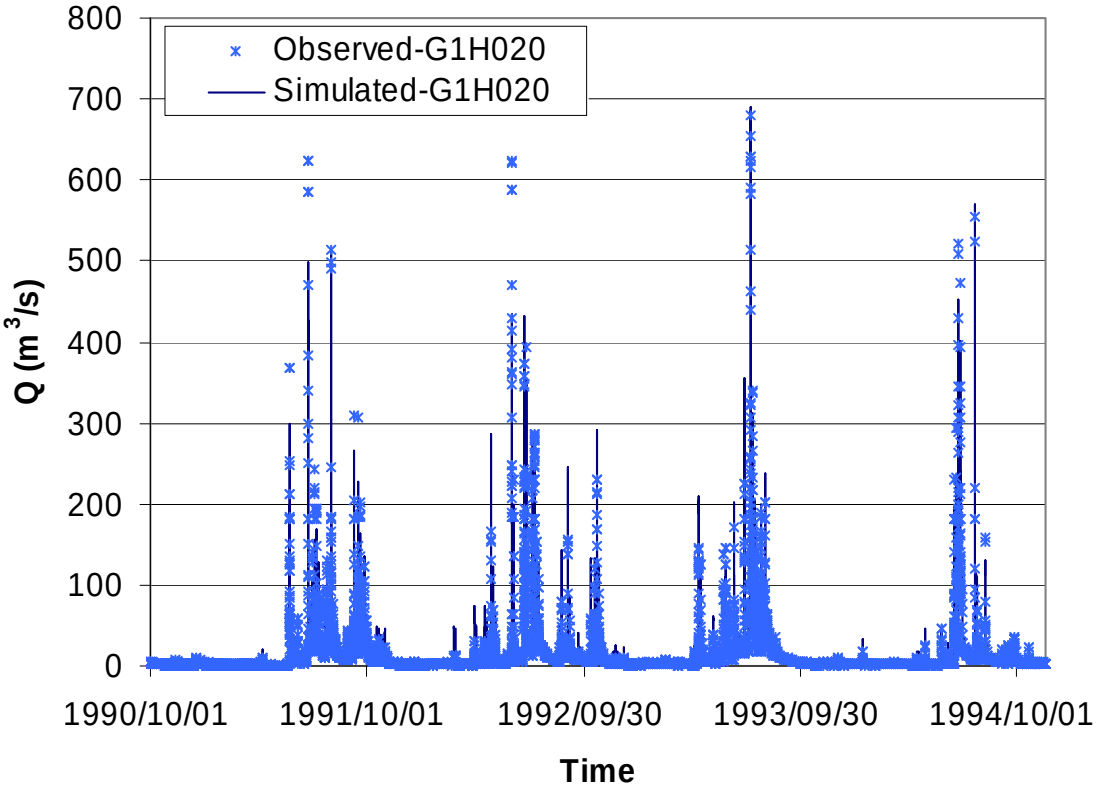

Figure 5.4.9 Calibration of flows at Paarl (G1H020)

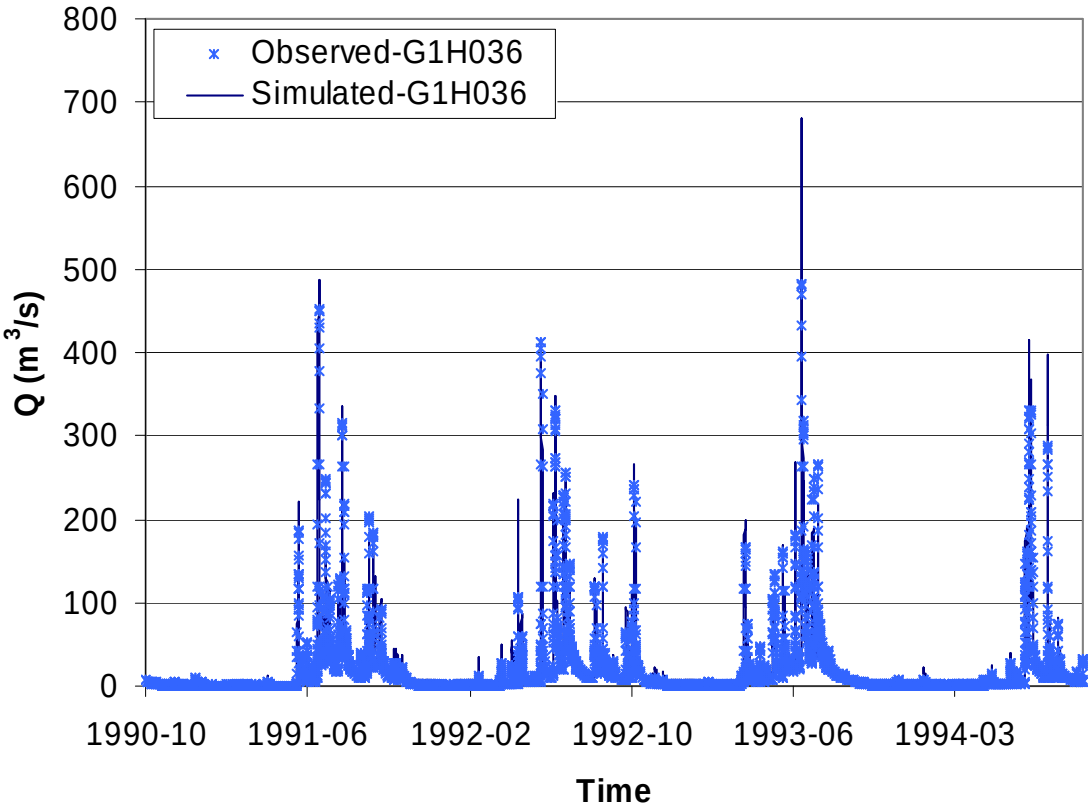

Figure 5.4.10 Calibration of flows at Hermon (G1H036)

5.4.4 Effect of proposed Skuifraam Dam

- Flood peaks:

Recurrence interval floods have been determined based on a statistical analysis of flow records at the G1H004 station (Skuifraam Dam), Paarl, G1H020, and at Hermon, G1H036, and are indicated in **Table 5.4.5**.

Table 5.4.5 Flood recurrence intervals (current development)

Recurrence interval (yr)	G1H004 - Skuifraam Dam (m^3/s)	G1H020 - Paarl (m^3/s)	G1H036 - Hermon (m^3/s)
2	240	350	230
10	440	600	460
20	610	690	560
50	780	820	690
100	920	920	800

Skuifraam Dam will reduce the flood peaks by about 40% in the upper reaches and by about 20% downstream of Paarl, as indicated in **Table 5.4.6**. The expected recurrence interval flood peaks were determined by obtaining a reduction factor from the routed 10-year flow record, and applying that to the long-term observed flood peaks.

Table 5.4.6 Flood recurrence intervals (Skuifraam Dam)

Recurrence interval (yr)	G1H004 - Skuifraam Dam (m^3/s)	G1H020 - Paarl (m^3/s)	G1H036 - Hermon (m^3/s)
2	160	280	190
10	330	480	370
20	410	550	450
50	510	660	560
100	610	740	640

- Possible planform changes

As a result of the reduced flood peaks the braided character of the upper Berg River could change to a meandering pattern, as illustrated in **Figure 5.4.11** (without considering the possible changes in bed slope).

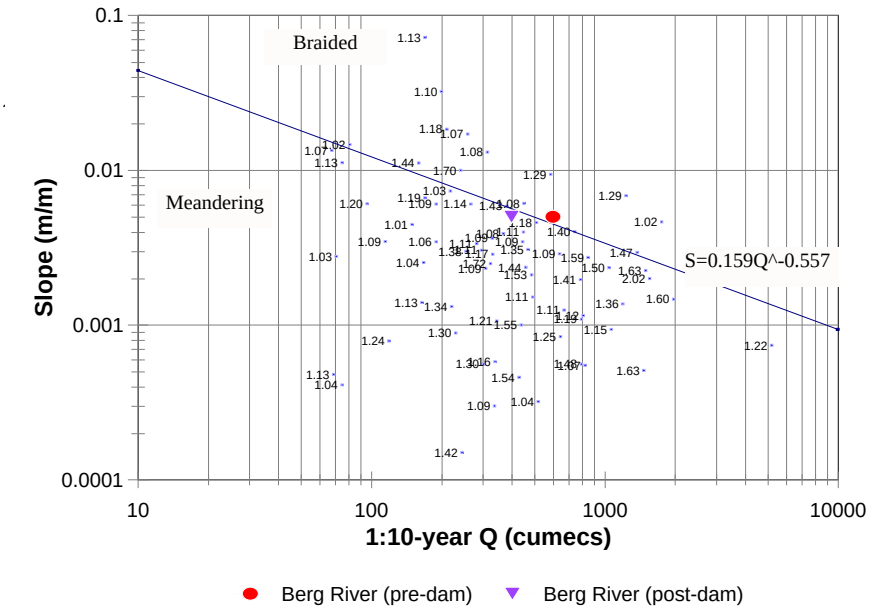

Figure 5.4.11 Threshold line separating braided and meandering rivers – Berg River indicated

5.4.5 Hydrodynamic and Morphological Model Simulations: Set-up

The computational model was set up with the full 10-year flow records as well as sediment input from the five major tributaries and the upstream boundary of the Berg River. The sediment input was in the form of a series of sediment discharges representing two sediment fractions: 0.03 mm (fraction 1) and 0.5 mm (fraction 2). Fraction 2 represents the median particle size of samples taken during field investigations. However, there is usually finer material present in the suspended load that is not found in the bed, since it is generally moved right through the system. It is important, however, in that it affects the sediment transport capacity of the river. It was found that about 60% of the suspended load consisted of sediment finer than 0.5 mm, which was represented by fraction 1 during the simulations. The same two fractions were also used for the bed material, but with a different distribution, as shown in **Table 5.4.7**. The larger boulders and cobbles constitute only a minor fraction of the incoming sediment load (see **Table 5.4.9**) and were therefore not included in the incoming sediment loads. Because of model limitations these particle sizes were also not included in the bed material, but rather bedrock was specified at a level 100 mm below the current bed level between the dam site and Paarl, since it is was established that these particle sizes would be

very difficult to re-entrain.

Table 5.4.7 Graded sediment

	Fraction 1: 0.03 mm	**Fraction 2: 0.5 mm**
Suspended load	60%	40%
Bed material	1%	99%

The Manning n-value used in the simulations was 0.06, which was increased to 0.07 between the dam site and Paarl for the dam scenarios to account for the increased roughness due to encroaching vegetation.

Narrowing of the river channel was considered by reducing the widths of the main channel by 15% between the dam site and Paarl and 10% for the lower reach (see **Figure 5.4.12**). The reduction factors were determined by considering the changes in flow pattern as a result of dam construction, based on methods developed in **Chapter 3**.

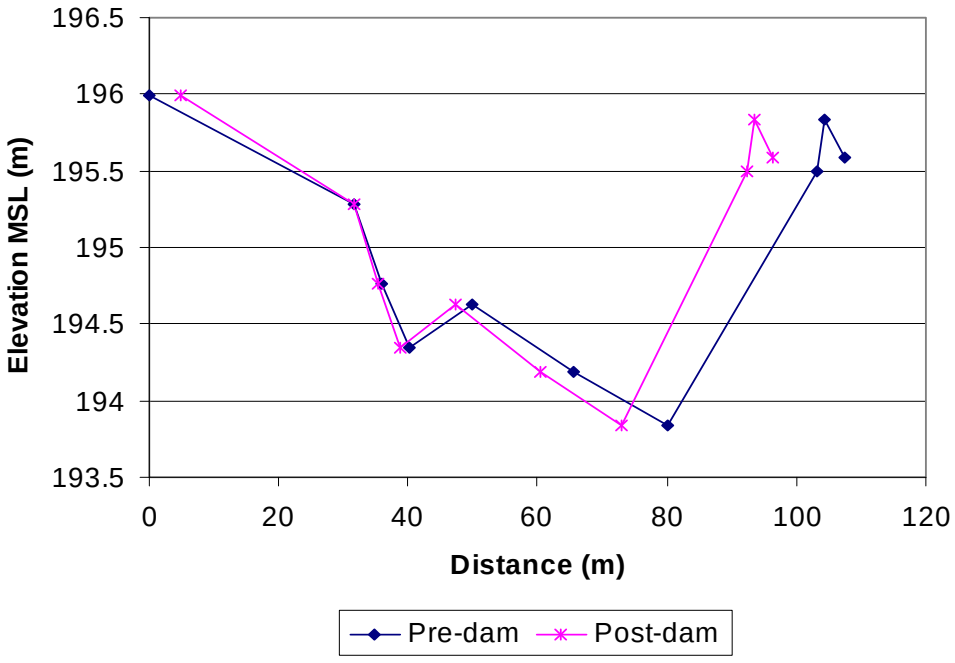

Figure 5.4.12 Cross-section reduction

Three simulations were carried out: current development level and Skuifraam Dam with and without artificial flood releases. The time steps were 50 seconds.

The sediment transport equation used for these simulations is Engelund and Hansen's total load formula and the default bottom level update method as explained in **Section 5.3.1** was used.

5.4.6 Hydrodynamic and Morphological Model Simulations: Results

From **Table 5.4.8** it can be seen that at the current development level large quantities of sediment are being transported on the upper, steep reaches of the Berg River, reducing considerably further downstream (**Figure 5.4.13**). Increasingly larger percentages of fraction 1 in the bed material were observed with distance downstream. With the proposed Skuifraam Dam (**Figure 5.4.14**) the annual sediment loads are reduced by about 7% just below the Franschhoek and Wemmershoek inflows, probably due to the reduced incoming sediment at the upstream boundary. The effect becomes increasingly more severe downstream of Paarl in spite of the large quantities of sediment supplied by the tributaries, which could be a result of the reduced flood peaks, which could cause increased deposition on the flatter reaches between Paarl and Hermon and also just upstream of Paarl. The decrease in simulated sediment loads at Hermon agrees with the reduction in flood peaks. The artificial flood releases (**Figure 5.4.15**) have had some effect on the upper reaches of the Berg River, effectively increasing the annual sediment loads. This means that some erosion had taken place, especially over the first few kilometres, seeing that the sediment loads have increased by 13% below the Franschhoek and Wemmershoek inflows.

Table 5.4.8 Changes in annual sediment loads

Location	Current development level	Skuifraam Dam without artificial flood releases	Skuifraam Dam with artificial flood releases
Dam site (km 0)	9418	0	0
Below Franschhoek inflow (km 7)	179452	166732 (-2%)*	191347 (+13%)
Below Dwars inflow (km 12)	255975	207937 (-16%)	261635 (-6%)
G1H020 (Paarl, km 31)	58749	46897 (-5%)	48167 (-2%)
G1H036 (Hermon, km 72)	42330	26730 (-19%)	26735 (-19%)

*: Percentage change relative to (current development level – 9418 ton/a)

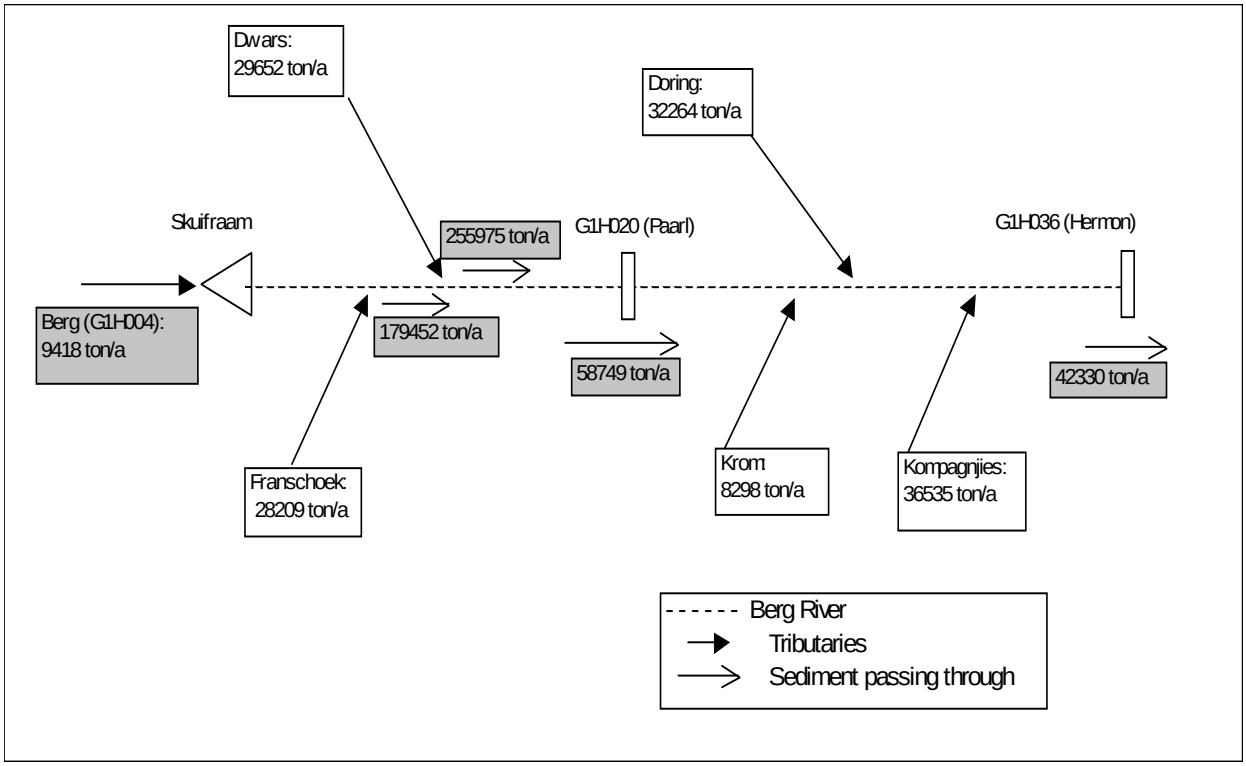

Figure 5.4.13 Long-term sediment balance: current development level

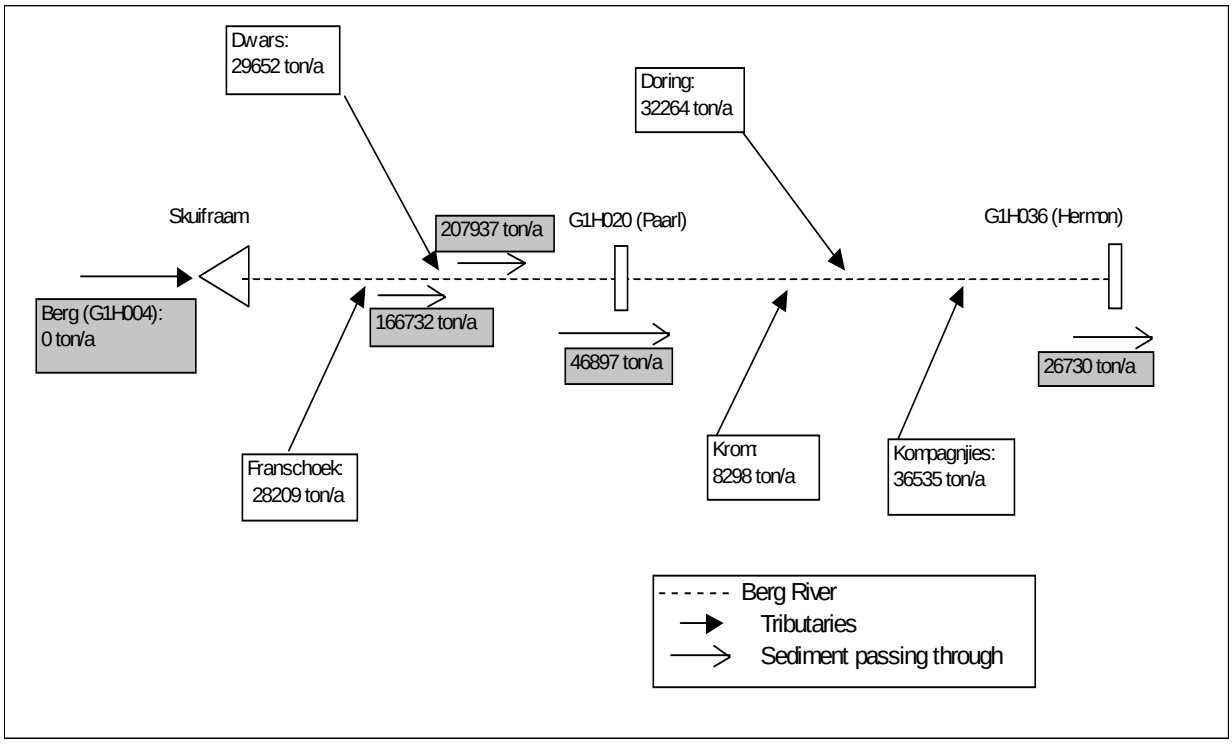

Figure 5.4.14 Long-term sediment balance: Skuifraam Dam without artificial flood releases

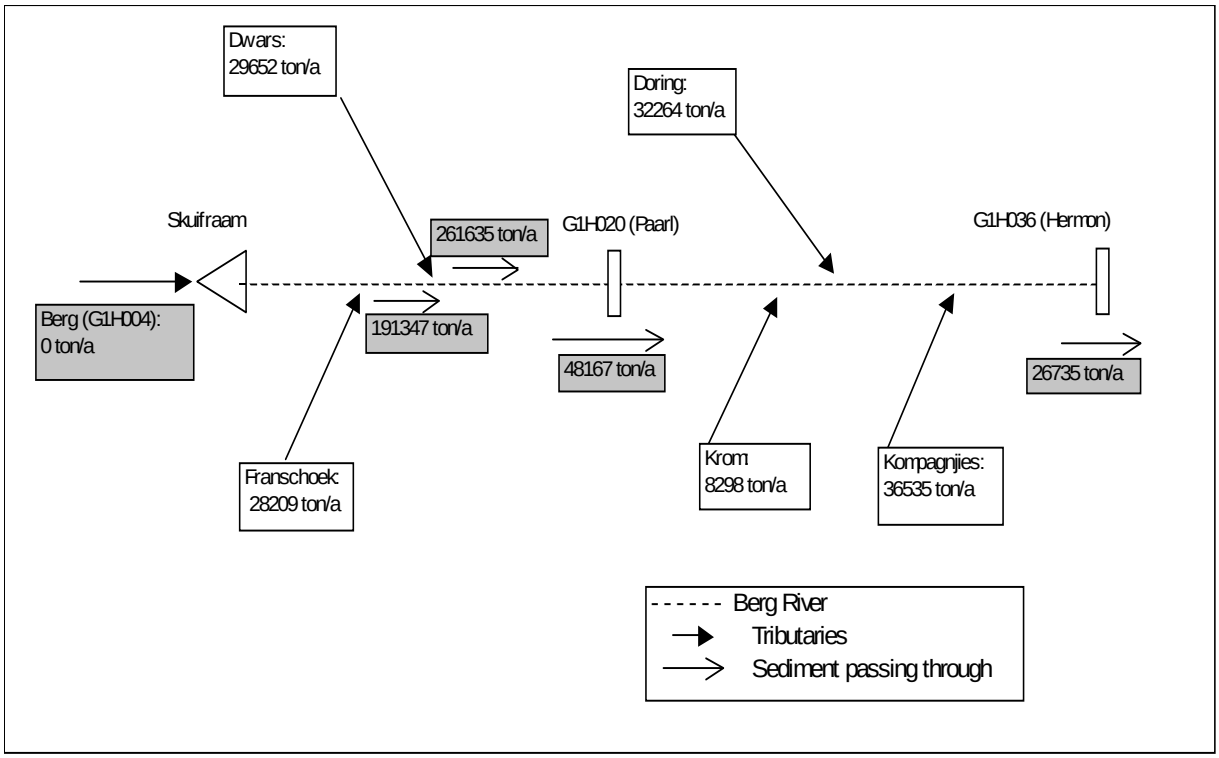

Figure 5.4.15 Long-term sediment balance: Skuifraam Dam with artificial flood releases

All the simulated scenarios indicate much higher sediment loads downstream of the Dwars River, than the sum of the sediment inputs upstream. This is due to scour down to the "bedrock" level specified in the model, which was necessary since sediments coarser than sand fractions were not included in the model. Sediment deposition was also simulated at some places in the upper reach for the current development level, as observed in the field (**Figure 5.4.16**). Relative changes in sediment transport between the scenarios are of importance in this study. Oversaturated sediment transport conditions occur at Paarl due to the flatter bed slopes and most of the sediment scoured upstream is deposited again.

In reality cobbles and boulders would create a shielding effect, making it more difficult to entrain sand. Medium and large floods will however still be able to scour the sand, with the same deposition pattern downstream.

Further downstream the effect of the artificial floods is less noticeable, probably because the 160 m^3/s flood peak is reduced to only 65 m^3/s at Hermon (when simulated on its own), which means it will lose most of its effectiveness. The artificial flood releases seemed to have been the most effective around Paarl.

Figure 5.4.16 Sand deposition about 3 km downstream of proposed dam site

The movement of the larger particle sizes, although not included in the simulations, was also considered. Since the bed material consists of a wide range of particles, as can be seen in **Table 5.4.3**, hiding and shielding of the smaller particle sizes by the larger fractions had to be considered. The approach used was such that the critical conditions for re-entrainment, in this case the Shield's parameter (Shields, 1936), was adjusted to account for the effect of hiding and shielding based on Egiazarof's method (Egiazarof, 1950) (**Figure 5.4.17**). This means that the smaller fractions are much more difficult to move than the larger sizes, because these are more exposed. As can be seen from **Figure 5.4.17** the critical value increases dramatically for the smaller fractions.

The annual sediment loads of the larger sediment fractions (**Table 5.4.9**) were determined with hiding considered just upstream of Paarl. The floods in the 10-year period considered were not sufficient to initiate movement of the 250 mm size. The flood peak necessary to initiate movement of 250 mm particle size is about 1200 m^3/s, corresponding to a 1:200-year flood at the current development level (see **Table 5.4.10**).

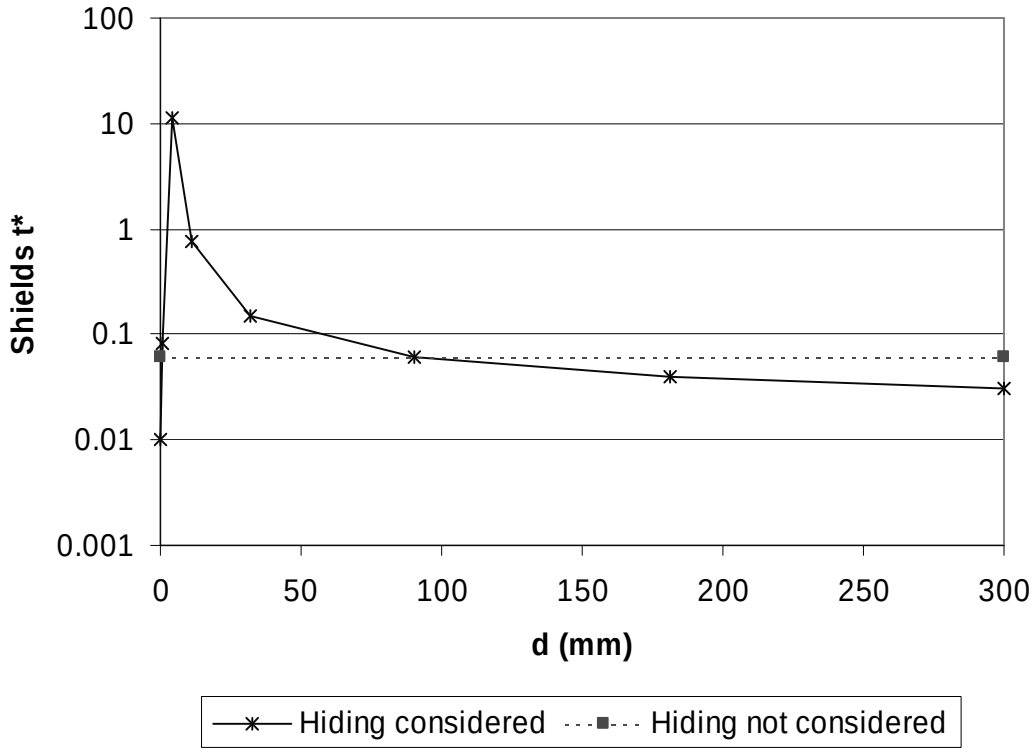

Figure 5.4.17 Critical conditions for re-entrainment of sediment (based on d_{50} = 94 mm in pool at IFR site 1)

Table 5.4.9 Annual sediment loads of larger sediment sizes not included in model set-up

Particle size (mm)	Current development level (ton/a)	After Skuifraam Dam with 160 m^3/s artificial flood releases (ton/a)
40*	347	2341
96	42	26
250	0	0

*: Mean particle size of upper particle size ranges found at IFR site 1

Table 5.4.10 Flood peaks required to initiate movement of large sediment sizes (including shielding and exposure)

Particle size (mm)	Flood peak (m^3/s)	Velocity (m/s)
40	294 (3)*	2.4
96	451 (10)	3.5
250	1200 (200)	5.3

*: Recurrence interval (yr) based on current development level at dam site

The annual sediment load of the 40 mm fraction increased, probably because of the artificial flood releases.

Another way of illustrating the effect of Skuifraam Dam with and without the proposed artificial flood releases is by comparing the simulated sediment load-discharge rating curves at various locations along the Berg River. **Figures 5.4.18** to **5.4.20** show these rating curves at just below the Franschhoek/Wemmershoek inflow, Paarl and Hermon, respectively. In **Figure 5.4.18** it can be seen that the rating curve for the proposed Skuifraam Dam plots above that of the current development level at lower flows. This is because of the reduced flood peaks with more material available to be transported at lower flows. With the addition of the artificial flood releases the sediment transport capacity has been increased, but apparently too much for that reach, because instead of bringing the rating curve back to the current position, it has moved even further away.

At the Paarl gauging station (**Figure 5.4.19**) the situation is quite different compared to the one depicted in **Figure 5.4.18**, indicating a slightly reduced sediment transport capacity after Skuifraam Dam has been built. This decreased sediment transport capacity is also apparent at the Hermon gauging station (**Figure 5.4.20**). In this instance it is also apparent that the artificial flood releases do not have a sufficient restoring capacity, since the sediment load-discharge rating curve does not recover to the “original” position. This is probably because the 160 m^3/s flood peak released from the reservoir reduces to only 65 m^3/s by the time it reaches Hermon (if it does not coincide precisely with a natural flood and is therefore not maintained by tributary flows). The area around Paarl seems to be the least affected by the dam.

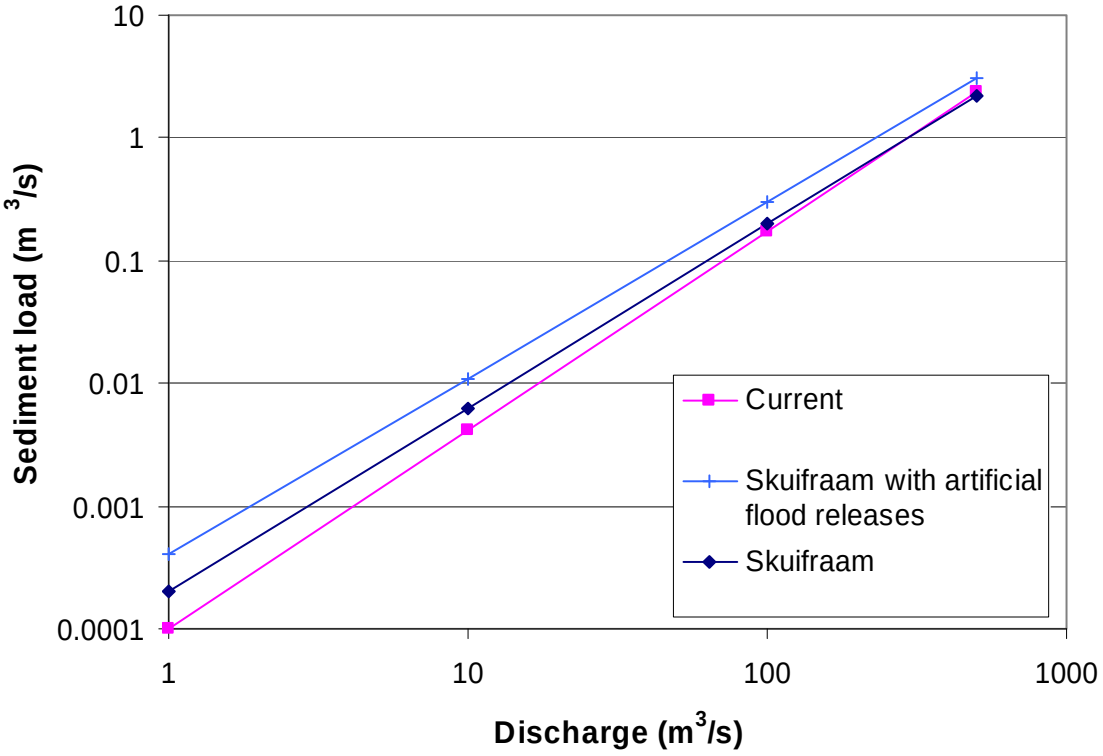

Figure 5.4.18 Effect of Skuifraam Dam with and without artificial flood releases (downstream of Franschhoek inflow – km 7)

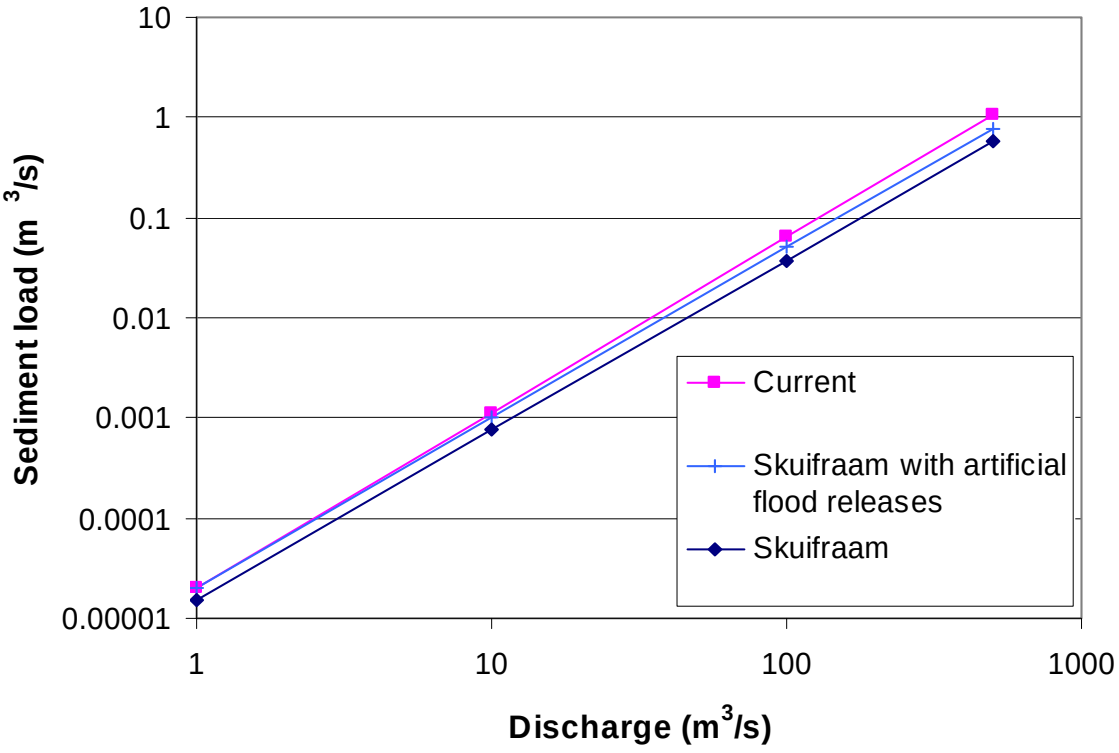

Figure 5.4.19 Effect of Skuifraam Dam with and without artificial flood releases (Paarl – km 31)

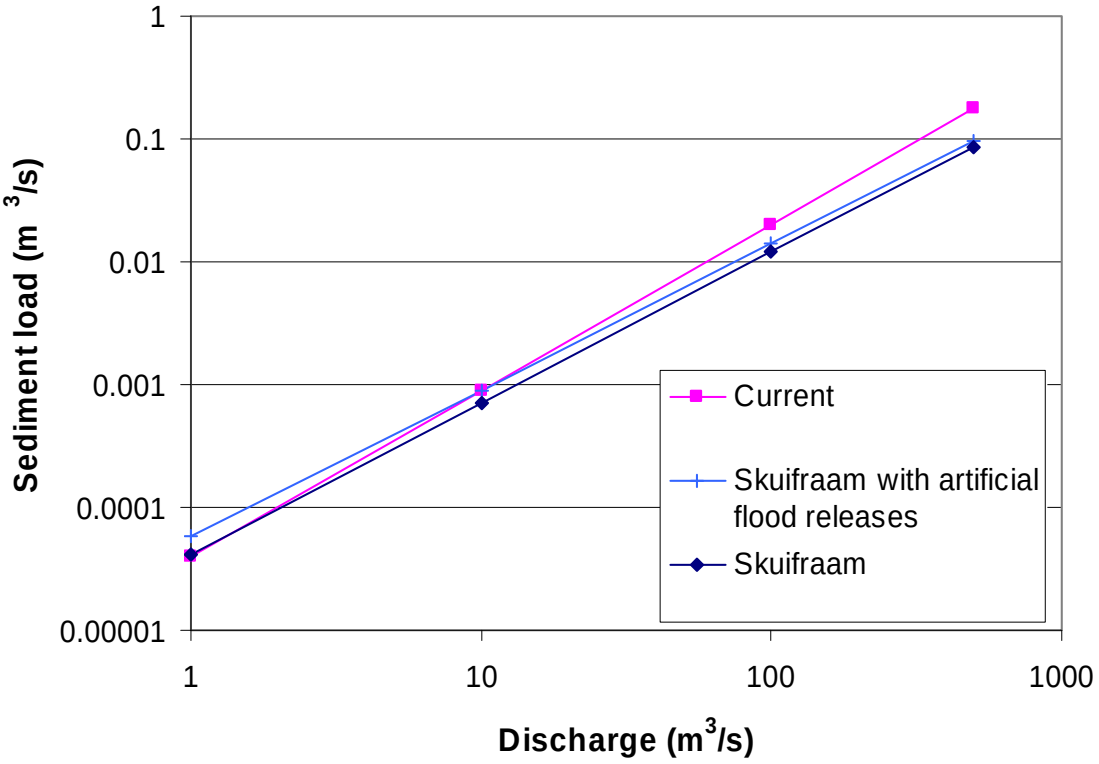

Figure 5.4.20 Effect of Skuifraam Dam with and without artificial flood releases (Hermon – km 73)

5.4.6.1 Resetting Flood

An aspect still to be considered is that the substantially reduced sediment loads at Paarl indicate significant deposition on the upstream reaches, which could become a problem in the long term. It would be of interest to find out whether a resetting flood, such as the 1:50-year flood (779 m^3/s flood peak at dam site at current development level) would manage to remove those deposits.

A representative 1:50-year flood hydrograph was incorporated into the inflow record at the dam site (at the same time as floods from the catchment) and the quantities of sediment transported for the duration of that flood were determined. Although quite a large sediment load was simulated at Paarl (87900 ton), this reduced considerably to only 5200 ton at Hermon. So it would seem that even such a large flood couldn't move all the accumulated sediment through the system.

5.4.7 Conclusions

Simulations carried out with a fully hydrodynamic-morphological model indicated:

- Flood routing through the proposed Skuifraam Reservoir showed a decrease in peak discharge of 40 % in the upper Berg River and about 20 % further downstream.
- With the dam and annual artificial floods, more erosion will occur in the upper 4 km than under current conditions.
- More sediment deposition will occur downstream of the Dwars River to Hermon than under current conditions. The decrease in sediment load at Hermon is 19 % which is associated with the general flood peak reduction of about 20 %.
- The annual artificial flood at 160 m^3/s seems to be too constant in the upper reach.
- Boulder movement is limited. When shielding and exposure of particles are considered a flow velocity of 5.3 m/s would be required to re-entrain a 250 mm diameter boulder. The discharge required to achieve this is 1200 m^3/s at Skuifraam site. For a 90 mm diameter particle the flow velocity required is 3.5 m/s at a discharge of 450 m^3/s.
- The 10-year simulation period included a 1:10 year flood. The effect of a 1:50 year resetting flood was however also simulated. This flood transported 5200 ton past Hermon, versus the 26735 ton/year achieved by smaller more regular floods over the 10-year simulation period.
- Planform changes in the upper reach are possible.
- A higher artificial flood would be required to limit sediment deposition to the same conditions as the current development level.

It should be noted that the relative results of the pre-dam and post-dam simulations have been compared, and not the absolute values.

5.5 Case Study: Proposed Jana and Mielietuin Dams - Thukela Estuary

Although this project is primarily concerned with the impact of dams on the river morphology, an estuary is really just an extension of the river and will therefore also be affected by any changes in the catchment.

The catchment area of the Thukela River at the estuary is 29000 km^2. The Thukela River is relatively steep and has a high sediment transport capacity with a mean annual sediment yield (present day) of about 9.3 million ton.

At the estuary the main channel is relatively wide (about 500 m). The sediment consists mostly of fine sand (d_{50} = 0.22 mm at the N2-bridge). The alluvial bed is deep with bedrock 55 m below sea level at the N2-bridge. At flow gauging station V5H002 upstream of John Ross Bridge, the river is steep (1:130) with bedrock conditions, but downstream of the N2-bridge at the estuary the general slope is much flatter at 1:1500.

The estuary is dominated by floods in the river and is relatively shallow and short (5 km in length). During low flow conditions (< 10 m^3/s) the river meanders through several sand banks in the main channel. The Thukela River flood peaks are high and therefore the system is very dynamic with rapid changes in the river morphology from time to time. During falling stages of flood hydrographs sediment deposition has been observed in the river mouth (**Figure 5.5.1**), but this sediment is later scoured by the south to north long-shore currents. A typical morphology of the estuary is shown in **Figure 5.5.2**.

Several large dams have been constructed in the catchment such as Woodstock, Spioenkop, Chelmsford, Zaaihoek and Wagendrift. These dams would trap most of the sediment yield in their respective catchments and would also attenuate floods. The impact of these dams on the estuary would however be minimal, since they are located high up in the catchment.

However, significant land use changes and overgrazing to date could have led to an increase in the sediment yield, meaning that under natural conditions the sediment yield could have been around 200 ton/km^2.a. This would mean that the estuary was a lot longer (around 8.5 km) and also deeper compared to the present day. Further catchment developments, again causing the sediment yield to increase, could have a significant effect on the Thukela Estuary fluvial morphology.

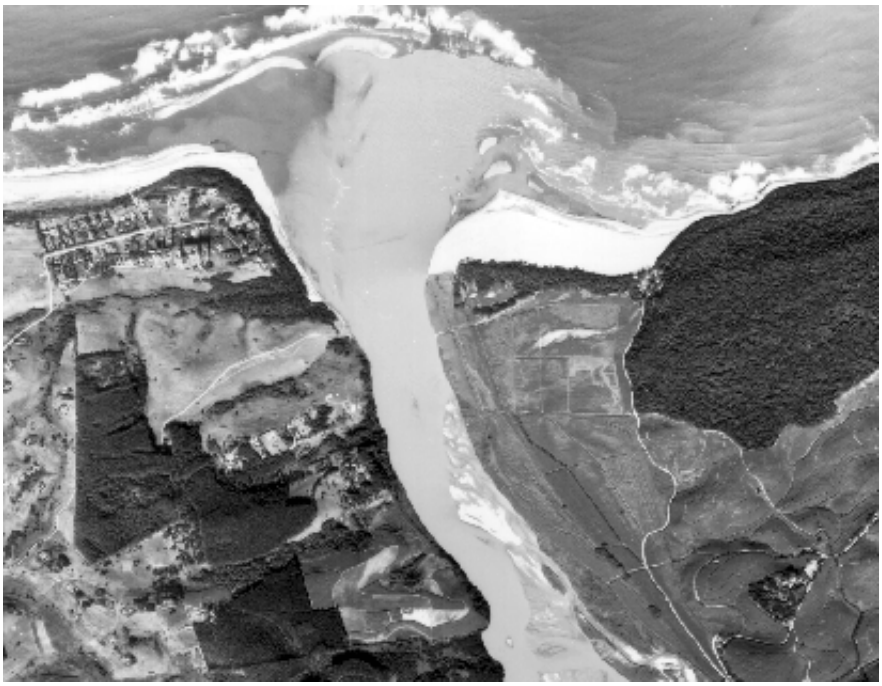

Figure 5.5.1 Sediment deposition (May 1976)

Figure 5.5.2 Aerial view of Thukela Estuary

5.5.1 Fluvial Morphological Simulation Scenarios

In order to assess how the sediment dynamics of the Thukela Estuary might change with further catchment development, mathematical modelling of the hydraulics and morphology of the Thukela Estuary was carried out. Six scenarios were selected:

- **Scenario 0**: "natural" conditions (sediment yield of 200 ton/km^2.a)
- **Scenario 1**: present day (corresponding to the 'Present Day' scenario of the Reserve Determination)
- **Scenario 2**: full demand placed on proposed dams, with environmental flow releases (worst case in terms of floods)
- **Scenario 3**: scenario 1 including a resetting flood
- **Scenario 4**: scenario 2 including a resetting flood
- **Scenario 5**: scenario 2 with a higher sediment yield of 600 ton/km^2.a

Different scenarios than for the reserve determination were selected since most of those described in the hydrological report (Hughes, 2002), except Natural and Present Day, are basically the same in terms of floods and therefore will not yield different results in terms of sediment dynamics.

The 15-year period used for the simulations was a combination of flows from 1962 to 1967, and 1990 to 2000. This was done since it yielded the longest continuous and representative flow series from observed flow records (primary, break point data of DWAF).

5.5.2 Flood Routing

Before any estuary simulations could be done the flows from the proposed dam sites had to be routed to the estuary, since both the proposed Jana Dam (Thukela River) and the Mielietuin Dam (Bushmans River) are situated relatively high in the catchment, with Jana Dam approximately 270 km from the estuary as set out in **Figure 5.5.3**.

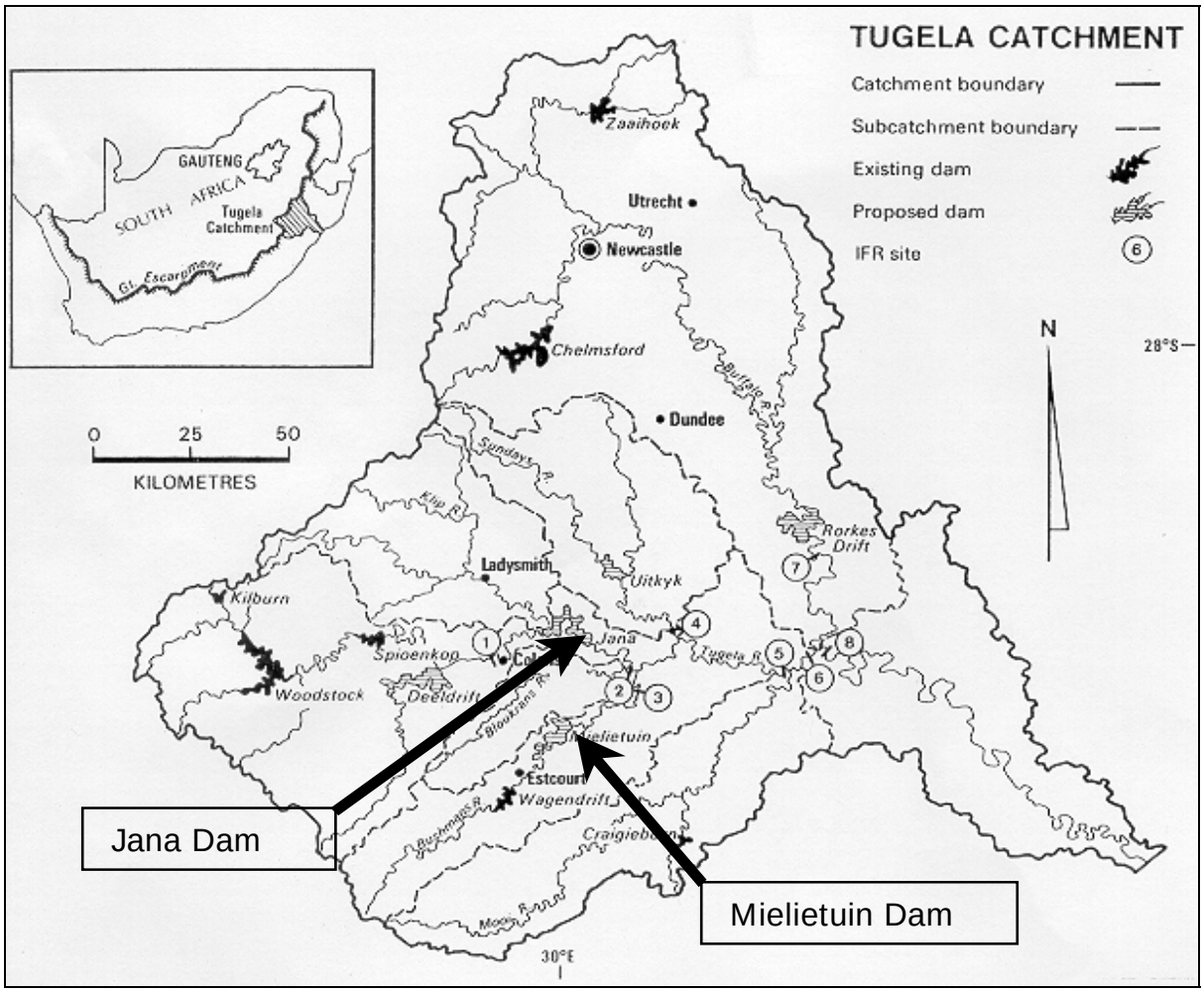

Figure 5.5.3 Thukela catchment layout (Rowntree & Wadeson, 1999)

The one-dimensional mathematical model MIKE 11 (Danish Hydraulics Institute) was set up for a 270 km reach of the Thukela River with cross-sections taken from 1:10 000 orthophotos at 3 km intervals. Only the hydrodynamic module was set up because this exercise was intended solely for the purpose of routing the flows from the dam sites to the estuary and not for morphological investigations. Tributary flows were included for all major subcatchments, with gauging stations on the Mooi, Buffels, Bushmans and Sundays River. A schematic layout is shown in **Figure 5.5.4**. The observed flows were scaled up to account for the whole subcatchment, based on a function of the mean annual runoff (MAR) ratio (**Table 5.5.1**). Ungauged catchments close to the estuary were considered by scaling the flows from the Buffels River, since the MAR's are very similar.

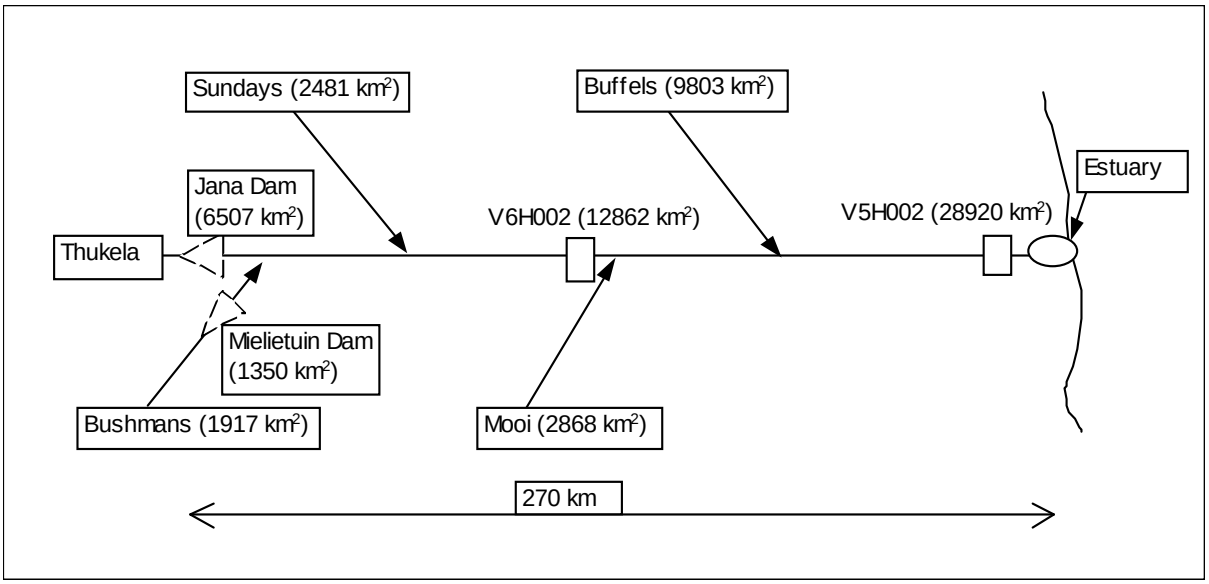

Figure 5.5.4 Schematic layout of Thukela and major tributaries

Table 5.5.1 Scaling factors

Tributary	Catchment area at gauging station (km^2)	Total catchment area (km^2)	MAR at gauging station (Mm^3)	Total MAR (Mm^3)	Scaling factor
Mooi (V2H004)	1546	2868	292.3	402.5	1.37
Bushmans (V7H020)	744	1917	222.1	312.7	1.4
Buffels (V3H010)	5887	9803	701.9	1016.8	2
Sundays (V6H004)	658	2481	86.5	224.3	2.6

The hydrodynamic model was calibrated based on observed flows at two gauging stations on the Thukela River (V6H002 at Thukela Ferry and V5H002 at Mandini). The discharge table limit had to be extended for V5H002 from 1990 onwards to include medium and large floods. This made the calibration process somewhat difficult since extending the discharge table introduces a certain amount of inaccuracy. However, the simulated flows could be predicted to within 30% of the observed floods, which is similar to the accuracy of the gauging stations. The observed and simulated flows at Mandini are shown in **Figure 5.5.5**.

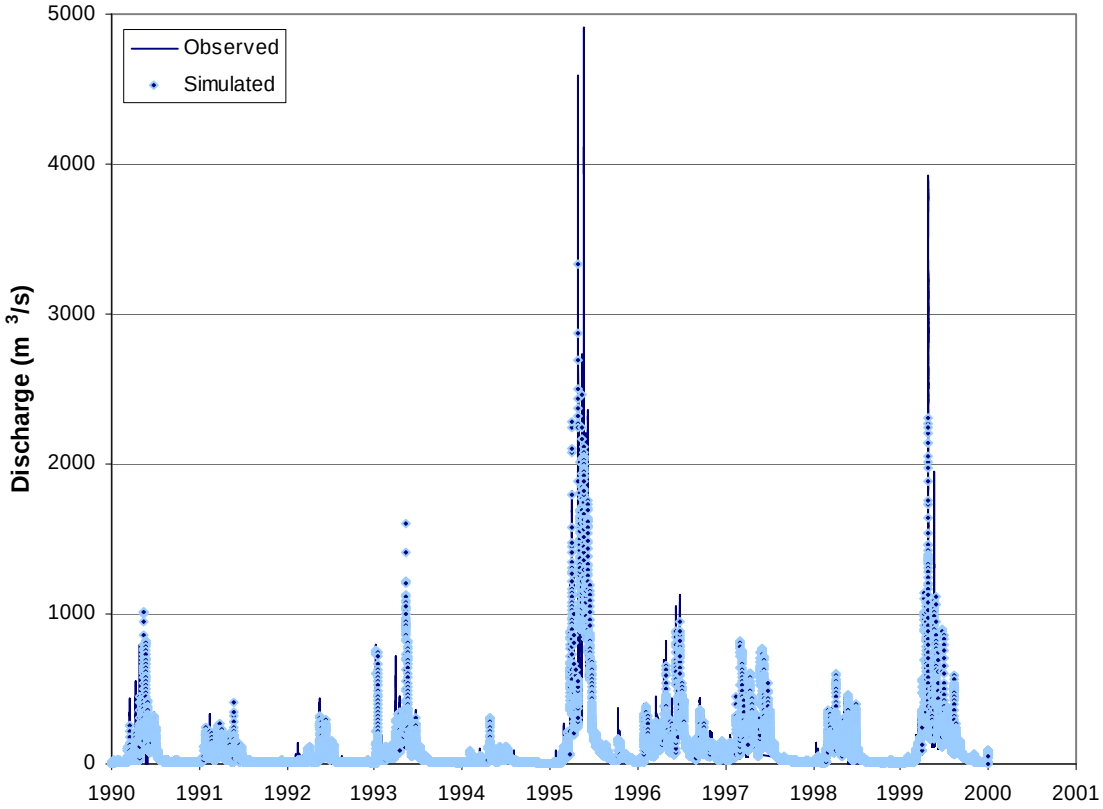

Figure 5.5.5 Observed and simulated flows at Mandini (V5H002)

The present day flows (without Jana and Mielietuin Dam) could thus be obtained at the estuary. In order to generate flows for the second scenario (including both Jana and Mielietuin Dams), hydrological reservoir routing was carried out with the proposed dam characteristics taken from the DWAF website (**Table 5.5.2**).

Table 5.5.2 Reservoir characteristics

	FSC[1] (million m^3)	**FSL[2] (masl)**	**Spillway length (m)**	**HFY[3] (million m^3/a)**	**MAR at dam site (million m^3)**
Jana Dam	1500	RL 860	165	507.7	1446
Mielietuin Dam	350	RL1025	69	192.8	288

[1]: Full Supply Capacity; [2]: Full Supply Level; [3]: Historical Firm Yield

Observed flows at gauging stations V1H001 for Jana Dam and V7H020 for Mielietuin Dam were used as inflows. The historical firm yield (WRP, 2001**)** was taken as the net demand (including environmental releases of 13% of the MAR as set out in the hydrological report (Hughes, 2002) for Reserve B). The pre-dam flows at the proposed Jana Dam and Mielietuin Dam sites, as well as the post-dam flows are shown in **Figures 5.5.6** to **5.5.9**.

Similar to the present day scenario the flows thus obtained were routed to the estuary. The pre-dam and post-dam flows at the estuary are shown in **Figures 5.5.10** and **5.5.11**.

As can be seen from these figures, the dams do not have a very dramatic effect on the flows at the estuary, because they are located relatively far up in the catchment and the incremental downstream catchment area comprises still more than 50% of the total catchment. Immediately downstream of both dams, however, many years have no flood spillage, which will have to be rectified by the release of freshets and floods for the river.

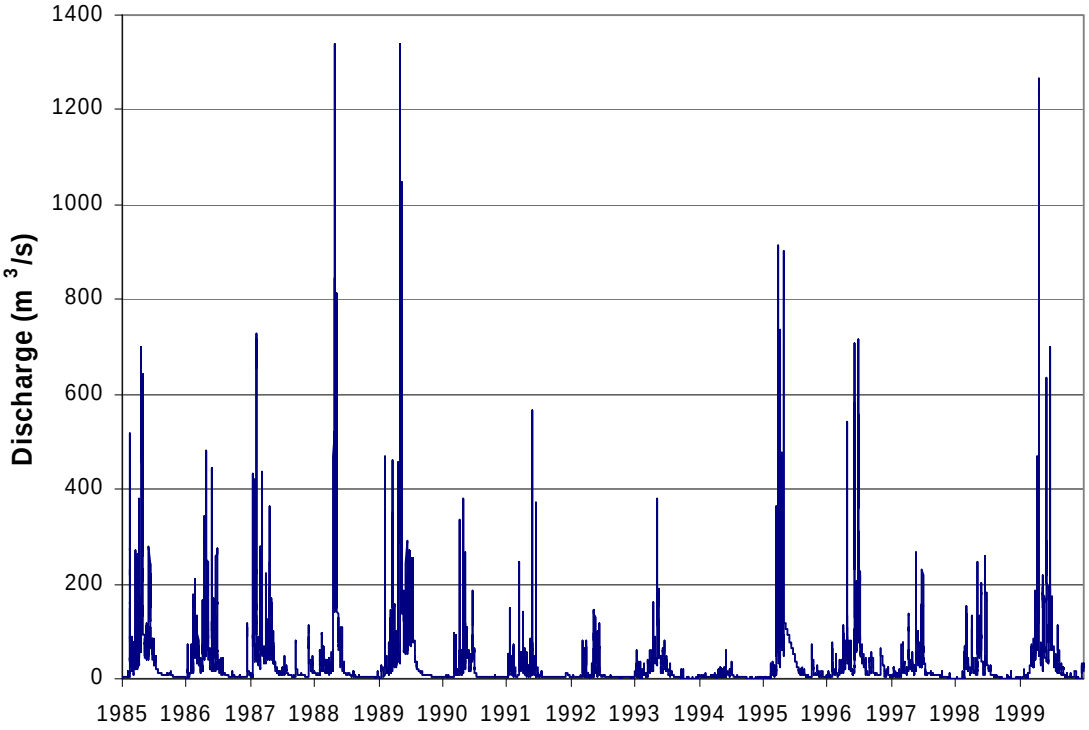

Figure 5.5.6 Pre-dam flows at proposed Jana Dam site (hourly data)

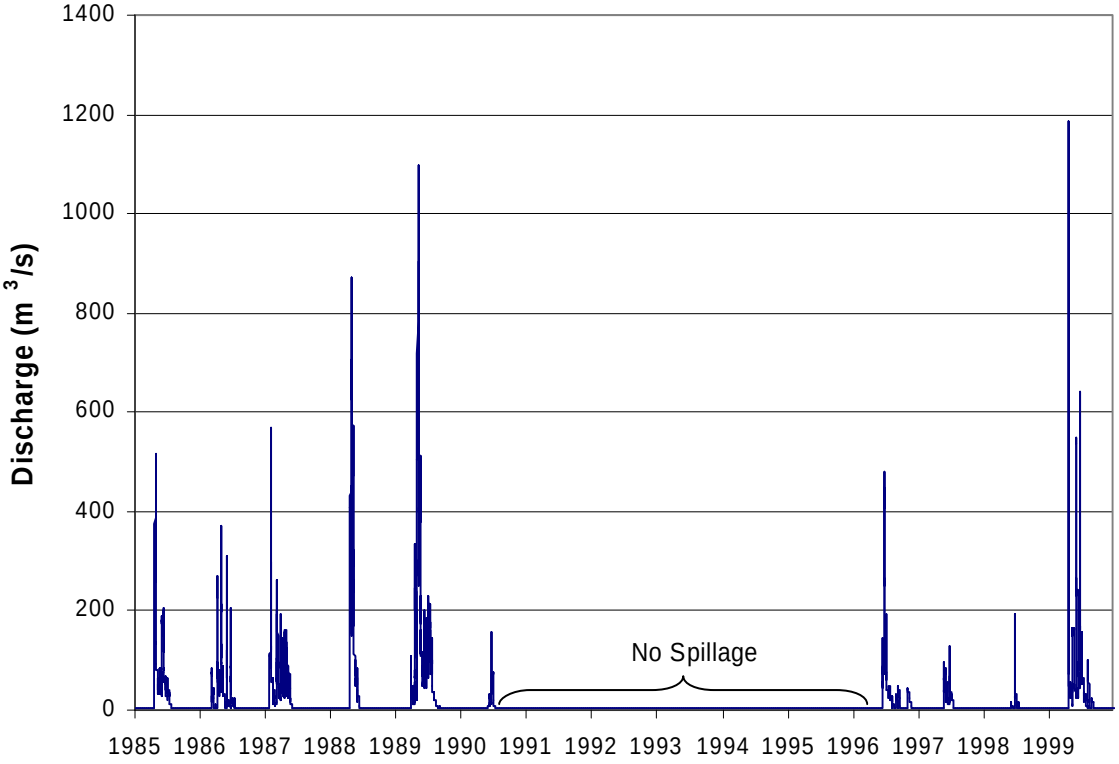

Figure 5.5.7 Post-dam flows at proposed Jana Dam site (hourly data)

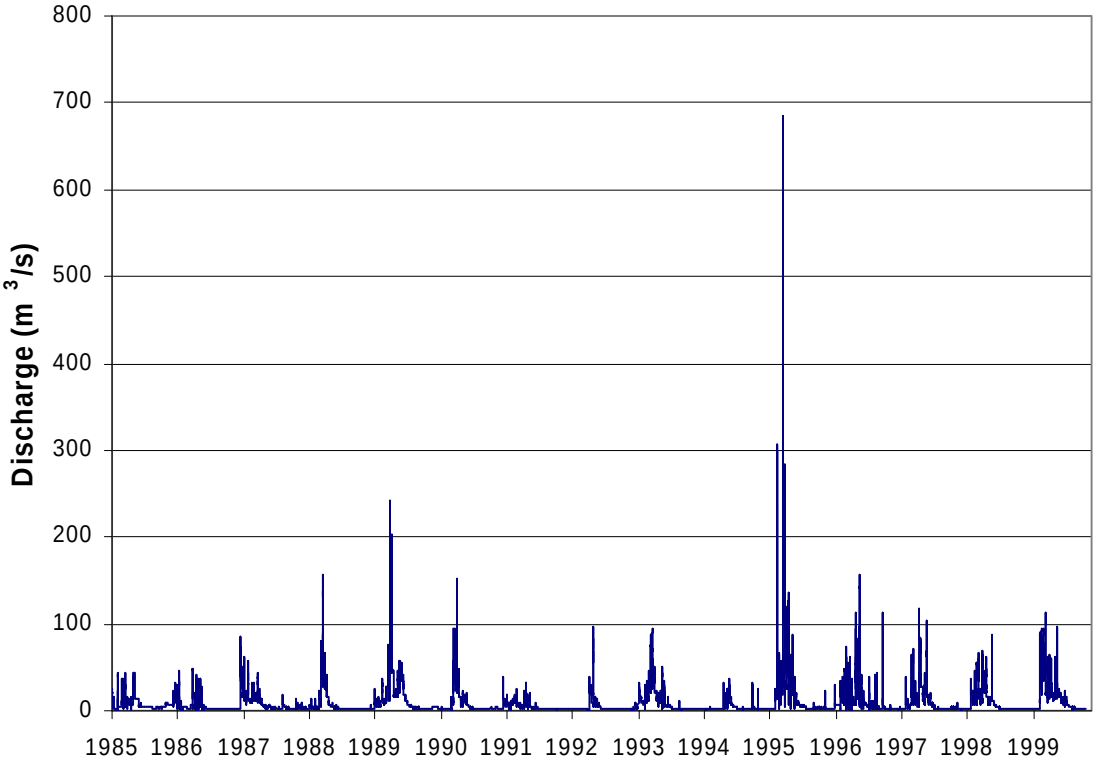

Figure 5.5.8 Pre-dam flows at proposed Mielietuin Dam site (hourly data)

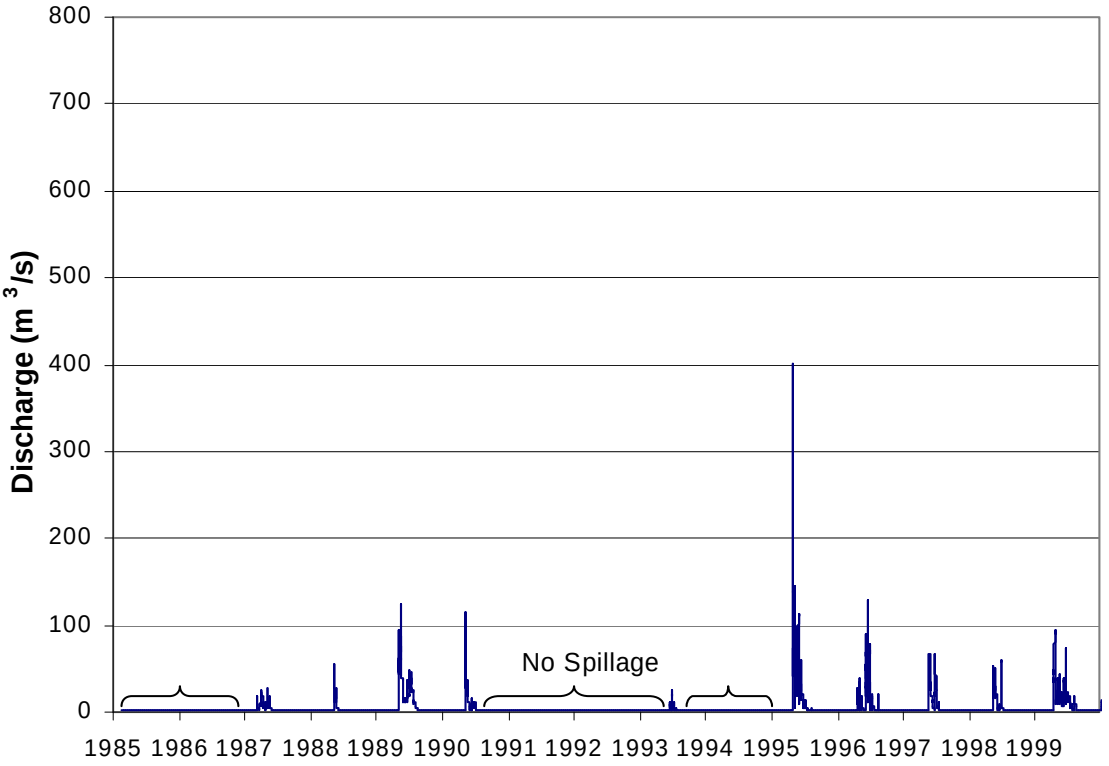

Figure 5.5.9 Post-dam flows at proposed Mielietuin Dam site (hourly data)

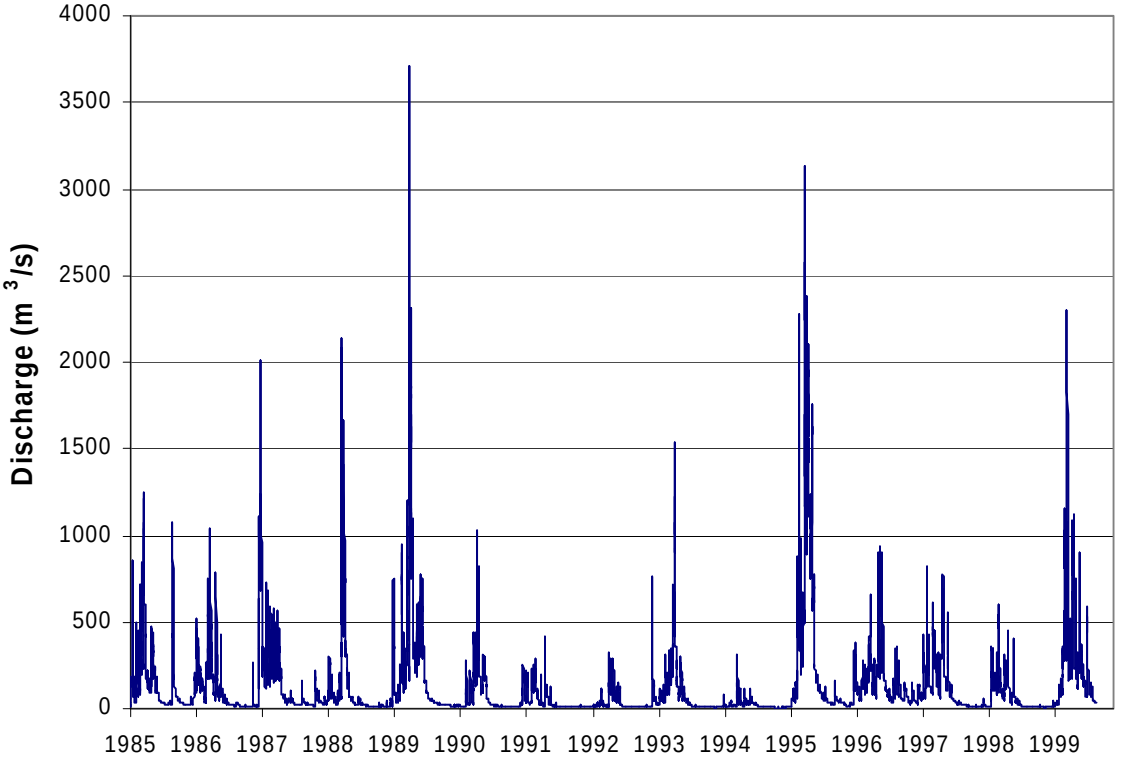

Figure 5.5.10 Pre-dam flows at Thukela Estuary (hourly data)

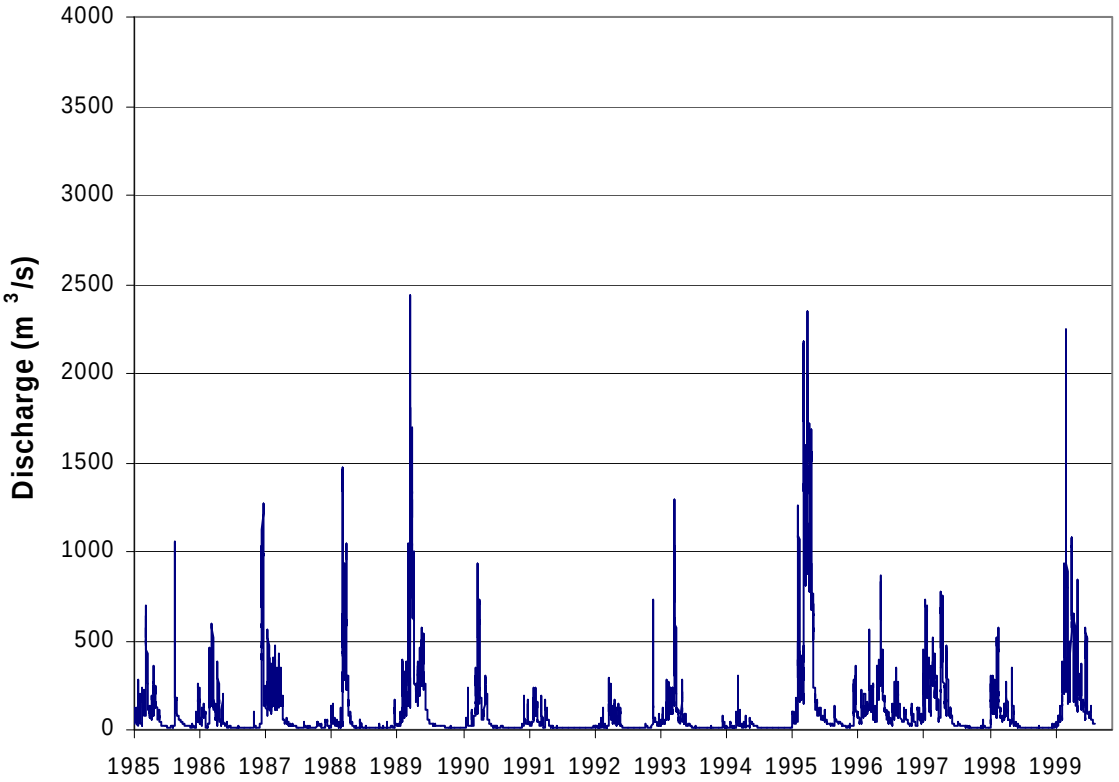

Figure 5.5.11 Post-dam flows at Thukela Estuary (hourly data)

The present day, as well as post-dam recurrence interval flood peaks are indicated in **Table 5.5.3**. The present day recurrence interval flood peaks were determined based on the statistical analysis of the complete flow record V5H002 (39 years). The post-dam flood peaks were determined by adjusting the pre-dam flood peaks (based on the complete flow record) by a factor based on the reduction in flood peaks during the 15 years simulated as a result of the dam developments.

Table 5.5.3 Pre-dam and post-dam flood peaks

Recurrence interval (Years)	Present day flood peaks (m^3/s)	Post-dam flood peaks (m^3/s)
2	1000	850
10	4500	3600
20	6800	5400
50	11000	8700

5.5.3 Thukela Estuary Model Set-up

With the generated flow sequences for the scenarios the model for the estuary could be set up. Cross-sections were obtained from a survey done by DWAF in 1996, spaced between 200 and 500 m apart (closer at the mouth). The model extends from the John Ross Bridge to the estuary mouth over 13 km. The Manning n-value was taken as 0.042 for the main channel and 0.055 for the more densely vegetated higher ground (see **Figure 5.5.12**), as obtained from calibrations done in 1990 (Basson and Rooseboom, 1990).

Figure 5.5.12 Thukela Estuary

Two sediment fractions (d_1 = 0.035 mm and d_2 = 0.22 mm) were specified in the bed material (see **Table 5.5.4**). The first fraction represents the median particle size of bed samples taken during 1990 at the N2-bridge (Basson and Rooseboom, 1990). More samples taken at the estuary in 2001 are shown in **Appendix C2**. The data are from core samples taken in the estuary. Although these samples do not indicate the presence of cohesive material, it was found during a site visit that there are areas with cohesive sediments as indicated in **Figure 5.5.13**. Fine sediment deposition occurs at the banks in reed beds. Finer material is generally present in the suspended load, which is not always present in the bed since it generally moves right through the system. It was found that about 50% of the suspended load consists of sediment finer than 0.22 mm, which was represented by fraction 2 during the simulations.

Table 5.5.4 Graded sediment (as simulated)

	Fraction 1: 0.035 mm	Fraction 2: 0.22 mm
Bed material	5%	95%
Suspended load	50%	50%

Figure 5.5.13 Presence of cohesive sediment at Thukela Estuary (left bank at mouth)

The upstream boundary of the model consisted of the above-mentioned flow sequence together with a sequence of sediment loads. The sediment loads were determined with the aid of a sediment load–discharge rating curve obtained from suspended sediment samples taken between 1971 and 1984 at V5H002. There was a seasonal variability in the suspended sediment samples, with higher concentrations observed during the beginning of the rainy season. For this reason a different rating curve was used between September and December than for the rest of the year as indicated in **Figure 5.5.14**.

The sediment loads determined with these rating curves had to be adjusted in order to obtain the adopted sediment yield. There is a significant variability (between 184 and 559 ton/km^2.a)

in the sediment yields for different parts of the Thukela system found in literature (Dollar, 2001), but only those applicable at the estuary are shown in **Table 5.5.5**.

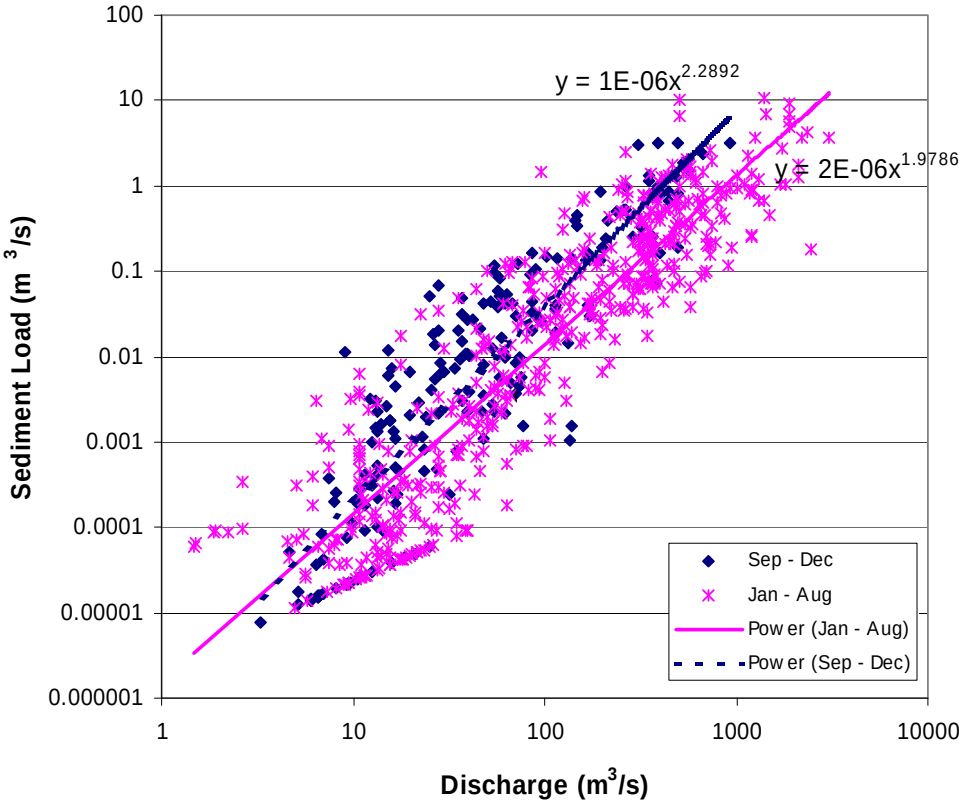

Figure 5.5.14 Sediment load-discharge relationship – Thukela River

Table 5.5.5 Sediment yields

Reference (Dollar, 2001)	Place	Catchment area (km^2)	Yield ($ton/km^2.a$)
Orme (1974)	Thukela	29046	375
Dingle & Scrutton (1974)	Thukela	29046	427
Flemming & Hay (1983)	Thukela	29046	386
Goodlad (1986)	Thukela	29046	406
Nicholson (1983)	Thukela	29046	390*

*: Average value

The average sediment yield for the lower Thukela obtained from those shown in **Table 5.5.5** is about 400 $ton/km^2.a$. The sediment yield obtained from the suspended sediment samples is the similar at 395 $ton/km^2.a$ (including 25% for non-uniformity and bed load). A maximum sediment yield of 571 $ton/km^2.a$ was found by Rooseboom (1992), but this was obtained from

samples taken at Colenso, which is high up in the catchment, which generally has a higher sediment yield than further downstream, and the period was also relatively wet (1950 – 1958). A sediment yield of 400 ton/km^2.a was therefore thought to be representative for the present state.

The sediment yield under natural conditions is difficult to determine, since very little information is available. There is, however, an indication that the sediment yield could have been lower than at present from observations that indicate that the estuary was a lot longer than at present. The lowest sediment yield from those mentioned above is just under 200 ton/km^2.a. However, the source of some of those observations is questionable and therefore the sediment yield under natural conditions is estimated to be no lower than 200 ton/km^2.a.

For scenarios 1 and 2 a sediment yield of 400 ton/km^2.a is actually somewhat high because no large floods occur in that period, but this situation is representative of a relatively dry period just before a large resetting flood occurs, when the availability of the sediment is not limited. However, for scenarios 3 and 4 the sediment availability is very much limited, especially during the resetting flood. The highest concentration observed at V5H002 was around 40 000 mg/ℓ, and no data are available on concentrations during large floods. During the Domoina flood of 1984, the average volumetric concentration on the Pongola River (further north) was about 2%. It was assumed that the same average concentration could be expected on the Thukela River during a large resetting flood. The concentrations during the flood were calculated with the aid of the sediment load-discharge rating curve and then scaled down to reduce the average volumetric concentration during the flood to 2%. The average sediment yield for the simulation period was kept at 400 ton/km^2.a. For scenario 5 the sediment yield was increased to 600 ton/km^2.a, which could occur if increasing areas of the catchment are under cultivation and with overgrazing.

Due to the fact that the planned reservoirs will trap most of the incoming sediment, the sediment loads had to be adjusted again for the second scenario, because the mean annual sediment load will reduce by up to 27% if all the sediment is trapped in the reservoirs.

The downstream boundary of the model consisted of a time series of tidal water levels based on tidal constituents from the Richards Bay area. No sediment input was specified at the

downstream boundary since it was assumed that most of the sediment from the ocean would be scoured around the mouth of the estuary, which is included in the model, and that the sediment availability from the ocean is not limited.

The cross-sections are updated so that erosion and deposition are uniformly distributed over the whole cross-section below bank level, i.e. not including the floodplains.

The changing geometry of the mouth was not incorporated in the model because it was found that most of the time the tidal action dominates the downstream water level, and only at flows of over 300 m^3/s does the river flow begin to dominate, at which stage the mouth should be completely open. Also, should the mouth close, it will not affect the sediment transport in the estuary, since the flows at that stage are very low and the mouth also does not stay closed for long periods. A study done on the width changes of the mouth opening (Pollard, 2001) has shown that the width of the mouth is a function of the discharge in the form of a regime equation (with a maximum width of 500 m):

$$B = aQ^b$$

where B = mouth width (m), Q = discharge (m^3/s)
with a = 9.6 and b = 0.59

The length of the estuary is defined as the length from the mouth to the point where the final bed level reaches 1.2 m MSL, which is generally regarded as the average spring tide level.

The simulations were carried out with the one-dimensional MIKE 11 model, where the sediment transport and hydrodynamics (fully hydrodynamic) are coupled at each time step, with one minute time steps for the hydrodynamics and two minute time steps for the sediment transport calculations.

5.5.4 Simulation Results

Under natural conditions due to the lower sediment yield the estuary would have been quite long (around 8.5 km) and deep (see **Figure 5.5.15**). The mean annual sediment load would

have been around 5.9 million ton.

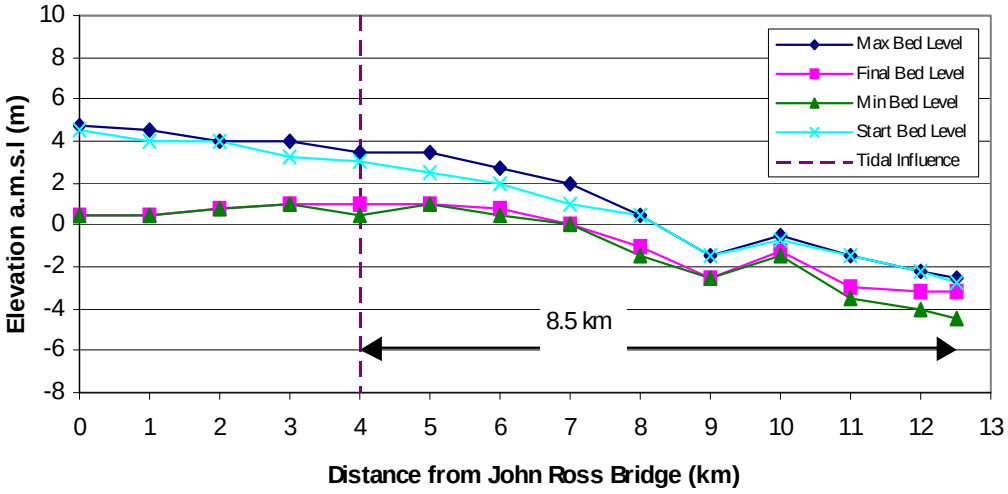

Figure 5.5.15 Bed levels – scenario 0 (15 year simulated period)

The present mean annual sediment yield of the Thukela is quite high, with more than 9 million ton at the estuary. The simulations of the present day scenario still show very high sediment loads transported through the estuary (see **Figure 5.5.16**), although there is a slight decrease in the annual sediment loads towards the mouth. This is probably due to the decreasing velocities as the river enters the estuary, and sediment deposits. From the bed levels shown in **Figure 5.5.17**, the same trend can be observed, as some deposition occurred up to 6 km from the mouth. The estuary, however, is in dynamic equilibrium, with the bed level changing constantly throughout the simulation period (maximum and minimum values are indicated in **Figure 5.5.17**).

With the Jana and Mielietuin Dams fully developed the incoming sediment load is of course reduced, as mentioned in **Section 5.5.3**. The effect becomes evident when looking at the simulated annual sediment loads in **Figure 5.5.16**, which are also reduced by about 36% from the sediment loads simulated under present day conditions. The combination of reduced incoming sediment and flood peaks is the reason why there is no evidence of severe scour or aggradation in the estuary (see **Figure 5.5.18**). The band (i.e. maximum and minimum) within which the bed level seems to move is also narrower than for the present day scenario. However, this could indicate that a further reduction in the streamflow due to further catchment development could lead to aggradation in the estuary, especially if the sediment yield should increase due to changing land use.

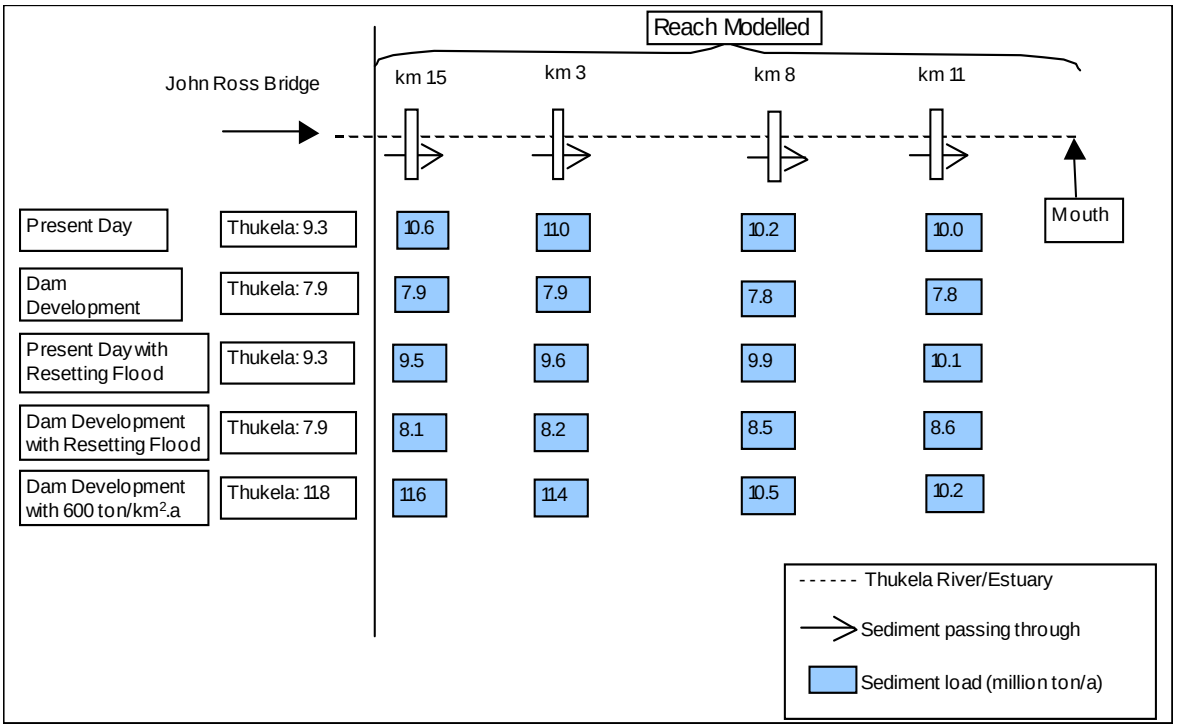

Figure 5.5.16 Simulated long-term sediment balance

Simulations of scenario 5 have indicated aggradation of up to 2 m. This means that the estuary becomes somewhat shorter (at a stage only 3.5 km), but the aggradation is confined mainly to the river and the estuary itself will not become much shallower (see **Figure 5.5.19** for details). **Figure 5.5.16** also shows that the annual sediment loads have decreased by more than 1 million ton at the estuary, indicating that the sediment has deposited upstream in the river.

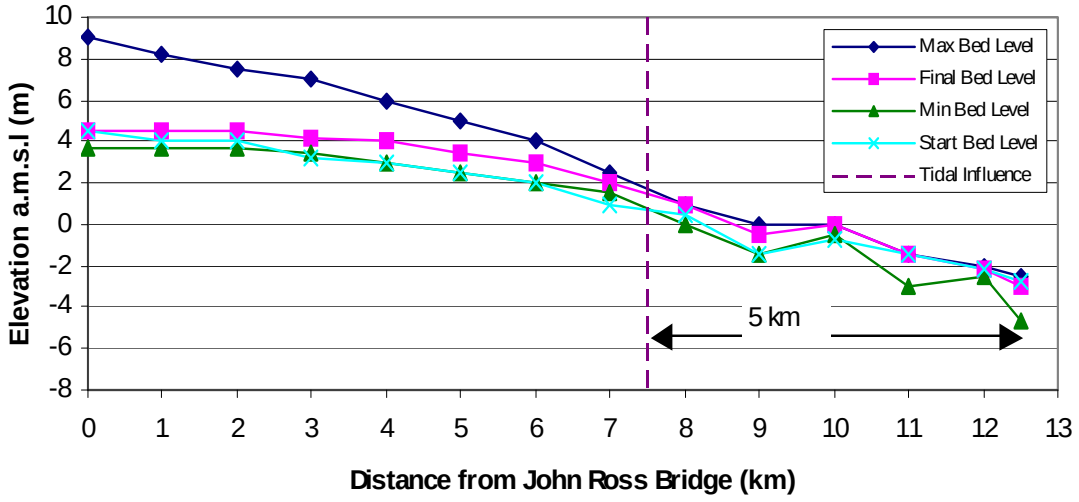

Figure 5.5.17 Bed levels - scenario 1 (15 year simulated period)

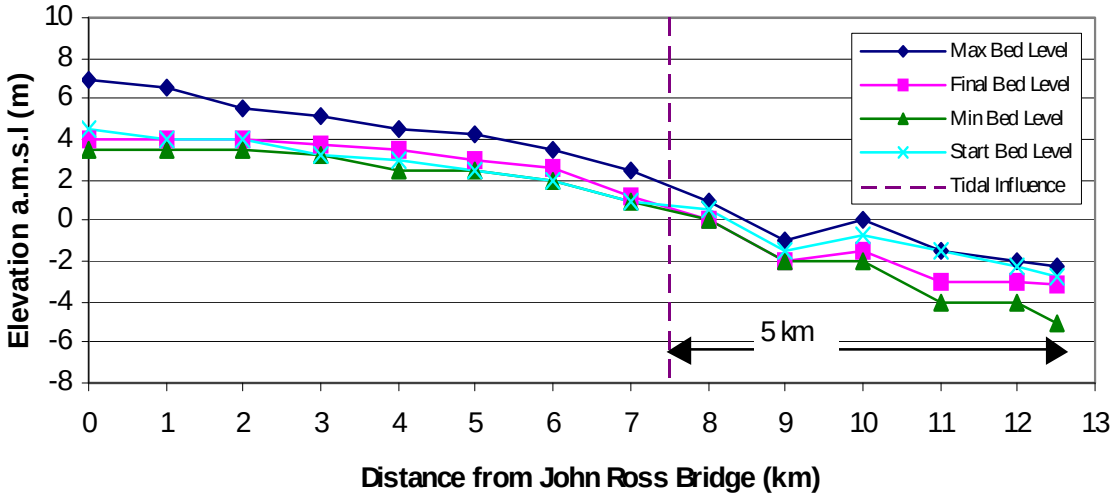

Figure 5.5.18 Bed levels - scenario 2 (15 year simulated period)

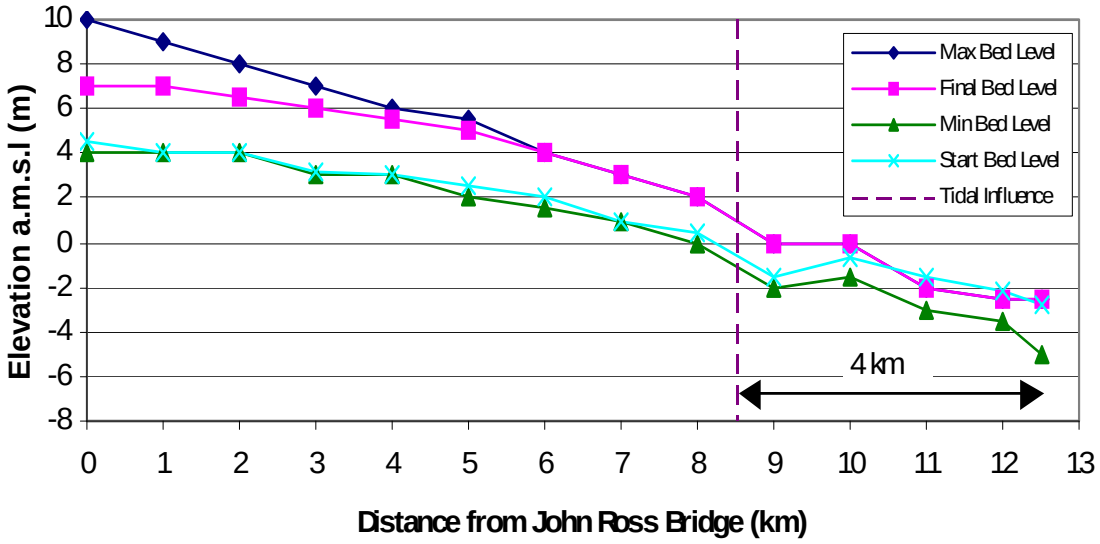

Figure 5.5.19 Bed levels – scenario 5 (15 year simulated period)

The length of the estuary (about 5 km) did not change very much, varying between 5 and 6 km, for the present day scenario. The same is true for the post-dam scenario, which is a result of the fact that no dramatic scouring or aggradation took place for both scenarios.

As mentioned in **Section 5.5.3** cohesive sediments were found in the estuary and the simulations have shown that the proportion of fraction 1 could increase dramatically between flood events, but would decrease again during a flood. During the present day scenario

fraction 1 would on average build up from 5 to 60% in the bed, and during the post-dam scenario to about 40%. The amount of cohesive sediment might therefore decrease as a result of the dam developments, but there will still be large quantities present. The system is, however, very dynamic and the mean percentage of cohesive sediment in the bed may be as low as 5%. All this is only applicable to the estuary and more than 7 km from the mouth the percentage of cohesive sediment will remain between 5 and 10%.

The percentage cohesive sediment in the bed sediment depends mostly on the availability of sediment as well the size of the estuary, since the larger the estuary the larger the area over which the sediment can be distributed. Under natural conditions (with a mean annual sediment load of 5.9 million ton at the estuary) the percentage fine material rarely builds up to more than 40%, generally staying between 20 and 30%, staring from the mouth and progressively building up back into the estuary for about 5 to 6 km. Under present day conditions (mean annual sediment load of 9.3 million ton) the fine sediment build-up is greater (generally up to 60%) extending 2 to 4 km into the estuary from the mouth. In future with the dams the fine sediment will still extend for about 2 to 4 km but will only build up to about 40%. With an increased sediment yield the percentage fine material builds up to about 75% extending only 2 to 3 km into the estuary from the mouth. Further upstream in the estuary and the river the fine fraction will generally remain between 5 and 10% for all scenarios but will vary from place to place along the river (see **Figure 5.5.20** for an example).

The amount of time that the fine sediment remains in the estuary depends on the occurrence of floods. If there are no floods in the dry season the fine sediment can stay in the estuary for about five months from May to October, which was the case in nine out of the fifteen years that were simulated. Even with floods the fine sediment can remain in the estuary for at least a month in the dry season.

As a result of the reduction in flood peaks the estuary could become narrower. Based on regime equations developed in Chapter 3 the estuary could narrow by about 11% (from present state), which means the cross-section width could reduce to around 445 m.

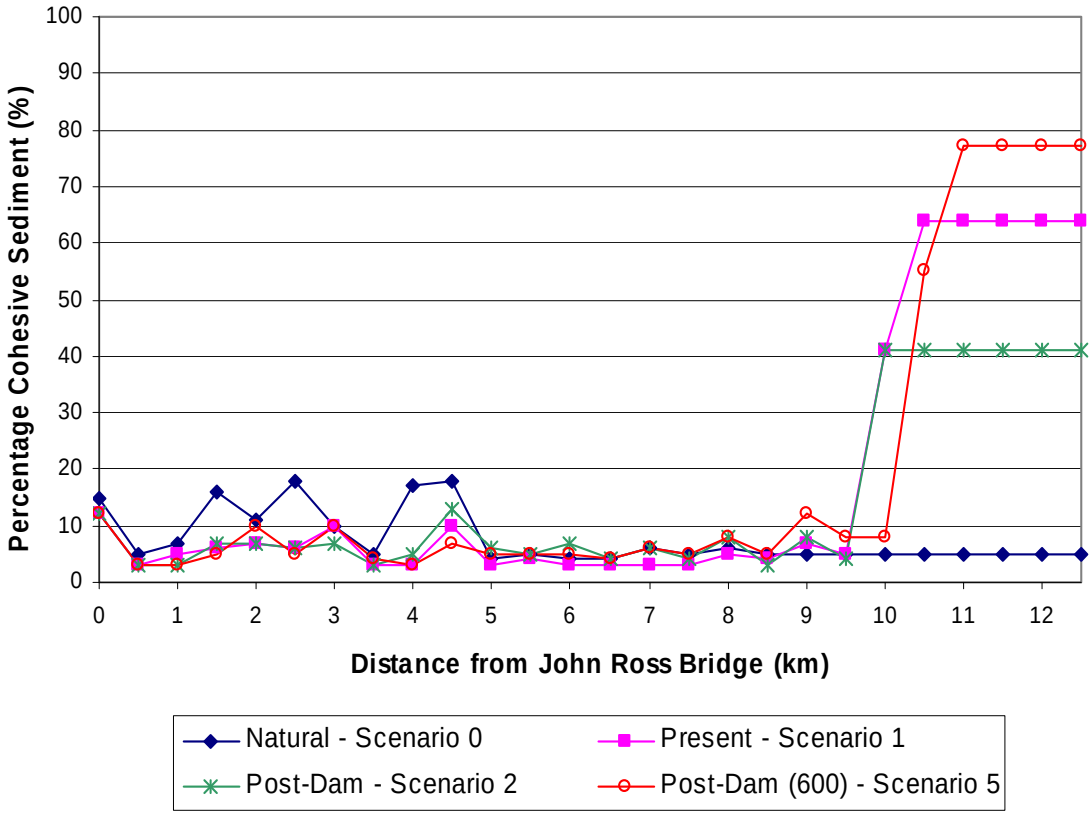

Figure 5.5.20 Example of fine sediment build-up in estuary (at a certain point in time)

5.5.5 Resetting Floods

Since the largest flood in the simulation period is only about a 1:10-year flood, it was important to also investigate what the effect of a large resetting flood, such as the 1:50-year flood, could be on the estuary. These floods are generally not affected to a great degree by dams, but Jana Dam does have a large storage capacity and therefore the flood peak could be reduced. The resetting flood was included in the simulations for both scenarios, right at the start of the simulation period. The resetting floods for the two scenarios and the corresponding concentrations are indicated in **Figures 5.5.21** and **5.5.22**.

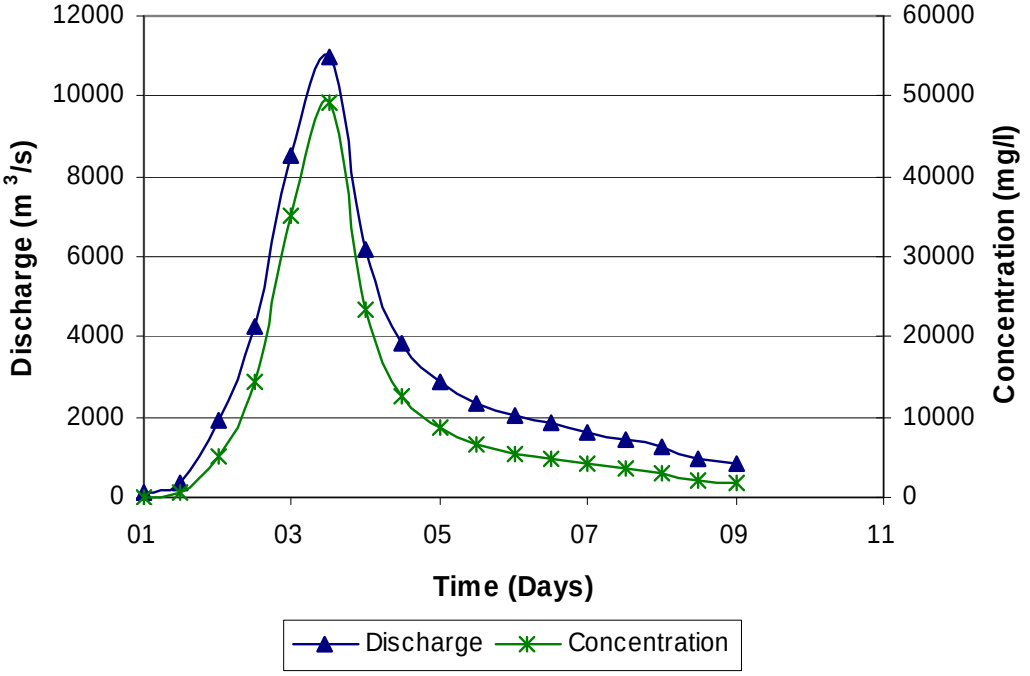

Figure 5.5.21 Resetting flood (1:50-year) for scenario 3

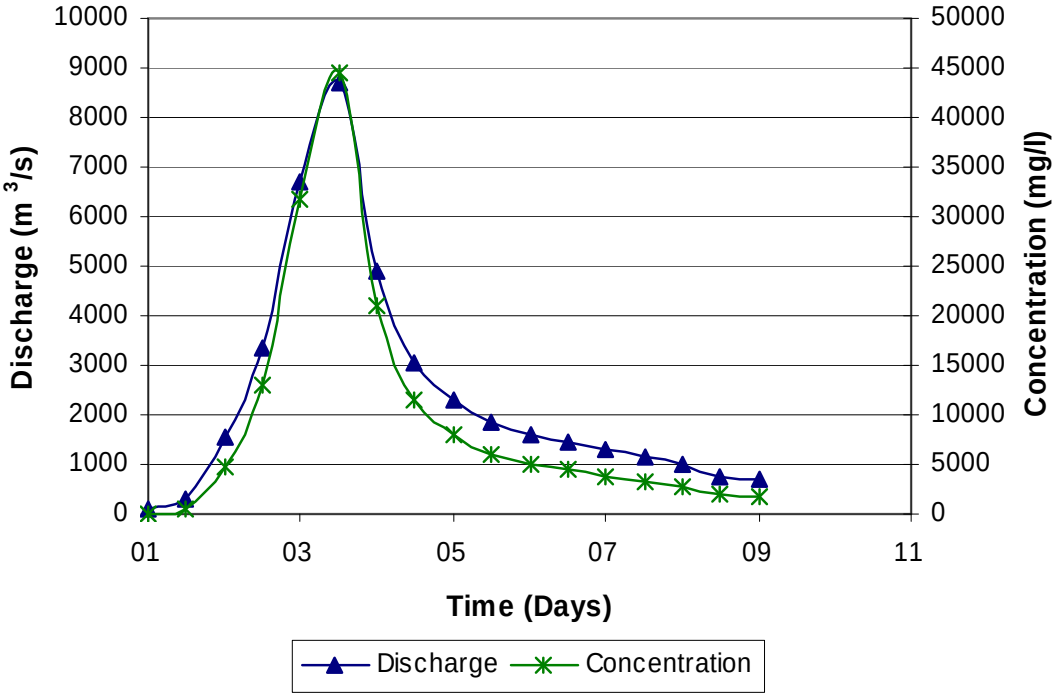

Figure 5.5.22 Resetting flood (1:50-year) for scenario 4

The surprising result was that for both scenarios some aggradation actually took place immediately after the flood in the upper part of the reach modelled, but severe scouring was simulated in the estuary itself closer to the mouth (see **Figure 5.5.23** and **5.5.24**). The overall effect was that the bed slope increased dramatically during the flood, but returned to normal within a few months. It took only a few months to remove most of the sediment again, and because the resetting flood carries so much sediment, less sediment is available for the rest of the time and therefore eventually the bed level ended up lower than at the start of the simulations. The fact is that these floods can have a major effect on both the Thukela River and the estuary, but it looks like the estuary is able to recover to a certain degree.

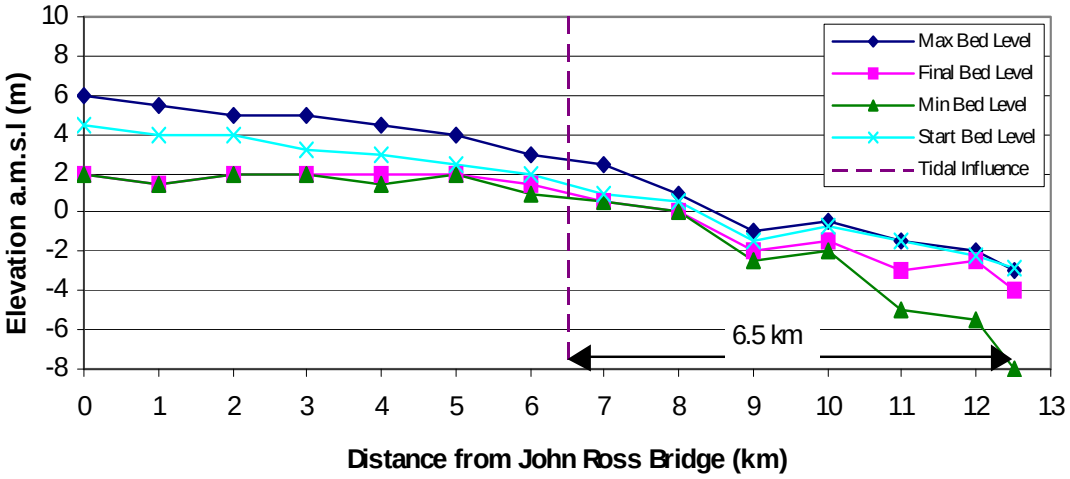

Figure 5.5.23 Bed levels - scenario 3 (15 year simulated period)

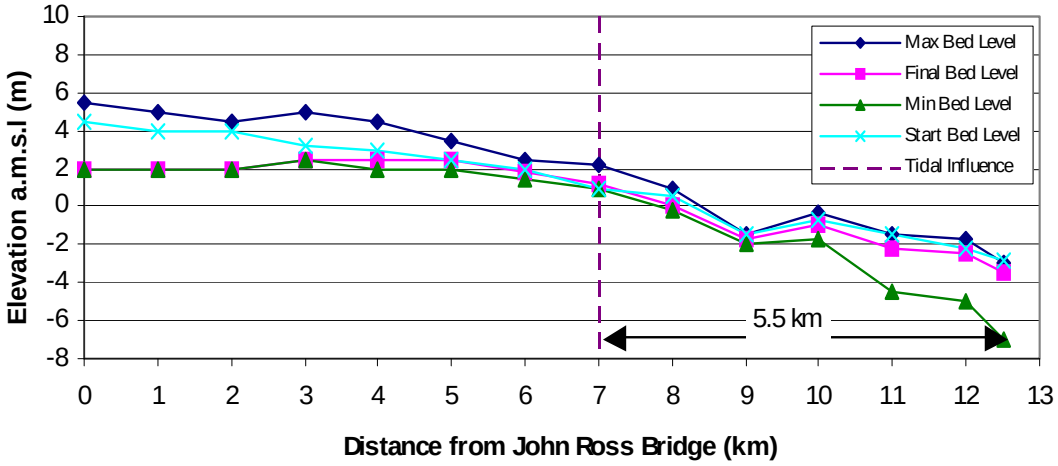

Figure 5.5.24 Bed levels - scenario 4 (15 year simulated period)

5.5.6 Conclusions

The key findings are:

- A number of large dams have been constructed high up in the catchment. Their effects on floods and sediment dynamics at the estuary are, however, minimal. The decrease in flood peaks at the estuary from natural to present day condition is estimated at 8%, while from present day to post-dam conditions the average peak discharge decrease is 19%.
- The estuary sediment dynamics is in a dynamic equilibrium under present day conditions. Simulations for the post-dam (worst case) scenario also indicate dynamic equilibrium of the fluvial morphology similar to present day conditions.
- Under natural conditions (assuming that the sediment yield would have been lower than at present) the estuary would have been about 8.5 km long and deeper than at present.
- The typical present-day (pre-dam) as well as future post-dam estuary length is 5 km.
- The flood attenuation, caused by the proposed dams, will decrease the estuary width by about 11% from present state, equivalent to 55 m on a 500 m wide cross-section.
- If the sediment yield from the catchment increases in future, it would shorten the estuary and it will become shallower.
- The role of the large resetting floods is important in scouring the river mouth, especially previously deposited cohesive sediments. Regular floods are therefore required to limit possible consolidation of cohesive sediment.
- The pre-dam and post-dam scenarios indicate a decrease in flood peaks at the estuary, but the floods are still regular enough with high sediment transport capacity to maintain the sediment balance in the estuary. No artificial flood releases from the Jana or Mielietuin Dams are therefore recommended for the estuary morphology, but this should be considered for the river immediately downstream of both dams during long periods without spillage.

5.5.7 Semi-Two-Dimensional Modelling of Thukela River Downstream of Proposed Jana Dam

A short reach (6 km) of the Thukela River just downstream of the proposed Jana Dam was modelled. The first three years of the flow sequence shown in **Figures 5.5.6** and **5.5.7** were used (average daily values). The model set-up was as follows:

- Five cross-sections 1.5 km apart

- Three stream tubes
- Two sediment fractions in bed material and incoming sediment
- Pre- and post-dam conditions

The cross-sectional changes during those five years simulated are shown in **Figures 5.5.25** and **5.5.26**. The fact that the river is a lot deeper after five years under natural conditions, is because the original cross-sections were taken from orthophotos and that the depth of the main river channel was unknown, and therefore assumed to be a certain depth, which was obviously too shallow. The river width has, however, not changed during those five years. The aggradation in the river between 1988 and 1990 is due to a continuous period (half a year) of low flows. With the proposed dam in place erosion of the river channel is significant, which is to be expected considering that no sediment is released from the reservoir. The width of the river channel has decreased from 40 m to between 25 and 30 m, which is in line with a predicted width of 32 m with the aid of the alternative width equations of **Section 3.6.2**.

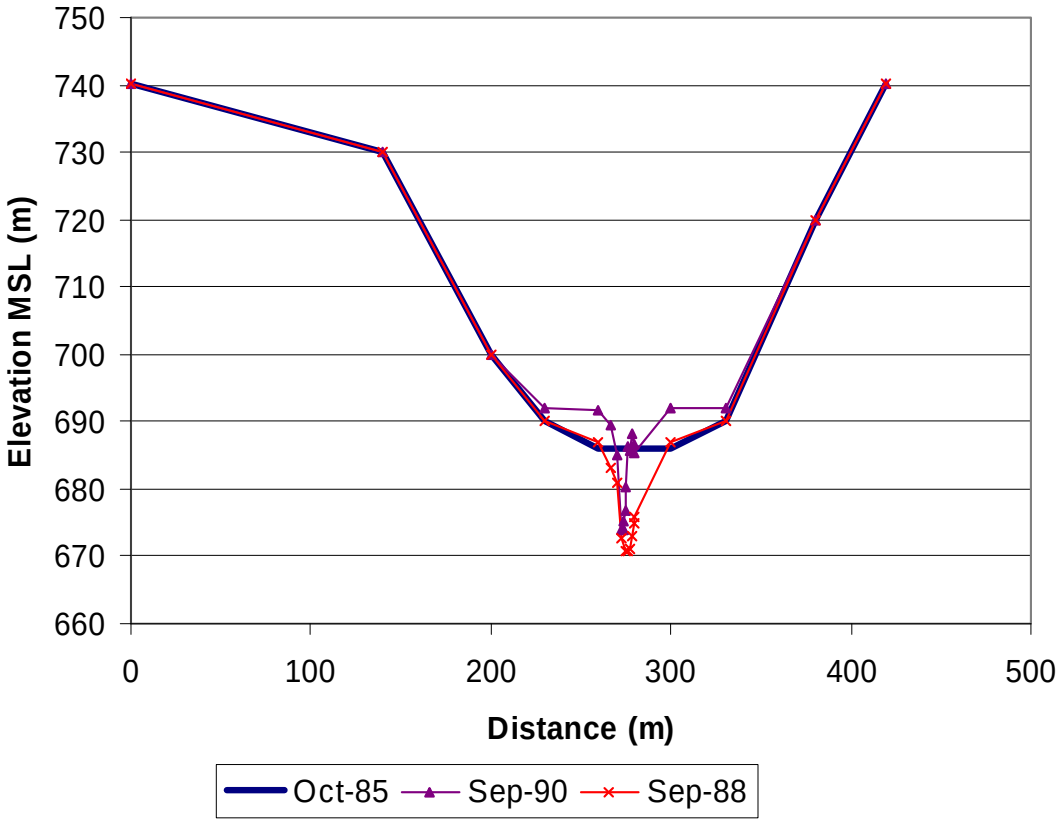

Figure 5.5.25 Pre-dam cross-sectional changes 3 km downstream of Jana Dam site

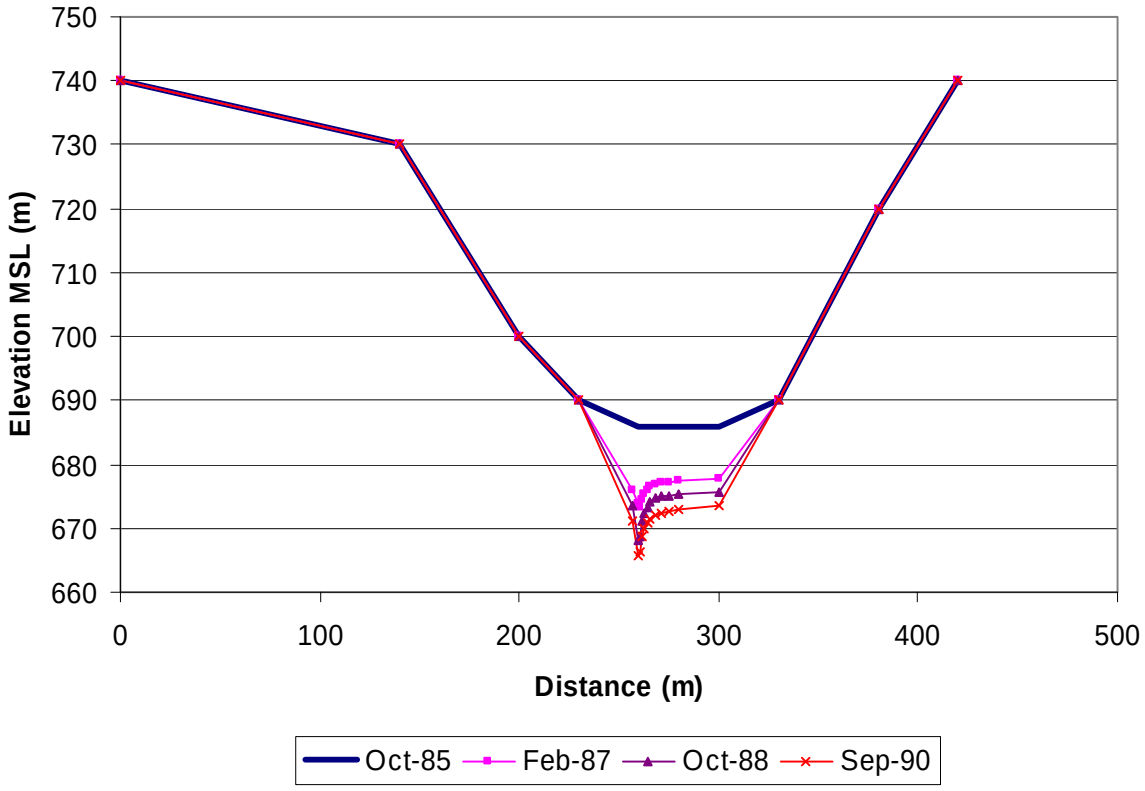

Figure 5.5.26 Post-dam cross-sectional changes 3 km downstream of Jana Dam site

For the most detailed investigations into the impacts of dams, both one- and two/three-dimensional mathematical models could be used. The one-dimensional models are suitable for long-term simulations of sediment balances, and erosion and deposition patterns, while two- and three-dimensional models should be used for short-term simulations, investigating certain areas in greater detail.

6. Development of Procedures to Determine and Limit the Impacts of Dams on the Downstream River Morphology

The major downstream impacts of dams are a reduction of the magnitude and frequency of flood peaks, changes in flow duration and reduced downstream sediment supply due to the trapping of sediments in the reservoir. These changes can lead to riverbed degradation close to the dam and aggradation further downstream, as the river strives for a new equilibrium. In order to reverse some of the changes that have taken place, or prevent major changes from occurring, researchers have been attempting to define a regulated flow regime, which will have much the same effects as the natural pre-dam flow regime. The problem, however, is to define those flows that form and maintain the river channel and the floodplain. The relative importance of different flows can best be evaluated by determining the amount of sediment transported by each. The discharge that transports the greatest amount of sediment over time is termed the effective discharge and identifying that discharge could help to determine a flow regime that will maintain the river in a natural or at least equilibrium state.

6.1 Determination of the Effective Discharge (Dollar *et al.*, 2000)

The method outlined by Dollar *et al*. (2000) to determine the effective discharge is as follows:

- Daily flow data are used to generate flow duration curves.
- The flow duration curves are divided into individual flow classes. It is assumed that the flows equalled or exceeded 10% of the time or less are most likely the most significant in terms of sediment transport. Therefore the flows from the 99.99% equalled or exceeded to the 10% equalled or exceeded are divided into 10% duration flow classes. The flow exceedences less than this are divided into flow class durations of 5%, 4%, 0.9% and 0.09%, respectively.
- The geometric mean of each flow class is then calculated.
- For each flow class the sediment concentration is calculated using a sediment transport equation like Engelund and Hansen or Yang.
- The sediment transported for each flow class is thus determined and expressed as a percentage of the total sediment transported.
- The effective discharge can then be determined.

This approach is used to determine the effective discharge of the Pongola River in its natural state. The flow record used contains 39 years of flow data. Engelund and Hansen's total load equation was used and the all the necessary parameters obtained from a surveyed cross-section, with d_{50} = 0.12mm. The use of the sediment transport equation does, however, not take into consideration that the sediment transport may be supply limited. For this reason a sediment rating curve was used to determine the sediment load and the results were compared to those obtained by utilizing Engelund and Hansen's sediment transport equation. The results are illustrated in **Figure 6.1.1**, and summarised in **Table 6.1.1**.

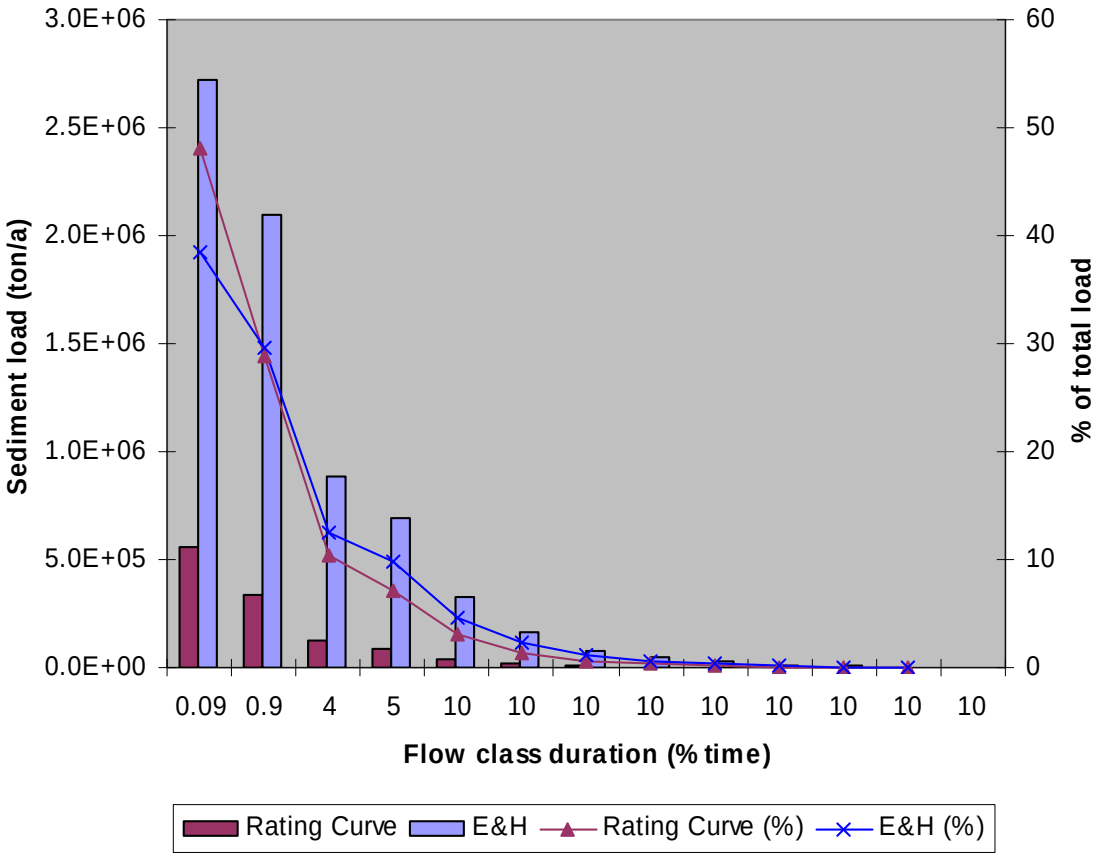

Figure 6.1.1 Sediment load distribution

From **Table 6.1.1** it can be seen that both approaches yield similar results in that the effective discharge is the discharge that is equalled or exceeded 0.01% of the time, although this is much more obvious for the sediment rating curve approach, with almost 50% of the total sediment transported by the effective discharge. The mean flow for that flow class represents a 1:10-year discharge for the Pongola River at that site (see **Table 6.1.2**). This is contrary to

the general opinion that the effective discharge generally occurs more frequently, usually in the 5% to 0.01% flow duration class (Dollar *et al.*, 2000).

Table 6.1.1 Flow classes and associated sediment transport

		Rating curve		E&H*	
% time equalled or exceeded	**Mean flow (m^3/s)**	**Sediment load (*1000 ton/a)**	**% of total load**	**Sediment load (*1000 ton/a)**	**% of total load**
99.99					
90	2	0.09	0.004	1.8	0.02
80	5	0.34	0.015	5.7	0.05
70	7	0.87	0.04	13.0	0.12
60	10	1.82	0.08	24.6	0.23
50	14	3.57	0.2	44.4	0.42
40	19	6.99	0.3	79.9	0.8
30	29	16.07	0.7	165.4	1.6
20	41	35.27	1.6	328.7	3.1
10	62	82.86	3.7	693.5	6.5
5	103	120.51	5.4	881.7	8.3
1	185	334.84	15.0	2093.8	19.7
0.1	475	559.35	25.0	2716.5	25.5
0.01	1914	1071.20	48.0	3585.4	33.7
	Σ	2233.8	Σ	10634.4	

*Engelund and Hansen's sediment transport formula

Table 6.1.2 Pongola flood peaks

Recurrence interval (years)	Flood peak (m^3/s)
2	800
5	1400
10	1900
20	4600
50	10500

The one significant problem with the outlined approach, is the determination of the different flow classes. Choosing different intervals could yield different results. Also all the flow classes should really have the same duration to be able to compare the contribution of each flow class. Another aspect of that problem is the fact that all flows equalled or exceeded less than 0.01% of the time are not included in the evaluation. It may be argued that these flows do not occur frequently enough to be effective, but as can be seen in **Table 6.1.3**, this is not the case. Another flow class was added, representing the discharges equalled or exceeded between 0.01% and 0.001% of the time. The flow duration is very short, and yet these flows manage to transport more than 35% of the total sediment load.

Table 6.1.3 Extended flow classes and associated sediment transport

		Rating Curve			E&H*	
% time equalled or exceeded	$\overline{Q}$ **(m^3/s)**	**Sediment load (ton/a)**	**% of total load**	**Cumulative %**	**Sediment load (ton/a)**	**% of total load**
99.99						
90	2	0.1	0.002	0.00	1.8	0.01
80	5	0.3	0.01	0.01	5.7	0.04
70	7	0.9	0.02	0.03	13.0	0.08
60	10	1.8	0.05	0.08	24.6	0.15
50	14	3.6	0.09	0.17	44.4	0.27
40	19	7.0	0.2	0.4	79.9	0.5
30	29	16.1	0.4	0.8	165.4	1.0
20	41	35.3	0.9	1.7	328.7	2.0
10	62	82.9	2.2	3.9	693.5	4.2
5	103	120.5	3.1	7.0	881.7	5.4
1	185	334.8	8.7	15.7	2093.8	12.8
0.1	475	559.3	14.6	30.3	2716.5	16.6
0.01	1914	1071.2	27.9	58.2	3585.4	21.9
0.001	10541	1605.0	41.8	100	5772.2	35.2
	Σ	3838.7		Σ	16406.6	

*Engelund and Hansen's sediment transport formula

From **Table 6.1.3** it can also be seen that all flows greater than 50 m^3/s are significant, accounting for 98% of the total sediment load.

The concept of an effective discharge can be very useful when determining a flow regime that will maintain a river in its natural or equilibrium state. However, the method outlined above still holds some problems, such as the determination of the flow duration intervals and the exclusion of the less frequently occurring floods.

6.2 Proposed Procedures to Determine and Limit the Impact of Dams on the Downstream River Morphology

A better approach will be the one followed in the case studies in **Chapter 5**, investigating the changes in the sediment balance and sediment load-discharge relationship between the pre- and post-dam periods.

The following methodology was followed in all three case studies in **Chapter 5**:

- Delineate the study area in terms of the morphological processes.

- Determine the reference condition and present geomorphological state, using:
  - Historical aerial photos and surveys.
  - Investigate possible changes in sediment yield.

- Describe the morphological processes of the river, including sediment transport, based on flow patterns, sediment characteristics (field work) and the downstream boundary conditions.

- Establish a sediment load–discharge relationship from observed suspended sediment concentration data considering seasonal trends and sediment transport capacity, which might limit the concentration.

- Use the sediment load–discharge relationship with the observed flow record to determine the catchment sediment yield, taking into account trapping of sediment by existing upstream dams.

- Compare this sediment yield with observed or estimated mean annual values of sediment yield determined by one of the following methods:
  - Sediment load-discharge rating curves obtained from observed suspended sediment concentrations in conjunction with long-term flow records.
  - Surveys of reservoir sediment deposits.
  - Sediment yield maps.
  - Statistical analysis of Southern African sediment yields.

- Should no observed suspended sediment data be available, the sediment transport capacity can be used. The sediment transport capacity and corresponding sediment loads are calculated for a long time period (> 15 years) based on observed flow data. The sediment load is integrated over the whole period and the sediment yield thus determined. The sediment transport capacity is then, if necessary, adjusted to yield the observed sediment yield.

- Generate long-term time series data of natural flow and concentration/sediment load by using the sediment load- discharge relationship.

- Simulate the natural condition with a numerical hydrodynamic and morphological model:
  - Upstream boundary – concentration (C_{in})/sediment load (Q_{sin}) and flow (Q_{in})
  - Downstream boundary – f(discharge or water level)
  - Calibrate hydrodynamic model bed roughness, based on field measurements or possible correlation between gauging station discharge and flow depth.

- Establish the natural sediment transport processes, including erosion and deposition, in the river.

- Generate current and future scenario flows and sediment transport:
  - Reduce sediment yield (t/a) by sediment trapping in future planned upstream dams
  - Use generated flows with development, or if not available, simulated new flows at the dam, by considering water use, net evaporation, full supply capacity of reservoir, etc. If the effect of more than one dam has to be investigated, or the point of interest is far downstream of the dam flows may have to be routed through the catchment, together with the downstream catchment flows. Abstractions downstream should be lumped to reduce total catchment flow.
  - Adjust the sediment load-discharge relationship to obtain the reduced mean annual sediment yield (t/a), also considering sediment transport capacity (concentration should not be higher than the maximum observed concentration, if reliable long-term observed data is available).
  - Generate time series of flows and concentration/sediment load.
  - Generate time series of flows and concentration/sediment load with increased sediment yield above natural (due to changing land use).

- Simulate the sediment transport through the river with dam operated with storage operation: evaluate deposition and erosion patterns and compare with natural conditions.

- Determine the critical conditions for re-entrainment of sediment from the riverbed and associated flood discharge, considering possible effects of cohesive sediment (sediment characteristics to be obtained from bed sediment samples and grading analysis).

- Simulate sediment transport through the river with realistic artificial flood releases from dam(s), considering the following:
  - Magnitude: annual up to 1:10-year flood.
  - Duration: as close as possible to natural hydrograph shape (typically a few days).
  - Frequency: once or twice a year, depending on the flood magnitude and availability of water.
  - Timing: together with a large enough natural runoff event and at the beginning of the rainy season (for the greatest effectiveness).

Use future development scenario flows with floods added, after comparison with natural runoff record.

- Recommend IFR/EFR flood peaks, frequency and duration.

It should be noted that in order to develop proper guidelines it would be necessary to hold a workshop attended by all parties concerned, during which all the abiotic and biotic components and their interrelationship are discussed.

In addition to the clear water artificial flood releases, sluicing through and/or flushing of sediment from the reservoir can be considered at relatively small reservoirs where excess water is available.

6.2.1 Passing High Sediment Loads Through the Reservoir

Sluicing:

When the storage capacity-mean annual runoff (MAR) ratios of reservoirs in the world are plotted against the capacity-sediment yield ratio, the data plot as shown in **Figure 6.2.1 (**Basson and Rooseboom, 1997). Most dams have a capacity-MAR ratio of between 0.2 to 3, and a life of 50 to 2000 years when considering reservoir sedimentation.

When the capacity-MAR ratio is less than 0.03, sediment sluicing or flushing should be carried out during floods and through large bottom outlets, preferably with free outflow conditions. Flushing is a sustainable operation and a long-term equilibrium storage capacity would be reached. When capacity-MAR ratios are however larger than 0.2, not enough excess water is available for flushing.

Successful sluicing depends on the availability of excess water and relatively large bottom outlets at the dam. First Falls and Second Falls on the Mtata River have been operated in series with sluicing through two large bottom radial gates at each dam. After about 20 years of operation the reservoir storage capacity remains more than 70 percent of the original capacity. For successful flushing the reservoir capacity-mean annual runoff ratio should be quite small, say less than 0.05 year. Free outflow conditions are preferable, but not a

requirement like with flushing, and only partial water level drawdown is required as long as the sediment transport capacity through the reservoir is high during a flood.

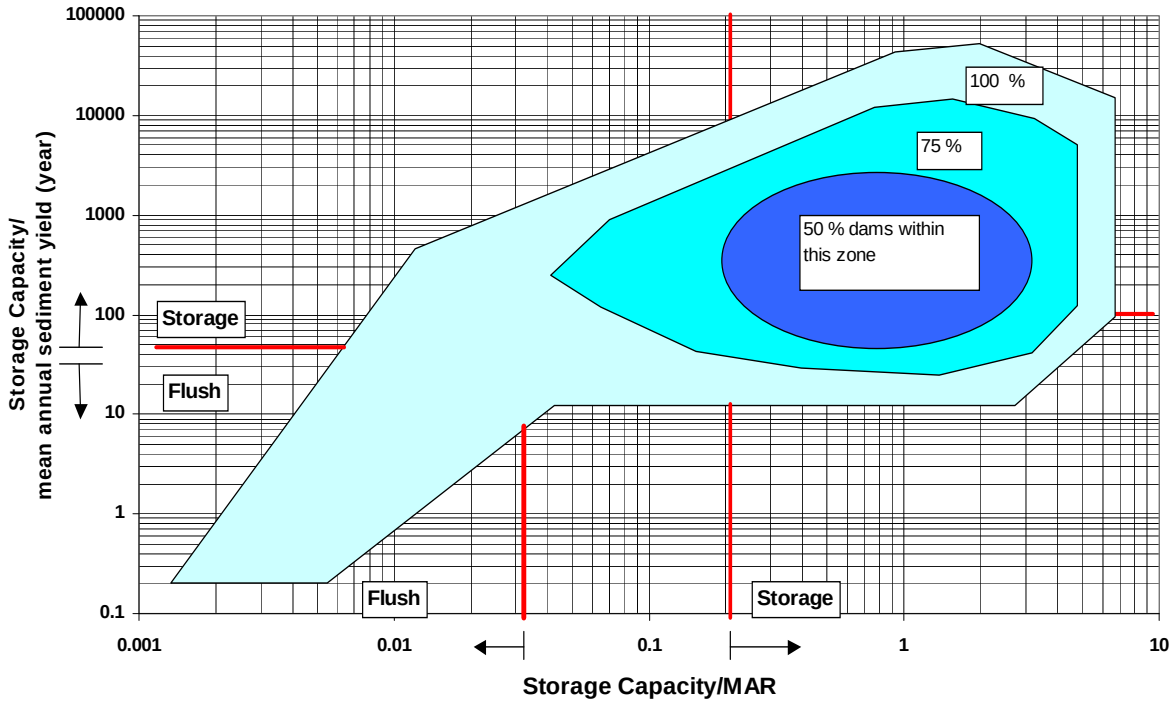

Figure 6.2.1 Universal reservoir classification system in terms of storage, runoff and sediment yield

6.2.2 Removal of Sediment

Flood Flushing:

Flushing can be a very effective way to remove accumulated sediment deposits from a reservoir. As with sluicing, excess water is required with large low-level outlets capable of passing the say 1:5 year flood under free outflow conditions. Successful flood flushing is carried out at Phalaborwa Barrage on the Olifants River where 22 large, 12 m wide radial gates were installed, covering the whole width of the river (**Figure 6.2.2**). The reservoir has been operated since the 1960s, and maintains a long-term capacity in the order of 40 % of the original capacity.

At other reservoirs the flushing is less effective for example the case of Welbedacht Dam which has 5 large radial gates but which are not located at the river bed but 15 m above it. After 20 years of operation, 85 percent capacity was lost and today only about 9 million m³

storage capacity remains and this is with regular flushing during floods above 400 m³/s. The flushing duration is limited to about 10 hours, the period of time during which water purification to the city of Bloemfontein can be temporarily stopped. During 1994, 3 million m³ sediment was flushed out during two floods with total flushing duration of 20 hours. The storage capacity is however still decreasing.

Figure 6.2.2 Phalaborwa Barrage flood flushing

Planning, design and judicious operation of water resources are of key importance in limiting the impacts of reservoir sedimentation. In small reservoirs as much as 40% of the original capacity can be maintained in the long-term by regular flushing of sediments. As long as the flushing discharge sediment concentrations do not exceed the maximum values recorded at the dam site before dam construction, based on an observed sediment load-discharge rating curve, the river morphology should experience similar conditions as under natural conditions.

7. Conclusions and Recommendations

7.1 Conclusions

The objectives of this project were to obtain a better understanding of the river sediment transport processes due to the impacts of dam developments. Specifically the development of a methodology to both determine and limit the impacts of dams on the downstream river morphology.

The following results have been obtained:

- The impacts of dams on the downstream river morphology depend to a large degree on the operation of the reservoir as well as the reservoir capacity in relation to the MAR, since these two factors determine the magnitude, duration and frequency of all but the largest floods. Some examples of impacts are presented in **Table 7.1.1**:

Table 7.1.1 Impacts and causes

Impact	**Cause**
Riverbed degradation	Clear water spillage due to sediment trapped in reservoir
Coarsening of bed material	Clear water releases
Reduced sediment transport capacity	Attenuated flood peaks, coarser bed materials, flatter slopes
Riverbed aggradation	Reduced sediment transport capacity, tributary sediment supply
Increased riparian vegetation	Long periods of low or no flows
Narrowing of river channel	Increased riparian vegetation and smaller floods

- Regime equations describing the average width and depth of a river were developed, based on South African river data. The equations were verified with the aid of international river data, and compared to results obtained from semi-theoretical regime

equations developed in the United States. The new regime equations compared favourably to these regime equations.

- The regime equations developed in **Chapter 3**, as well as other international regime equations are not suitable for predicting the channel geometry of rivers downstream of dams with highly unnatural release patterns, mainly as a result of the problems with the determination of the dominant discharge. Alternative regime width equations were developed.

- It has been found, through laboratory experiments, that as little as 7% clay and silt can affect the sediment transport behaviour of sand. When sediments contain more than 23% sand the erosion could be affected by armouring. At higher clay and silt contents (> 7%) almost no bedforms develop.

- A methodology was developed by which the critical conditions for mass erosion of cohesive sediments and cohesive – non-cohesive mixtures can be described in terms of the applied stream power at the bed. The applied stream power at the bed can be related to the percentage clay and silt in the bed material.

- Sediment transport equations in terms of the unit input stream power for cohesive and non-cohesive sediments, as well as mixtures of the two, were developed with data gained from laboratory experiments. The equations were successfully verified against independent flume data, as well as United States river data.

- One-dimensional modelling of the impact of existing and proposed new dams on two South African rivers and an estuary was carried out. By comparing sediment transport characteristics of pre-and post-dam scenarios, problem areas could be identified and mitigating procedures evaluated.

- Procedures were developed by which the impacts of dams on the downstream river morphology can be determined and mitigating measures developed.

- Environmental flood releases at medium and large dams, and sediment sluicing/flushing at small reservoirs (relative to the MAR), are required to limit the upstream and downstream impacts of a dam on the river and estuary morphology. By using observed and simulated discharge-sediment load relationships along a river for various development/operational scenarios, it is possible to design the peak discharge, frequency and duration of these environmental floods.

- Environmental flood releases will cause riverbed degradation close to the dam, but are required for channel maintenance of the greater part of the river further downstream to limit the overall impact of a dam.

7.2 Recommendations

7.2.1 Design and Operation

- Dams have dramatic impacts on the river morphology, far upstream and even further downstream. These impacts should not be underestimated in terms of ecological damage and costs, and should be investigated in great detail during planning, design and operation of the dam using suitable hydraulic techniques.

- It is recommended that the proposed procedures on the methodology to investigate the morphological impacts of dams be implemented in environmental flood requirement studies. The design of flood releases (or not) considering flood peak, duration, and frequency should be carried out using this methodology.

- Post-dam river width changes can be simulated by using regime equations developed in this study, but for more detailed investigations semi-two-dimensional or two-dimensional modelling should be carried out.

- River morphological simulations should be carried out over at least 15 years. Daily data are often not good enough due to the flood peak averaging.

- Flood flushing and managed flood releases from reservoirs should be implemented to take place simultaneously with a natural flood event for maximum efficiency.

- Generally the quality of the water released from reservoirs is very different than under natural conditions. In order to achieve the desired water quality, the design of multi-level outlet structures should be optimised to allow managed flood releases.

- Hydropower generation, causing large water level fluctuations, can seriously damage a river. Planned flood releases are difficult to implement in order not to interfere with the hydropower generation, so the hydropower releases have to be optimised to reduce geomorphological impacts, by limiting maximum release discharges and rate of change of discharges.

- The proposed analysis procedures rely on long-term suspended sediment data taken in rivers to determine a sediment load – discharge relationship. Such data are available on most rivers in Africa and internationally, but are limited in South Africa. It is important that suspended sediment sampling is continued as soon as possible at most of the South African flow gauging stations.

- The natural river geomorphology is generally used as a reference condition against which to evaluate any future changes. At future planned dam sites monitoring of the river morphology should be carried out, such as repeat surveys, in order to establish the reference condition and any subsequent changes.

- The impacts of a dam are not limited to rivers, but if the reservoir is large enough or close to the sea, the estuarine and marine environment can also be affected. It is recommended that the flood and sediment transport requirements of the estuarine and marine environment be investigated.

- It has been established that a range of flows is important in forming and maintaining the river geomorphology, but the relative importance between freshets and major flood releases in terms of the sediment transport need to be investigated.

7.2.2 Research

- More data are necessary on the sediment transport of fine sediments and non-cohesive – cohesive mixtures in order to be able to test the theory developed during this project on the critical conditions for mass erosion.

- In order to calibrate the proposed cohesive sediment transport equation for a wider range of sediment sizes, data on other types of cohesive sediments are necessary.

- The effect of consolidation and drying of fine sediments on the sediment transport behaviour should be investigated in greater detail.

- The sediment transport theory of sand, gravel and even fine sediment is well established. However, the sediment transport of cobbles and boulders should be investigated to establish characteristics such as the flows necessary to move larger-sized sediment and their sediment transport.

- A problem with determining IFR/EFR requirements is the difficulty in establishing the correct link between the abiotic drivers, e.g. hydrology and sediment transport, and the biotic components, such as the role of fine sediment transport. Detailed hydrodynamic and morphological simulations can yield more information, which can be significant for the biotic components.

8. References

Ackers, P. (1988). Alluvial Channel Hydraulics. *Journal of Hydrology*, 100, pp. 177- 204.

Ackers, P. and Charlton, F.G. (1970). Meander Geometry arising from varying flows. *Journal of Hydrology*, 11, pp. 230-252.

Acreman, M. (2000). *Managed Flood Releases from Reservoirs: Issues and Guidance*. Contributing Paper to the World Commission on Dams, Cape Town. www.dams.org

Alexander, W.J.R. (1990). *Flood Hydrology for Southern Africa.* SANCOLD. South Africa.

Andrews, E.D. (1986). Downstream Effects of Flaming Gorge Reservoir on the Green River, Colorado and Utah. *Geological Society of America Bulletin*, 97(8), pp. 177-204.

Andrews, E.D. and Pizzi, L.A. (2000). Origin of the Colorado River Experimental Flood in Grand Canyon. *Hydrological Sciences*, 45(4), pp. 607 – 627.

Bagnold, R.A. (1966). An Approach to the Sediment Transport Problem from General Physics. *Geological Survey Professional Paper 422-I*, U.S. Government Printing Office, Washington, D.C.

Basson, G.R. and Rooseboom, A (1990). *Report on the Hydraulic Model Investigation of the Proposed Tugela River Bridge B351 on National Route 2 Section 27.* South African Roads Board.

Basson, G.R. and Rooseboom, A. (1997). *Dealing with Reservoir Sedimentation.* South African Water Research Commission, Report No. TT91/97, South Africa.

Blench, T. (1957). *Regime Behaviour of Canals and Rivers.* Butterworth Scientific Publications, London.

Brandt, S.A. (1999). Reservoir Desiltation by Means of Hydraulic Flushing. PhD Thesis, University of Copenhagen, Copenhagen, Denmark.

Bray, D.I. (1982). Regime Equations for Gravel-Bed Rivers. In: Hey, R.D., Bathurst, J.C., Thorne, C.R. (eds.) *Gravel-bed Rivers.* John Wiley & Sons, Chichester, UK.

Brierley, G.J. and Fitchett, K. (2000). Channel Planform Adjustments along the Waiau

River, 1946-1992: Assessment of the Impacts of Flow Regulation. In: Brizga, S. and Finlayson, B. (eds.) *River Management: the Australasian Experience.* John Wiley & Sons, Chichester, UK, pp. 51 – 71.

Carling, P.A. (1988). Channel Change and Sediment Transport in Regulated UK Rivers. *Regulated Rivers: Research and Management,* 2, pp. 369-387.

Carson, M.A. (1984). The Meandering – Braided Threshold: A Reappraisal. *Journal of Hydrology,* 73, pp. 315 –334.

Chang, H.H. (1979). Minimum Stream Power and River Channel Patterns. *Journal of Hydrology*, 41, pp. 303-327.

Chang, H.H. (1988). *Fluvial Processes in River Engineering.* John Wiley & Sons, New York.

Chien, N. (1985). Changes in River Regime after the Construction of Upstream Reservoirs. *Earth Surface Processes and Landforms*, 10, pp. 143 – 159.

Chitale, S.V. (1966). Cited in Wargadalam.

Clark, P.B. and Davies, S.M.A. (1988). The Application of Regime Theory to Wadi Channels in Desert Conditions. In: White, W.R. (ed.) *International Conference on River Regime.* John Wiley & Sons, Chichester, UK, pp. 67-82.

DHI (1992). *MIKE 11: A Microcomputer Based Modelling System for Rivers and Channels, Reference Manual*. Danish Hydraulic Institute Software. Denmark.

Dollar, E.J.S., Rowntree, K.M., Wadeson, R.A. (2000). *Geomorphological Research for the Conservation and Management of Southern African Rivers, Volume 2.* Draft Report to the Water Research Commission.

Dollar, E.S.J (2001). *A Review of the Information Relating to the Geomorphology and Sediment Yield of the Thukela Basin with a Comment on it Implications for the Instream Flow Requirement Assessment.* University of Witwatersrand, South Africa.

DT (1997). *Road Drainage Manual.* Department of Transport, Chief Directorate Roads. South Africa.

DWA (1987). *Mathematical Model of the Hydraulics of the Pongolo River Flood Plain –*

Draft. Department of Water Affairs. South Africa.

DWAF (1998). *Hydrological Calculation Files.* Department of Water Affairs and Forestry, South Africa.

DWAF Website: http://www-dwaf.pwv.gov.za/thukela

Egiazarof, I.V. (1950). Coefficient (f) de la Force d'Entrainement Critique des Matérieaux par Charriage. *Proc. Acad. of Sci., Armenian S.S.R. Translation EDF No. 499.*

Engelbrecht, G. (1996). *Fluvial Geomorphological Impact Assessment of the Proposed Skuifraam Dam on the Berg River. Skuifraam Feasibility Study EIA.*

Gilbert, G.K. (1914). The Transportation of Debris by Running Water, Based on Experiments Made with the Assistance of E.C. Murphy. *Geological Survey Professional Paper 86.*

Glen Canyon Dam Website, 2002 - http://www.canyon-country.com/lakepowell/gcdam.htm

Guy, H.P., Simons, D.B., Middleton, B.J. (1966). Summary of Alluvial Channel Data from Flume Experiments, 1956-61. Sediment Transport in Alluvial Channels. *Geological Survey Professional Paper 462-I*, U.S. Government Printing Office, Washington, D.C.

Hadley, R.F. and Emmett, W.W. (1998). Channel Changes Downstream of a Dam. *Journal of the American Water Resources Association*, 34(4), pp. 629 –637.

Harvey, A.M. (1969). Channel Capacity and the Adjustment of Stream to the Hydrologic Regime. *Journal of Hydrology*, 8, pp. 82-98.

Henderson, F.M. (1963). Cited in Wargadalam.

Hey, R.D. and Thorne, C.R. (1986). Stable Channels with mobile Gravel Beds. *Journal of Hydraulic Engineering*, 112(8), pp. 671-689.

HTDC – Highlands Delivery Tunnel Consultants (1999). *Lesotho Highlands Water Project Contract No. TCTA-10 – Delivery Tunnel North: Report on the Erosion along the Ash and Liebenbersgvlei Rivers.* South Africa.

HTDC - Highlands Delivery Tunnel Consultants (2000). *Lesotho Highlands Water Project Contract No TCTA-10 –Delivery Tunnel North: Upgrading of the Ash River Stage 2 -*

Field Inspections and Analyses – October 2000 Follow-up Reconnaissance Report South Africa.

HTDC - Highlands Delivery Tunnel Consultants (2002). *Ash River Upgrading Stages 1,2 and 2A – Ash CD-Rom No 01 and No 02*. South Africa.

Hughes, D.A. (2002). *Thukela Water Project Decision Support Phase – Reserve Determination Module - Hydrology Estuary Scenarios*. Rhodes University, South Africa.

Julien, P.Y. and Wargadalam, J. (1995). Alluvial Channel Geometry: Theory and Applications. *Journal of Hydraulic Engineering*, 121(4), pp. 312-325.

Kamphuis, J.W. and Hall, K.R. (1983). Cohesive Material Erosion by Unidirectional Currents. *Journal of the Hydraulics Division,* 109(1), pp. 49-61.

Kellerhals, R. (1967). Stable Channels with Gravel-Paved Beds. *Journal of the Waterways and Harbours Division*, 93(WW1), pp. 63-84.

Kovacs, Z.P., Du Plessis, D.B., Bracher, P.R., Dunn, P., Mallory, G.C.L. (1985). *Documentation of the 1984 Domoina Floods*. Department of Water Affairs. South Africa.

Lacey, G. (1930). Cited in Wargadalam.

Le Grange, A.duP. (1994). *Techniques for Predicting the Deformation and Hydraulic Resistance of Sand-Bed Rivers.* PhD. Thesis, University of Stellenbosch, Stellenbosch, South Africa.

Leopold, L.B. and Maddock, T. (1953). Cited in Wargadalam.

Leopold, L.B. and Wolman, G. (1957). River Channel Patterns: Braided, Meandering and Straight. *Geological Survey Professional Paper 282-B*, U.S. Government Printing Office, Washington, D.C.

Mehta, A.J., Hayter, E.J., Parker, R., Krone, R.B., Teeter, A.M. (1989). Cohesive Sediment Transport I: Process Description. *Journal of Hydraulic Engineering*, 115(8), pp.1076-1093.

Midgley, D.C., Pitman, W.V., Middleton, B.J. (1990). *Water Surface Resources of South*

Africa 1990, Volume VI, Appendices. South African Water Research Commission, Report No. 298/6.1/94, South Africa.

Nitsche, N.C. (2000). *Assessment of a Hydrodynamic Water Quality Model, Duflow, for a Winter Rainfall River.* M.Eng. Thesis, University of Stellenbosch.

Nouh, M. (1988). Regime Channels of an Extremely Arid Zone. In: White, W.R. (ed.) *International Conference on River Regime.* John Wiley & Sons, Chichester, UK, pp. 55-66.

NS – Ninham Shand (2001). Pers. Com.

Osterkamp, W.R. and Hedman, E.R. (1979). Cited in Wharton, G. (1995). Information from Channel Geometry-Discharge Relations. In: Gurnell, A. and Petts, G. (eds.) *Changing River Channels.* John Wiley & Sons. Chichester, UK.

Panagiotopoulos, I., Voulgaris, G., Collins, M.B. (1997). The Influence of Clay on the Threshold of Movement of Fine Sandy Beds. *Coastal Engineering,* 32, pp. 19-43.

Parchure, T.M. and Mehta, A.J. (1985). Erosion of Soft Cohesive Sediment Deposits. *Journal of Hydraulic Engineering,* 111(10), pp.1308-1326.

Partheniades, E. (1971). Erosion and Deposition of Cohesive Materials. In: Shen, H.W. (ed.) *River Mechanics,* Volume II, Fort Collins, Colorado, pp. 25.1 – 25.91.

Partheniades, E. and Paaswell, R.E. (1970). Erodibility of Channels with Cohesive Boundary. *Journal of the Hydraulics Division,* 96(3), pp. 755-771.

Pollard, I. (2001). *Die Effek van Damontwikkeling op die Morfologie van die Thukela Estuarium.* B.Ing. Thesis, University of Stellenbosch. South Africa.

Qian, Y., Cheng, X., Fu, C., Shang, H. (1993). Influence of the Upstream Reservoirs on the Adjustment of Downstream Alluvial Channel. *International Journal of Sediment Research,* 8(3), pp. 1-20.

Rooseboom, A. (1992). *Sediment Transport in Rivers and Reservoirs - a South African Perspective.* South African Water Research Commission, Report No. 297/1/92, South Africa.

Rowntree, K.M. and Wadeson, R.A. (1999). *A Hierarchical Geomorphological Model for*

the Classification of Selected South African Rivers. South African Water Research Commission, Report No.497/1/99, South Africa.

Rowntree, K.M., Du Plessis, A.J.E., McGregor, G.K. (2000). *Geomorphological Research for the Conservation and Management of Southern African Rivers, Volume 1.* Draft Report to the Water Research Commission.

Rutherford, I. (2000). Some Human Impacts on Australian Stream Channel Morphology. In: Brizga, S. and Finlayson, B. (eds.) *River Management: the Australasian Experience.* John Wiley & Sons, Chichester, UK, pp. 11-49.

Schumm, S.A. (1969). River metamorphosis. *Journal of the Hydraulics Division,* 95(1), pp. 255-273.

Schumm, S.A. and Galay, V.J. (1994). The River Nile in Egypt. In: Schumm, S.A. and Winkley, B.R (eds.) *The Variability of Large Alluvial Rivers.* ASCE, United States, pp. 75-100.

Shields, I.A. (1936). Anwendungen der Ähnlichkeitsmechanik und Turbulenzforschung auf die Geschiebebewegung. *Mitteilungen der Preussischen Versuchsanstalt für Wasser und Schiffsbau*, Berlin, No.26, 1936.

SI and CESDC – Soils Incorporated (Pty) Ltd and Chalo Environmental and Sustainable Development Consultants (2000). *Kariba Dam Case Study,* prepared as an input to the World Commission on Dams, Cape Town. www.dams.org

Topping, D.J., Rubin, D.M., Nelson, J.M., Kinzel III, P.J., Corson, I.C. (2000). Colorado River Sediment Transport: 2. Systematic Bed-Elevation and Grain-Size Effects of Sand Supply Limitation. *Water Resources Research*, 36(2), pp. 543 – 570.

Topping, D.J., Rubin, D.M., Vierra JR, L.E. (2000). Colorado River Sediment Transport: 1. Natural Sediment Supply Limitation and the Influence of Glen Canyon. *Water Resources Research*, 36(2), pp. 515 – 542.

Torfs, H., Huygens, M., Tito, L. (1994). Influence of the Cross-section on the Erosion Criteria for Partly Cohesive Sediments. *Water, Science and Technology,* 29, pp. 103-111.

USBR – United States Bureau of Reclamation, 2002 -

http://www.uc.usbr.gov/feature/gcd_flows

USGS – United States Geological Survey , 2002a - http://az.waterdata.usgs.gov/nwis

USGS – United States Geological Survey, 2002b - http://wwwdaztcn.wr.usgs.gov/flood.html

Wargadalam, J. (1993). *Hydraulic Geometry Equations of Alluvial Channels.* PhD. Thesis, Colorado State University, Fort Collins, Colorado.

WCD (2000a). *Dams and Development: A new Framework for Decision-Making.* World Commission on Dams. www.dams.org

WCD (2000b). *Orange River Development Project, South Africa*. Case study prepared as input to the World Commission on Dams, Cape Town. www.dams.org

Wegner, D. (1996). Faking the Flood – Scientists Experiment with Floodlike Releases to Restore Habitat Below Glen Canyon Dam. *World Rivers Review*, 11(3).

Western Cape System Analysis, (1990). *Evaluation and Calibration of Flow Gauging Stations.*

White, R. (2000). Introduction: World Stock of Reservoirs. In: *Reservoir Sedimentation – One-Day Seminar*. HR Wallingford, UK.

Williams, G.P. (1978), Bankfull Discharge of Rivers. *Water Resources Research*, 14(6), pp. 1141-1154.

Williams, G.P. and Wolman, M.G. (1984). Downstream Effects of Dams on Alluvial Rivers. *Geological Survey Professional Paper 1286*, U.S. Government Printing Office, Washington, D.C.

Wolman, M.G. and Miller, J.P. (1960). Cited in Wharton, G. (1995). Information from Channel Geometry-Discharge Relations. In: Gurnell, A. and Petts, G. (eds.) *Changing River Channels.* John Wiley & Sons. Chichester, UK.

WRP – Water Resource Planning and Conservation (2001). Pers. Com.

Yang, C. T. and Simões, F.J.M. (2000). *User's Manual for GSTARS 2.1 (Generalised Stream*

Tube model for Alluvial River Simulation version 2.1). U.S. Department of the Interior.

Yang, C.T. (1972). Unit Stream Power and Sediment Transport. *Journal of the Hydraulics Division,* 98(10), pp. 1805-1826.

Yang, C.T. (1973). Incipient Motion and Sediment Transport. *Journal of the Hydraulics Division,* 99(10), pp. 1679-1704.

Yang, C.T. (1979).Unit Stream Power Equations for Total Load. *Journal of Hydrology,* 40, pp. 123-138.

Yang, C.T. (1984). Unit Stream Power Equation for Gravel. *Journal of the Hydraulic Engineering,* 110(12), pp. 1783-1797.

Yang, C.T. and Molinas, A. (1982). Sediment Transport and Unit Stream Power Function. *Journal of the Hydraulics Division,* 108(6), pp. 774-793.

Yang, C.T., Molinas, A., Wu, B. (1996). Sediment Transport in the Yellow River. *Journal of Hydraulic Engineering,* 122(5), pp. 237-244.

Zanke, U. (1977). Cited in Basson and Rooseboom (1997).

Zhou, Z. and Pan, X. (1994). Lower Yellow River. In: Schumm, S.A. and Winkley, B.R (eds.) *The Variability of Large Alluvial Rivers.* ASCE, United States, pp. 363-393.

APPENDIX A

- **A1: SOUTH AFRICAN RIVER DATA**
- **A2: VERIFICATION DATA**
- **A3: CHANNEL PATTERN DATA**
- **A4: REGRESSION RESULTS**

APPENDIX A1: SOUTH AFRICAN RIVER DATA

River Information

No.	Dam	River	S_0	A (km^2)	w (m/s)	d_{50} (mm)
1	Albertfalls	Mgeni	0.00015	905	0.052	0.241
2	Allemanskraal	Sand	0.00109	2925	0.002	0.043
3	Armenia	Leeu	0.00140	734	0.000	0.009
4	Boskop	Mooi	0.00278	2098	0.130	0.381
5	Bospoort	Hex	0.00233	555	0.002	0.050
6	Buffeljags	Buffeljags	0.00363	550	0.051	0.239
7	Buffelskloof	Waterval	0.01112	289	0.002	0.049
8	Buffelspoort	Strekstroom	0.00603	123	0.002	0.050
9	Bulshoek	Olifants	0.00612	736	0.224	0.500
10	Calitzdorp	Nels	0.00664	218	0.002	0.050
11	Chelmsford	Ngagane	0.00100	920	0.001	0.040
12	Clanwilliam	Olifants	0.00055	1942	0.167	0.432
13	Craigie Burn	Mnyamvubu	0.00300	182	0.224	0.500
14	Dagama	White Waters	0.00347	212	0.002	0.050
15	Darlington	Sundays	0.00051	13066	0.000	0.022
16	Doorndraai	Sterk	0.00448	564	0.002	0.050
17	Doringrivier	Doring	0.00056	269	0.002	0.052
18	Duiwenhoks	Duiwenhoks	0.07198	123	0.224	0.500
19	Ebenezer	Groot Letaba	0.00345	73	0.000	0.005
20	Erfenis	Groot Vet	0.00094	4364	0.001	0.028
21	Gamka	Gamka	0.03233	428	0.000	0.005
22	Gamkapoort	Gamka	0.00463	14275	0.000	0.009
23	Gariep	Oranje	0.00074	68885	0.001	0.025
24	Glen Alpine	Mogalakwena	0.00115	10689	0.002	0.041
25	Grassridge	Groot Brak	0.00125	3937	0.000	0.005
26	Gubu	Gubu	0.01464	93	0.000	0.006
27	Hartebeespoort	Crocodile	0.00685	3838	0.035	0.198
28	Hazelmere	Mdloti	0.00585	340	0.000	0.012
29	Hluhluwe	Hluhluwe	0.00235	688	0.000	0.018
30	Kalkfontein	Riet	0.00137	8346	0.001	0.028
31	Kammanassie	Kammanassie	0.00288	1600	0.078	0.295
32	Katrivier	Kat	0.01001	79	0.000	0.009
33	Klein Maricopoort	Klein Marico	0.00304	940	0.002	0.050
34	Klipberg	Konings	0.01346	228	0.163	0.426
35	Klipvoor	Pienaars (Moretele)	0.00399	5051	0.002	0.050
36	Kommandodrift	Tarka	0.00274	857	0.000	0.005
37	Koster	Koster	0.00335	266	0.002	0.050
38	Kouga	Kouga	0.00294	2706	0.214	0.490
39	Krugersdrift	Modder	0.00056	4258	0.004	0.064
40	Lindleyspoort	Elands	0.00606	729	0.002	0.050
41	Loerie	Loeriespruit	0.00940	154	0.012	0.114
42	Longmere	Wit	0.00079	77	0.002	0.050
43	Loskop	Olifants	0.00200	5774	0.157	0.418
44	Magoebaskloof	Politsie	0.01718	79	0.000	0.005
45	Midmar	Mgeni	0.00046	789	0.004	0.067
46	Nooitgedacht	Komati	0.00308	1734	0.207	0.481
47	Pietersfontein	Pietersfontein	0.01118	82	0.007	0.088

No.	Dam	River	S_0	A (km^2)	w (m/s)	d_{50} (mm)
48	Pongolapoort	Pongolo	0.00147	7834	0.010	0.108
49	Poortjieskloof	Groot	0.00607	645	0.032	0.190
50	Primkop	Wit	0.00735	63	0.002	0.050
51	Roode-Elsberg	Sanddrif	0.01836	124	0.220	0.496
52	Roodeplaat	Pienaars (Moretele)	0.01310	888	0.008	0.097
53	Rust de Winter	Elands	0.00287	1104	0.023	0.016
54	Rustfontein	Modder	0.00152	748	0.002	0.050
55	Van Ryneveldpas	Sundays	0.00197	3308	0.000	0.005
56	Wagendrift	Boesmans	0.00211	682	0.014	0.126
57	Waterdown	Klipplaat	0.00250	633	0.000	0.023
58	Westoe	Usutu	0.00132	600	0.221	0.497
59	Xonxa	White Kei	0.00236	1440	0.000	0.005

SA River Information (before and after dam development)

		Width (m)		MAR (Mm^3)		Mean annual max. flood peak (m^3/s)		Highest flood peak (m^3/s)		Mean annual average daily flow (m^3/s)	
Dam	**River**	**Before**	**After**	**Before**	**After**	**Before**	**After**	**Before**	**After**	**Before**	**After**
Albertfalls	Mgeni	31.7	27.6	256.5	252.8	50.8	49.0	74.3	72.9	8.7	7.3
Allemanskraal	Sand	49.0	21.0	-*	9.8	-	18.4	-	19.8	-	0.3
Bloemhof	Vaal	91.0	82.4	2494.0	-	745.9	-	772.6	1005.0	72.0	-
Erfenis	Groot Vet	23.7	26.0	-	20.5	-	63.6	-	81.2	-	1.1
Gamkapoort	Gamka	55.0	66.8	54.8	37.7	127.1	30.9	151.1	37.7	1.6	1.1
Gariep	Orange	269.0	255.0	4001.0	6934.0	1622.3	1018.9	-	-	135.8	219.3
Glen Alpine	Mogalakwena	36.0	24.0	-	101.7	-	64.6	-	83.9	-	3.0
Krugersdrift	Modder	24.0	31.0	123.5	86.2	305.7	114.8	-	-	4.0	2.8
Pongolapoort	Pongola	71.0	60.0	1023.8	586.7	223.5	424.7	787.8	457.9	35.5	18.7
Roodeplaat	Pienaars	26.0	15.0	-	19.0	-	19.8	278.4	30.9	-	0.7
Spioenkop	Thukela	53.2	36.3	425.5	352.5	224.7	162.1	441.3	218.8	16.7	10.3
Theewaterskloof	Sonderend	37.0	33.0	171.4	167.0	29.8	43.4	32.9	50.4	5.6	5.3
(Vioolsdrif)	Orange	221.4	207.5	9304.5	5271.5	2733.0	977.0	2907.7	1020.8	266.8	150.0

*: No data available

APPENDIX A2: VERIFICATION DATA

Verification Data

S (m/m)	B (m)	D (m)	Q (m^3/s)	d_{50} (mm)
0.001140	193.55	5.55	3143.08	0.610
0.000400	142.95	5.21	1812.22	0.400
0.000800	83.21	1.46	285.99	0.315
0.001705	21.64	0.49	11.81	0.212
0.000230	295.00	3.01	1310.00	0.500
0.000460	195.00	2.18	475.00	1.080
0.000480	610.00	3.94	2710.00	1.050
0.000360	785.00	2.80	2630.00	0.405
0.000130	400.00	4.62	2720.00	0.920
0.000200	454.00	5.29	3080.00	0.375
0.000450	280.00	2.88	652.00	0.265
0.000110	605.00	3.08	2085.00	0.320
0.000160	410.00	6.57	2858.00	0.310
0.000062	582.00	13.28	10200.00	0.210
0.001920	4.33	0.44	1.48	0.899
0.002750	3.92	0.15	0.65	0.286
0.000144	214.70	4.28	1523.45	0.227
0.001155	43.89	0.34	10.78	0.368
0.001480	8.00	0.65	4.85	1.440
0.001660	8.00	0.20	2.24	1.330
0.000140	253.10	2.30	403.57	0.310
0.000187	117.03	2.83	362.46	0.300
0.000134	162.43	3.59	443.16	0.195
0.000193	113.09	2.90	310.61	0.350
0.000207	149.09	3.08	387.66	0.280
0.000389	136.11	1.45	132.24	0.315
0.000044	451.10	13.23	10222.07	0.188
0.000035	1097.28	15.67	26560.40	0.342

APPENDIX A3: CHANNEL PATTERN DATA

Channel Patterns

River	Dam	Q_{10} (m^3/s)	Slope (m/m)	Sinuosity
Mgeni	Albertfalls	245	0.00015	1.42
Sand	Allemanskraal	795	0.00109	1.19
Leeu	Armenia	165	0.0014	1.13
Brak	Bellair	168	0.00253	1.04
Mooi	Boskop	71	0.00278	1.03
Hex	Bospoort	310	0.00233	1.09
Bronkhorstspruit	Bronkhorstspruit	340	0.00058	1.16
Buffeljags	Buffeljags	330	0.00363	1.09
Waterval	Buffelskloof	160	0.01112	1.44
Strekstroom	Buffelspoort	190	0.00603	1.09
Olifants	Bulshoek	451	0.00612	1.08
Nels	Calitzdorp	170	0.00664	1.19
Ngagane	Chelmsford	440	0.001	1.55
Olifants	Clanwilliam	824	0.00055	1.07
Mnyamvubu	Craigie Burn	255	0.003	1.38
White Waters	Dagama	115	0.00347	1.09
Sundays	Darlington	1473	0.00051	1.63
Sterk	Doorndraai	150	0.00448	1.01
Doring	Doringrivier	302	0.00056	1.30
Duiwenhoks	Duiwenhoks	170	0.07198	1.13
Groot Letaba	Ebenezer	190	0.00345	1.06
Groot Vet	Erfenis	1070	0.00094	1.15
Buffels	Floriskraal	647	0.00084	1.25
Gamka	Gamka	200	0.03233	1.10
Gamka	Gamkapoort	1760	0.00463	1.02
Oranje	Gariep	5200	0.00074	1.22
Mogalakwena	Glen Alpine	810	0.00115	1.12
Groot Brak	Grassridge	670	0.00125	1.11
Gubu	Gubu	81	0.01464	1.02
Crocodile	Hartebeespoort	1234	0.00685	1.29
Mdloti	Hazelmere	380	0.00585	1.43
Hluhluwe	Hluhluwe	1046	0.00235	1.50
Riet	Kalkfontein	1200	0.00137	1.36
Kammanassie	Kammanassie	641	0.00288	1.09
Kat	Katrivier	242	0.01001	1.70
Klein Marico	Klein Maricopoort	297	0.00304	1.11
Mooi	Klerkskraal	75	0.00041	1.04
Konings	Klipberg	68	0.01346	1.07
Loopspruit	Klipdrift	338	0.0003	1.09
Pienaars (Moretele)	Klipvoor	449	0.00399	1.11
Tarka	Kommandodrift	851	0.00274	1.59
Koster	Koster	283	0.00335	1.11
Kouga	Kouga	1379	0.00294	1.47
Klein Marico	Kromellenboog	369	0.00391	1.08
Modder	Krugersdrift	797	0.00056	1.48
Tarka	Lake Arthur	745	0.004	1.40
Leeu	Leeu Gamka	446	0.00345	1.09

River	Dam	Q_{10} (m^3/s)	Slope (m/m)	Sinuosity
Elands	Lindleyspoort	268	0.00606	1.14
Loeriespruit	Loerie	588	0.0094	1.29
Wit	Longmere	119	0.00079	1.24
Olifants	Loskop	1560	0.002	2.02
Politsie	Magoebaskloof	259	0.01718	1.07
Groot Marico	Marico Bosveld	346	0.00106	1.21
Mgeni	Midmar	430	0.00046	1.54
Komati	Nooitgedacht	470	0.00308	1.35
Hex	Olifantsnek	510	0.0046	1.18
Pietersfontein	Pietersfontein	75	0.01118	1.13
Pongolo	Pongolapoort	1979	0.00147	1.60
Groot	Poortjieskloof	96	0.00607	1.20
Wit	Primkop	219	0.00735	1.03
Sanddrif	Roode-Elsberg	211	0.01836	1.18
Pienaars (Moretele)	Roodeplaat	315	0.0131	1.08
Leeuspruit	Roodepoort-Cornelia	69	0.00048	1.13
Elands	Rust de Winter	332	0.00287	1.17
Modder	Rustfontein	492	0.00152	1.11
Olifants	Stompdrift	520	0.00032	1.04
Kaffer	Tierpoort	230	0.00089	1.30
Sundays	Van Ryneveldpas	790	0.00197	1.41
Boesmans	Wagendrift	486	0.00211	1.53
Klipplaat	Waterdown	325	0.0025	1.72
Caledon	Welbedacht	1500	0.00225	1.63
Usutu	Westoe	221	0.00132	1.34
White Kei	Xonxa	460	0.00236	1.44

APPENDIX A4: REGRESSION RESULTS

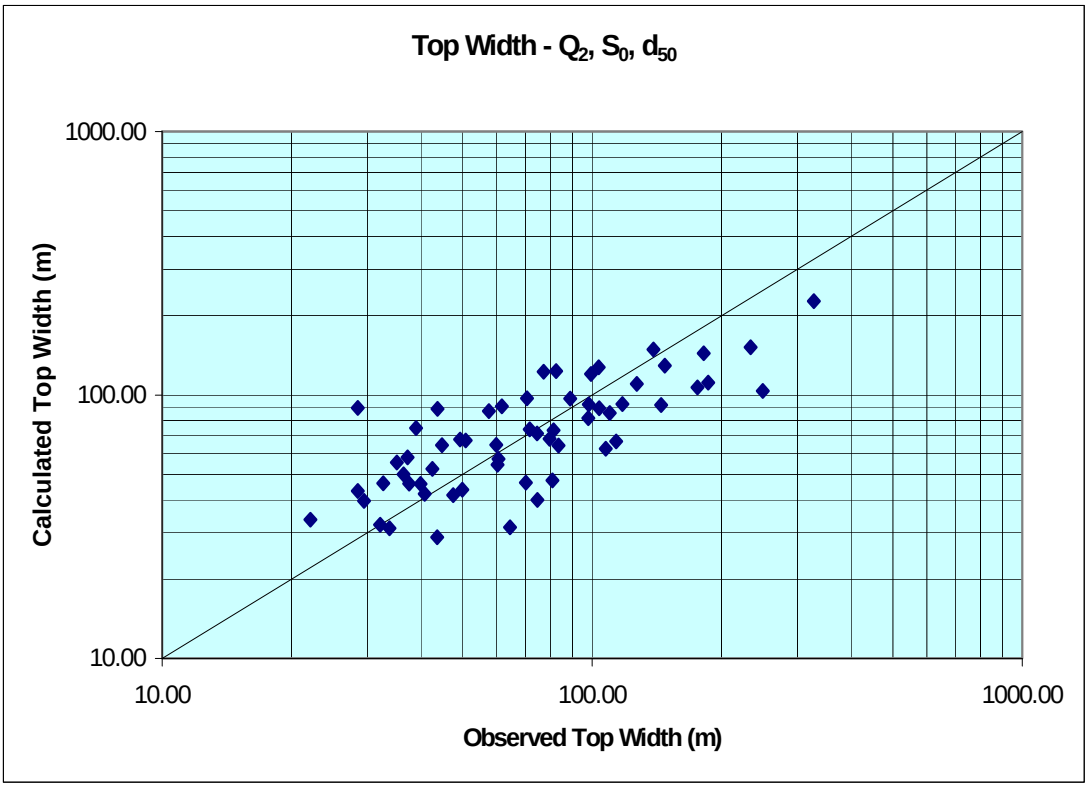
Top Width - Q_2, S_0, d_{50}
1000.00
100.00
10.00
Calculated Top Width (m)
10.00
100.00
1000.00
Observed Top Width (m)

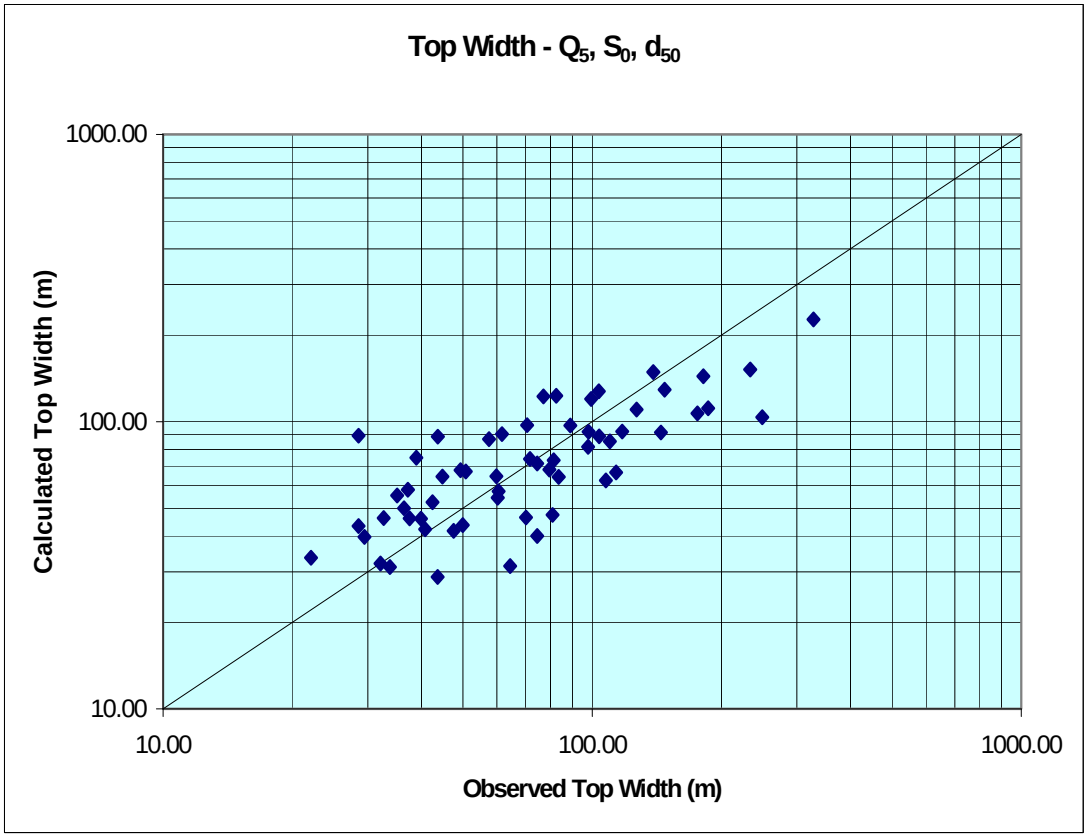
Top Width - Q_5, S_0, d_{50}
1000.00
100.00
10.00
Calculated Top Width (m)
10.00
100.00
1000.00
Observed Top Width (m)

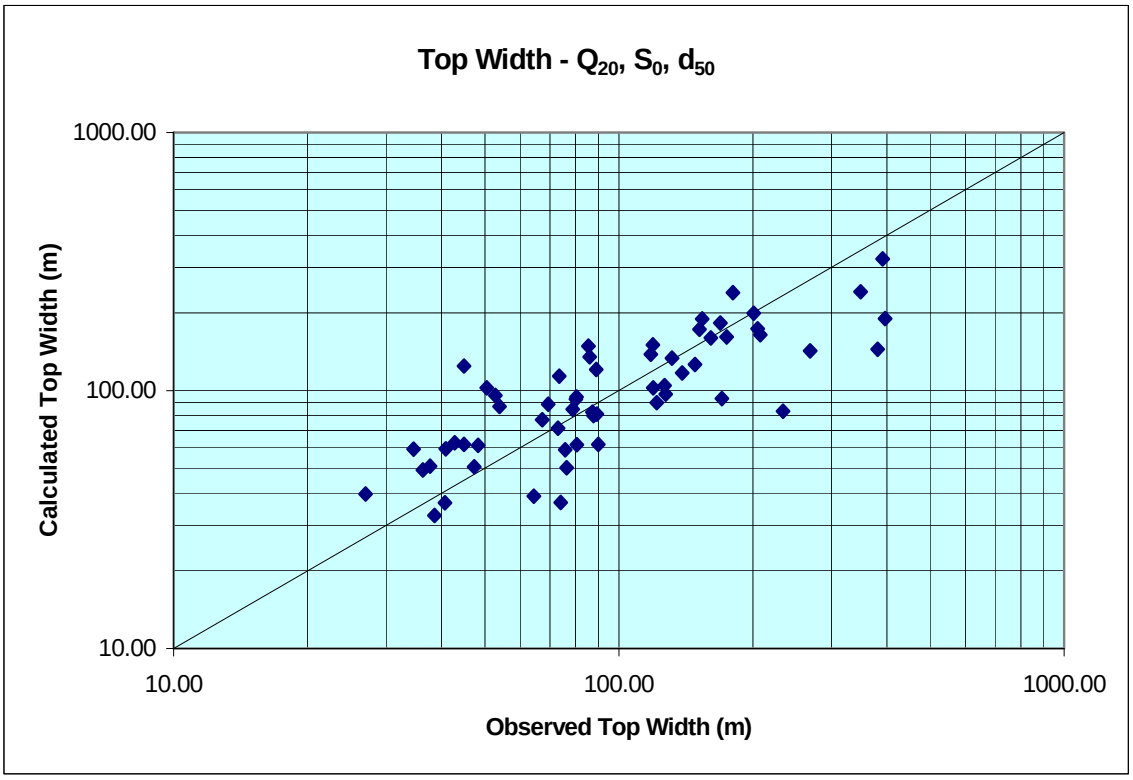

Regression results: $B = C_b\ Q_T^{\ a}\ S^b\ d_{50}^{\ c}$

					Accuracy ranges			
Recurrence interval T	C_b	a	b	c	0.67-1.5	0.5-2	0.33-3	r^2
2	5.75	0.368	-0.209	0.085	51%	86%	97%	0.4
5	4.63	0.361	-0.182	0.036	61%	93%	98%	0.58
20	2.79	0.33	-0.269	0.011	73%	90%	100%	0.63

Regression results: $B = C_b\ Q_T^{\ a}\ S^b$

					Accuracy ranges			
Recurrence interval T	C_b	a	b	c	0.67-1.5	0.5-2	0.33-3	r^2
2	2.49	0.369	-0.208	-	53%	83%	95%	0.38
5	3.33	0.357	-0.183	-	71%	92%	98%	0.57
20	2.54	0.329	-0.27	-	71%	92%	100%	0.63

Regression results: $B = C_b\ Q_T^{\ a}$

					Accuracy ranges			
Recurrence interval T	C_b	a	b	c	0.67-1.5	0.5-2	0.33-3	r^2
2	4.94	0.475	-	-	47%	83%	97%	0.31
5	5.47	0.458	-	-	64%	92%	98%	0.48
20	4.89	0.473	-	-	63%	85%	98%	0.45

APPENDIX B

- **B1: LABORATORY RESULTS**
- **B2: CONCENTRATIONS**
- **B3: DENSITIES AND SHEAR STRENGTHS**
- **B4: PARTICLE SIZE DISTRIBUTIONS**

APPENDIX B1: LABORATORY RESULTS

Flume Experiments: Sand

Run	Water Surface Slope	Bed Slope	Average Slope	Depth (m)	Discharge (m^3/s)	Velocity (m/s)	Froude No.	Hydraulic Radius (m)	k_s (m)	d_{50} (mm)	C (mg/l)	T (°C)	Bedform
1	0.0012	0.0007	0.0010	0.179	0.051	0.478	0.361	0.112	0.00357	0.12	566	24.5	Ripples
2	0.0015	0.0008	0.0012	0.187	0.061	0.544	0.401	0.115	0.00330	0.12	500	30.5	Dunes
8	0.0013	0.0009	0.0011	0.167	0.052	0.521	0.407	0.107	0.00280	0.12	553	29.0	Dunes
3	0.0023	0.0019	0.0021	0.138	0.070	0.850	0.732	0.094	0.00050	0.12	1552	27.0	Transition
4	0.0024	0.0019	0.0022	0.136	0.073	0.891	0.772	0.094	0.00036	0.12	1500	29.0	Transition
5	0.0026	0.0023	0.0025	0.132	0.078	0.986	0.867	0.092	0.00024	0.12	1616	32.0	Transition
6	0.0041	0.0052	0.0047	0.119	0.079	1.112	1.031	0.085	0.00080	0.12	2668	28.0	Antidunes
7	0.0080	0.0070	0.0075	0.086	0.052	1.011	1.101	0.067	0.00249	0.12	35745	28.5	Antidunes

Flume Experiments: Clay (88% Fines) - 1 day

Run[1]	Water Surface Slope	Bed Slope	Energy Slope	Depth (m)	Discharge (m^3/s)	Velocity (m/s)	Froude	Hydraulic Radius (m)	k_s (m)	T (°C)	d_{50} (mm)	C (mg/l)	τ (Pa)
1	0.00034	-0.00008	0.00042	0.158	0.0078	0.0819	0.066	0.103	0.2526	14.9	0.001	1434	0.650
2	0.00035	-0.00024	0.00048	0.155	0.0101	0.1087	0.088	0.102	0.1685	16	0.001	1479	0.730
3	0.00022	-0.00037	0.000167	0.153	0.0131	0.1427	0.116	0.102	0.0145	18	0.001	1428	0.251
4	0.0003	-0.00047	0.00032	0.153	0.0159	0.1724	0.141	0.101	0.0254	19	0.001	1732	0.482
5	0.00034	-0.00038	0.0004	0.154	0.0200	0.2162	0.176	0.102	0.0160	20	0.001	2159	0.604
6	0.0004	-0.00025	0.00027	0.152	0.0250	0.2749	0.225	0.101	0.0014	17	0.001	2570	0.402
7	0.0005	-0.00025	0.00042	0.151	0.0301	0.3320	0.273	0.100	0.0017	19	0.001	2600	0.623
8	0.00055	-0.00035	0.00045	0.152	0.0350	0.3840	0.314	0.101	0.0008	20.2	0.001	6500	0.671
9	0.00072	-0.00038	0.00051	0.152	0.0399	0.4390	0.360	0.101	0.0005	21.5	0.001	10040	0.759
10	0.001	0.0008	0.00097	0.151	0.0500	0.5513	0.453	0.100	0.0010	22	0.001	17170	1.438

Flume Experiments: Clay (88% Fines) - 4 days

Run[1]	Water Surface Slope	Bed Slope	Energy Slope	Depth (m)	Discharge (m^3/s)	Velocity (m/s)	Froude	Hydraulic Radius (m)	k_s (m)	T (°C)	d_{50} (mm)	C (mg/l)	τ (Pa)
1	0.00035	0.0051	0.00044	0.225	0.0078	0.0573	0.039	0.129	0.5831	17.5	0.001	458	0.973
2	0.0004	0.0048	0.00037	0.223	0.0101	0.0756	0.051	0.128	0.3755	19.5	0.001	444	0.808
3	0.00035	0.0049	0.00024	0.221	0.0131	0.0992	0.067	0.127	0.1535	21	0.001	606	0.520
4	0.00035	0.005	0.00035	0.219	0.0159	0.1208	0.082	0.127	0.1489	22.5	0.001	600	0.752
5	0.0003	0.0051	0.00041	0.213	0.0200	0.1565	0.108	0.124	0.0906	18.5	0.001	630	0.856
6	0.00035	0.0051	0.0003	0.210	0.0250	0.1985	0.138	0.124	0.0228	21	0.001	800	0.618
7	0.00035	0.0051	0.00038	0.205	0.0301	0.2444	0.172	0.122	0.0148	24	0.001	2030	0.765
8	0.0003	0.0005	0.00034	0.199	0.0350	0.2939	0.211	0.120	0.0039	19	0.001	2400	0.663
9	0.00035	0.0049	0.00044	0.197	0.0399	0.3383	0.243	0.119	0.0036	21	0.001	3180	0.850
10	0.00055	0.0046	0.00065	0.196	0.0500	0.4240	0.305	0.119	0.0030	23	0.001	7530	1.253

Flume Experiments: Clay (88% Fines) - 7 days

Run[1]	Water Surface Slope	Bed Slope	Energy Slope	Depth (m)	Discharge (m^3/s)	Velocity (m/s)	Froude	Hydraulic Radius (m)	k_s (m)	T (°C)	d_{50} (mm)	C (mg/l)	τ (Pa)
1	0.00035	0.00091	0.000367	0.145	0.0078	0.0890	0.075	0.098	0.1753	15	0.001	1280	0.522
2	0.000295	0.00079	0.000305	0.144	0.0101	0.1167	0.098	0.097	0.0757	16	0.001	1380	0.432
3	0.00038	0.00099	0.00025	0.144	0.0131	0.1519	0.128	0.097	0.0228	18	0.001	2237	0.353
4	0.000715	0.00075	0.000894	0.148	0.0159	0.1788	0.148	0.099	0.1047	15.5	0.001	1850	1.297
5	0.00034	0.00096	0.000504	0.148	0.0200	0.2247	0.186	0.099	0.0204	17	0.001	2100	0.733
6	0.00041	0.00094	0.000403	0.148	0.0250	0.2814	0.233	0.099	0.0040	18	0.001	2840	0.586
7	0.00044	0.00094	0.000412	0.147	0.0301	0.3412	0.284	0.099	0.0013	20	0.001	3840	0.594
8	0.00059	0.00077	0.000596	0.147	0.0350	0.3983	0.332	0.098	0.0015	21	0.001	5100	0.857
9	0.00072	0.00069	0.00081	0.146	0.0399	0.4564	0.381	0.098	0.0017	22	0.001	6980	1.159
10	0.0011	0.00109	0.00112	0.144	0.0500	0.5776	0.486	0.097	0.0010	17	0.001	14390	1.585
11	0.00117	0.0014	0.00113	0.148	0.0547	0.6172	0.513	0.099	0.0007	19	0.001	19530	1.638

Flume Experiments: Dry Clay (88% Fines) - 35 days

Run	Water Surface Slope	Bed Slope	Energy Slope	Depth (m)	Discharge (m^3/s)	Velocity (m/s)	Froude	Hydraulic Radius (m)	k_s (m)	d_{50} (mm)	τ (Pa)
1	0.00035	0.00091	0.000367	0.145	0.0078	0.0890	0.075	0.098	0.1753	0.001	0.522
2	0.000295	0.00079	0.000305	0.144	0.0101	0.1167	0.098	0.097	0.0757	0.001	0.432
3	0.00038	0.00099	0.00025	0.144	0.0131	0.1519	0.128	0.097	0.0228	0.001	0.353

Flume Experiments: Mixture 1 (77% Fines)

Run[1]	Water Surface Slope	Bed Slope	Energy Slope	Depth (m)	Discharge (m^3/s)	Velocity (m/s)	Froude No.	Hydraulic Radius (m)	k_s (m)	τ (Pa)	d_{50} (mm)	C (mg/l)	T (°C)
1	0.00043	0.0011	0.00036	0.194	0.0079	0.068	0.049	0.118	0.3735	0.685	0.001	430	15.5
2	0.00038	0.0011	0.00036	0.193	0.0101	0.087	0.063	0.117	0.2528	0.682	0.001	475	18
3	0.00033	0.00092	0.00042	0.192	0.0136	0.118	0.086	0.117	0.1631	0.790	0.001	585	19.5
4	0.00028	0.00098	0.00036	0.194	0.0155	0.134	0.097	0.118	0.1027	0.685	0.001	645	16
5	0.00031	0.00099	0.00029	0.193	0.0200	0.173	0.126	0.117	0.0318	0.548	0.001	900	18.5
6	0.00032	0.00099	0.00035	0.191	0.0250	0.219	0.160	0.117	0.0176	0.655	0.001	1465	21.5
7	0.00037	0.00101	0.00041	0.183	0.0292	0.265	0.198	0.114	0.0095	0.737	0.001	1830	15.5
8	0.00031	0.00102	0.00022	0.181	0.0328	0.302	0.227	0.113	0.0006	0.391	0.001	2595	18
9	0.00047	0.00118	0.00053	0.178	0.0383	0.359	0.272	0.112	0.0034	0.924	0.001	3545	19.5
10	0.0006	0.00101	0.00063	0.172	0.0460	0.444	0.342	0.110	0.0014	1.066	0.001	6470	21.5

Flume Experiments: Mixture 2 (54% Fines)

Run[1]	Water Surface Slope	Bed Slope	Energy Slope	Depth (m)	Discharge (m^3/s)	Velocity (m/s)	Froude No.	Hydraulic Radius (m)	k_s (m)	τ (Pa)	d_{50} (mm)	C (mg/l)	T (°C)	Remarks
1	0.00036	0.00087	0.00055	0.191	0.0083	0.072	0.053	0.117	0.4418	1.029	0.017	1555	14	
2	0.0003	0.00086	0.00061	0.192	0.0101	0.088	0.064	0.117	0.3694	1.146	0.017	1550	18	
3	0.00036	0.00069	-0.0001	0.191	0.0136	0.118	0.087	0.117	0.1353	0.675	0.017	1575	20	Use Water Slope
4	0.00024	0.00078	0.00006	0.189	0.0161	0.143	0.105	0.116	0.0011	0.444	0.017	1425	21	
5	0.00032	0.00095	0.00025	0.185	0.0200	0.180	0.133	0.115	0.0180	0.446	0.017	1770	16.5	
6	0.00027	0.00083	-5.6E-05	0.185	0.0244	0.221	0.164	0.114	0.0085	0.489	0.017	1800	18	Use Water Slope
7	0.00028	0.00087	0.00016	0.184	0.0291	0.264	0.197	0.114	0.0005	0.285	0.017	2170	21	
8	0.00039	0.00091	0.00032	0.181	0.0326	0.300	0.225	0.113	0.0022	0.559	0.017	2455	18	
9	0.00050	0.00092	0.00039	0.174	0.0380	0.364	0.278	0.110	0.0011	0.662	0.017	4195	24	
10	0.00079	0.00096	0.00088	0.168	0.0457	0.452	0.352	0.108	0.0035	1.461	0.017	5095	25	
11	0.00102	0.00096	0.00107	0.163	0.0540	0.552	0.437	0.106	0.0016	1.710	0.017	7095	26	
12	0.00135	0.00127	0.00157	0.160	0.0638	0.667	0.533	0.104	0.0016	2.457	0.017	11235	26	

Flume Experiments: Mixture 3 (20% Fines)[2]

Run[1]	Water Surface Slope	Bed Slope	Energy Slope	Depth (m)	Discharge (m^3/s)	Velocity (m/s)	Froude No.	Hydraulic Radius (m)	k_s (m)	τ (Pa)	d_{50} (mm)	C (mg/l)	T (°C)	Remarks
4	0.00026	0.00195	0.00033	0.186	0.0160	0.143	0.106	0.115	0.0696	0.601	0.105	3550	17	
6	0.00032	0.00198	0.00031	0.183	0.0250	0.228	0.170	0.114	0.0101	0.556	0.105	3593	21	
7	0.00023	0.00182	0.0002	0.184	0.0289	0.262	0.195	0.114	0.0012	0.415	0.105	3958	18	
8	0.00034	0.00192	0.00044	0.172	0.0330	0.320	0.246	0.109	0.0036	0.574	0.105	4333	21	
9	0.00044	0.00185	0.00057	0.170	0.0380	0.372	0.288	0.108	0.0030	0.950	0.105	5163	22	
10	0.00064	0.0021	0.00084	0.165	0.0450	0.455	0.358	0.106	0.0027	1.034	0.105	6575	16	Sand Ripples
11	0.00087	0.00193	0.00106	0.163	0.0529	0.540	0.426	0.106	0.0019	1.700	0.105	8925	19	Sand Ripples
12	0.0013	0.00168	0.00147	0.160	0.0640	0.667	0.533	0.104	0.0013	2.306	0.105	13655	20	Sand Ripples

Flume Experiments: Mixture 4 (7% Fines)[2]

Run[1]	Water Surface Slope	Bed Slope	Energy Slope	Depth (m)	Discharge (m^3/s)	Velocity (m/s)	Froude No.	Hydraulic Radius (m)	k_s (m)	τ (Pa)	d_{50} (mm)	C (mg/l)	T (°C)	Remarks
4	0.00043	0.00296	0.00057	0.186	0.0160	0.143	0.106	0.115	0.1429	1.039	0.11	2300	12	
7	0.00026	0.00244	0.00046	0.185	0.0289	0.261	0.193	0.114	0.0139	0.835	0.11	3080	20	Dunes (+-6mm)
9	0.00074	0.00308	0.0007	0.174	0.0380	0.364	0.279	0.110	0.0066	1.262	0.11	6760	23	Dunes
10	0.00097	0.00306	0.00119	0.169	0.0450	0.445	0.346	0.108	0.0086	1.605	0.11	9500	22	Dunes
11	0.00126	0.00312	0.00141	0.162	0.0529	0.544	0.431	0.105	0.0042	2.242	0.11	14840	22	Dunes
12	0.00152	0.00113	0.00134	0.156	0.0638	0.683	0.552	0.103	0.0007	2.324	0.11	12020	19	Dunes+Flat
13	0.00183	0.00089	0.00142	0.147	0.0738	0.839	0.700	0.098	0.0001	2.043	0.11	10420	23	Transition

1: Runs with the same numbers indicate that they were done at similar discharges and flow depths

2: Mixtures 3 and 4 were started at higher flow rates because of the larger amounts of sand

APPENDIX B2:

CONCENTRATIONS

Sediment	Run	Duration (h)	C (mg/l)
Sand[1]	1	11.75	566
	2	18	1682
	3	16.5	1552
	4	9.3	513
	5	5.5	1616
	6	3.8	2668
	7	2	35745
	8	26.1	553

Sediment	Run	Duration (h)	C (mg/l)
Clay (88% Fines)[2]	1		656
		0.5	458
	2		486
		2	444
	3		530
		1	606
	4		600
		1.8	630
	5		555
		1	600
	6		620
		2	800
	7		840
		3.5	2030
	8		1495
		1.3	2400
	9		2570
		1.8	3180
	10		3400
		2	7530

Sediment	Run	Duration (h)	C (mg/l)
Mixture 1 (77% Fines)[2]	1		493
		2.8	430
	2		435
		1.5	475
	3		550
		2	585
	4		570
		2	645
	5		655
		2	900
	6		940
		3	1465
	7		1380
		1.5	1830
	8		1885
		2	2595
	9		2660
		2	3545
	10		4100
		2	6470

[1] Concentrations taken at the end of each run

[2] Concentrations taken at the start and end of each run

Sediment	Run	Duration (h)	C (mg/l)	Sediment	Run	Duration (h)	C (mg/l)	Sediment	Run	Duration (h)	C (mg/l)
Mixture 2 (54% Fines)[2]	1		1985	**Mixture 3 (20% Fines)[2]**	4		3873	**Mixture 4 (7% Fines)[2]**	4		2340
		1.7	1555			5	3550			1.3	2300
	2		-		6		3373		7		2440
		2.5	1550			5	3593			6.3	3080
	3		1535		7		2975		9		3800
		2.3	1575			4.3	3958			1.5	6760
	4		1600		8		3953		10		6840
		1.8	1425			2.7	4333			9.5	9500
	5		1745		9		4378		11		7680
		2.5	1770			2.3	5163			14.8	14840
	6		1760		10		4855		12		11120
		2.4	1800			2	6575			23.3	12020
	7		1875		11		6457		13		10680
		2.3	2170			2.8	8925			4.8	10420
	8		2220		12		8910				
		3.2	2455			24.3	13655				
	9		2480								
		20.8	4195								
	10		3695								
		5.6	5095								
	11		5250								
		3.3	7095								
	12		2755								
		2.5	11235								

[2] Concentrations taken at the start and end of each run

APPENDIX B3: DENSITIES AND SHEAR STRENGTHS

Densities and shear strengths of the bed measured after each experiment

Bed Sediment	Wet density (kg/m^3)	Dry density (kg/m^3)	Moisture content (%)	Shear Strength (kPa)
Sand	1971	1602	23	1.4
Clay (1day)	2288	1678	36	
Clay (4 days)	1169	310	298	0.7
Clay (7 days)	2251	1523	47	
Clay (35 days) dry	2108	1674	25	
Mixture 1	1890	1131	67	0.4
Mixture 2	1693	1273	34	0.68
Mixture 3	2139	1865	16	0.93
Mixture 4	1747	1460	20	0.58

APPENDIX B4: PARTICLE SIZE DISTRIBUTIONS

Particle size distributions

		d (mm)	0.002	0.02 - 0.002	0.05 - 0.02	0.106 - 0.05	0.25 - 0.106	0.5 - 0.25	2 - 0.5
		d_{ave} (mm)	0.0014	0.0063	0.032	0.073	0.163	0.354	1
		w (m/s)	1.76E-06	3.57E-05	0.00092	0.00479	0.0187	0.0525	0.1176
S0	Sand - bed material before tests	% in Category	0	0	2	29	61	8	0
C0	Sand - bed material after tests	% in Category	73	9	11	7	0	0	0
SSUR	Clay (88% fines)- bed material before tests	% in Category	0	0	1	24	67	7	0
CS1	Clay (88% fines) - bed material after tests	% in Category	79	10	7	4	0	0	0
M0	Mixture 1 (77% fines) - bed material before tests	% in Category	64	9	8	9	9	1	0
M21	Mixture 1 (77% fines) - bed material after tests	% in Category	74	8	9	6	3	0	0
S4C6-1.1	Mixture 2 (54% fines) - bed material before tests	% in Category	44	7	6	15	24	4	0
S4C6-12.3	Mixture 2 (54% fines) - bed material after tests	% in Category	27	9	20	38	6	0	0
S4C6-Monsters	Mixture 2 (54% fines) - suspended sediments	% in Category	57	25	8	10	0	0	0
S6C4-4-1	Mixture 3 (20% fines) - bed material before tests	% in Category	16	3	5	22	48	6	1
S6C4-12.3	Mixture 3 (20% fines) - bed material after tests	% in Category	2	1	2	22	62	10	1
S6C4-Monsters	Mixture 3 (20% fines) - suspended sediments	% in Category	63	18	7	12	0	0	0
S8C2-1.1	Mixture 4 (7% fines) - bed material before tests	% in Category	6	0	2	26	58	7	1
S8C2-13.3	Mixture 4 (7% fines) - bed material after tests	% in Category	0	1	2	29	60	7	1
S8C2-Kombinasie	Mixture 4 (7% fines) - suspended sediments	% in Category	43	9	13	20	13	2	0

APPENDIX C

- **C1: PONGOLA RIVER WIDTHS BEFORE AND AFTER DAM**
- **C2: THUKELA ESTUARY SEDIMENT CORE SAMPLES/ GRADINGS**

APPENDIX C1: PONGOLA RIVER WIDTHS BEFORE AND AFTER DAM

Pongola River widths before and after Pongolapoort Dam

		Width (m)	
Section	Chainage (km)	1956	1996
1	0.46	82.7	90.5
2	0.95	183.1	135.7
3	1.43	224.5	60.3
4	1.91	177.2	60.3
5	2.39	141.8	62.1
6	2.87	159.5	62.1
7	3.36	189.0	62.1
8	3.86	153.6	54.3
9	4.33	153.6	46.6
10	4.81	82.7	46.6
11	5.32	88.6	38.8
12	5.58	130.0	46.6
13	6.13	82.7	46.6
14	6.62	130.0	62.1
15	7.09	118.1	62.1
16	7.58	153.6	77.6
17	8.07	124.0	62.1
18	8.58	206.7	62.1
19	9.10	153.6	54.3
20	9.52	342.6	77.6
21	10.05	153.6	69.8
22	10.53	135.9	62.1
23	11.01	112.2	62.1
24	11.48	194.9	69.8
25	11.97	177.2	77.6
26	12.49	147.7	66.7
27	12.99	200.8	58.3
28	13.53	177.2	116.7
29	14.04	124.0	50.0
30	14.52	147.7	66.7
31	15.00	130.0	75.0
32	15.48	147.7	83.3
33	15.96	106.3	75.0
34	16.43	183.1	91.7
35	16.96	200.8	108.3
36	17.45	159.5	100.0
37	17.92	135.9	75.0
38	18.40	141.8	75.0
39	18.86	130.0	100.0
40	19.36	130.0	83.3
41	19.82	141.8	83.3
42	20.30	112.2	75.0
43	20.78	106.3	91.7
44	21.27	141.8	100.0
45	21.77	76.8	56.5
46	22.26	135.9	96.8
47	22.72	130.0	80.7
48	23.19	118.1	80.7

		Width (m)	
Section	Chainage (km)	1956	1996
49	23.72	118.1	64.5
50	24.24	94.5	63.3
51	24.69	118.1	71.2
52	25.29	135.9	79.1
53	25.86	82.7	63.3
54	26.29	230.4	79.1
55	26.75	130.0	94.9
56	27.24	159.5	79.1
57	27.79	88.6	79.1
58	28.29	100.4	63.3
59	28.76	82.7	47.4
60	29.24	112.2	55.3
61	29.73	70.9	56.6
62	30.21	65.0	56.6
63	30.68	112.2	48.5
64	31.15	65.0	48.5
65	31.67	70.9	48.5
66	32.15	53.2	48.5
67	32.63	76.8	56.6
68	33.11	82.7	48.5
69	33.58	76.8	48.5
70	34.05	147.7	48.5
71	34.53	88.6	48.5
72	35.01	76.8	56.6
73	35.48	130.0	48.5
74	35.97	230.4	73.2
75	36.44	53.2	40.7
76	36.92	29.5	40.7
77	37.41	35.4	48.8
78	37.91	47.3	48.8
79	38.40	70.9	40.7
80	38.89	106.3	48.8
81	39.44	76.8	56.9
82	40.20	59.1	32.5
83	40.79	59.1	32.5
84	41.38	47.3	32.5
85	41.87	53.2	65.1
86	42.44	70.9	40.5
87	42.92	59.1	24.3
88	43.42	53.2	16.2
89	43.95	48.0	40.5
90	44.51	53.3	32.4
91	45.37	21.3	24.3
92	45.79	42.6	24.3
93	46.29	21.3	32.4
94	46.83	48.0	32.4
95	47.34	26.6	40.5
96	47.83	53.3	24.3
97	48.36	32.0	32.4
98	48.79	26.6	32.5

		Width (m)	
Section	Chainage (km)	1956	1996
99	49.27	10.7	32.5
100	49.77	53.3	40.6
101	50.24	59.7	32.5
102	50.75	35.8	48.7
103	51.26	74.6	40.6
104	51.76	47.8	40.6
105	52.26	41.8	32.5
106	52.76	41.8	48.7
107	53.26	65.7	32.5
108	53.77	53.3	40.6
109	54.27	42.6	24.4
110	54.76	42.6	32.5
111	55.28	42.6	24.4
112	55.70	42.6	16.2
113	56.18	37.3	24.4
114	56.67	32.0	33.0
115	57.17	37.3	33.0
116	57.65	37.3	24.8
117	58.16	32.0	16.5
118	58.64	32.0	33.0
119	59.17	64.0	16.5
120	60.21	37.3	24.8
121	60.71	48.0	24.8
122	61.21	53.3	24.8
123	61.71	48.0	16.5
124	62.17	42.6	16.5
125	62.67	53.3	16.5
126	63.17	37.3	24.8
127	63.67	42.6	16.5
128	64.16	48.0	25.0
129	64.66	53.3	16.7
130	65.14	48.0	16.7
131	65.63	53.3	16.7
132	66.11	42.6	16.7
133	66.59	42.6	25.0
134	67.09	42.6	16.7
135	67.59	42.6	16.7
136	68.10	41.8	25.0
137	68.62	38.8	25.0
138	69.13	47.8	25.0
139	69.63	35.8	16.7
140	70.11	35.8	25.0
141	70.61	35.8	16.7
142	71.09	44.8	25.0
143	71.61	38.8	32.8
144	72.12	44.8	32.8
145	72.63	59.7	32.8
146	73.14	47.8	32.8
147	73.65	59.7	41.1
148	74.16	47.8	32.8

		Width (m)	
Section	Chainage (km)	1956	1996
149	74.67	41.8	16.4
150	75.18	44.8	24.6
151	75.68	47.8	32.8
152	76.19	42.6	16.4
153	76.70	48.0	24.6
154	77.22	53.3	24.6
155	77.74	42.6	24.6
156	78.28	64.0	49.3

APPENDIX C2: THUKELA ESTUARY SEDIMENT CORE SAMPLES/ GRADINGS

No 1	**Depth (m)**	**Coordinate**: 29°12'92"S 31°28'50"E			
Sieve Size (mm)	0 - 0.15	0.15 - 0.3	0.3 - 0.45	0.45 - 0.6	0.6 - 0.8
4.75	100%	100	100	100	99.96
2.36	99.68	99.6	99.96	99.87	99.78
1.18	97.56	98.46	99.16	97.38	98.58
0.6	76.99	85.85	91.27	69.22	79.1
0.3	33.62	41.68	58.42	20.31	23.32
0.15	1.92	1.22	1.28	1.63	0.7
0.075	0.06	0.08	0.04	0.06	0.04
<0.075	0	0	0	0	0

No 2	**Depth (m)**	**Coordinate**: 29°13'30"S 31°29'19"E			
Sieve Size (mm)	0 - 0.15	0.15 - 0.3	0.3 - 0.45	0.45 - 0.6	0.6 - 0.75
4.75					100
2.36	100%	100	100	100	99.98
1.18	99.78	99.86	99.9	99.94	99.82
0.6	90.39	92.55	93.35	93.51	98.28
0.3	29.64	21.82	23.44	21.49	40.5
0.15	1.02	0.82	0.76	0.74	2.06
0.075	0.02	0	0	0	0.04
<0.075	0	0	0	0	0

No 3	**Depth (m)**	**Coordinate**: 29°13'60"S 31°29'87"E			
Sieve Size (mm)	0 - 0.15	0.15 - 0.3	0.3 - 0.45	0.45 - 0.6	0.6 - 0.75
4.75					
2.36					
1.18	100%	100	100	100	100
0.6	98.98	98.6	99.22	98.86	98.92
0.3	42.82	45.35	29.74	45.93	45.98
0.15	1.8	1.56	1.34	2.36	1.62
0.075	0.06	0.06	0.02	0.1	0.06
<0.075	0	0	0	0	0

No 4	**Depth (m)**	**Coordinate**: 29°13'60"S 31°30'07"E				
Sieve Size (mm)	0 - 0.15	0.15 - 0.3	0.3 - 0.45	0.45 - 0.6	0.6 - 0.75	0.75 - 0.9
4.75						
2.36	100%	100	100	100	100	100
1.18	99.74	99.8	99.76	99.7	99.28	99.82
0.6	86.62	87.92	88.33	86.07	73.59	93.14
0.3	19.7	30.32	31.97	23.28	13.02	33.3
0.15	0.42	0.7	0.9	0.66	0.14	0.8
0.075	0	0	0	0	0	0
<0.075	0	0	0	0	0	0

No 5	**Depth (m)**	**Mouth**	
Sieve Size (mm)	0 - 0.15	0.15 - 0.3	0.3 - 0.45
4.75			
2.36	100%		
1.18	99.96	100	100
0.6	82.47	91.64	93.7
0.3	18.92	15.19	27.65
0.15	0.8	0.42	1.4
0.075	0	0	0
<0.075	0	0	0

APPENDIX D: JULY 2002 FLOOD RELEASE FROM PONGOLAPOORT DAM

UNIVERSITEIT·STELLENBOSCH·UNIVERSITY
jou kennisvennoot • your knowledge partner

HYDRAULIC ASSESSMENT OF THE PROPOSED PONGOLA RIVER FLOOD RELEASE OF JULY 2002

GR BASSON & JS BECK

June 2002

Department of Civil Engineering, University of Stellenbosch, Stellenbosch
Tel: (021) 808 4355
Fax: (021) 808 4351
Email: **grbasson@sun.ac.za**; **jsbeck@sun.ac.za**

1. INTRODUCTION

During 2001 no large managed flood was released from Pongolapoort Dam due to flood protection measures that failed in Mozambique. Following meetings between the Department of Water Affairs and Forestry (DWAF), the local community and Mozambique, it was decided that the current dry conditions in the region warrant a flood release during July 2002. The proposed flood release is indicated in Table 1.

Table 1 Proposed flood release July 2002

DATE	DAY	FLOOD DAY	TIME	DISCHARGE (m^3/s)	DAILY RELEASE (m^3) (millions)	CUMULATIVE RELEASE (millions)	DAM CAPACITY (%)
12/07	Friday	1	12H00	50	0.00	0.00	**95.6**
13	Saturday	2	12H00	50	4.32	4.3	95.4
14	Sunday	3	12H00	50	4.32	8.6	95.2
15	Monday	4	08H00	100	3.60	12.2	95.1
			09H00	200	0.36	12.6	95.1
			10H00	300	0.72	13.3	95.1
			11H00	400	1.08	14.4	95.0
			12H00	500	1.44	15.8	95.0
			13H00	600	1.80	17.6	94.9
			14H00	700	2.16	19.8	94.8
			15H00	800	2.52	22.3	94.7
16	Tuesday	5	15H00	400	69.12	81.4	92.3
17	Wednesday	6	15H00	150	34.56	115.9	90.9
18	Thursday	7	15H00	150	12.96	128.9	90.3
19	Friday	8	15H00	50	12.96	141.8	89.8
20	Saturday	9	08H00	50	3.06	144.9	89.7
21	Sunday	10	08H00	50	4.32	149.2	89.5
22	Monday	11	08H00	10	4.32	153.5	89.3
23	Tuesday		08H00	10	0.86	154.4	89.3
24	Wednesday		08H00	10	0.86	155.3	89.3
25	Thursday		08H00	10	0.86	156.1	89.2
26	Friday		08H00	10	0.86	157.0	89.2
27	Saturday		08H00	10	0.86	157.9	89.2
28	Sunday		08H00	10	0.86	158.7	89.1
29	Monday		08H00	10	0.86	159.6	89.1
30	Tuesday		08H00	10	0.86	160.5	89.1
31	Wednesday		08H00	10	0.86	161.3	89.0
1/08	Thursday		08H00	10	0.86	162.2	89.0

Prof GR Basson and Ms JS Beck (Dept. Civil Engineering, University of Stellenbosch) have been investigating the hydraulics of the annual flood releases at Pongolapoort Dam since 1999, as a part of a Water Research Commission Project. Close cooperation was maintained with the DWAF-Durban office throughout the study.

The 1D model MIKE 11 of the Danish Hydraulics Institute was used to analyse the impact of Pongolapoort Dam on the geomorphology of the downstream river and pans, as well as the effect of the artificial flood releases as part of a Water Research Commission Project: *The Hydraulics of the Impacts of Dam Developments on the Downstream River Morphology* (2002).

During 2002 the model was extended to the Mozambique border and hydrodynamic calibration was completed during May 2002. The model simulations can be used to determine flood peak attenuation along the river and water levels in pans, for managed floods and dam spillage. In future the modelled reach can be extended into Mozambique.

This report discusses the hydrodynamic simulation results of the proposed July 2002 flood release.

2. HYDRODYNAMIC MODEL

The MIKE 11 hydrodynamic (HD) module is an implicit, finite difference model for the computation of unsteady flows in rivers and reservoirs, based on the St Venant equations representing conservation of mass and momentum. The model can describe both subcritical as well as supercritical flow conditions, and modules are incorporated that describe flow past hydraulic structures. The model can be applied to looped networks and quasi two-dimensional flow simulation on floodplains. The model is based on a fully hydrodynamic flow description. The old model (DWA, 1987) is a steady-state backwater model using the Manning equation, with cells representing the main river channel and the floodplains between consecutive sections. The pans were treated as special cells with certain stage-storage relationships and weir links between cells.

The new model was set up over a period of a year and it should be much more reliable than the 1987 model, since unsteady fully hydrodynamic simulations are carried out, and it would also be much more reliable to predict flood routing of floods outside the calibration range. The model has also recently been used to simulate a 1:50-year flood peak of 10500 m^3/s.

3. MODEL SET-UP AND CALIBRATION

The MIKE 11 model was set up for 100 km (almost up to the border to Mozambique) of the Pongola River downstream of Pongolapoort Dam (Figure 1):

- The set-up includes all major pans (18) that could be identified from 1:50 000 topographical maps, as well as from the DWA report *Mathematical Model of the Hydraulics of the Phongolo River Floodplain* (1987).

- Two minor tributaries were included, but for the July 2002 flood release it was assumed that there would only be very low flows of about 1 m^3/s in these tributaries during July.
- Pans were linked to the main river channel with short link channels and weirs. This allowed in- and outflows from the pans.
- Some pans were also connected to other pans allowing for cross-flows between pans.
- Sill levels, i.e. the level at which flows spill from the river into the pans, were determined from contour maps as well the DWA report mentioned above.
- Extra storage capacities were specified for some pans.
- Cross-sections were taken from contour maps (1933 and 1957) at 500 m intervals.
- The model was calibrated based on water levels in certain pans taken during the 1984 and 1986 flood releases. The Manning n-value for the main river channel and floodplains was adjusted and extra storage capacity was added to some pans in order to get peak and timing right. The simulated water levels deviated from the observed water levels between –0.65 and +0.65 m, with an average of +0.2 m. The simulated peak generally occurs about half a day too early, which is conservative for flood warnings. The reason for the poor accuracy on some of the pans is due to the fact that the topographical maps from which the cross-sections were taken are quite old and the river has certainly changed to some degree, especially since the dam has been built.

4. HYDRODYNAMIC FLOOD ROUTING OF THE PROPOSED FLOOD RELEASE

The 800 m^3/s flood peak of the proposed release corresponds to a 1:2-year natural flood peak and the shape of the hydrograph resembles a natural hydrograph more closely than previous flood releases (Figure 1), although the volume is quite large and the 24 hour duration of the flood peak is very long. The flood peak of the proposed flood release attenuates quite dramatically over 100 km, depending to a certain degree on the storage capacity of the pans, but also on the initial water levels in the pans. If they are starting full, i.e. up to their sill levels, the flood peak reduces to about 310 m^3/s and takes five days to cover 100 km (Figure 3), while if the pans are starting empty the flood peak reduces to 220 m^3/s and takes six days (Figure 4). Both of these are extremes and it is more likely that the pans will be about 50% full, which means that the flood peak at Ndumu should reduce to about 260 m^3/s, taking five and a half days to reach Ndumu (Figure 5). Between the new Pongola Bridge and the Ndumu Game Reserve the flood peak attenuation is quite significant since the river in that area is very flat and wide. The water levels in the pans can rise by between 2 and 5 m taking between one and five and a half days to reach their highest water levels (Figures 6 to 11).

The 260 m^3/s flood peak at Ndumu (starting 50% full) can be reduced to about 200 m^3/s by decreasing the peak duration significantly.

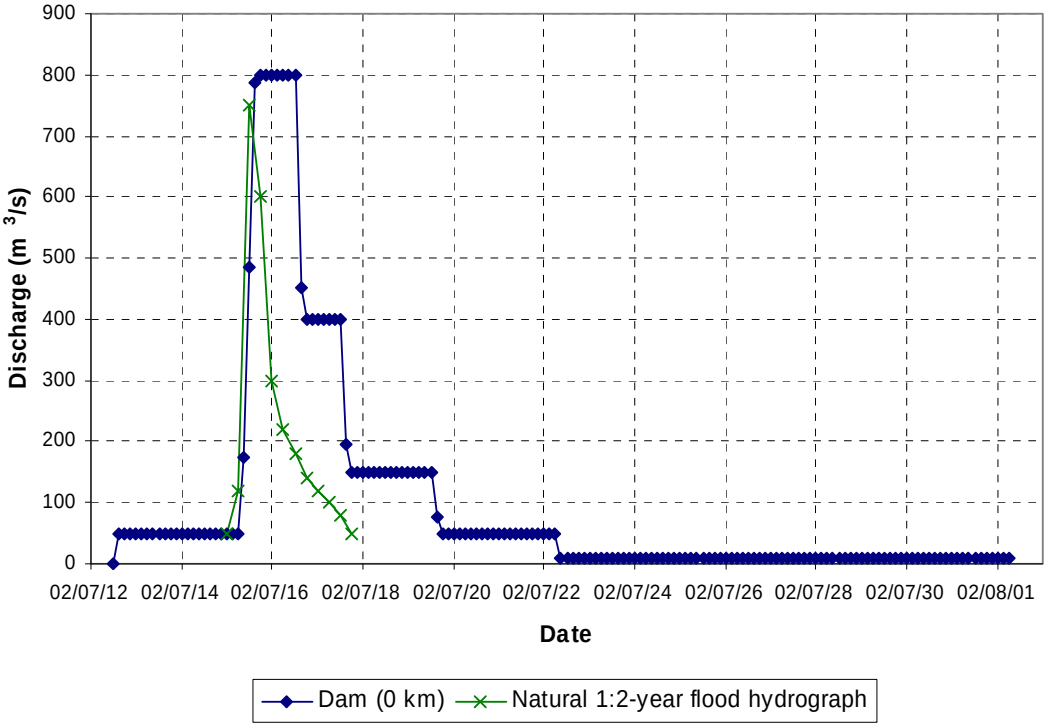

Figure 1 Proposed flood release and natural hydrograph

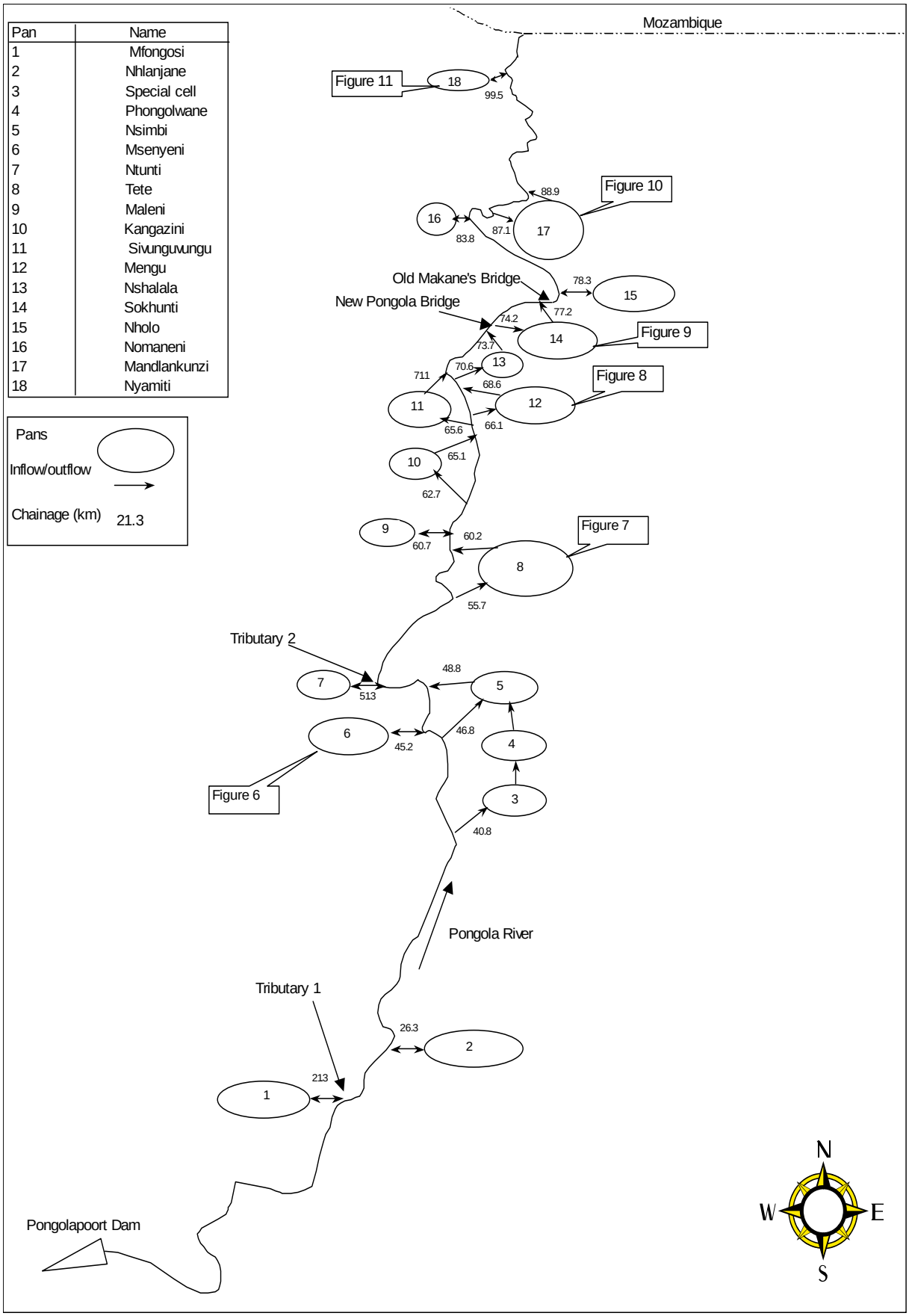

Figure 2 Pongola River layout

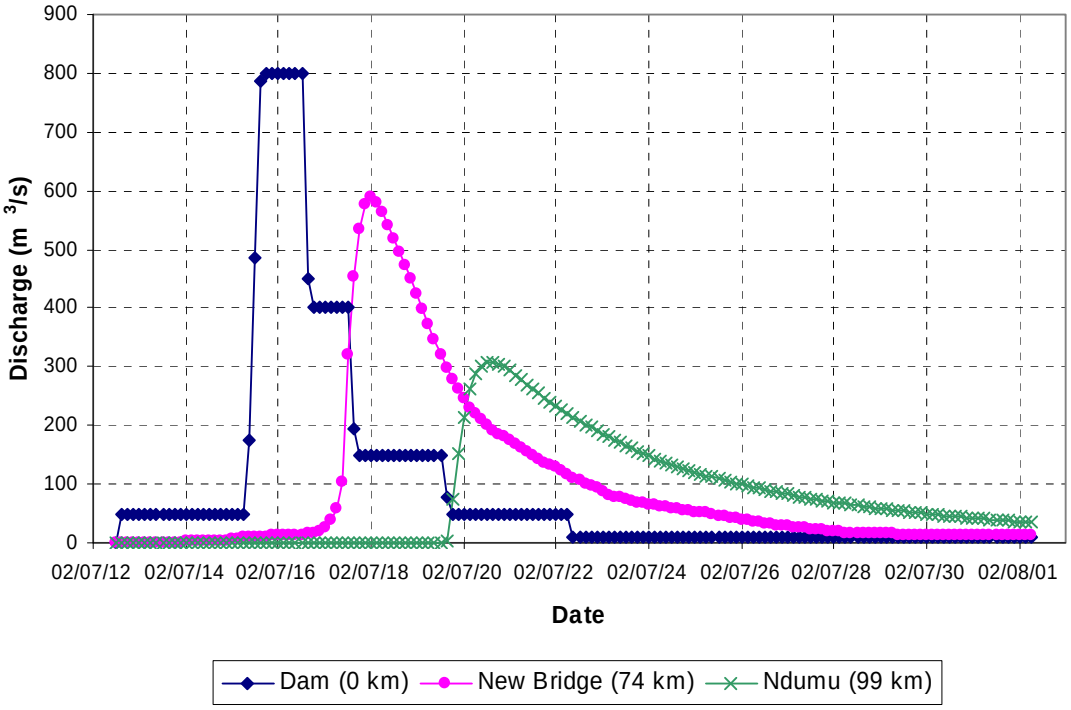

Figure 3 Simulated flood attenuation in the river – pans starting full

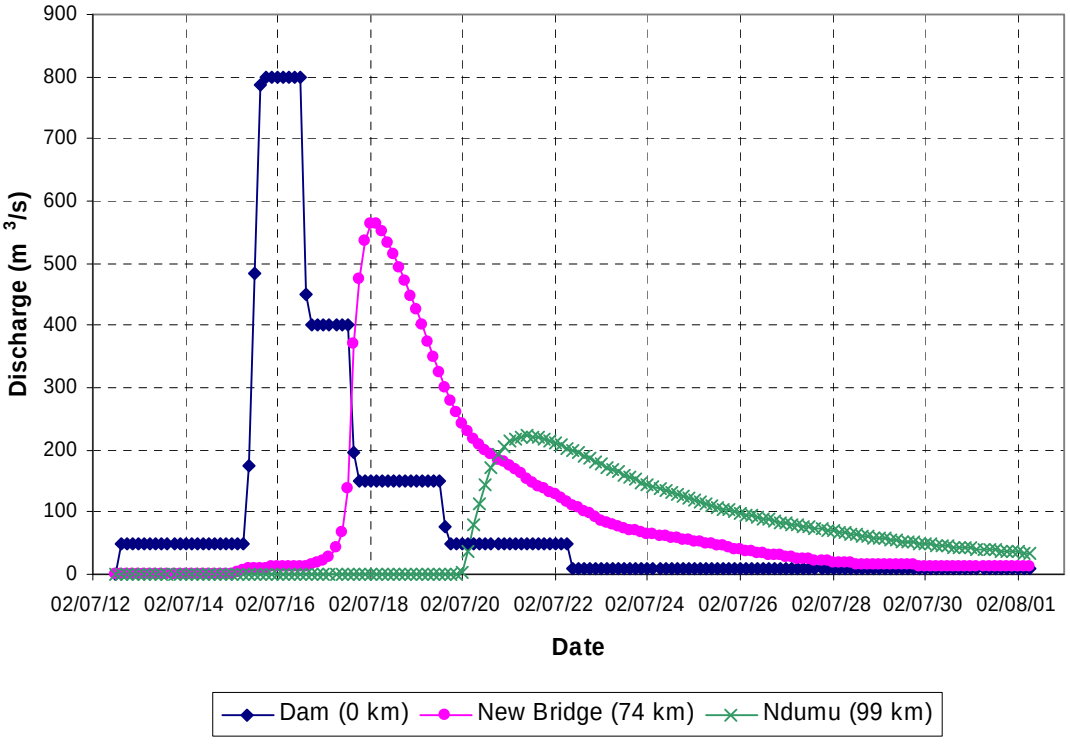

Figure 4 Simulated flood attenuation in the river– no initial pan water levels specified

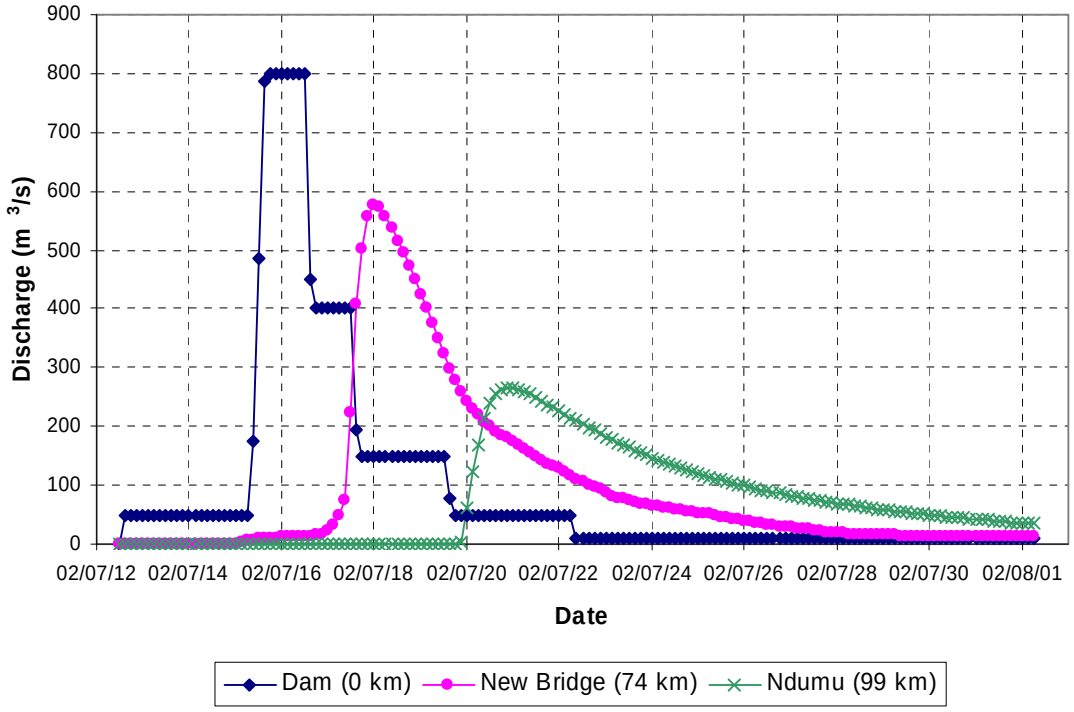

Figure 5 **Simulated flood attenuation in the river – initial pan water levels 0.5 to 1.5 m below sill level**

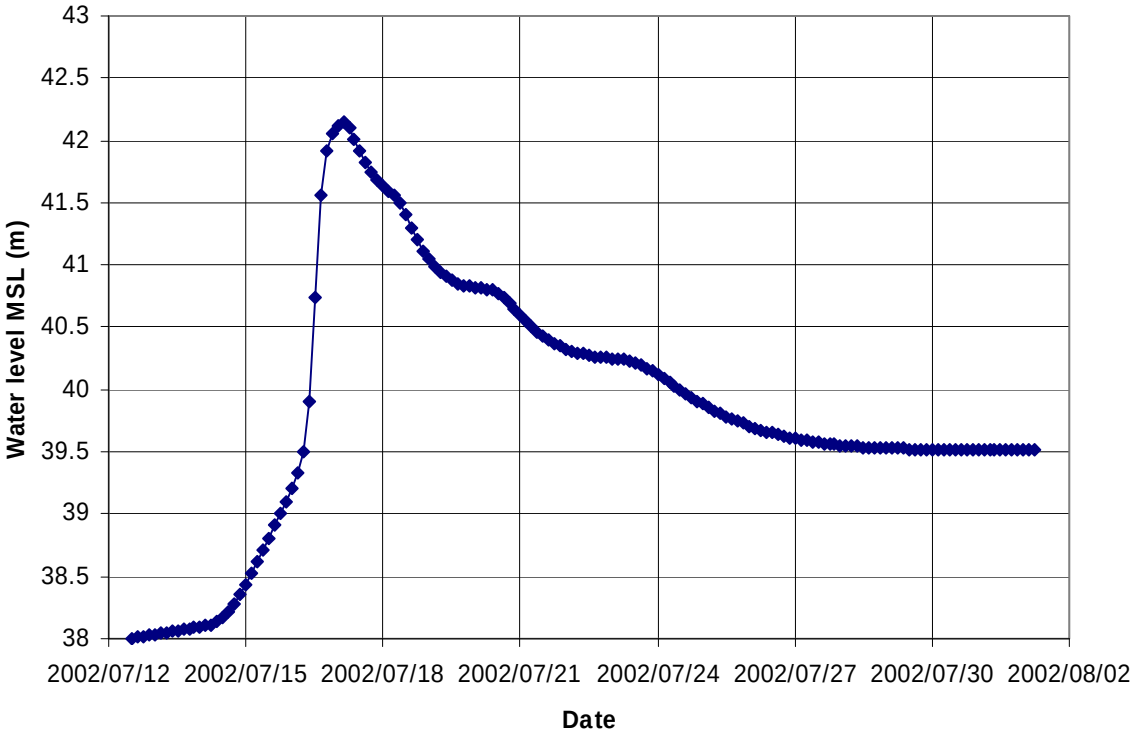

Figure 6 **Msenyeni Pan simulated water level**

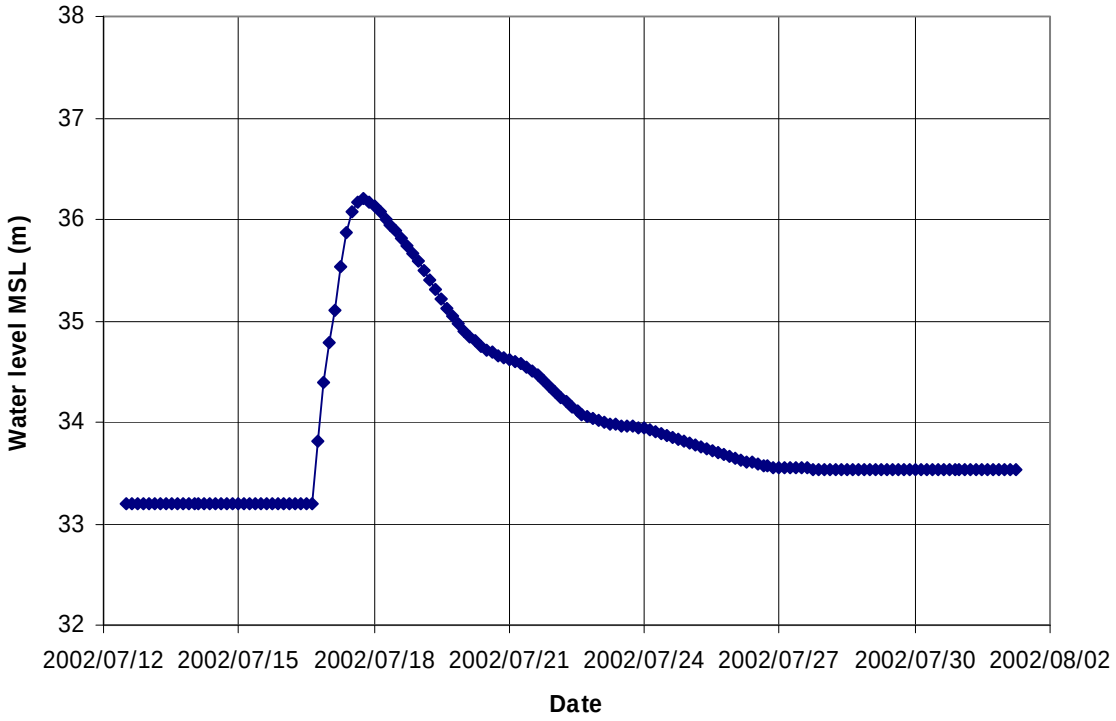

Figure 7 Tete Pan simulated water level

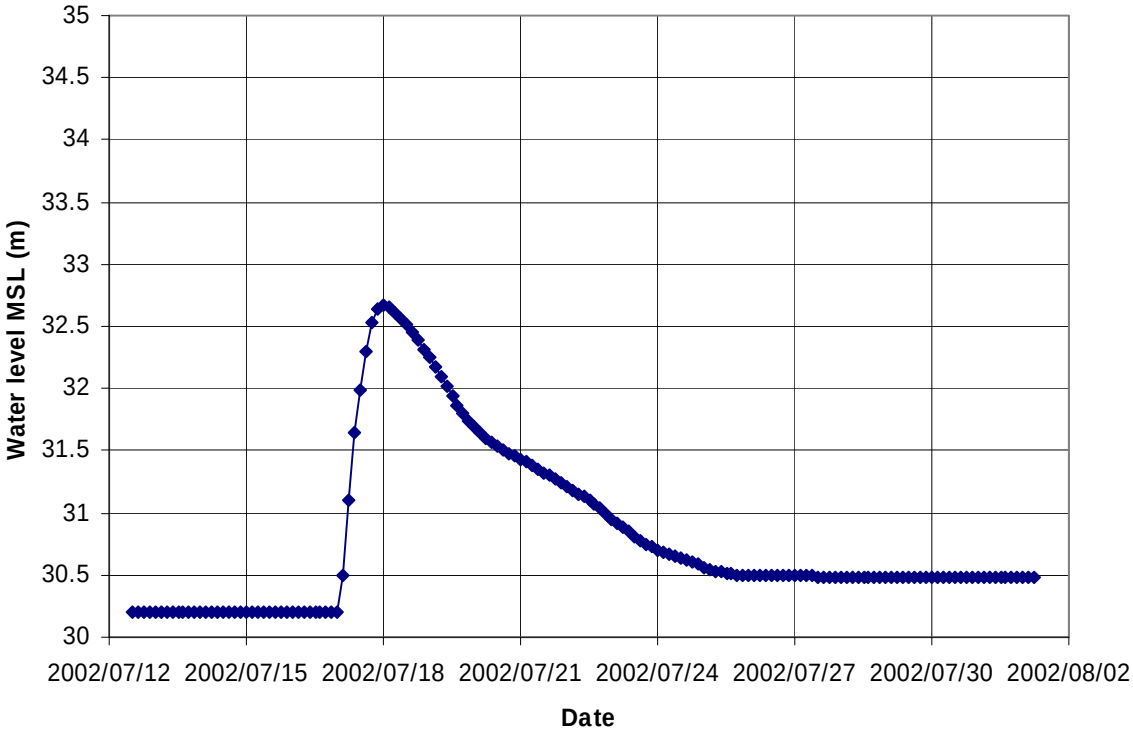

Figure 8 Mengu Pan simulated water level

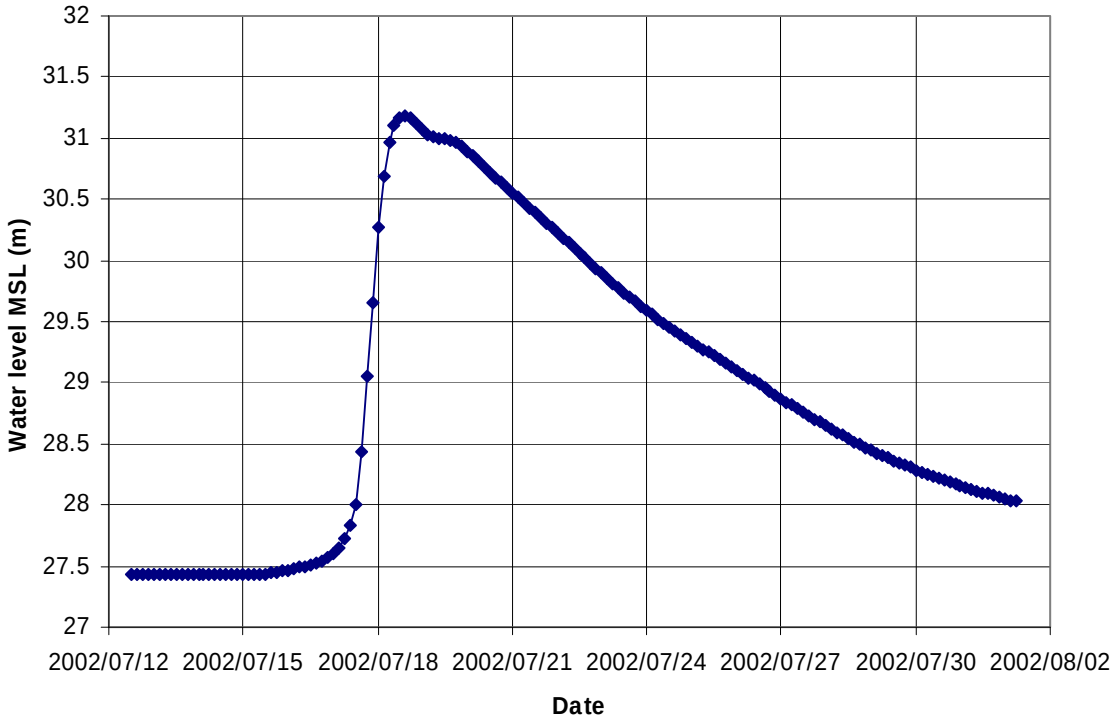

Figure 9 Sokhunti Pan simulated water level

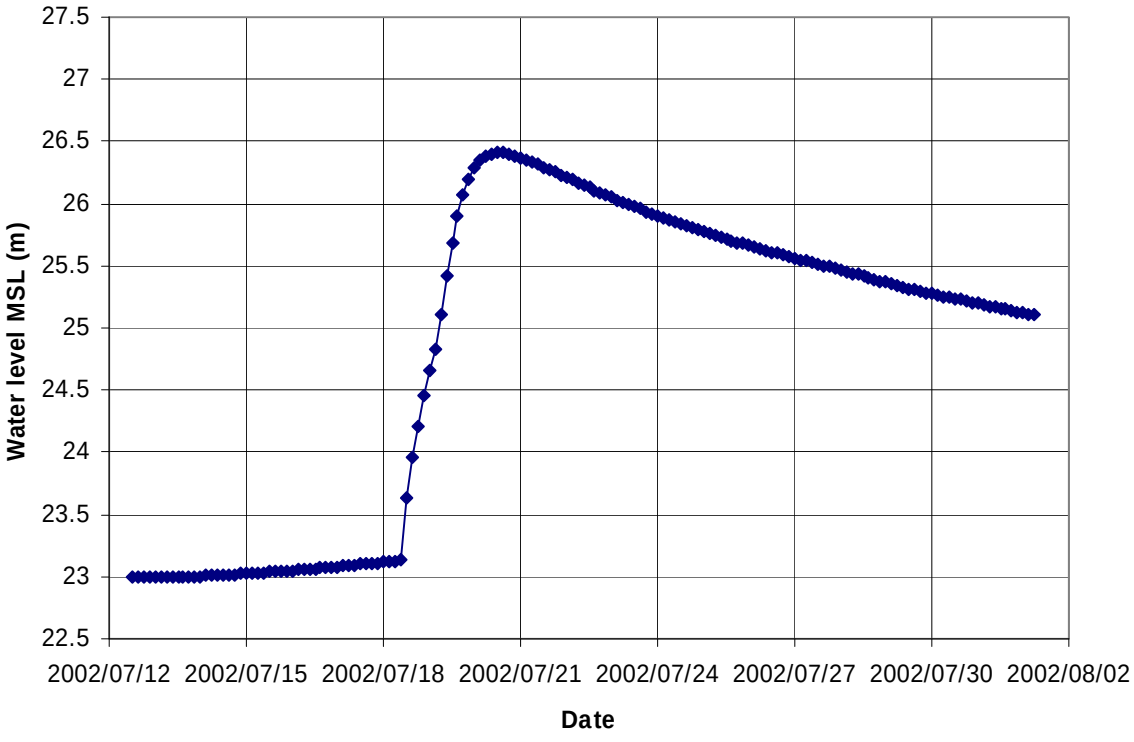

Figure 10 Mandlankunzi Pan simulated water level

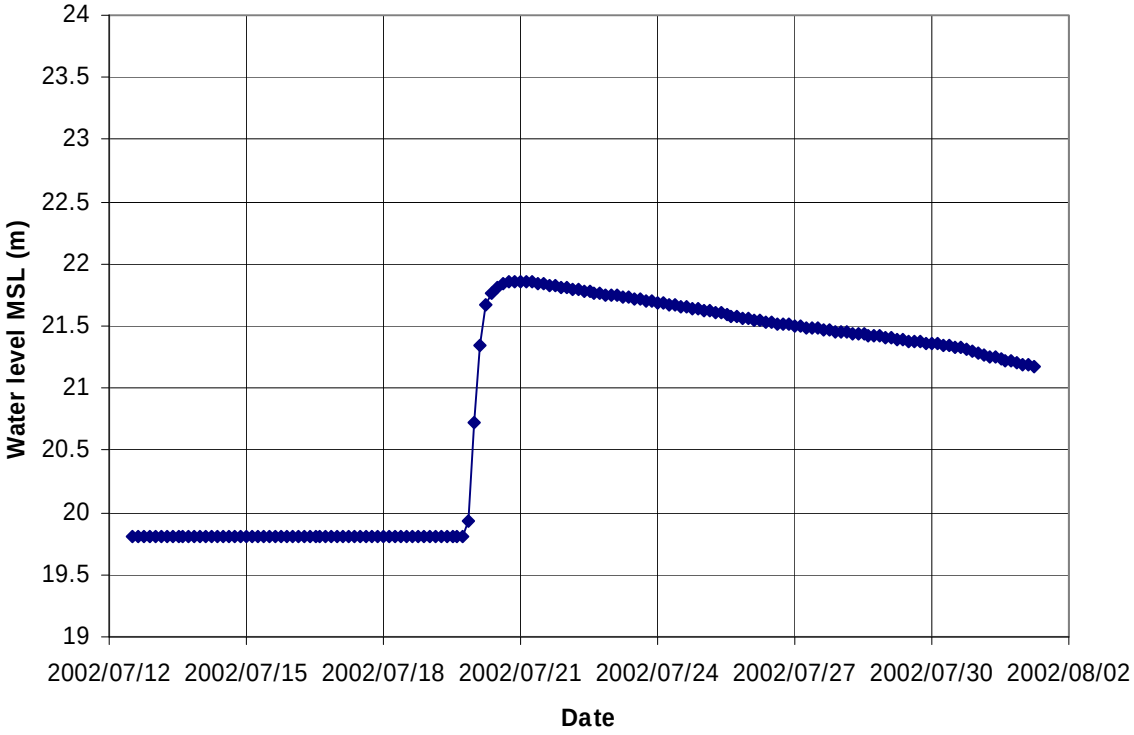

Figure 11 Nyamiti Pan simulated water level